The synthesis and evaluation of magneto-plasmonic nanoparticles for biosensing applications.

Author:
Mehdipour, Milad

Publication Date:
2021

DOI:
https://doi.org/10.26190/unsworks/1967

The synthesis and evaluation of magneto-plasmonic nanoparticles for biosensing applications.

By

Milad Mehdipour

A thesis submitted in fulfilment of the requirements for the degree of

Doctor of Philosophy

School of Chemistry

Faculty of Science

The University of New South Wales

Sydney, Australia

September 2021

Surname/Family Name	:	**Mehdipour**
Given Name/s	:	**Milad**
Abbreviation for degree as give in the University calendar	:	**PhD**
Faculty	:	**Science**
School	:	**Chemistry**
Thesis Title	:	**The synthesis and evaluation of magneto-plasmonic nanoparticles for biosensing applications**

Abstract 350 words maximum: (PLEASE TYPE)

This thesis aims to synthesise gold-coated magnetic nanoparticles (Au@MNPs). These nanoparticles provide unique properties such as magnetism, localized surface plasmon resonance (LSPR), conductivity, and ease of modification. These properties make Au@MNPs ideal for optical and electrochemical bio-sensing. The main challenges synthetic chemists faced when synthesising these nanoparticles are partial coating, aggregation, low yield, and reduction of saturation magnetisation after coating MNPs with gold. Our strategy to address these issues was to develop two unique types of Au@MNPs and develop a novel method for gold coating of the MNPs.

Firstly, the properties of the state-of-the-art commercially available Au@MNPs were investigated. This was performed to increase our understanding of the challenges facing the scientific community regarding these nanoparticles. Then, a novel particle ''gold-coated conglomerates of superparamagnetic nanoparticles'' was synthesized. To make practical biosensors, having MNPs that respond to magnets quickly and are stable against aggregation is crucial. Although using big MNPs as cores guarantees fast magnetic response, they are irreversibly magnetized and easily aggregate once placed next to a magnet. Superparamagnetic nanoparticles are stable against magnetic aggregation, but their saturation magnetization is small. To make an Au@MNPs with a fast magnetic response and good stability against aggregation, a number of superparamagnetic nanoparticles were encapsulated inside each silica shell and then coated with gold. The nanoparticles were characterized and their effectiveness for bio-sensing was demonstrated. Next, gold-coated zero-valent iron core-iron oxide shell nanoparticles were synthesized. Iron has the highest magnetization saturation amongst magnetic elements. The challenge was to avoid the rapid oxidation of iron when exposed to air or water. Thus, a synthetic method was developed to keep parts of the zero-valent iron-core intact while coating with gold. The final gold-coated zero-valent iron core-iron oxide shell showed superparamagnetic behaviour and high magnetization saturation. Finally, a new route for the large scale synthesis of Au@MNPs was developed. The method was designed based on fluidic systems. The gold nanoshell manufacturing systems were consisted of a two and three syringe set-up, delivering streams of reagents to a Y-shaped piece. This system was designed to be fast, cost-effective, and easy to handle.

ORIGINALITY STATEMENT

'I hereby declare that this submission is my own work and to the best of my knowledge it contains no materials previously published or written by another person, or substantial proportions of material which have been accepted for the award of any other degree or diploma at UNSW or any other educational institution, except where due acknowledgement is made in the thesis. Any contribution made to the research by others, with whom I have worked at UNSW or elsewhere, is explicitly acknowledged in the thesis. I also declare that the intellectual content of this thesis is the product of my own work, except to the extent that assistance from others in the project's design and conception or in style, presentation and linguistic expression is acknowledged.'

Signed .....

Date .....

COPYRIGHT STATEMENT

Signed …….....

Date …….....

AUTHENTICITY STATEMENT

‘I certify that the Library deposit digital copy is a direct equivalent of the final officially approved version of my thesis.’

Signed …….....

Date …….....

UNSW is supportive of candidates publishing their research results during their candidature as detailed in the UNSW Thesis Examination Procedure.

Publications can be used in their thesis in lieu of a Chapter if:

- The candidate contributed greater than 50% of the content in the publication and is the "primary author", ie. the candidate was responsible primarily for the planning, execution and preparation of the work for publication
- The candidate has approval to include the publication in their thesis in lieu of a Chapter from their supervisor and Postgraduate Coordinator.
- The publication is not subject to any obligations or contractual agreements with a third party that would constrain its inclusion in the thesis

Please indicate whether this thesis contains published material or not:

☐ This thesis contains no publications, either published or submitted for publication
(if this box is checked, you may delete all the material on page 2)

☐ Some of the work described in this thesis has been published and it has been documented in the relevant Chapters with acknowledgement
(if this box is checked, you may delete all the material on page 2)

☒ This thesis has publications (either published or submitted for publication) incorporated into it in lieu of a chapter and the details are presented below

CANDIDATE'S DECLARATION

I declare that:

- I have complied with the UNSW Thesis Examination Procedure
- where I have used a publication in lieu of a Chapter, the listed publication(s) below meet(s) the requirements to be included in the thesis.

Candidate's Name	**Signature**	**Date (dd/mm/yy)**
Milad Mehdipour		

POSTGRADUATE COORDINATOR'S DECLARATION *To only be filled in where publications are used in lieu of Chapters*

I declare that:

- the information below is accurate
- where listed publication(s) have been used in lieu of Chapter(s), their use complies with the UNSW Thesis Examination Procedure
- the minimum requirements for the format of the thesis have been met.

PGC's Name	PGC's Signature	Date (dd/mm/yy)
Alex William Donald		

For each publication incorporated into the thesis in lieu of a Chapter, provide all of the requested details and signatures required

Details of publication #1:

Full title: Synthesis of gold-coated magnetic conglomerate nanoparticles with fast magnetic response for bio-sensing

Authors: Milad Mehdipour, Lucy Gloag, Danielle T. Bennett, Sharmin Hoque, Raheleh Pardehkhorram, Padmavathy Bakthavathsalam, Vinicius R. Gonçales, Richard D.Tilley and J. Justin Gooding

Journal or book name: Journal of Materials Chemistry C
Volume/page numbers: **9**/ 1034-1043

Date accepted/ published: 06 Dec 2020/ 08 Dec 2020

Status	*Published*	***X***	*Accepted and In press*		*In progress (submitted)*	

The Candidate's Contribution to the Work

Synthesized magnetite nanoparticles, silica-coated conglomerates of superparamagnetic nanoparticles, gold-coated conglomerates of superparamagnetic nanoparticles

Characterised nanoparticles using TEM, SQUID magnetometry, UV-Vis spectroscopy,

Carried out stability against magnetic aggregation and colloidal stability experiments

Drafted and proofread the manuscript

Addressed reviewer's comments

Location of the work in the thesis and/or how the work is incorporated in the thesis:
In lieu of Chapter 4

PRIMARY SUPERVISOR'S DECLARATION

I declare that:

- the information above is accurate
- this has been discussed with the PGC and it is agreed that this publication can be included in this thesis in lieu of a Chapter
- All of the co-authors of the publication have reviewed the above information and have agreed

to its veracity by signing a 'Co-Author Authorisation' form.		
Primary Supervisor's name **J. Justin Gooding**	**Primary Supervisor's signature**	**Date (dd/mm/yy)**

Add additional boxes if required

For each publication incorporated into the thesis in lieu of a Chapter, provide all of the requested details and signatures required

Details of publication #2:
Full title: Synthesis of strongly magnetic gold-coated zero-valent iron core-iron oxide shell nanoparticles with superparamagnetic behaviour
Authors: Milad Mehdipour, Lucy Gloag, Jiaxin Lian, Richard D Tilley and J. Justin Gooding
Journal or book name: *ChemComm*
Volume/page numbers:
Date accepted/ published:

Status	*Published*		*Accepted and In press*		*In progress (submitted)*	***X***

The Candidate's Contribution to the Work
Synthesized zero-valent iron nanoparticles, silica-coated zero-valent iron core-iron oxide shell nanoparticles, gold-coated zero-valent iron core-iron oxide shell nanoparticles
Characterised nanoparticles using TEM, SQUID magnetometry, UV-Vis spectroscopy, Darkfield image
Carried out stability against magnetic aggregation and colloidal stability experiments
Drafted and proofread the manuscript

Location of the work in the thesis and/or how the work is incorporated in the thesis:
In lieu of Chapter 5

PRIMARY SUPERVISOR'S DECLARATION
I declare that:

- the information above is accurate
- this has been discussed with the PGC and it is agreed that this publication can be included in this thesis in lieu of a Chapter
- All of the co-authors of the publication have reviewed the above information and have agreed to its veracity by signing a 'Co-Author Authorisation' form.

Primary Supervisor's name **J. Justin Gooding**	**Primary Supervisor's signature**	**Date (dd/mm/yy)**

Add additional boxes if required

For each publication incorporated into the thesis in lieu of a Chapter, provide all of the requested details and signatures required

Details of publication #3:

Full title: Facile, flow reactor synthesis of gold-coated magnetic nanoparticles for biosensing applications

Authors: Milad Mehdipour, Lucy Gloag, Daniel Hagness, Jiaxin Lian, Md Saiful Alam, Xueqian Chen, Richard. D Tilley, and J. Justin Gooding

Journal or book name: Aggregate

Volume/page numbers:

Date accepted/ published:

Status	*Published*		*Accepted and In press*		*In progress (submitted)*	***X***

The Candidate's Contribution to the Work

Experimental design

Synthesized magnetite nanoparticles, silica-coated conglomerates of superparamagnetic nanoparticles, gold-coated conglomerates of superparamagnetic nanoparticles

Characterised nanoparticles using TEM, SQUID magnetometry, UV-Vis spectroscopy

Design of the Y-shaped pieces

Drafted and proofread the manuscript

Location of the work in the thesis and/or how the work is incorporated in the thesis:

In lieu of Chapter 6

PRIMARY SUPERVISOR'S DECLARATION

I declare that:

- the information above is accurate
- this has been discussed with the PGC and it is agreed that this publication can be included in this thesis in lieu of a Chapter
- All of the co-authors of the publication have reviewed the above information and have agreed to its veracity by signing a 'Co-Author Authorisation' form.

Primary Supervisor's name	**Primary Supervisor's signature**	**Date (dd/mm/yy)**
J. Justin Gooding		

Add additional boxes if required

Acknowledgements

My dad passed away on the 22nd of August 2021, less than a month before I submit my PhD thesis. It has been a long way until here, from early childhood up to now when I am about to submit my PhD Thesis. Throughout all these years he was always by my side, cheering and supporting me. He always valued education and loved the fact that I and my brother were doing fine in school. As of this moment which I am writing this last part of my PhD thesis all I can think of is our memories together, and how happy he would have been, knowing I have finished my PhD. Dad, it breaks my heart that you are not here anymore, but deep down I know you are always with me, in my heart, in my mind, in every part of my life. So, to my dear dad, thank you from bottom of my heart for everything, I am forever grateful for your love, support, and guidance. To my beautiful and perfect Mum, thank you from the bottom of my heart for everything you have done for me. Thank you for your unconditional love and support throughout all these years. There are no words that can describe how much you and dad did for me and I can never thank you enough. To my brother, who we have so much in common, and yet we are so different, thank you, bro.

To my supervisor, Professor Justin Gooding, I appreciate the opportunity you gave me to move to Sydney and study in one of the best universities in the world. Your dedication to science and hard hardworking attitude was always inspirational to me. Thank you for all the advice and discussions throughout the three and half years of my PhD.

To my Co-supervisor, Professor Richard Tilley, thank you for not letting me do that autoclave synthesis. Thank you for caring for our safety and well-being. Thank you for all the advice and recommendations especially on how to synthesis nanoparticles.

To my post-doc supervisor, Dr Lucy Gloag, thank you for the support, guidance, and scientific feedbacks. Thank you for teaching me how to make nanoparticles for the first time. Above all thank you for being a great friend, I will never forget how you supported me when I was going through hard times.

To James webb, the best lab manager in the history of Chemistry, thank you, my dude. You were always there for me in happiness and sadness. I cannot thank you enough. I wish you and Vikki a happy and wonderful life.

Special thank you to Dr Bijan Pouryousefi Markhali and Dr Adam D. Farahani for being my family in Sydney. Thank you for all the good times and thank you for always having my back no matter what.

To my lunch and WeSave buddies, Shreedhar Gautam and Munkhshur Myekhlai (Shuree), thank you guys for being my best friends.

To Kim Duong, thank you for being a great friend. I loved our conversations about life, music, YouTube, movies and ..., especially that one time we googled the university of Melbourne's notable alumni.

To Peter O'Mara, thank you for being such a good friend to me, I enjoyed our talks about politics and religion over coffee.

Shout out to my neighbours and buddies in the office, G.I. Joe Harding, and Daniel Hagness, thank you for being awesome.

To my friends Saiful, Pan, Kristine, and Sweetchen (Xueqian), I have always enjoyed hanging out with you guys. Thank you for being so cool and amazing.

To my friends, Ashkan Abdibastami, and Parisa Moazzam, thank you for your support especially in a time when I needed support more than ever.

To all my friends, Shahin Sinaki, Maziyar Mehdipour, Mehdi Cheraghi, Dr Raheleh Pardekhoram, Dr Mohaddeseh Kahram, Dr Majid Asnavandi, Danielle Bennett, Frederik Sondergaaed-Pedersen, Ujjaval Kerketta, Dr Masoud Masjoodi, Dr Eric Du, Dr Jiaxin Lian, Dr Iman Tehrani, Dr Ali Chamazketi, Dr Iman Roohaniesfahani, Dr Hsiang-Shen (Johnson) Chen, Dr Wenxian Tang, Belinda Zhang, Dr Agus Poerwoprajitno, Dr Rafael Colombo, Simone Bonaccorsi, Liam Barrera, Leo James, Kevin Mariandry, Peilin Tian, Han Han, … thank you for your support, some great time and good company.

Katie Levic, Sean Lim, Dr, Simon Hager and Dr Yin Yao from the electron microscope unit at UNSW. Thank you for training and all the help throughout the years of my PhD.

To Dr John Almeida, Dr Donna Zhuang, and all the nurses and doctors in Prince of Wales hospital, thank you so much for taking such good care of me when I was sick.

Also, I would like to thank UNSW and the Australian Government for UIPA Scholarship.

Finally, to my beautiful Shima, thank you from the bottom of my heart. In my dark nights, you are shining like the stars-you are my shining star.

It was an honour for me to work in the SMS group. Thanks and I love you all!

Milad Mehdipour

Abbreviations and Synonyms

3D	three-dimensional
acac	acetylacetonate
APTES	(3-aminopropyl)triethoxysilane
AEAPTMS	[3-(2-aminoethylamino)propyl]trimethoxysilane
Au	gold
Au@MNP	gold-coated magnetic nanoparticles
CV	cyclic voltammogram
DMSO	dimethyl sulfoxide
DNA	deoxyribonucleic acid
EDC	1-ethyl-3-(3-dimethylaminoprpyl) carbodiimide
EDX	energy-dispersive X-ray spectroscopy
LSPR	localized surface plasmon resonance
MNPs	magnetic nanoparticles
M_S	magnetization saturation
NHS	n-hydroxysuccinimide
rcf	relative centrifugal force
rpm	revolutions per minute
SAM	self-assembled monolayer
SEM	scanning electron microscopy
SERS	surface-enhanced Raman spectroscopy
SQUID	superconducting quantum interference device
TEM	transmission electron microscopy
XRD	x-ray diffraction

List of publications

1. **Mehdipour, M**., Gloag, L., Bennett, D.T., Hoque, S., Pardehkhorram, R., Bakthavathsalam, P., Gonçales, V.R., Tilley, R.D., and Gooding, J.J. (2021) Synthesis of gold-coated magnetic conglomerate nanoparticles with a fast magnetic response for bio-sensing. J. Mater. Chem. C, 9 (3), 1034–1043.

2. Gloag, L., **Mehdipour, M**., Ulanova, M., Mariandry, K., Nichol, M.A., Hernández-Castillo, D.J., Gaudet, J., Qiao, R., Zhang, J., Nelson, M., Thierry, B., Alvarez-Lemus, M.A., Tan, T.T., Gooding, J.J., Braidy, N., Sachdev, P.S., and Tilley, R.D. (2020) Zero valent iron core-iron oxide shell nanoparticles as small magnetic particle imaging tracers. *Chem. Commun.*, **56** (24), 3504–3507.

3. Gloag, L., **Mehdipour, M**., Chen, D., Tilley, R.D., and Gooding, J.J. (2019) Advances in the Application of Magnetic Nanoparticles for Sensing. Adv. Mater., 31 (48), 1904385.

Abstract

This thesis aims to synthesise gold-coated magnetic nanoparticles (Au@MNPs). These nanoparticles provide unique properties such as magnetism, localized surface plasmon resonance (LSPR), conductivity, and ease of modification. These properties make Au@MNPs ideal for optical and electrochemical bio-sensing. The main challenges synthetic chemists faced when synthesising these nanoparticles are partial coating, aggregation, low yield, and reduction of saturation magnetisation after coating MNPs with gold. Our strategy to address these issues was to develop two unique types of Au@MNPs and develop a novel method for gold coating of the MNPs.

Firstly, the properties of the state-of-the-art commercially available Au@MNPs were investigated. This was performed to increase our understanding of the challenges facing the scientific community regarding these nanoparticles. Then, a novel particle ‘’gold-coated conglomerates of superparamagnetic nanoparticles’’ was synthesized. To make practical biosensors, having MNPs that respond to magnets quickly and are stable against aggregation is crucial. Although using big MNPs as cores guarantees fast magnetic response, they are irreversibly magnetized and easily aggregate once placed next to a magnet. Superparamagnetic nanoparticles are stable against magnetic aggregation, but their saturation magnetization is small. To make an Au@MNPs with a fast magnetic response and good stability against aggregation, a number of superparamagnetic nanoparticles were encapsulated inside each silica shell and then coated with gold. The nanoparticles were characterized and their effectiveness for bio-sensing was demonstrated. Next, gold-coated zero-valent iron core-iron oxide shell nanoparticles were synthesized. Iron has the highest magnetization saturation amongst magnetic elements. The challenge was to avoid the rapid oxidation of iron when exposed to air or water. Thus, a synthetic method was developed to keep parts of the zero-valent iron-core intact while coating with gold. The final gold-coated zero-valent iron core-iron oxide shell showed superparamagnetic behaviour and high magnetization saturation. Finally, a new route for the large scale synthesis of Au@MNPs was developed. The method was designed based on fluidic systems. The gold nanoshell manufacturing systems were consisted of a two and three syringe set-up, delivering

streams of reagents to a Y-shaped piece. This system was designed to be fast, cost-effective, and easy to handle.

Contents

List of Figures

Figure 1.12. Nanoparticles solution extinction measurements of (A) faceted (B) and gold-coated. magnetic nanoparticles (i) when cores are not coated (r1 31.5 ± 9.7 and 28.5 ± 7.3 nm), (ii) gold decorated nanoparticles (r1 32.6 ± 9.0 and 28.6 ± 8.5 nm) in aqueous solution, and (iii–vi) gold-coated nanoparticles with gold shell increasing of particles sized is 100, r2 is 59.9 ± 12.4, 65.0 ± 19.9, 73.1 ± 11.7, and 76.6 ± 9.8 nm for the faceted cores and 40.0 ± 6.7, 49.1 ± 10.7, 53.8 ± 4.6, and 66.4 ± 5.0 nm for the tetra cubic cores in aqueous solution. (C) picture of nanoparticles in solution A.

Figure 1.13. Calculated extinction spectrum of the gold-coated magnetite nanoparticles in comparison with other core-shell nanoparticles with the same diameter (Dtotal=50 nm, gold shell thickness 5 nm).

Figure 1.14. Top absorption spectra of the gold-coated iron oxide nanoparticles with different shapes A) core-shell nanospheres B) core-shell nano popcorn and C) core-shell nanostars. Bottom TEM images of the D) nanosphere E) nano popcorn F) nanostars. The sizes labelled in the graphs are the base size of the particles that do not include the protrusions in popcorns and tips in the stars.

Figure 1.15. A schematic of the accumulation of gold-coated magnetic nanoparticles onto the surface of a gold working electrode in a magnetic field.

Figure 1.16. TEM images of multiple synthesis methods used for making the gold-coated magnetic nanoparticles(a) based on a method reported by Goon et al[138], (b) based on method reported by Jin et al[140],(c) a combination of method a and b, and (d) based on a method reported by Freitas et al[139].

Figure 1.17. Schematic illustration of the Separation and Detection method by Using gold-coated magnetic nanoparticles and silver Nanoparticles through Ligation.

Figure 1.18. Schematic of the sensing strategy using gold-coated magnetic nanoparticles to detect microRNA, a,b, gold-coated magnetic nanoparticles modified with probe DNA complementary to target miRNA (a) are mixed in the blood for 30 minutes (b). c magnetic separation of the gold-coated magnetic nanoparticles from unhybridized sequences. d, gold-coated magnetic nanoparticles both hybridized and unhybridized deposited on the gold electrode. e, Electrical reconfiguration of gold-

coated magnetic nanoparticles in their heterogeneous network (hybridized and unhybridized) occurs by applying 10 cycles of square-wave voltammetry in the potential range between 200 and − 500 mV.

Figure 1.19. Schematic illustration of the two main routes for gold coating.

Figure 1.20. Schematic illustration of the three growth modes of secondary metal on a seed substrate.

Figure 1.21. Schematic illustration of the hydroxylamine seeding of colloidal gold nanoparticles.

Figure 1.22. TEM images of the A) citrate capped magnetic nanoparticles B) one incremental addition of the gold atoms to the magnetic nanoparticles C) three incremental additions of the gold atoms to the magnetic nanoparticles and D) five incremental additions of the gold atoms to the magnetic nanoparticles. insets show the histogram of the size of the nanoparticles for each step.

Figure 1.23. Schematic illustration gold coating process of the magnetite nanoparticles (i) gold-coating in organic phase (ii) water dispersible gold-coated magnetite nanoparticles (iii). (B) TEM image of the gold-coated magnetic nanoparticles (iii); (C) HRTEM image of part of a gold-coated magnetite nanoparticle from (B). (D) UV−vis absorption spectra of the gold-coated magnetite nanoparticles (i) in hexane, (ii) in hexane, and (iii) in Milli-Q water.

Figure 1.24. Top: Scheme and Bottom: TEM images of the nanoparticles at different stages of the synthesis process.

Figure 1.25. (a) TEM image of PEI-coated magnetite cores; (b) HRTEM image of a PEI-coated magnetite particle; (c) TEM image of gold-seeded PEI-coated magnetite cores; (d) HRTEM image of a gold-seeded PEI-coated magnetite particle; (e) TEM image of gold-coated PEI-coated magnetite nanoparticles; (f) high-magnification TEM image of a gold-coated PEI-coated magnetite nanoparticle.

Figure 1.26. Top: Schematic illustration of synthesis route to make the gold-coated magnetic nanoparticles. Bottom: TEM images of 1) JHU magnetic nanoparticles 2)

Figure 3.5. A) TEM image of the gold-coated magnetic nanoparticles acquired from Creative Diagnostics®(50 nm) B) TEM images of the gold-coated magnetic nanoparticles acquired from Creative Diagnostics® (250 nm) C) the corresponding histogram of the size of gold-coated magnetic nanoparticles acquired from Creative Diagnostics®(50 nm) D) the corresponding histogram of the size of gold-coated magnetic nanoparticles acquired from Creative Diagnostics® (250 nm) E) Dynamic light scattering (DLS) of the gold-coated magnetic nanoparticles acquired from Creative Diagnostics® 50 nm (blue) and 250 nm (red).

Figure 3.6. EDX map of the elements A) gold B) iron and C) merged gold and iron of the gold-coated magnetic nanoparticles acquired from Creative Diagnostics®.

Figure 3.7. X-Ray Diffraction patterns of gold-coated magnetic nanoparticles acquired from Creative Diagnostics® (navy blue) 50 nm and (purple) 250 nm.

Figure 3.8. A) SQUID magnetometry measurements of gold-coated magnetic nanoparticles acquired from Creative Diagnostics® (cyan) gold-coated magnetic nanoparticles 250 nm and (navy) gold-coated magnetic nanoparticles 50 nm; Inset shows the low field region, B) UV-Vis spectra of gold-coated magnetic nanoparticles acquired from Creative Diagnostics®, (navy) gold-coated magnetic nanoparticles 50 nm, (pink) gold-coated magnetic nanoparticles 250 nm.

Figure 3.9. A) TEM image of the 50 nm gold-coated magnetic nanoparticles acquired from Nanoimmunotech B) TEM image of the 250 nm gold-coated magnetic nanoparticles C) the corresponding histogram of the size of 50 nm gold-coated magnetic nanoparticles acquired from Nanoimmunotech D) the corresponding histogram of the size of 250 nm gold-coated magnetic nanoparticles acquired from Nanoimmunotech, and E) Dynamic light scattering (DLS) of the 50 nm (red) and 250 nm (blue) gold-coated magnetic nanoparticles acquired from Nanoimmunotech.

Figure 3.10. EDX map of the elements A) gold B) iron and C) merged gold and iron of the gold-coated magnetic nanoparticles acquired from Nanoimmunotech.

Figure 3.11. X-Ray Diffraction patterns of (purple) 50 nm and (blue) 250 nm gold-coated magnetic nanoparticles were acquired from Nanoimmunotech.

Figure 3.12. A) SQUID magnetometry measurements (blue) 50 nm gold-coated magnetic nanoparticles, (green) 250 nm gold-coated magnetic nanoparticles acquired from Nanoimmunotech, and B) UV-Vis spectroscopy measurements of (blue) 50 nm gold-coated magnetic nanoparticles, (purple) 250 nm gold-coated magnetic nanoparticles acquired from Nanoimmunotech.

List of Tables

In loving memory of my dear Father

In my thoughts,

In my heart,

You are always with me, Dad,

And always will be.

To my Mum

With love and eternal appreciation

Chapter 1

Introduction

1. General overview

People diagnosed earlier with cancer are not only more likely to survive, but importantly also to have better experiences of care, and improved quality of life compared with those diagnosed late.[1,2] So, there is a frequent effort to push the medical tests to detect lower levels of the biomarker to facilitate the diagnosis and treatment of diseases. Ultrasensitive biosensors are one of the promising ways to lower detection limits while using simple technologies.[3] The main challenge facing ultrasensitive biosensors is related to diffusion. Detectors with sufficient sensitivity are normally nanoscale in size which means that although the detector can detect the ultralow level of biomarkers the diffusion of these molecules to this nanoscale detector may take an excessively long time.[4]

Magnetic nanoparticles are one of the most effective tools to overcome the diffusion problem. As illustrated in Figure 1.1 magnetic nanoparticles can be distributed throughout a sample and collect and preconcentrate the analyte in the bulk and then can be transferred to the detector with a help of a magnet.[4,5] This means instead of waiting for the analyte to find the sensing interface, the sensor (magnetic nanoparticles) finds the analyte.[4]

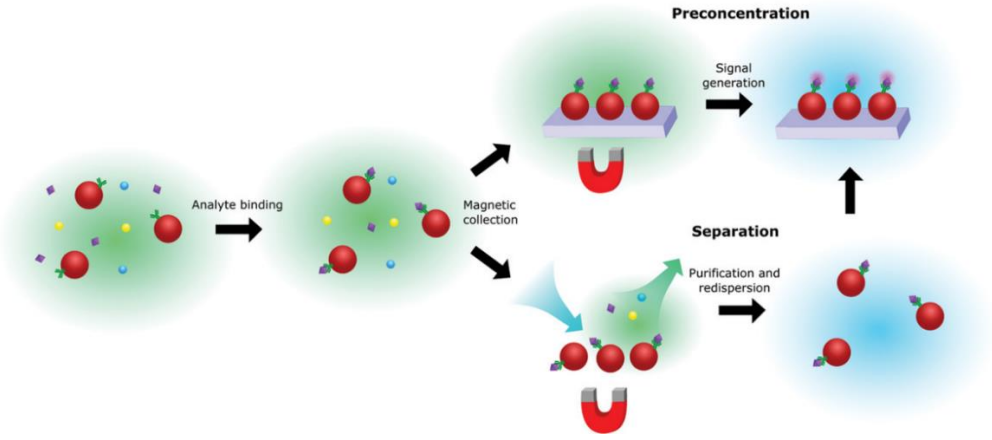

Figure 2.1. Scheme illustrating preconcentration and separation techniques with magnetic nanoparticles. Reprinted with permission from[4].Copywrite (2021) John Wiley and Sons.

For applications where the magnetic nanoparticles are used to collect or separate the analyte for sensing or imaging, the bigger the magnetic nanoparticle, the more powerful

their magnetic moment, thus a stronger signal can be achieved.[6] However, big magnetic nanoparticles are also heavily attracted to each other and as a result, magnetic nanoparticles with bigger sizes are prone to aggregation.[7] To address this issue, we can reduce the size of nanoparticles to a limit, in which the nanoparticle is still responding to the external field in a timely manner, but when the field is removed, they are no longer magnetic. These nanoparticles are called superparamagnetic nanoparticles. Even though this phenomenon can help, there are still challenges facing magnetic nanoparticles such as superparamagnetic nanoparticles are not coming to a magnet fast enough, magnetic nanoparticles not being stable in biological media, magnetic nanoparticles not being optically active or conductive and also them being quite hard to be modified with biological molecules.[8,9]

Coating the magnetic nanoparticles with noble metals, and especially gold, is a great way to address all these issues. This thesis aims to make gold-coated magnetic nanoparticles with good qualities for bio-sensing. In the following sections, a detailed discussion of the literature evolving around gold-coated magnetic nanoparticles and their importance in bio-sensing is presented.

1.1. Principles of magnetism:

The ancient Greeks especially those who lived near the province of Magnesia were the first humans started to notice the strange effect of some rare stones (loadstones) which could attract iron. Magnetism in practice is all about electrons, it is caused by the motion of electric charges. When a magnetic field (H) is applied to a material, magnetic induction (B) happens in which is the response of the material to the magnetic field. The relationship between H and B (equation 1.1) is an intrinsic property of the material.[10]

$$B = \mu_0(H + M) \qquad 1.1$$

Where μ_0 is the permeability of free space, and M (magnetization of medium) defines as magnetic moment per unit volume.

$$M = \frac{M}{V} \qquad 1.2$$

M depends on both the single magnetic moment of integral atoms, molecules, or ions and how these dipole moments interact with each other. Inside the medium magnetic induction (B) is the same as the magnetic flux density (φ), so within a material $B = \frac{\varphi}{A}$ by resemblance with $H = \frac{\varphi}{A}$ in free space.[11] Generally, the magnetic flux density outside of a material is different from inside of the material and by this notion, magnetic materials could be classified into different groups based on their differences in internal and external magnetic flux density (Figure 1.2). If the magnetic flux density inside the material is less than outside the material, it is called diamagnetic. Materials with a magnetic flux density inside slightly larger than outside are called either paramagnetic or antiferromagnetic.[12] The constituent's atoms or ions in many of these materials have a magnetic dipole moment. The difference is that in paramagnetic materials the dipoles are randomly oriented while in antiferromagnetic materials they are oriented antiparallel toward each other. In both cases, the overall magnetization is zero. Finally, ferromagnetic and ferrimagnetic materials have much higher flux densities inside than outside.[13]

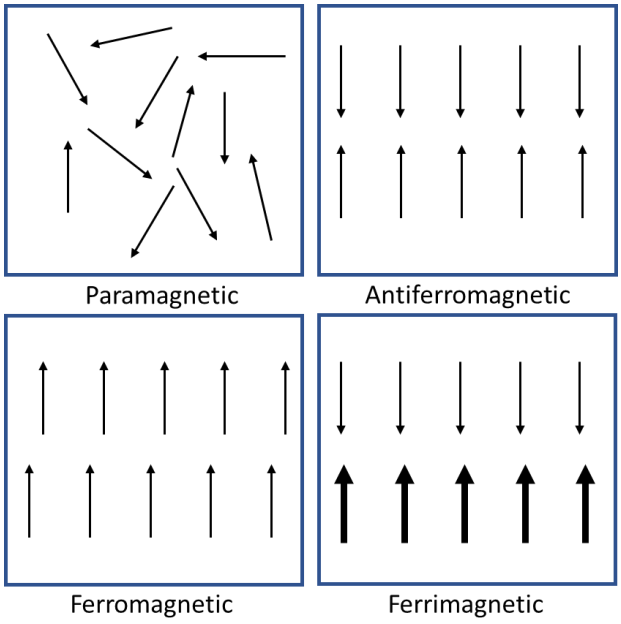

Figure 1.1. Types of magnetic materials according to their dipoles ordering.

In ferromagnetic materials the magnetic dipoles tend to line up in the same direction while ferrimagnetic materials have semi-similar behaviour like antiferromagnetic

materials (dipoles are oriented in antiparallel fashion), however, some dipole moments are larger than others, thus material having a net overall magnetic moment.[13]

Variation of each of the terms above with the respect to the external magnetic field could also affect the magnetic properties of a material. Susceptibility of a magnetic material is the ratio between M to H (equation 3) and could be defined as how quick to react material is toward an applied external magnetic field:

$$\mathrm{X} = \frac{M}{H} \qquad 1.3$$

Another important term is permeability, which is the ratio of B to H and indicates how permeable the material is toward the magnetic field (equation 4).

$$\mu = \frac{B}{H} \qquad 1.4$$

If a material concentrates high flux density inside it means that the permeability of the material is high too. The relationship between permeability and susceptibility of material could be defined in equation 5:

$$\frac{\mu}{\mu 0} = 1 + \mathrm{X} \qquad 1.5$$

Where the $\mu 0$ is the permeability in free space.[13]

1.1.1. Hysteresis loops

The plots of M or B vs H are called magnetization curves. These curves are characteristics of materials. The magnetization curves (M-H curve) of diamagnetic, paramagnetic, and antiferromagnetic materials are linear, which means a large magnetic field should be applied to any of these materials to achieve small magnetization, and after removal of the external magnetic field the magnetization is zero (Figure 1.3 A).[14]

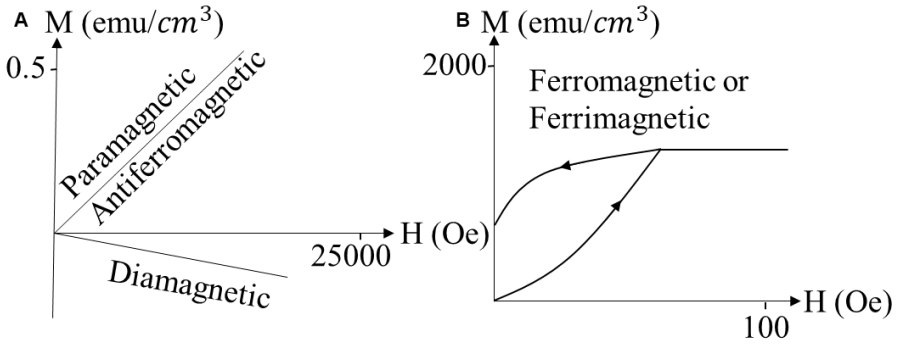

Figure 1.3. Schematic magnetization curves of A) paramagnetic, antiferromagnetic, and diamagnetic and B) ferromagnetic and ferrimagnetic materials.

As can be seen from Figure 1.3 A, the slope of the graph for diamagnetic materials are negative, thus the susceptibility is small and negative, and the permeability is slightly less than one. For paramagnets and antiferromagnets materials, the slope is positive, and the susceptibility and permeability are small and positive, and slightly greater than one.[14]

In the case of ferromagnetic and ferrimagnetic materials as it can be seen from Figure 1.3 B application of a small external magnetic field result in a large magnetization, and magnetization saturates after a certain point. Both permeability and susceptibility as a function of the external magnetic field are positive. Finally, and most importantly, as it can be seen from Figure 1.3 B, decreasing the external magnetic field to zero after the saturation point, does not result in zero magnetization. This phenomenon which has a huge effect on the technological application of magnetic materials is called hysteresis. If a magnetic material is placed inside an external magnetic field, the magnetic material is at first unmagnetized.[15] As the external magnetic field increases the magnetization increases to the point M_S (magnetization saturation) and from that point, it will be constant. When starting to reduce the magnetic field M starts to decrease too but as it can be seen from Figure 1.4 even after reducing the applied field to zero the magnetization does not reach zero (M_R). The M_R is called the remanence and define as the remaining magnetization of the material when the applied magnetic field is zero. The reversed magnetic field required to decrease the magnetization is called coercivity (H_C).[15]

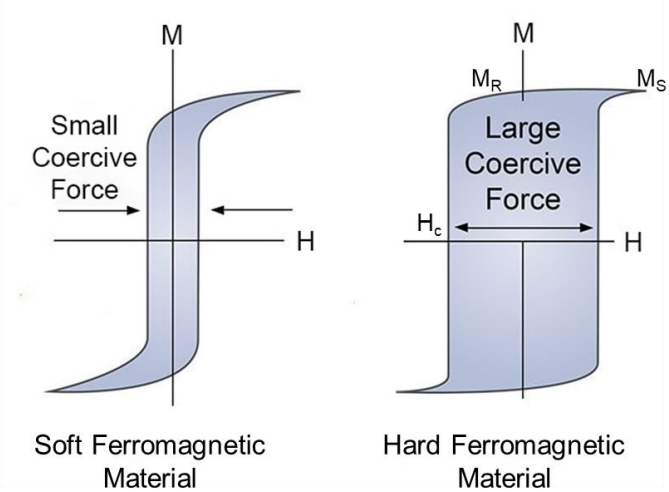

Figure 1.4. Schematic illustration of a typical hysteresis loop of soft and hard ferromagnetic materials.

Depending on the coercivity of a magnetic material, ferromagnetic materials could be categorized into hard and soft materials. Hard ferromagnets are those that need a high magnetic field to saturate magnetization and the demagnetization is not fast too. While soft ferromagnets are easy to saturate and demagnetized fast. Characteristics shown by hysteresis loops determines the suitability of ferrimagnetic and ferromagnetic materials for any application.[15]

1.1.2. Finite-size effect

So far, we have established some of the laws governing the behaviour of bulk magnetic materials. However, as the size of a material decreases, its magnetic properties are affected resulting in the behaviour deviating from the well-established laws. Two important phenomena namely the most interesting points of differentiation of properties of magnetic materials in nanoscale size compared to the bulk materials; these are single domain limit and superparamagnetic limit.[16] As it can be seen from Figure 1.5 the blue curve shows the size dependence of coercivity vs nanoparticles size. When the particle size approaches infinite (large) radius, the curve approaches an asymptotic limit which means that ferro-ferrimagnetic material is going to have a magnetic field even in the absence of an externally applied magnetic field. As the size of the particle starts to shrink down it is evident the coercivity is going up until it comes to a peak, because the particle is becoming a single domain.[16]

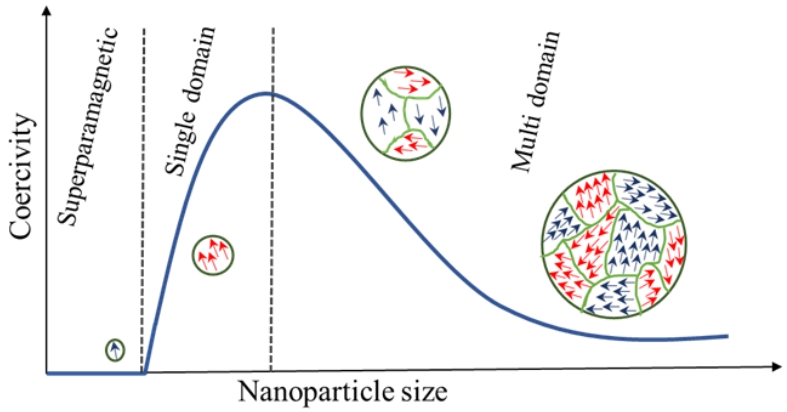

Figure 1.5. A schematic illustration of a coercivity-size graph of small magnetic materials.

If the nanoparticle size continues to shrink, the coercivity becomes zero and the particle makes the transition to becoming superparamagnetic. In large ferro-ferrimagnetic materials, the spins of unpaired electrons undergo spontaneous magnetization, where their energy is lowered by aligning with spins in neighbouring atoms.[16] To decrease the overall energy of the system, magnetic materials divide into magnetic domains in the absence of an external magnetic field. The boundaries (walls) between these domains can be moved by the application of a magnetic field, and it is the movement of these boundaries that causes the hysteresis curve of ferro-ferrimagnetic materials. Usually, if a particle is smaller than this characteristic domain size it will contain a single magnetic domain. More precisely: a particle remains as a single domain only if the required energy to create domain boundaries is greater than the reduction of energy that would be obtained by the resulting decrease in magnetic flux. [17]

When the size of a single domain magnetic particle falls below a critical threshold diameter, thermal energy allows the particles to freely reorient their spins so that no external energy needs to be applied to demagnetize the system in the absence of the externally applied magnetic field (zero coercivity). For superparamagnetic nanoparticles changing the direction of the spins can be achieved at relatively low fields, meaning that superparamagnetic nanoparticles can have very high initial susceptibilities while the external magnetic field required to fully align all spins, needs to be high, and as a result magnetization saturation is going to be high too.[18]

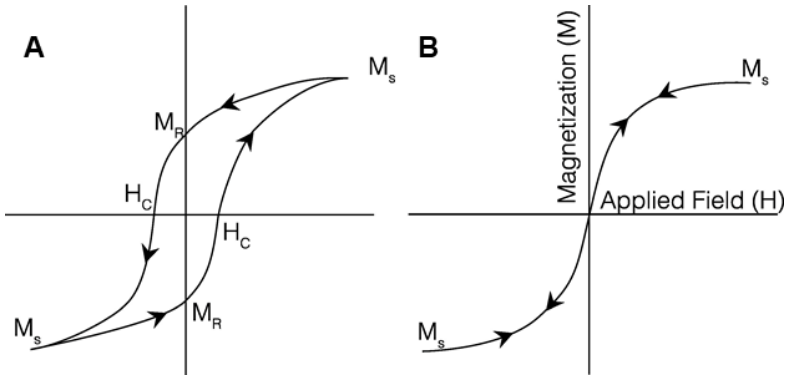

Figure 1.6. Hysteresis curves of A) ferro-ferrimagnetic materials and B) when the particles are in the superparamagnetic size range. Reprinted with permission from[19].Copyright (2021) American Chemical Society.

Figure 1.6 could help to better understand the differences between the magnetic behaviour of particles with different sizes (above and below the superparamagnetic region). As it can be seen from Figure 1.6 A, ferro-ferrimagnetic nanoparticles (≥30 nm) have rather large coercivity (H_C) and remanence (M_R) in their hysteresis curves which means even after removal of an external magnetic field they will remain magnetic and have a high tendency of attracting each other. This can lead to aggregation as nanoparticles have a high surface to volume ratio and they want to reduce their surface energy by becoming bigger.[10,15,20] In contrast, superparamagnetic nanoparticles (Figure 1.6 B) show neglectable coercivity and remanence which means after removal of the external magnetic field, the nanoparticles behave as if they are not magnetic and are not attract each other. Hence, nanoparticles are less prone to aggregation.[21,22]

1.2. Magnetic nanoparticles and biomedicine

The synthesis of magnetic nanoparticles is of scientific and technological interest due to the possibilities they can offer for a variety of medical applications. First, the position of magnetic nanoparticles could be controlled *via* the help of an external magnetic field.[23] Secondly, it is possible to control their size from a few nanometres to hundreds of nanometres, Which means that they are in the size range smaller or comparable to many biological entities such as cells, viruses, genes, or proteins. Thus, magnetic particles not only can get close to biological entities, but it is also possible to coat the

magnetic nanoparticles with biological units.[24] Third, their interaction with the external magnetic field could be used to transform energy from the outside source to the nanoparticle or influence the external magnetic field.[25] As the result of the physical properties of magnetic particles, applications such as biosensing, magnetic resonance imaging (MRI), magnetic particle imaging (MPI), hyperthermia, magnetic separation, drug delivery, etc has opened new opportunities in both diagnosis and treatments of diseases.[26,27]

1.2.1. Magnetic nanoparticles and composition

1.2.1.1. Iron oxides

Iron oxide magnetic nanoparticles are the most important and highly explored nanoparticles, due to the variety of synthesis methods, low toxicity, and stability.[28–33] There are four stable types of iron oxide nanoparticles (Figure 1.7): magnetite (Fe_3O_4), maghemite (γ-Fe_2O_3), hematite (α-Fe_2O_3) and wüstite (Fe_xO).[34] Magnetite is a ferromagnetic semiconductor with a cubic inverse spinel structure and the highest magnetization saturation (Ms=84 - 92 emu g^{-1}) amongst all the stable phases of iron oxide. Fe_2O_3 has four crystalline phases γ-Fe_2O_3, β-Fe_2O_3, ε-Fe_2O_3, and α-Fe_2O_3, of which only maghemite (γ-Fe_2O_3) and hematite (α-Fe_2O_3) are stable at room temperature.[35] Maghemite is a ferrimagnetic insulator material exhibiting a cubic structure and has a magnetization saturation (Ms) of 74 - 80 emu g^{-1}. While hematite is a weak ferromagnetic (Ms=0.1-0.4 emu g^{-1}) material at room temperature and, the most thermodynamically stable iron oxide phase. Finally, wüstite (Fe_xO, x= 0.84 - 0.95) is a nonmagnetic material (0 emu g^{-1} in bulk) with a NaCl-like crystal structure.[34]

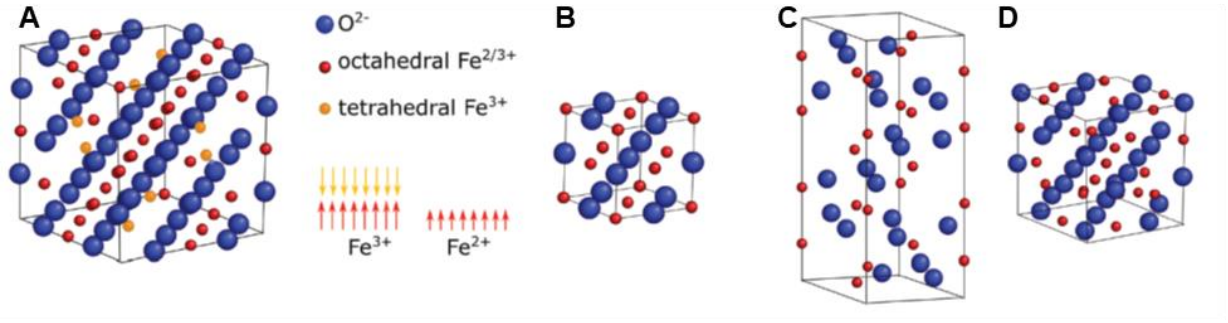

Figure 1.7. Crystal structure of iron oxides A) magnetite (Fe3O4) B) wüstite (FexO) C) hematite (α-Fe2O3) and D) maghemite (γ-Fe2O3). Reprinted with permission from[36].Copyright (2021) John Wiley and Sons.

Maghemite and magnetite nanoparticles are the most widely used magnetic nanoparticles in the realm of biosensing and biomedicine mostly due to their high magnetic saturation and biocompatibility.[34] Their high magnetic saturation is related to the crystal structure and the position of atoms in the octahedral and tetrahedral sites. As it can be seen from the crystal structure of magnetite, illustrated in Figure 1.7 A which shows a face-centred cubic lattice of oxygen ions packed with Fe^{3+} and Fe^{2+} cations in octahedral sites and Fe^{3+} in tetrahedral sites.[37] The number of tetrahedral sites is double the octahedral sites. Thus, the parallel alignment of magnetic spins in octahedral sites relative to the antiparallel alignment of spins in tetrahedral sites is not balanced and consequently, a strong attraction toward the external magnetic field is produced. Magnetite is superparamagnetic when its size is below 25 nm and remains a single domain up to the size of 80 nm.[23] Maghemite has a similar structure as magnetite, but the octahedral sites are packed with the Fe^{+3} cations and vacancies. Although the lower density of Fe cations reduces saturation magnetization of maghemite compared to magnetite, the chemical stability and low toxicity of maghemite in biological media makes it an interesting choice for bio-sensing.[38]

1.2.1.2. Iron nanoparticles

Bulk iron has the highest magnetization saturation (218 emu/g^{-1}) at 25$^{\circ}C$ amongst magnetic materials. So smaller zero-valent iron nanoparticles could achieve higher saturation magnetization compared to their counterpart iron oxide nanoparticles. Furthermore, iron is a very soft magnetic material and has a low magnetocrystalline anisotropy which makes it an interesting choice for biosensing and bio-imaging applications. To better understand the effectiveness of iron compared to other magnetic materials table 1.1 compares some of the most important magnetic properties of most common magnetic materials.[39–43]

Table 1.1. Properties of magnetic materials.

Element	M_s at 0 K	M_s at 293 K	T_c
Fe	222	218	1043
Co	162	161	1388
Ni	57	54	627

Although gadolinium has higher saturation magnetization at 0 K, its low Curie temperature (0 K) and acute side effects make it a poor candidate to use for a variety of bio-sensing applications.[44–47] In contrast, iron's Curie temperature is high enough to be of no concern for the majority of bio-sensing applications.[48] While properties such as high saturation magnetization, high Curie temperature, low magnetocrystalline anisotropy and low cytotoxicity make iron nanoparticles a good choice for bio-sensing and bio-imaging, the high reactivity, especially toward water and oxygen, and complicated and time-consuming synthesis routes hinder the widespread use of iron nanoparticles in such applications.[49–51]

Even though iron nanoparticles could oxidize rapidly and form other types of iron oxide nanoparticles. If iron nanoparticles were grown to a certain size or bigger, part of their zero valent-iron core could be saved and produce a core-shell nanoparticles compromise of zero-valent iron core and iron oxide shell.[43,52] It has been reported that iron nanoparticles with a size 8 nm or below, oxidize almost instantly when exposed to the air.[53] For bigger size iron nanoparticles, upon exposure to air, a 3-4 nm oxide shell will form on the surface of iron nanoparticles resulting in a core-shell nanoparticle. The synthesis of iron nanoparticles (above 8 nm) and different shapes have been reported in the literature using different precursors such as iron pentacarbonyl, iron oleate complex and iron amido complexes.[54–56] As most of these precursors are toxic and hard to handle Cheong *et al*, reported the synthesis and application of zero-valent iron core-iron oxide shell from an easy to handle and stable iron precursor [$Fe(C_5H_5)(C_6H_7)$] in the presence of oleylamine for biomedical application.[57,58] The highly crystalline zero-valent iron core-iron oxide shell were further coated with dimercaptosuccinic acid (DMSA) to make them water dispersible and shown that the particles are an effective choice as a T_2 contrast agent for MRI. Recently Gloag *et al*, reported that zero-valent iron core-iron oxide shell (≤15 nm) could be used as an effective magnetic particle imaging (MPI) agent.[59] The high magnetization saturation provided by the small zero-valent iron core-iron oxide shell nanoparticles enabled them to get a similar MPI signal in case of magnitude and resolution as twice as big of size state-of-the-art iron oxide nanoparticles.

1.2.2. Synthesis of magnetic nanoparticles

Several methods have been reported for the synthesis of magnetic nanoparticles. These methods can be grouped into two main categories: top-down and bottom-up approaches (Figure 1.8).[60]

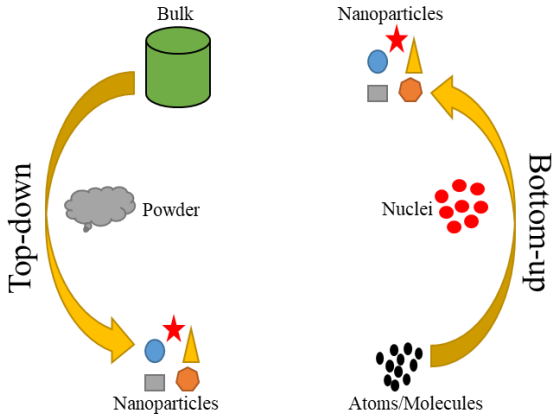

Figure 1.8. Bottom-up and the top-down approaches in the synthesis of magnetic nanoparticles.

Top-down synthesis methods involve the breaking down of the bulk material into nano-sized structures or particles. Amendola *et al* used a laser ablation synthesis in solution method to prepare FeO_x-MNPs compromise of 75% magnetite and 22% hematite. They further functionalized their particles with a variety of ligands such as carboxylated phosphonates, fluorescent alkylamines, fluorescent isothiocyanates and bovine serum albumin.[61] In another study Mignot *et al* used a top-down method to prepare ultra-small (≤5 nm) gadolinium-based silica nanoparticles. They have shown that the synthesized particles have low toxicity and also they are a good candidate for use as bio-sensing and MRI agents.[62]

Bottom-up refers to the development of material from the bottom: atom-by-atom, molecule-by-molecule, or cluster-by-cluster in a gas phase or solution.[63] Predominantly, the bottom-up approaches are favoured due to the possibility to gain smaller particles with better size distribution and better control over the shape of the particles.[64,65] The most common 'bottom-up' methods include coprecipitation reactions,[66] polyol methods,[67,68] microemulsion,[69] sol-gel syntheses,[70] thermal decompositions,[71] hydrothermal and high-temperature reactions,[72] sonochemical syntheses,[73] and flow injection synthesis.[74]

1.2.2.1. Coprecipitation

One of the oldest methods to make magnetic nanoparticles is the coprecipitation method.[75–77] The principle process behind this method for synthesis of magnetite nanoparticles (Fe_3O_4) is usually by mixing ferric and ferrous ions in a 1:2 M ratio at a basic solution (pH range 8–14) according to the following reaction:[78]

$$Fe^{+2} + 2Fe^{+3} + 8OH^- \rightarrow Fe_3O_4 + 4H_2O$$

By using different salts as precursors, changing reaction temperature and pH, the size and shape of magnetite nanoparticles can be adjusted. The main advantage of this method is the large-scale synthesis of the magnetic nanoparticles. In an example, Mascolo *et al* made magnetite nanoparticles in a wide pH range (10.0–13.0) at room temperature by co-precipitation.[66] Mascolo *et al* concluded that the size reduction of the magnetic nanoparticles are dependent on the pH and the rate to which the basic solution is added to the mixed solution of Fe^{2+} and Fe^{3+} ions.[66] In another example Petcharoen and Sirivat synthesized magnetite nanoparticles *via* co-precipitation using ammonium hydroxide as the precipitating agent.[79] Reaction temperature and surfactants were crucial to controlling the size of the magnetic nanoparticles.[79] One drawback of the chemical co-precipitation approach is the wide size distribution of nanoparticles made by this method, which made chemists to came up with new methods.

1.2.2.2. Hydrothermal and solvothermal synthesis

Other approaches to produce high-quality magnetic nanoparticles are the hydrothermal (solvent is aqueous) and solvothermal (solvent is not aqueous) methods. These methods rely on phase transformation and separation mechanisms at interfaces of liquid, solid, and solution during synthesis (Figure 1.9). Monodisperse noble metal, quantum dots, and magnetic nanoparticles can be obtained by reduction of metal ions through wet-chemical technologies of crystallizing substances in a sealed container (autoclave).

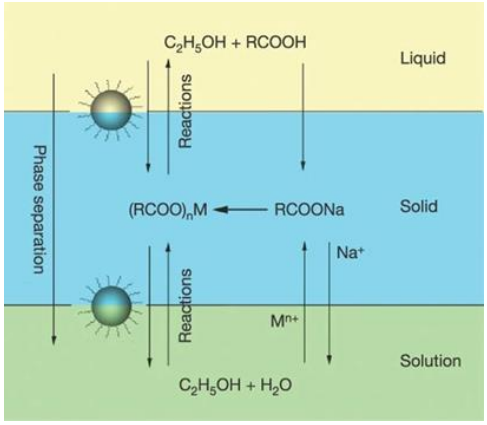

Figure 1.9. Scheme of liquid-solid-solution phase transfer for the synthesis of magnetic nanoparticles. Reprinted with permission from[80]*.Copyright (2021) Springer Nature.*

The high temperature and extreme pressure are the keys to the synthesis of the variety of nanoparticles with this method.[80] Ge *et al* synthesized magnetite nanoparticles with a size range from 15 nm to 31 nm by oxidation of $FeCl_2 \cdot 4H_2O$ in basic aqueous solution at 134°C and extreme pressure.[81] Nanoparticles were highly crystalline with a size range from 15 nm to 31 nm. Although this method can make highly crystalline nanoparticles on large scale, the high cost of autoclaves could be of concern.

1.2.2.3. Thermal decomposition

Thermal decomposition of organometallic compounds in high-boiling organic solvents containing surfactants leads to monodisperse magnetic nanoparticles.[82] Existence of hydrophobic surfactant and high temperature allows perfect control over nucleation and growth of the nanoparticles which results in monodisperse magnetic nanoparticles.[83,84]

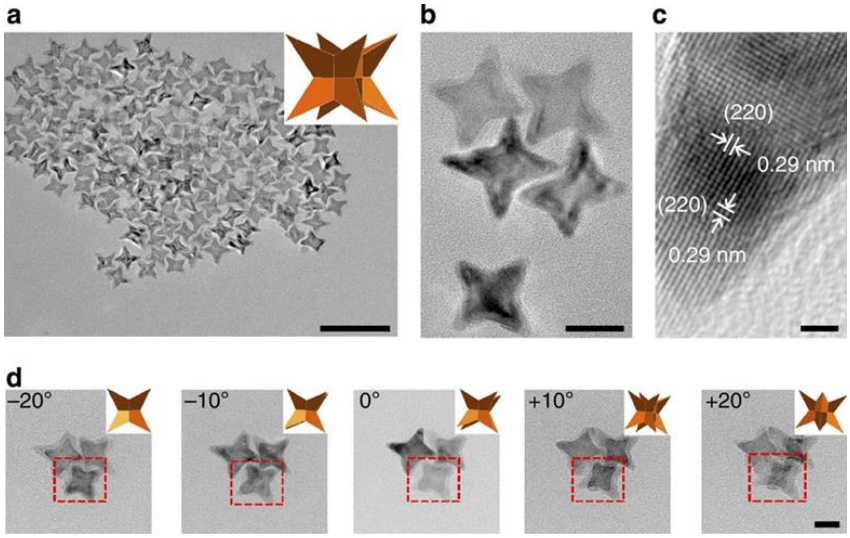

Figure 1.10. TEM image of Octapod-shaped magnetic nanoparticles inset shows geometric cartoon. Scale bar, 100 nm. (b) HRTEM image of Octapod-magnetic nanoparticle. Scale bar, 20 nm. (c) HRTEM image of Octapod-magnetic nanoparticles, proving that the nanoparticles are magnetite. Scale bar, 2 nm. (d) Tilted TEM images of three Octapod-magnetic nanoparticles. insets show corresponding geometric cartoon. Scale bar, 20 nm. Reprinted with permission from[85]*.Copyright (2021) Springer Nature.*

Kemp *et al* made magnetite nanoparticles *via* a two-step thermal decomposition method.[86] By using Iron oleate as a precursor they first made wüstite in presence of oleic acid and 1-octadecene at 324°C. The wüstite nanoparticles were then oxidized in presence of 1% oxygen in argon gas for 3 hours to synthesize magnetite nanoparticles.[86] The nanoparticles' size (15 nm-30 nm) were controlled by varying the oleic acid ratio to the precursor. The magnetite nanoparticles showed nearly perfect magnetizations saturation of 80 emu g^{-1}.[86] In another study, Zhao *et al* used the thermal decomposition method and synthesized highly crystalized octapod magnetite nanoparticles.[85] Iron oleate was decomposed at 320°C in presence of the sodium chloride and oleic acid to form the octapod nanoparticles.[85] As can be seen from Figure 1.10 the nanoparticles consist of 4-armed star liked magnetite nanoparticles. The unique shape of the magnetic nanoparticles made here allowed for ultrahigh transverse relaxivity of (679.3 ± 30mM^{-1} s^{-1}) and proved to be a perfect T_2 contrast agent for MRI.[85]

Thermal decomposition was used as the main route for the synthesis of magnetic nanoparticles in this thesis. The good control over shape, size and monodispersity this

method possesses along with the relatively facile synthesis protocols available were the main reasons we choose this method.

Although other methods are available for the synthesis of the magnetic nanoparticles such as microemulsion and sonochemical synthesis, they are not as prevalent and easy to use as the main three methods discussed here.[87]

1.2.3. Protection and surface functionalization of magnetic nanoparticles for nanomedicine

As it was discussed in the previous section, thermal decomposition of the organometallic compounds in boiling organic solvents produces highly monodisperse magnetic nanoparticles with good shape and magnetic properties. However, these magnetic nanoparticles are not stable in physiological conditions, and their surface must be coated with other elements and molecules to prevent aggregation.[23] Furthermore, by coating the magnetic nanoparticles we can add active chemical groups and also other properties to the magnetic nanoparticles.[24] A variety of coatings such as polymers or sugar molecules, silica and noble metals have been used for coating the magnetic nanoparticles for different applications.[88] In the following the most important ones are discussed.

1.2.3.1. Silica coating

Silica is one of the best surface coatings for magnetic nanoparticles.[89–91] Several reasons are behind the popular use of silica as a surface coating for magnetic nanoparticles. These include providing high stability especially in aqueous media, chemical inertness, the ability to easily control the thickness of the coating layer and porosity and finally, a well-established coating process.[92,93] Stöber and microemulsion are the two general methods for generating a silica layer on the surface of magnetic nanoparticles.[94–96]

Lu *et al* have used a water-dispersible ferrofluid (EMG 340) containing maghemite and magnetite nanoparticles with a size range of 5-15 nm. Hydrolysis of the sol-gel precursor tetraethyl orthosilicate (TEOS) on the surface of the magnetic nanoparticles and further condensation produced the silica shell.[97] Silica shell thickness could be changed between 2-100 nm by simply varying the concentration of TEOS.[97] In another

study Zhang *et al* used a reverse microemulsion method to form an ultra-thin (2 nm) silica shell around magnetite nanoparticles.[98] The interaction between Igepal CO 520 hydrophobic tail with the oleic acid capped magnetite nanoparticles was the key to achieve silica-coated magnetic nanoparticles in the microemulsion system. By adjusting the concentration of the reagents they have managed to change the size of the overall nanoparticles.[98] Due to easy modification of the silica with amine terminal groups, these nanoparticles could readily be used for DNA separation, hybridization and biosensing.[99,100] Moreover silica is a great intermediate layer for further coating of the magnetic nanoparticles with other metallic substances specially for the formation of gold shell around magnetic nanoparticles. A detailed discussion of the importance of silica as an intermediate layer for gold coating will be provided in the later sections.

1.2.3.2. Noble metal coating

Silver and gold are the two most important noble metal coatings for magnetic nanoparticles. They convey several key features to the magnetic nanoparticles such as plasmonic property, conductivity, ease of modification with biomolecules, stability and inertness.[101–103] The potent antiviral and antimicrobial activity of silver, and its SERS applicability, combined with the magnetism of iron oxide nanoparticles have been used for the detection of molecules and also fight against antibacterial resistance.[104,105] Song *et al* synthesized a hybrid nanostructure of Fe_3O_4@SiO_2@Ag nanoparticles through mild reduction of the $AgNO_3$ by formaldehyde on the gold-seeded silica-coated magnetite nanoparticles. The silver-coated magnetic nanoparticles were used to detect malachite green (MG) in water samples.[106] In another study Mahmoudi and Serpooshan synthesized newly designed nanoparticles compromising a magnetic core that was separated from its silver shell by a ligand gap. The silver-coated magnetic nanoparticles were shown to enhance the antimicrobial activity of silver while being able to penetrate within the bacterial biofilm due to the magnetic properties of magnetite cores.[107]

Despite the advantages of silver as a coating for magnetic nanoparticles. Lethal and sublethal hazards silver poses on biological entities such as human cells made the scientific community focus on gold as a safer and better alternative.[108–110]

Gold-coated magnetic nanoparticles capable of providing both plasmonic and magnetic properties have created new avenues in nanomedicine research and developments. The inherent magnetic capability of iron oxide', combine with gold's inert nature, conductivity, plasmonic properties and high affinity toward both amine (-NH_2) and thiol (-SH) terminal groups, leads to a multifunction nanostructure ideal for both medical diagnosis and therapy. Furthermore, the ability to tune and change the properties of gold-coated magnetic nanoparticles by changing size, shape, surface charge, surface modification and tailoring them specifically for the intended application broadens the possible application of magnetic nanoparticles.[111] In the following sections, we will discuss some of the potential advantages' gold-coated magnetic nanoparticles will provide for bio-sensing.

1.3. Significance of gold for bio-sensing

1.3.1. Plasmonic properties

Localize surface plasmon resonance (LSPR) is a physical phenomenon that occurs at the nanometer-scale when a noble metal such as gold is being illuminated by a light source with a wavelength much bigger than the size of the nanoparticle. As it can be seen from Figure 1.11 the illumination will lead to a collective oscillation of conduction band electrons which results in sharp spectral absorption and scattering peaks.[112–114] This property of gold displays itself by the colour change of gold nanoparticles. The LSPR peak wavelength is directly dependent on size, shape, dielectric properties of the surrounding environment and the distance of nanoparticles from each other.[115] Bio-sensors based on the plasmonic nanoparticles take advantage of the change in the peak position and colour difference to detect a variety of bio-molecules and bio-chemicals on the surface of the nanoparticles.[116–120]

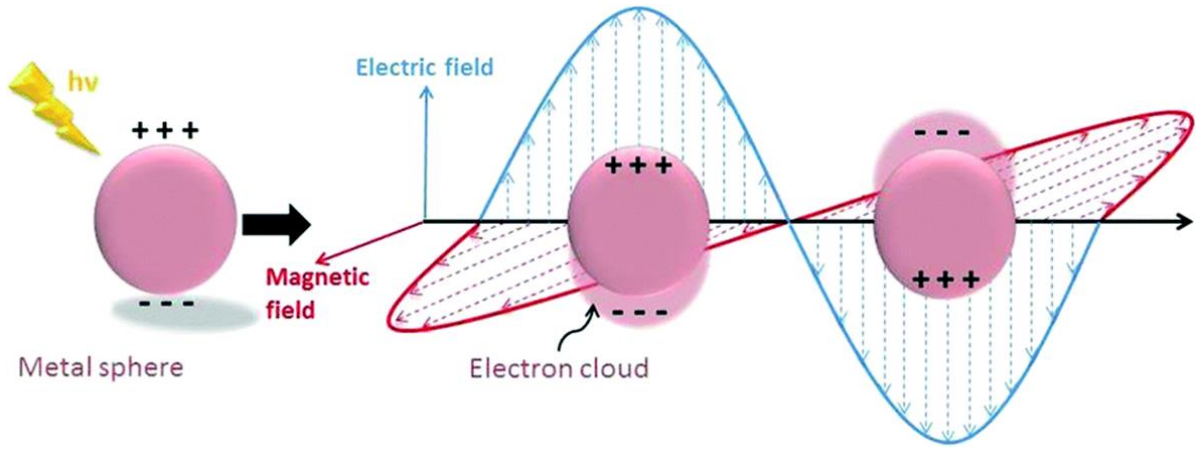

Figure 1.11. Schematic demonstration of localized surface plasmon resonance phenomena. Reproduced from[121] *with permission from the Royal Society of Chemistry.*

Introducing a complete gold shell on the surface of magnetic nanoparticles provides the particle with optical and electrochemical properties on top of magnetic properties. The optical properties of the core-shell magneto-plasmonic nanoparticles are dependent on the size and shape of the magnetic core, shell thickness and configuration and also the dielectric role of the core and shell.[122,123] Levin *et al* reported that by increasing or decreasing the thickness (Figure 1.12) of the gold layer on the surface magnetic nanoparticles position of the plasmonic peak could be shifted.[124] The study concluded that by increasing the gold shell thickness, plasmonic redshift occurs, which is due to the large dielectric permittivity of the core. Furthermore, investigating the effect of magnetic core shapes, it was concluded that the nanoparticles with cubic and concave cubic cores are slightly red shifted compared to the spherical particles. It was argued that the differences in optical properties of particles are originated from the lower symmetry in the case of cubic and concave cubic cores compare to the more symmetric spherical core.[124]

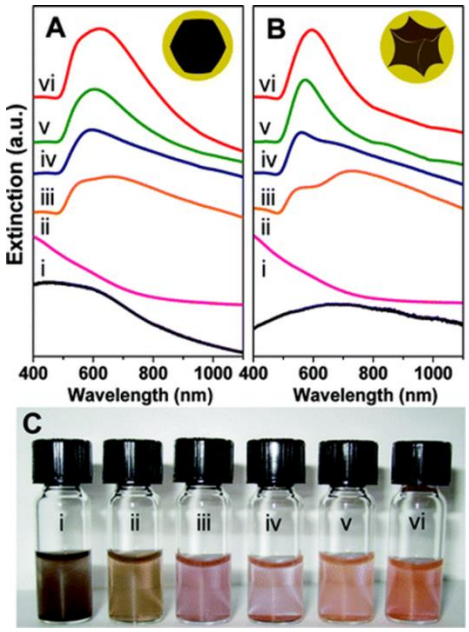

Figure 1.12. Nanoparticles solution extinction measurements of (A) faceted (B) and gold-coated magnetic nanoparticles (i) when cores are not coated (r1 31.5 ± 9.7 and 28.5 ± 7.3 nm), (ii) gold decorated nanoparticles (r1 32.6 ± 9.0 and 28.6 ± 8.5 nm) in aqueous solution, and (iii–vi) gold-coated nanoparticles with gold shell increasing of particles sized is 100, r2 is 59.9 ± 12.4, 65.0 ± 19.9, 73.1 ± 11.7, and 76.6 ± 9.8 nm for the faceted cores and 40.0 ± 6.7, 49.1 ± 10.7, 53.8 ± 4.6, and 66.4 ± 5.0 nm for the tetra cubic cores in aqueous solution. (C) picture of nanoparticles in solution A. Reprinted with permission from[124].Copyright (2021) American Chemical Society.

In another study conducted by Chaffin *et al*, based on Mie theory, the plasmonic properties of the gold-coated magnetite nanoparticles, gold-coated silica nanoparticles, gold-coated cobalt nanoparticles was calculated and further compared them with hollow gold nanoparticles and also similar size gold nanoparticles (Figure 1.13).[125] The overall size of the nanoparticles were assumed to be 50 nm with a 5 nm gold shell. Based on their model, gold-coated magnetite nanoparticles have redshifted the most, compared with the other nanoparticles explored, with an intensity comparable to the similar size gold nanoparticle. Interestingly, the gold-coated cobalt nanoparticles showed a very small peak which could be attributed to the dielectric properties of the core material. In contrast, the intensity of the LSPR peak for gold-coated silica nanoparticles and the hollow-core gold shell was much larger than the solid gold nanoparticles and gold-coated magnetic nanoparticles.[125] The definition of the reflective index of materials

which simply says how fast light can go through a material could help explain this phenomenon.[126] The fact that iron oxide nanoparticles (magnetite) are a non-transparent material and their refractive index is complex. While silica is a transparent material that does not absorb light and as a result has only a real refractive index. The plasmonic peak position is determined by the real component of the refractive index and its intensity is directly related to the imaginary part of the refractive index.[125,127,128] This is why the position and intensity of the plasmonic peaks of the similar size shell size were so different.

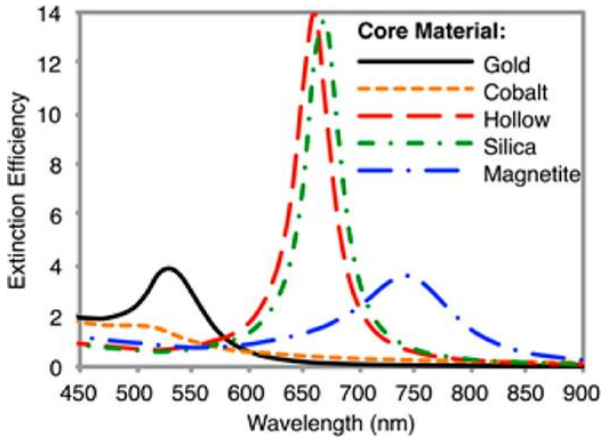

Figure 1.13. Calculated extinction spectrum of the gold-coated magnetite nanoparticles in comparison with other core-shell nanoparticles with the same diameter (Dtotal=50 nm, gold shell thickness 5 nm). Reprinted with permission from[125].Copyright (2021) American Chemical Society.

As it has been previously reported, optical properties of the anisotropic nanoparticles are greatly enhanced especially on the tips compared to simple nanoparticles due to their high curvature structure.[129] To better understand the effect of the shape of the nanoparticles on optical properties of the gold-coated magnetic nanoparticles Kwizera *et al*, synthesized three different shapes of gold-coated magnetic nanoparticles.[130] Sphere, popcorn and star-shaped core-shell gold-coated iron oxide magnetic nanoparticles with different shell thicknesses were synthesized. Figure 1.14. A show that a redshift from 538 nm to 575 nm occurs when the thickness of the gold shell and as the result the size of the nanoparticles increases from 77 nm to 140 nm. The redshift

of the particles regardless of the continuous gold shell thickening was attributed to the fact that the gold shell for all of the particles was bigger than 14 nm.[130]

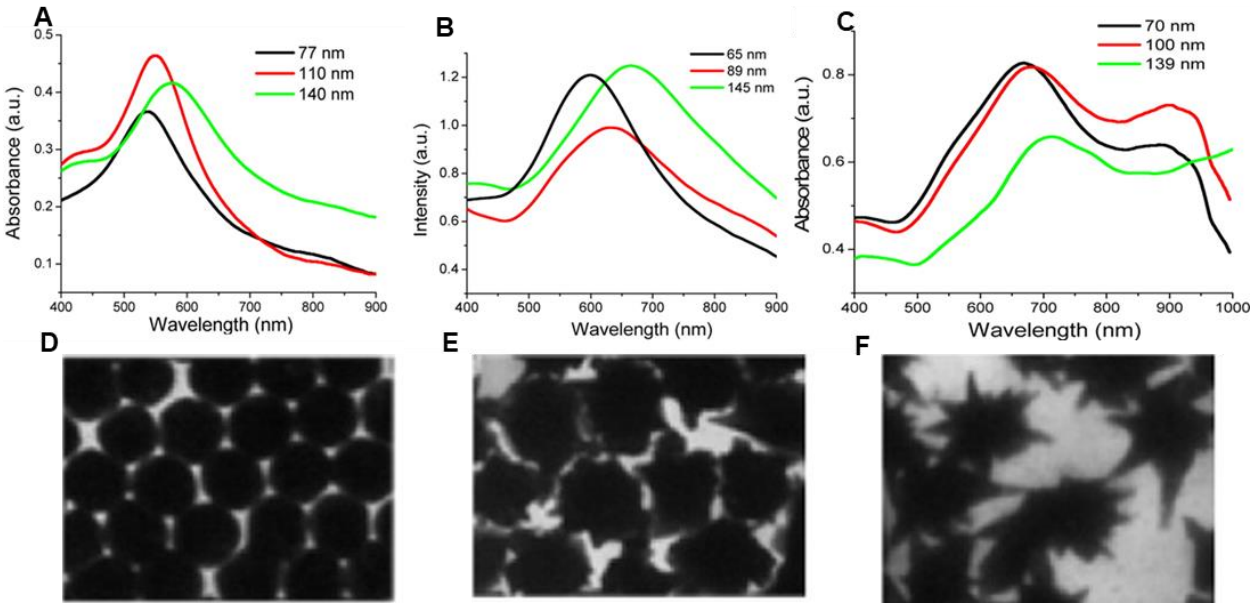

Figure 1.14. Top absorption spectra of the gold-coated iron oxide nanoparticles with different shapes A) core-shell nanospheres B) core-shell nano popcorn and C) core-shell nanostars. Bottom TEM images of the D) nanosphere E) nano popcorn F) nanostars. The sizes labelled in the graphs are the base size of the particles that do not include the protrusions in popcorns and tips in the stars. Reprinted with permission from[130].Copyright (2021) American Chemical Society.

UV-Vis spectra for the gold-coated magnetic nanoparticles with a popcorn shape is depicted in Figure 1.14 B. The LSPR peak positioned at 600, 633, and 665 nm could be observed from particles with the size of 65 nm, 89 nm, and 145 nm. Similar to the spherical gold-coated magnetic nanoparticles with an increase in size the position of the peaks moves to a higher wavelength. Due to the anisotropic shape of the gold shell, the shift is toward a longer wavelength and the peak is broader. Different from both gold shells with nanospheres and nano popcorn shapes, gold-coated magnetic nanoparticles with nano star shapes show three well-defined peaks (Figure 1.14 C). A weak peak at around 550 nm and two strong peaks at 700 nm and 850 nm. While the weak peak at the visible region seems to be insensitive to size increase the other two strong peaks redshifted. The fact that the nanoparticles with star shape have the elongated tip

morphology compared to the other two types of particles explains the bigger redshift of the nanostars shaped gold-coated magnetic nanoparticles.[130]

As was discussed above the LSPR properties of the gold-coated magnetic nanoparticles could be tuned by changing the size, shape and even changing the core material. Due to these properties, the optical addressability of the gold-coated magnetic nanoparticles could be exploited for a variety of biosensing applications using techniques such as surface-enhanced Raman scattering (SERS) and dark-field microscopy.

1.3.2. Conductivity

Unlike magnetic nanoparticles, such as magnetite or maghemite, gold is a conductive element. Introducing a gold shell on the surface of a magnetic nanoparticle provides practical means for electrochemical bio-sensing. Gold-coated magnetic nanoparticles have been used as electrochemical biosensors in two main ways. First, to aid the construction of the sensing interface by immobilizing the gold-coated magnetic nanoparticles on the electrode with the help of the external magnetic field.[131–133] Second, as ‘’dispersible electrodes’’ where the gold-coated magnetic nanoparticles are dispersed in the solution containing the analyte that needed to be detected (Figure 1.15). The gold-coated magnetic nanoparticles then can bind to the desired analyte and accumulated on the sensing interface *via* a magnet to produce a signal even at an ultra-low concentration of the analyte.[134–136]

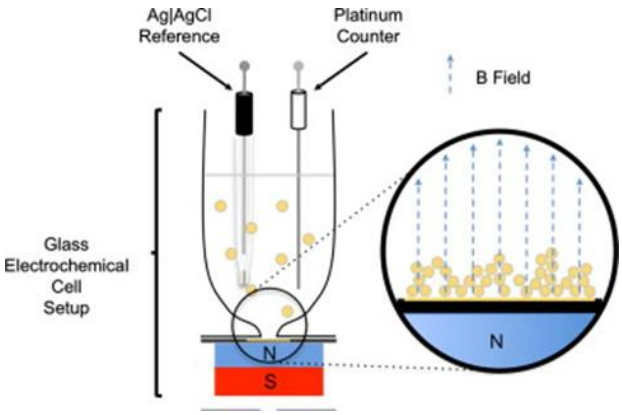

Figure 1.15. A schematic of the accumulation of gold-coated magnetic nanoparticles onto the surface of a gold working electrode in a magnetic field. Reprinted with permission from[135]. Copyright (2021) Elsevier B.V.

For gold-coated magnetic nanoparticles to be used as dispersible electrodes three main features (1) fast magnetic response to an external magnetic field, (2) well-defined electrochemistry and (3) uniform size and shape.[136,137] In a study conducted by Moraes Silva *et al*, four different types of gold-coated magnetic nanoparticles Goon *et al*,[138] Freitas *et al,*[139] Jin *et al,*[140] and cubic-Au@MNPs (Figure 1.16) were synthesized and their efficiency as disposable electrodes was investigated.[141] It was concluded that the cubic-Au@MNPs can fulfil all the requirements necessary for dispersible electrode applications. They were attracted to the external magnetic field in less than twenty seconds, had a well-defined shape and most importantly a stable electrochemical behaviour in acidic media. It is worth mentioning that although the gold-coated magnetic nanoparticles produced by the Goon *et al* method and cubic-Au@MNPs have slightly higher heterogeneous electron transfer rate constants (k^0) which could be crucial for the electrochemical bio-sensing applicability of these particles compared to the other two types.[141]

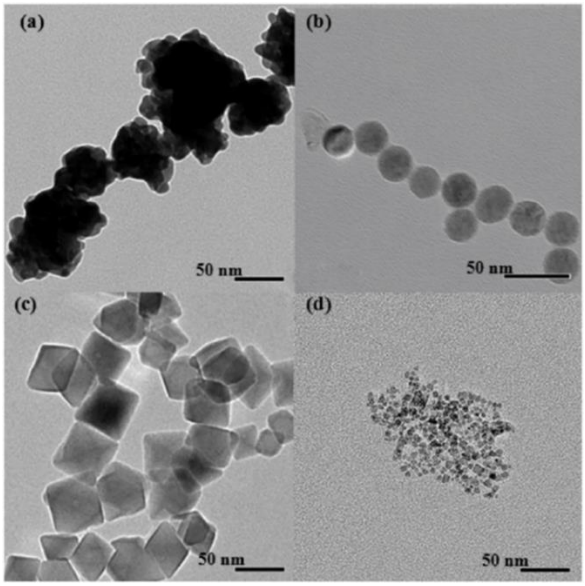

Figure 1.16. TEM images of multiple synthesis methods used for making the gold-coated magnetic nanoparticles(a) based on a method reported by Goon et al[138], (b) based on method reported by Jin et al[140],(c) a combination of method a and b, and (d) based on a method reported by Freitas et al[139]. Reprinted with permission from[141].Copyright (2021) John Wiley and Sons.

Electrochemical biosensors based on gold-coated magnetic nanoparticles and especially ‘’dispersible electrodes’’ despite their potential in bio-sensing are still in their infancy phase and many aspects of the method still need to be explored. The effectiveness of the dispersible electrodes’ is heavily reliant on the quality of the gold-coated magnetic nanoparticles. Thus, exploring new synthesis strategies to produce gold-coated magnetic nanoparticles that are more robust and more reliable is of the highest importance for further expansion of this technique and its final transition from lab to clinics and real-life applications.

1.3.3. Surface chemistry and protection

The development of biosensors at the nanoscale level is highly dependent on the immobilization of various bio-recognition elements, such as nucleic acids, enzymes and antibodies on the surface of the nanoparticles, enabling the selective targeting of biomarkers.[142,143] The surface of the magnetic nanoparticles is not normally compatible with regular surface chemistries used for modification of the biological entities. The growth of a gold layer on the magnetic nanoparticles not only protects the magnetic nanoparticles against corrosion and degradation in biological media due to the inertness of gold but enables the scientist to conjugate the nanoparticles with a variety of functional groups.[111]

The surface of gold can be modified with different groups such as proteins, DNA, saturated fatty acids and low molecular weight ligands.[144] There are two general approaches for the modification of the gold’s surface with functional groups, non-covalent and covalent methods.[145] These two broad categories could be divided into multiple methods such as amine modifications, carboxyl modifications, electrostatic interactions, thiol modifications, biotin-streptavidin system, and metal-mediated non-covalent conjugation, available for the modification of biomolecules (proteins, peptides, carbohydrates, polymers, DNA).[145,146]

One of the easiest ways to functionalize the surface of the gold shell with for example antibodies is a modification by non-specific absorption of gold-coated magnetic nanoparticles with an antibody. By controlling elements such as pH and taking advantage of the intermolecular forces (e.g. van der Waals and ionic force) gold-coated

magnetic nanoparticles could be modified with antibodies or other biological molecules.[145,147] The other prominent method of conjugation of gold surfaces is covalent conjugation. This method is more directional and controlled compared to the non-covalent methods.[148] For example gold-coated magnetic nanoparticles modified with carboxyl groups through thiol chemistry on their surface could be conjugated with antibodies *via* 1-ethyl-3-(3-di-methylaminopropyl)carbodiimide/*N*-hydroxysuccinimide (EDC/NHS) (EDC-NHS) conjugation chemistry.[149] In the EDC/NHS reaction, EDC is used to activate the carboxyl group on the surface of gold to create an active intermediate susceptible to nucleophilic attack. The resulting intermediate can bind to primary amines on the antibody but is unstable. The NHS is added to create a more stable amine-reactive intermediate, which will bind to the primary amines on the antibody and result in full conjugation.[145,147,148]

1.4. Applications of gold-coated magnetic nanoparticles in bio-sensing

As was discussed in sections 1.3.1 and 1.3.2, gold-coated magnetic nanoparticles could be used as agents for optical and electrochemical biosensors. In the following, the effectiveness of these nanostructures for bio-sensing will be demonstrated through several examples from the literature.

1.4.1. Optical sensors

The plasmon resonance property of the gold-coated magnetic nanoparticles could be exploited for developing optical bio-sensors.[119] The bio-sensors based on the LSPR property have gained attention due to two main reasons: high selectivity and extreme sensitivity.[116] For example, Markhali *et al* introduced a sensing system based on the colour change of gold nanoparticles for detection of interleukin 6 (IL-6). The core idea for this system was that the colour of the gold nanoparticles changes once in close contact with a smaller gold nanoparticle (core-satellite formation) under dark-field microscopy.[120] In another study Sriram *et al* developed a system that could evaluate λ_{max} of thousands of plasmonic nanoparticles in few seconds.[118] Addition of magnetic

property to a plasmonic property of gold could enhance the viability of these types of bio-sensors.

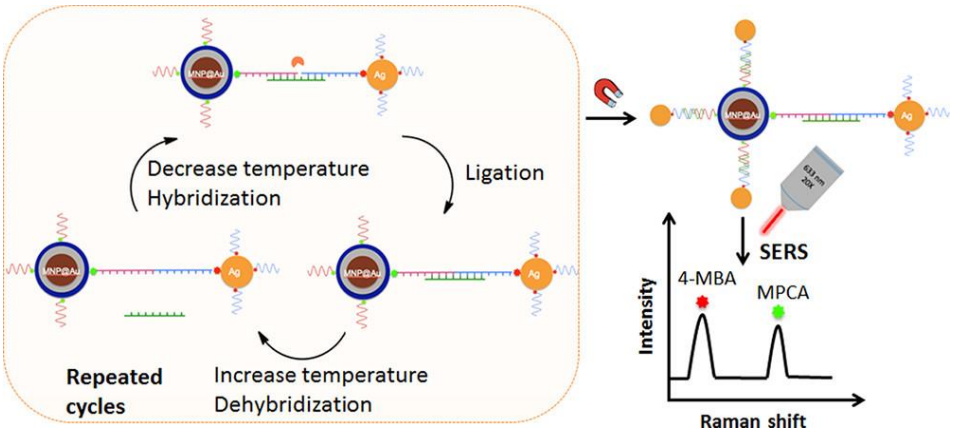

Figure 1.17. Schematic illustration of the Separation and Detection method by Using gold-coated magnetic nanoparticles and silver Nanoparticles through Ligation. Reprinted with permission from [150]*.Copyright (2021) American Chemical Society.*

Gold-coated magnetic nanoparticles have been used to detect a variety of biomolecules *via* the SERS platform. In a study conducted by Wang *et al,* synthesized gold-coated magnetic nanoparticles were modified with *Staphylococcus aureus* (*S. aureus*) antibody. Gold nanorods were also tagged *via* Raman active molecule 5,5-dithiobis (2-nitrobenzoic acid) (DTNB). By formation of a sandwich assay of SERS tags, target molecule and gold-coated magnetic nanoparticles they have managed to detect the *S. aureus* bacteria with a detection limit of 10 cells / mL.[151] The magnetism of the gold-coated magnetic nanoparticles helped to concentrate the nanoparticles several times throughout this study while the rough gold surface was used to produce the SERS signal in this study.[151] In another study Yu *et al* used gold-coated magnetic nanoparticles modified with 6-mercaptopyridine-3-carboxylic acid (MPCA) and silver nanoparticles tagged with 4-mercaptobenzonic acid (4-MBA). The nanoparticles were conjugated with a DNA probe in order to capture and detect single-stranded DNA containing the BRAF V600E mutation.[150] As it can be seen from Figure 1.17 gold-coated magnetic nanoparticles and silver nanoparticles were linked by ligation and separated from the solution by a magnet. They managed to detect the target analyte with extremely high sensitivity and specificity.[150]

1.4.2. Electrochemical sensors

As was discussed in section 1.3.2, the growth of a gold layer confers further electrochemical properties to the magnetic nanoparticles. The conductivity of gold and magnetism of magnetic nanoparticles could be used to design electrochemical biosensors.

Gold-coated magnetic nanoparticles have been used in a variety of ways as electrochemical biosensors. For instance, the nanoparticles could be used to construct the electrochemical sensing interface because of the magnetism. Xin *et al* used horseradish peroxidase (HRP) modified gold-coated magnetic nanoparticles to make a sensor to detect hydrogen peroxide.[132] To make the electrode (sensing interface) gold-coated magnetic nanoparticles were attracted to the graphene sheets (GS)–Nafion film modified screen-printed carbon electrode (SPCE) by a magnetic field. Using CV and impedance (EIS) they have managed to detect hydrogen peroxide with a detection limit of 12 Mm.[132] In another study Rawal *et al* fabricated an electrochemical sensor for the detection of sulfite based on gold-coated magnetic nanoparticles. By electrodeposition of the gold-coated magnetic nanoparticles onto a gold electrode by EDC-NHS process sensing interface was fabricated.[152]

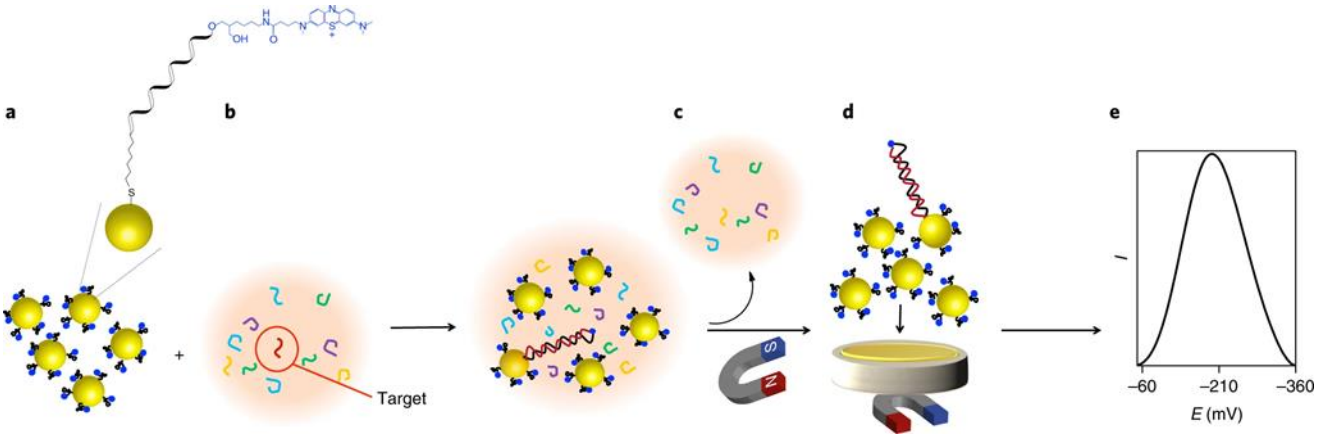

Figure 1.18. Schematic of the sensing strategy using gold-coated magnetic nanoparticles to detect microRNA, a,b, gold-coated magnetic nanoparticles modified with probe DNA complementary to target miRNA (a) are mixed in the blood for 30 minutes (b). c magnetic separation of the gold-coated magnetic nanoparticles from unhybridized sequences. d, gold-coated magnetic nanoparticles both hybridized and unhybridized deposited on the gold electrode. e, Electrical reconfiguration of gold-coated magnetic nanoparticles in their

heterogeneous network (hybridized and unhybridized) occurs by applying 10 cycles of square-wave voltammetry in the potential range between 200 and − 500 mV. Reprinted with permission from[153]. Copyright (2021) Springer nature.

One major challenge in ultrasensitive bio-sensing is the diffusion of the target analyte to the sensing interface. This means although the sensor can detect the analytes in very low concentrations, the time span for the analyte to reach the sensing interface is too long. To address that gap the dispersible electrode was introduced for ultra-sensitive detection of analytes in a timely manner.[136] Gold-coated magnetic nanoparticles in this method are actively participating in the selection of the target analyte and also directing them to the sensing platform.[137] In a study conducted by Tavallaie *et al*, using gold-coated magnetic nanoparticles conjugated by probe DNA, microRNA was detected directly in whole blood.[153] Figure 1.18 depicts the sensing platform in the study, as it can be seen the gold-coated magnetic nanoparticles modified with the methylene-blue-labelled probe DNA were mixed in the whole blood. The nanoparticles modified with probe DNA complementary to target miRNA in the blood could actively capture the target and then could be attracted to the sensing interface *via* magnetic force.[153] This work was shown for the first time it is possible to detect microRNA concentrations of from 10 aM to 1 nM in whole blood.[153] In another study Chen *et al* reported the detection of circulating DNA in whole blood with an ultralow detection limit of 3.3 aM. The sensing system was based on hybridization on a network of gold-coated magnetic modified with probe DNA.[154]

1.5. Gold coating processes

The growth of a gold nanoshell on the magnetic nanoparticles could be achieved *via* two general methods (Figure 1.19). First, the formation of the gold shell directly on the surface of the magnetic nanoparticles. The second introduction of an intermediate layer on the surface of the magnetic nanoparticles and then the growth of gold nanoshell (indirect) on the surface of the intermediate layer. The intermediate layer in the indirect gold coating process act as a glue, making the surface more favourable for the gold to be deposited on.[111]

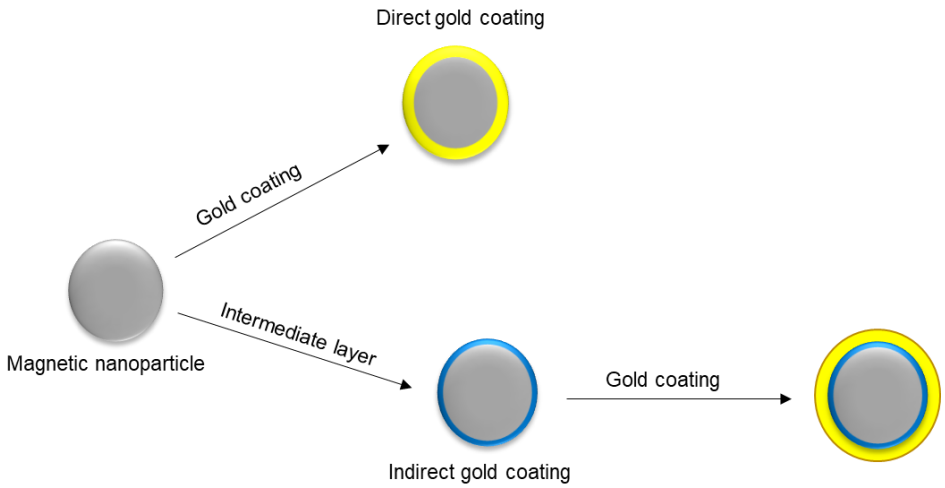

Figure 1.19. Schematic illustration of the two main routes for gold coating. Redrawn with modification from[111].

In the following sections, both methods are discussed in detail and several examples from the literature.

1.5.1. Direct gold coating

To grow a secondary metal on top of seed nanoparticles several factors such as crystallinity of the seed nanoparticles, surfactants in use, lattice mismatch etc should be considered.[155] Most importantly the lattice mismatch between the seed and secondary metal could play a huge role in the successful growth of the secondary metal on top of the substrate nanoparticles.[156] There are three (Figure 1.20) well-established growth modes for the deposition of a second metal in this case gold on a substrate (magnetite, maghemite etc): the island growth mode (Volmer-Weber, VW), island-on-performed layer mode (Stranski−Krastanov, SK) and finally the layer-by-layer growth (Frank−van der Merwe, FM).

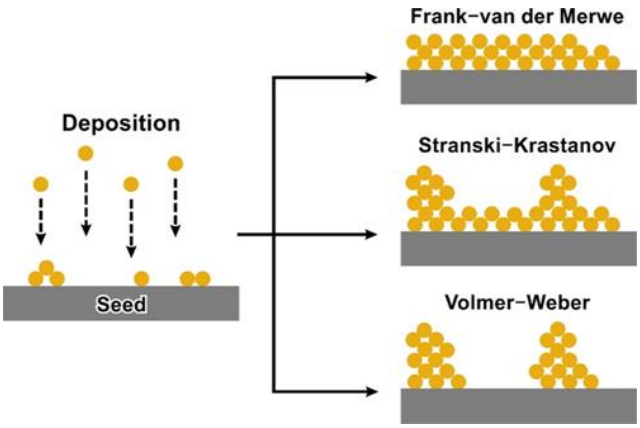

Figure 1.20. Schematic illustration of the three growth modes of secondary metal on a seed substrate. Reprinted with permission from[157]*.Copyright (2021) American Chemical Society.*

Direct coating of the surface of the magnetic nanoparticles with a gold shell could only be achieved if the layer-by-layer growth mode is followed.[158] Generally when the lattice mismatch between two metals are relatively small (≤5 %) the epitaxial growth (complete and uniform coverage of the second metal on a substrate) can happen.[157,158] If the lattice mismatch is bigger than 5% other types of growth could be observed.

Table 1.2. Standard atomic spacing for typical magnetic nanoparticles (Magnetite and Maghemite) and Gold.[159]

(*hkl*) index	Magnetite	Maghemite	Gold
111	4.85	4.82	2.35
220	2.97	2.95	1.44
311	2.53	2.52	1.23
400	2.10	2.09	1.02
422	1.71	1.70	0.83

As it can be seen from table 1.1 the atomic spacing between gold and typical magnetic nanoparticles are small enough so that direct coating of the magnetic nanoparticles with gold is possible.[160] To date several methods have been reported for the direct coating of a gold layer on the surface of the magnetic nanoparticles in both organic and aqueous solutions.[161–169]

As was discussed in section 1.2.2.1, co-precipitation of $FeCl_2$ and $FeCl_3$ in a strongly alkaline solution results in the synthesis of magnetite nanoparticles. Pham *et al* used this method to produce the iron oxide magnetic nanoparticles then by adding the

magnetic nanoparticles to the boiling solution of the $HAuCl_4$ in presence of the sodium citrate as a reducing agent they have managed to form gold-coated magnetic nanoparticles.[170] It is worth noting that sodium citrate not only acts as a reducing agent in high temperatures (normally above 70°C) but it also stabilizes the gold-coated magnetic nanoparticles.[171] In another example of direct coating of the gold layer on the surface of the magnetic nanoparticles Lo *et al* used the same protocol and produce the citrate capped gold-coated nanoparticles and then by a further ligand exchange process in a boiling solution containing L-homocysteine, they have managed to synthesize homocys-Au-Fe_3O_4 nanoparticles. The 12 nm gold-coated magnetite nanoparticles had a very thing gold shell (0.5 nm) and were well-dispersed in water and very stable in physiological pH with no sign of aggregation.[172] Furthermore, having homocysteine as a capping agent for the nanoparticles was shown to be beneficial for further surface modification with amine or carboxylate terminal groups.[172] Ahmad *et al*, synthesized similar gold-coated magnetic nanoparticles (22 nm average size with 2 nm gold shell) and used them as a T_2 contrast agent in MRI with 3 times higher relaxivity ratio of R_2/R_1 than conventional commercial contrast agent.[173]

In another example, gold-coated magnetic nanoparticles were synthesized at room temperature. Tamer *et al* added the magnetite nanoparticles produced *via* the co-precipitation method into the aqueous solution of $HAuCl_4$ under sonication. Sodium borohydride was used to reduce the gold onto the surface of the magnetite nanoparticles. The resultant gold-coated magnetic nanoparticles were monodispersed with an average size of 12.5±3 nm. It was argued that the sonication of nanoparticles during synthesis resulted in monodisperse gold-coated magnetic nanoparticles.[174] Another way to make the gold-coated magnetic nanoparticles is to use hydroxylamine as a reducing agent and iteratively deposit gold atoms on the surface of the iron oxide magnetic nanoparticles to obtain a uniform gold nanoshell.[175–178] It was reported that hydroxylamine encourages gold (III) surface catalysed reduction.[179] As can be seen from Figure 1.21 hydroxylamine ensures that the gold atoms are only deposited on the surface of the already synthesized seeds rather than forming new gold seeds.

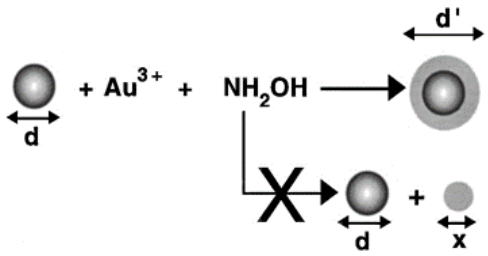

Figure 1.21. Schematic illustration of the hydroxylamine seeding of colloidal gold nanoparticles. Reprinted with permission from[179].Copyright (2021) American Chemical Society.

Gold atoms in the presence of NH_2OH prefer to go and deposit on the surface of the iron oxide nanoparticles and do not produce gold nanoparticles. Lyon *et al* used the iterative reduction of the gold atoms *via* hydroxylamine to produce gold-coated magnetic nanoparticles.[180] Maghemite and magnetite nanoparticles were first dispersed in sodium citrate solution to make the surface of the magnetic nanoparticles citrate terminated then the gold shell was grown by reduction of chloroauric acid by hydroxylamine at 25°C. Five separate iterations of gold atoms by hydroxylamine resulted in a complete gold shell on the surface of the magnetic nanoparticles.

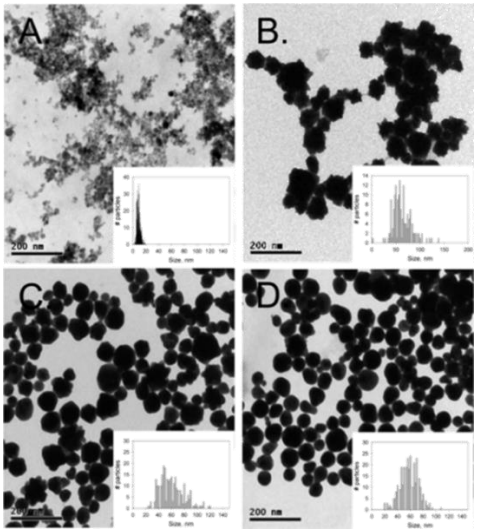

Figure 1.22. TEM images of the A) citrate capped magnetic nanoparticles B) one incremental addition of the gold atoms to the magnetic nanoparticles C) three incremental additions of the gold atoms to the magnetic nanoparticles and D) five incremental additions of the gold atoms to the magnetic nanoparticles. Insets show the histogram of the size of the nanoparticles for each step. Reprinted with permission from[180].Copyright (2021) American Chemical Society.

As is depicted in Figure 1.22, the size of the nanoparticles (60 nm on average) did not change significantly despite the continuous addition of the gold to the surface of the magnetic nanoparticle. This is because at the beginning gold nucleated on the surface of the magnetic nanoparticles and further reduction of the gold by hydroxylamine resulted in the gaps between the nuclei being filled by the gold shell.[180]

As it was discussed in section 1.2.2.3 synthesis of magnetic nanoparticles in the organic phase *via* thermal decomposition of the iron precursor at high temperature compared to co-precipitation results in monodisperse nanoparticles with better control over the size and shape.[181] As a result there are several reports on the addition of the gold shell directly to the magnetic nanoparticles which were made in organic solution.[182–184] For instance Xu *et al* made 10 nm magnetite nanoparticles by thermally decomposing the iron oleate in a boiling mixture of oleylamine and oleic acid at 300°C.[185] To add the gold shell onto the magnetite nanoparticles $HAuCl_4.3H_2O$ was dissolved in chloroform and oleylamine. Magnetite nanoparticles were added to a solution containing chloroform and oleylamine. By slow and dropwise addition of the solution containing the $HAuCl_4$ to the magnetic nanoparticles' solution gold was gently reduced and formed a nanoshell on the surface of the magnetite nanoparticles.

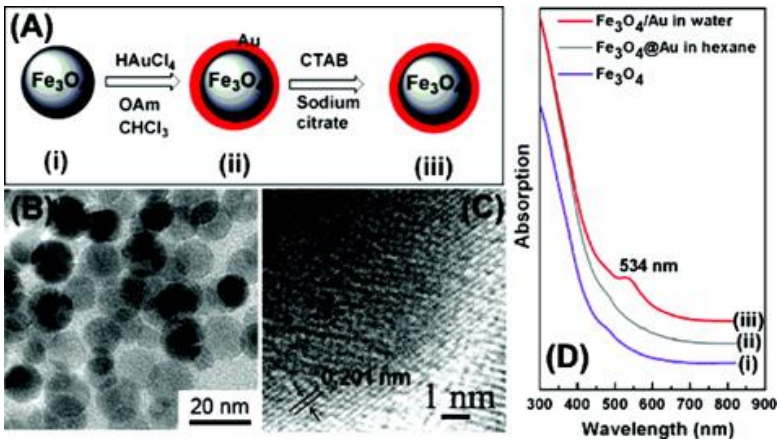

Figure 1.23. Schematic illustration gold coating process of the magnetite nanoparticles (i) gold-coating in organic phase (ii) water dispersible gold-coated magnetite nanoparticles (iii). (B) TEM image of the gold-coated magnetic nanoparticles (iii); (C) HRTEM image of part of a gold-coated magnetite nanoparticle from (B). (D) UV−vis absorption spectra of the gold-coated magnetite nanoparticles (i) in hexane, (ii) in hexane, and (iii) in Milli-Q water. Reprinted with permission from[185].Copyright (2021) American Chemical Society.

To make the gold-coated magnetite nanoparticles water-dispersible as can be seen from Figure 1.23, the nanoparticles were dried and then dispersed in a solution containing cetyltrimethylammonium bromide (CTAB) and sodium citrate. TEM, HRTEM and UV-Vis spectra proved the addition of the gold layer onto the surface of the magnetite solution (Figure 1.23. B and C). Further, by reduction of the gold by ascorbic acid in presence of CTAB onto the already gold-coated magnetite nanoparticles, they managed to control the thickness of the gold shell.[185]

Other methods such as microemulsion and nanoemulsion have been also used to synthesis the gold-coated magnetic nanoparticles as well but they are not as prevalent.[186] As an example Mikhaylova *et al*, by employing a microemulsion system of CTAB/octane/butanol/water managed to synthesized gold-coated magnetic nanoparticles.[187] The nanoparticles magnetic properties were measured at 5, 100 and 300 K, the nanoparticle showed superparamagnetic behaviour with magnetization saturation of 21 emu g^{-1} at 5 K and 18 emu g^{-1} at 300 K.[187]

1.5.2. Indirect gold coating

In the indirect method, magnetic nanoparticles are first coated with an intermediate layer (glue layer) and then a gold nanoshell will be formed on the surface of that intermediate layer.[111] One of the main advantages of the indirect gold coating is that the gold coating process could be divided into two-step 1) gold seeding and 2) gold shell growth. The seeding of the surface of the nanoparticles with small gold nanoparticles facilitates the growth of the gold shell as these gold nanoparticles serve as nucleation sites for the gold shell growth.[188–190] For any material to be considered as an effective intermediate layer for gold coating, it has to possess several key qualities and properties. A perfect intermediate material should completely cover the surface of the magnetic nanoparticles and make them both physically and chemically stable.[191] It also needs to have numerous metal-binding terminal groups on its surface to encourage attachments of gold atoms and finally it should be biocompatible too.[111,191] A variety of materials have been used as an intermediate layer (glue layer) for the synthesis of gold-coated magnetic nanoparticles.[192–198]

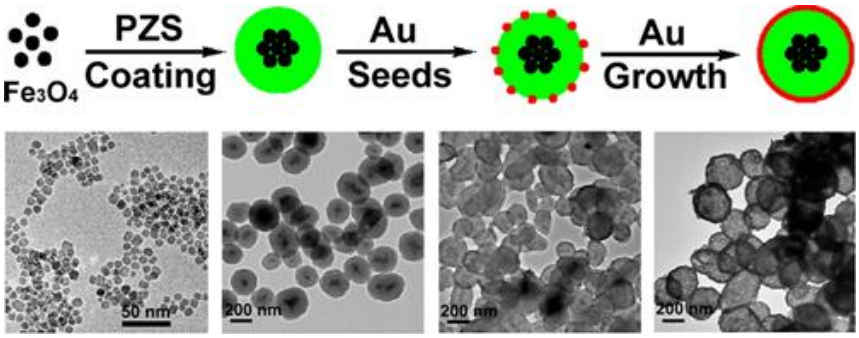

Figure 1.24. Top: Scheme and Bottom: TEM images of the nanoparticles at different stages of the synthesis process. Reprinted with permission from[191]*.Copyright (2021) American Chemical Society.*

Hu *et al*, used poly(cyclotriphosphazene-co-4,4′-sulfonyldiphenol) (PZS) as an intermediate layer between magnetite nanoparticles and the gold layer Figure (1.24).[191] PZS is a highly cross-linked polymer that is water dispersible and biocompatible. It also has numerous phenolic hydroxyl groups and atoms such as N, P and S which can interact with gold ions and atoms.[191,199,200] Magnetite nanoparticles were prepared by a polyol process using iron (III) acetylacetonate ($Fe(acac)_3$) in triethylene glycol at 278°C.[201] To form the PZS layer on the already water-dispersible magnetite nanoparticles a one-step polymerization process was used. Iron oxide magnetic nanoparticles were added to hexachlorocyclotriphosphazene. An aliquot of tetrahydrofuran, triethylamine and anhydrous alcohol were mixed and added to the magnetite nanoparticles solution in a flask. The reaction mixture was maintained under ultrasonic irradiation at room temperature for 6 hours to produce the PZS coated magnetite nanoparticles. It is important to note PZS coated an agglomeration of the magnetite nanoparticles and not a single core.[191] The surface of the polymer-coated magnetite nanoparticles was then seeded with around 3 nm gold seeds *via* rapid reduction of the $HAuCl_4$ by $NaBH_4$. Complete gold shell was grown on the surface of the seeded nanoparticles by reduction of the $HAuCl_4$ at high temperature in presence of the sodium citrate. The final Fe_3O_4@PZS@Au nanoparticles were around 253 nm with a rough surface and a saturation magnetization of 24.2 emu g^{-1}. The nanoparticles showed to be good MRI contrast agents while also could be used for photo-thermal therapy due to strong near-infrared absorption of the gold shell.[191]

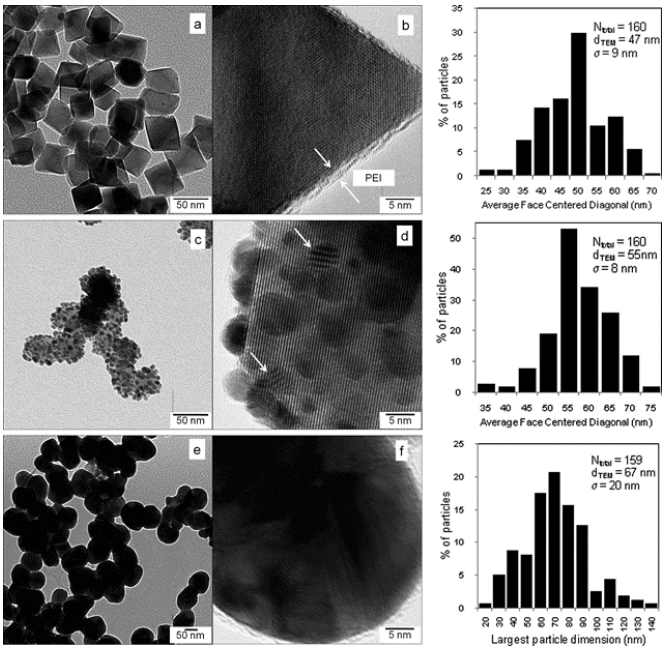

Figure 1.25. (a) TEM image of PEI-coated magnetite cores; (b) HRTEM image of a PEI-coated magnetite particle; (c) TEM image of gold-seeded PEI-coated magnetite cores; (d) HRTEM image of a gold-seeded PEI-coated magnetite particle; (e) TEM image of gold-coated PEI-coated magnetite nanoparticles; (f) high-magnification TEM image of a gold-coated PEI-coated magnetite nanoparticle. Reprinted with permission from[138]*. Copyright (2021) American Chemical Society.*

In another study, Goon *et al* used polyethyleneimine (PEI) as an intermediate layer between magnetic nanoparticles and gold shell (Figure 1.25).[138] PEI is a positively charged polymer thus, it can attract negatively charged gold seeds *via* electrostatic attraction.[202,203] PEI-coated magnetite nanoparticles were made using the coprecipitation method of $FeSO_4$ in a basic environment controlled by NaOH and in presence of KNO_3 and PEI at 90°C in an oxygen-free environment. Next, the 50 nm PEI-coated magnetic nanoparticles were seeded by reduction of $HAuCl_4$ by $NaBH_4$ in presence of sodium citrate. Another layer of PEI was synthesized on top of the already seeded magnetic nanoparticles by heating the nanoparticles at 60°C for one hour. Finally by repeated reduction (5 times) of $HAuCl_4$ by hydroxylamine onto the PEI surface to produce a complete gold shell.[138] The final gold-coated magnetic nanoparticles were free of capping agent which makes them favourable for a variety of applications due to their easy surface modification.[138]

In another study, Chin *et al* used dopamine as an intermediate layer to produce a gold shell on the surface of the magnetite nanoparticles.[204] Existence of amine terminal groups made the surface positively charged and as the result, they managed to attach the citrate capped gold seeds nanoparticles to the dopamine-coated magnetic nanoparticles.[204] The gold shell was formed by the reduction of $HAuCl_4$ by glucose in a slightly basic medium (pH≈9) to produce monodisperse gold-coated magnetic nanoparticles. The nanoparticles showed superparamagnetic behaviour with magnetization saturation of 35 emu g^{-1}.

One of the most important intermediate layers used to make gold-coated magnetic nanoparticles is silica.[196,205–208] Silica not only provides a favourable surface for the growth of the gold layer it helps prevent plasmonic damping of the magnetic core too.[92] Woodard *et al* synthesized a gold-coated magnetic nanoparticle capable of providing multi-dual functionality.[209]

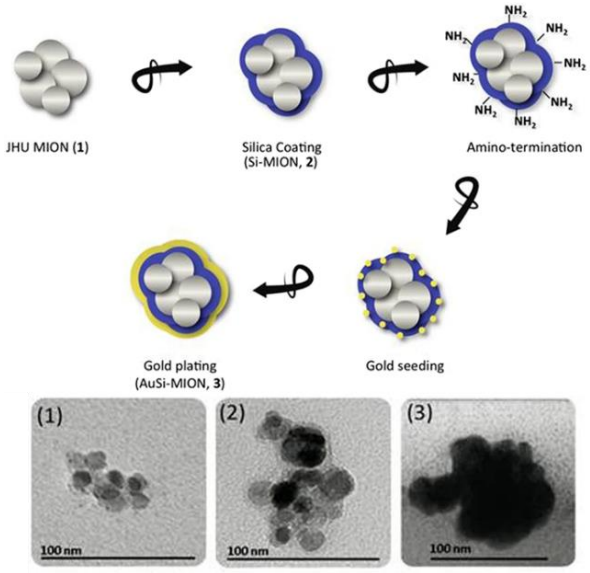

Figure 1.26. Top: Schematic illustration of synthesis route to make the gold-coated magnetic nanoparticles. Bottom: TEM images of 1) JHU magnetic nanoparticles 2) silica-coated JHU magnetic nanoparticles and 3) gold-coated JHU magnetic nanoparticles. Reprinted from[209].Open access article Springer Nature.

Figure 1.26. shows the multi-step synthesis strategy to prepare the nanoparticles. Citrate capped dense polycrystalline magnetic core (JHU) compromise of agglomerated

iron oxide nanoparticles was made through a high-gravity controlled precipitation method.[210] The magnetic cores (55 nm average size) were then coated with silica *via* a Stöber method with some modifications. The silica-coated magnetic nanoparticles were positively charged by the addition of the amine terminal group on the surface of the silica-coated nanoparticles *via* modification of the surface with 3-aminopropyltrimethoxy-silane (APTMS). The electrostatic interaction between positively charged silica surface and negatively charged gold nanoparticles (1-2 nm) produced the gold-seeded silica-coated magnetic nanoparticles. Finally, to add the gold shell, chloroauric acid was reduced by hydroxylamine.[209] The gold-coated magnetic nanoparticles made with this method were around 145 nm and shown good magnetic properties which allowed them to be used for dual MRI/CT imaging, hyperthermia, and biofunctionalization.[209]

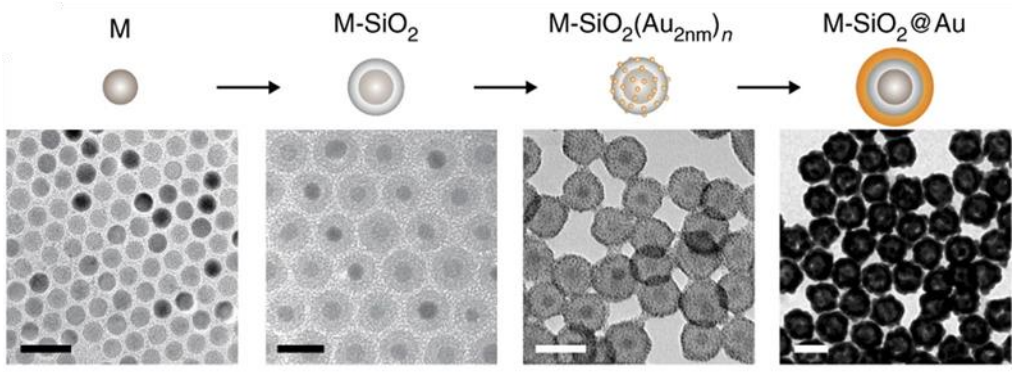

Figure 1.27. Top: Schematic illustration of the multi-step synthesis of the gold-coated magnetic nanoparticles. Bottom: TEM images of zinc doped magnetic nanoparticles, silica-coated zinc doped magnetic nanoparticles, gold-seeded silica-coated zinc doped magnetic nanoparticles and gold-coated magnetic nanoparticles. Scale bars, 50 nm. Reprinted with permission from[211].Copyright (2021) Springer Nature.

In another study, Kim *et al* reported the synthesis of gold-coated magnetic nanoparticles using zinc doped ferrite magnetic nanoparticles (Figure 1.27).[211] Zn-doped magnetic ferrite ($Zn_xFe_{3-x}O_4$) was synthesized using thermal decomposition of $Fe(acac)_3$ and Zinc (II) chloride in oleic acid and oleylamine. Controlling the stoichiometric ratio between the iron and zinc precursor 13 nm and 30 nm $Zn_{0.4}Fe_{2.6}O_4$ magnetic cores were synthesized. This critical ratio of zinc to iron was chosen as at this ratio Zn mainly occupies the tetrahedral sites, hence blocking antiparallel magnetic spins.[212,213] As the magnetic cores were made in organic solvents a water-in-oil microemulsion method was

employed to make the silica shell. Silica was further amine-modified and decorated with ultra-small gold seeds (2nm, prepared by fast reduction of gold chloride by tetrakis(hydroxymethyl)phosphonium chloride (THPC)). Final shell growth was done by mild reduction of $HAuCl_4$ with hydroxylamine hydrochloride ($NH_2OH{\cdot}HCl$). They have concluded that the dense decoration of the gold seeds on the silica-coated magnetic nanoparticles and also sufficient incubation of the gold plating solution mixture (absorbance of gold chloride solution ≈0.05) before the final step are the key for uniform growth of the gold shell on the surface of the silica-coated magnetic nanoparticles.[211]

1.5.3. Challenges of gold coating

One of the main challenges facing scientists in making gold-coated magnetic nanoparticles is the growth of a complete and uniform gold shell around magnetic cores (Figure 1.28), especially with direct coating. Incomplete or partial coating leads to divergence from optimal properties. This could significantly affect the possible applications of the nanoparticles. For example, partial coating of the magnetic nanoparticles with gold (i.e., exposure of the magnetic nanoparticles or intermediate layer) could change the expected LPSR peak position. Therefore, the ineffectiveness of the nanoparticles for a variety of optical applications. Furthermore, partial gold-coating could hugely affect the modification of nanoparticles. As was previously mentioned one of the main goals of having a gold shell on the surface of the magnetic nanoparticles is the high affinity of both amine and thiol functional groups for gold. This affinity for gold could further be exploited for robust thiol chemistry to interact with a variety of biomolecules and eventually the production of biosensors. Partial coating of the magnetic nanoparticles could disrupt the modification procedure and even result in the aggregation of nanoparticles due to ineffective surface chemistry. Although the indirect coating could elevate some of these issues regarding partial coating, it could also spark new challenges.

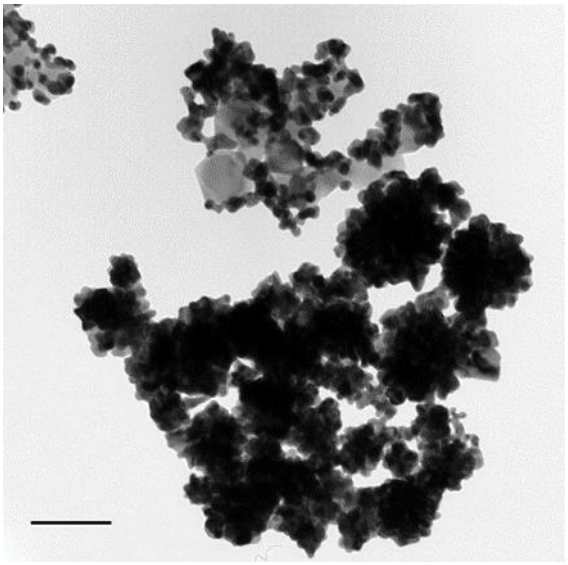

Figure 1.28. TEM image of gold-coated magnetic nanoparticles with part of the sample fully coated and part of the sample not coated with gold. Scale bar 100 nm.

As it was discussed in section 1.5.2 indirect gold coating requires multi-step synthesis procedures. Optimizing reaction conditions for each of these steps requires substantial experimental refinement. The seed-mediated method is one of the main routes of making gold-coated magnetic nanoparticles, constant charge convergence of the surface in each step could lead to agglomeration of the nanoparticles. For instance, to make the surface of the silica-coated magnetic nanoparticles positively charged APTES modification is used to cover the surface with an amine group.[214] After the surface is positively charged then negatively charged gold nanoparticles have to be attached to the surface, which means there is a chance for nanoparticles to get aggregated at any point.[208]

Another challenge is that encapsulating magnetic nanoparticles inside several non-magnetic layers causes a decline in the overall magnetization saturation of nanoparticles.[215,216] This diminution in magnetization saturation leads to less susceptibility toward the external magnetic field, which could seriously affect the application of the nanoparticles. For instance, in the case of magnetic separation or dispersible electrodes, the application relies on the fact the gold-coated magnetic nanoparticles respond to external magnetic fields promptly.[137] One solution to this issue could be using magnetic nanoparticles with bigger sizes as they provide higher

magnetization saturation compare to smaller magnetic nanoparticles and especially superparamagnetic nanoparticles.[217] However, once bigger magnetic nanoparticles (≥20 nm) get magnetized, even after removal of the external magnetic field they retain the magnetization. The retained magnetization means that the nanoparticles are attracted to each other and as a result, magnetic aggregation of nanoparticles could occur.[218]

Last but not least, one of the bigger hurdles to the widespread application of gold-coated magnetic nanoparticles is large scale synthesis methods. As it was discussed in the synthesis section, the production of gold-coated magnetic nanoparticles is a cumbersome and meticulous job. Most of the colloidal synthesis routes for making gold-coated magnetic nanoparticles result at best in milligram scale nanoparticles, with poor reproducibility. In recent years microfluidic systems gain lots of attention concerning the mass production of nanoparticles.[219–224] These processes offer many advantages over normal colloidal syntheses such as high reproducibility, the potential for online characterization and automation, mass production etc.[225–227] Frenz *et al* used droplet-based microfluidic microreactors to make ɣ-Fe_2O_3 by coprecipitation of Fe^2 and Fe^3 in a basic environment.[228] In another example, Abou-Hassan *et al* made fluorescent ɣ-Fe_2O_3@SiO_2 nanoparticles by using multistep continuous flow reactors.[229]

A more complicated gold-coated silica nanoparticle was synthesized by Duraiswamy and Khan in 2010.[230] Using a droplet-microfluidic reactor they have managed to form gold nanoshell on the surface of the pre-seeded silica nanoparticles within 2 minutes.[230] Recently, Ahrberg *et al* designed an automated droplet microfluidic system for the synthesis of gold-coated magnetic nanoparticles.[231] The unique design of the nanoparticles manufacturing system (Figure 1.29) was consist of capillary tubing connecting multiple tubes carrying the chemicals needed for each step of the reaction.[231]

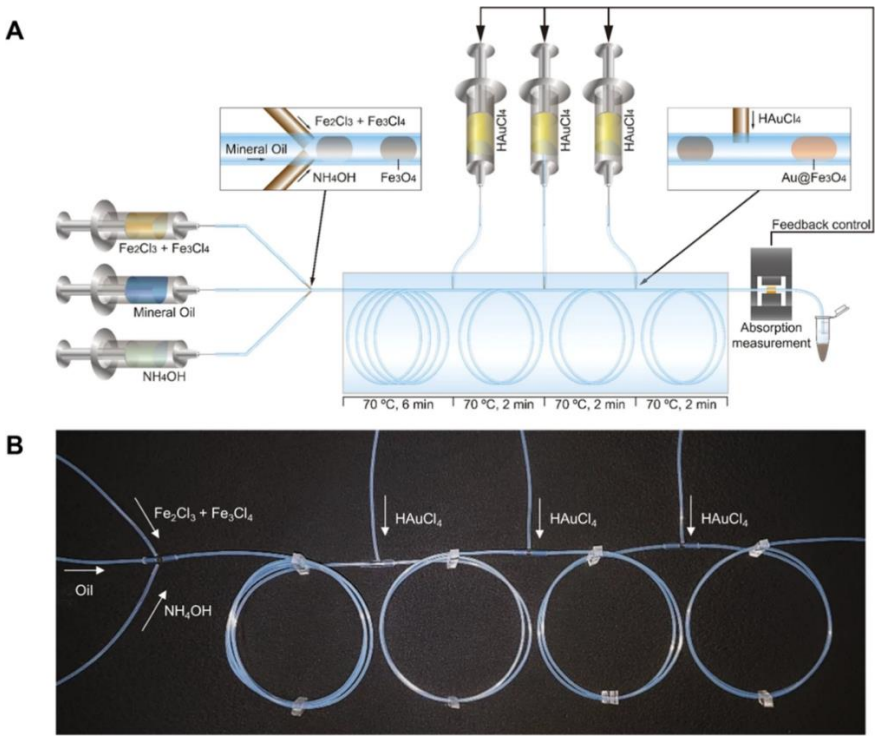

Figure 1.29. A) Schematic of the droplet reactor used to make gold-coated magnetic nanoparticles continuously. B) Picture of the droplet system used for continuous manufacturing of the gold-coated magnetic nanoparticles. Reprinted from[231].Open access article Springer Nature.

As it can be seen from Figure 1.29 The magnetic nanoparticles were made through coprecipitation of the Fe_2Cl_3 and Fe_3Cl_4 in NH_4OH inside the droplet. The continuous addition of the gold precursor first resulted in gold seeds on the surface of the magnetic nanoparticles and then grow into a complete shell.[231] Although microfluidic methods are starting to ease many of the issues related to the colloidal synthesis of gold-coated magnetic nanoparticles, there are still challenges facing them that need to be dealt with. For example, one of the biggest challenges is channel clogging which also could affect the mixing and compensation of the chemicals inside the channels. The cost related to the substrate materials and also the cost of moulding the substrate in cleanrooms is another crucial issue facing synthetics chemists. Finally, pre and post-treatment of nanoparticles such as cleaning of nanoparticles are still labour intensive and hard to be automated. [232]

All in all, the need for unique synthesis methods that are more robust and can produce better gold-coated magnetic nanoparticles is of the highest importance for synthetics chemists. Here we try to take a small step toward better synthetic routes for making gold-coated magnetic nanoparticles.

1.6. Thesis objective

This thesis aims to address some of the main issues regarding the synthesis of gold-coated magnetic nanoparticles. As it was discussed in the previous section lack of reliable and reproducible synthesis methods to produce the gold-coated magnetic nanoparticles hinders many of the intended applications from their jump from laboratory to commercial use. To address these issues, we proposed two unique nanoparticles and a synthetic route to produce the gold-coated magnetic nanoparticles. The acquired nanoparticles were subject to a variety of characterization techniques to evaluate their properties. A summary of the chapters in this thesis is provided below:

The first chapter provides a general overview of the literature regarding magnetic nanoparticles and their applications for bio-sensing. It further discusses the importance of gold-coated magnetic nanoparticles and shed some light on the general strategies of synthesis of gold-coated magnetic nanoparticles.

The second chapter explains the chemicals, instruments and general strategies used to produce different nanoparticles here. More detailed explanations of synthetics methods required for obtaining each of the unique nanoparticles are provided in the result chapters.

The third chapter provides a survey of the properties of the state-of-the-art commercially available gold-coated magnetic nanoparticles acquired from different companies in an

attempt to help the reader to understand the main challenges and issues facing when dealing with the synthesis of gold-coated magnetic nanoparticles.

The fourth chapter presents a new type of gold-coated magnetic nanoparticles called gold-coated conglomerates of superparamagnetic nanoparticles. This chapter aims to provide the reader with a new methodology for making gold-coated magnetic nanoparticles that are stable against magnetic aggregation and yet respond to the external magnetic field fast. The developed nanoparticles were characterized, and their effectiveness as electrochemical and optical sensors were shown.

The fifth chapter presents another new nanoparticle called gold-coated zero-valent iron core-iron oxide shell. The nanoparticle synthesized here aims to provide end-users with high magnetization saturation on top of good stability against magnetic aggregation and good colloidal stability.

The sixth chapter presents a new synthesis route for making gold-coated nanoparticles with higher reproducibility and ability for mass production. To achieve this a simple and cost-effective methodology based on microfluidic systems was developed. The effectiveness of the synthetic method to produce gold-coated nanoparticles was shown and the final products were characterized *via* multiple techniques.

The seventh chapter concludes the knowledge gained throughout the project and layouts suggestions for future work.

1.7. References:

1. Loomans-Kropp, H. A. & Umar, A. Cancer prevention and screening: the next step in the era of precision medicine. *npj Precis. Oncol.* **3**, (2019).
2. Chen, X. *et al.* Non-invasive early detection of cancer four years before conventional diagnosis using a blood test. *Nat. Commun.* **11**, 1–10 (2020).
3. Gooding, J. J. & Gaus, K. Single-Molecule Sensors: Challenges and Opportunities for Quantitative Analysis. *Angew. Chemie - Int. Ed.* **55**, 11354–11366 (2016).
4. Gloag, L., Mehdipour, M., Chen, D., Tilley, R. D. & Gooding, J. J. Advances in the Application of Magnetic Nanoparticles for Sensing. *Adv. Mater.* **31**, 1–26 (2019).
5. Wu, Y., Tilley, R. D. & Gooding, J. J. Challenges and Solutions in Developing Ultrasensitive Biosensors. *J. Am. Chem. Soc.* **141**, 1162–1170 (2019).
6. Gul, S., Khan, S. B., Rehman, I. U., Khan, M. A. & Khan, M. I. A Comprehensive Review of Magnetic Nanomaterials Modern Day Theranostics. *Front. Mater.* **6**, 1–15 (2019).
7. Akbarzadeh, A., Samiei, M. & Davaran, S. Magnetic nanoparticles: preparation, physical properties, and applications in biomedicine. *Nanoscale Res. Lett.* **7**, 1–13 (2012).
8. Wu, Y., Bennett, D., Tilley, R. D. & Gooding, J. J. How Nanoparticles Transform Single Molecule Measurements into Quantitative Sensors. *Adv. Mater.* **32**, 1–8 (2020).
9. Gossuin, Y., Gillis, P., Hocq, A., Vuong, Q. L. & Roch, A. Magnetic resonance relaxation properties of superparamagnetic particles. *Wiley Interdiscip. Rev. Nanomedicine Nanobiotechnology* **1**, 299–310 (2009).
10. Nolting, W. & Ramakanth, A. *Quantum Theory of Magnetism*. (Springer Berlin Heidelberg, 2009). doi:10.1007/978-3-540-85416-6.
11. Chiolerio, A., Chiodoni, A., Allia, P. & Martino, P. *Handbook of Nanomaterials Properties*. (2014). doi:10.1007/978-3-642-31107-9.
12. Lenglet, L. & Motte, L. *Neel Effect : exploiting the nonlinear behavior of superparamagnetic nanoparticles for applications in life sciences up to electrical engineering*. *In Rentschler, E. (Ed.) Novel Magnetic Nanostructures: Unique Properties and Applications. Elsevier* (Elsevier Inc., 2018). doi:10.1016/B978-0-12-813594-5.00008-4.
13. Kodama, R. H. *Magnetic nanoparticles*. *J. Magn. Magn. Materials* vol. 200 (1999).
14. Zabel, H. & Farle, M. *Magnetic Nanostructures - Spin Dynamics and Spin Transport*. (2013). doi:10.1007/978-3-642-32042-2.

15. Guimarães, A. P. *Principles of Nanomagnetism*. *Principles of Nanomagnetism* (2009).

16. Lu, A. H., Salabas, E. L. & Schüth, F. Magnetic nanoparticles: Synthesis, protection, functionalization, and application. *Angew. Chemie - Int. Ed.* **46**, 1222–1244 (2007).

17. Gatteschi, D. & Sessoli, R. Quantum Tunneling of Magnetization and Related Phenomena Inmolecular Materials. *Angew. Chemie-International Ed.* **42**, 268–297 (2003).

18. Thanh, N. T. Magnetic Nanoparticles From Fabrication to Clinical Applications. *CRC Press* 243–276 (2012) doi:10.1002/ddr.

19. Sandler, S. E., Fellows, B. & Thompson Mefford, O. Best Practices for Characterization of Magnetic Nanoparticles for Biomedical Applications. *Anal. Chem.* **91**, 14159–14169 (2019).

20. Lo, M. A. *Handbook of Nanomaterials Properties*. (2014). doi:10.1007/978-3-642-31107-9.

21. Mahmoudi, M., Hofmann, H., Rothen-Rutishauser, B. & Petri-Fink, A. Assessing the in vitro and in vivo toxicity of superparamagnetic iron oxide nanoparticles. *Chem. Rev.* **112**, 2323–2338 (2012).

22. Bumb, A. *et al.* Synthesis and characterization of ultra-small superparamagnetic iron oxide nanoparticles thinly coated with silica. *Nanotechnology* **19**, (2008).

23. Wu, K., Su, D., Liu, J., Saha, R. & Wang, J. P. Magnetic nanoparticles in nanomedicine: A review of recent advances. *Nanotechnology* **30**, (2019).

24. Chouhan, R. S. *et al.* Magnetic nanoparticles—a multifunctional potential agent for diagnosis and therapy. *Cancers (Basel).* **13**, 1–16 (2021).

25. Willard, M. A., Kurihara, L. K., Carpenter, E. E., Calvin, S. & Harris, V. G. Chemically prepared magnetic nanoparticles. *Int. Mater. Rev.* **49**, 125–170 (2004).

26. Hergt, R., Dutz, S., Müller, R. & Zeisberger, M. Magnetic particle hyperthermia: Nanoparticle magnetism and materials development for cancer therapy. *J. Phys. Condens. Matter* **18**, 2919–2934 (2006).

27. Reddy, L. H., Arias, J. L., Nicolas, J. & Couvreur, P. Magnetic nanoparticles: Design and characterization, toxicity and biocompatibility, pharmaceutical and biomedical applications. *Chem. Rev.* **112**, 5818–5878 (2012).

28. Walter, A. *et al.* Mastering the shape and composition of dendronized iron oxide nanoparticles to tailor magnetic resonance imaging and hyperthermia. *Chem. Mater.* **26**, 5252–5264 (2014).

29. Chatterjee, J., Haik, Y. & Chen, C.-J. Size dependent magnetic properties of iron oxide nanoparticles. *J. Magn. Magn. Mater.* **257**, 113–118 (2003).

30. Kim, D. *et al.* Synthesis of Uniform Ferrimagnetic Magnetite Nanocubes - Journal of the American Chemical Society (ACS Publications). *J. Am. Chem. Soc.* **131**, 454–5 (2009).

31. Palchoudhury, S. *et al.* Synthesis and growth mechanism of iron oxide nanowhiskers. *Nano Lett.* **11**, 1141–1146 (2011).

32. TARTAJ, P., Morales, M. del P. M., Veintemillas-Verdaguer, S., González-Carreño, T. & Serna, C. J. Progress in the preparation of magnetic nanoparticles for applications in biomedicine. *J. Phys. D. Appl. Phys.* **42**, 224002 (2009).

33. Bolisetty, S., Vallooran, J. J., Adamcik, J. & Mezzenga, R. Magnetic-responsive hybrids of Fe3O4 nanoparticles with β-lactoglobulin amyloid fibrils and nanoclusters. *ACS Nano* **7**, 6146–6155 (2013).

34. Dar, M. I. & Shivashankar, S. A. Single crystalline magnetite, maghemite, and hematite nanoparticles with rich coercivity. *RSC Adv.* **4**, 4105–4113 (2014).

35. Jain, T. K., Reddy, M. K., Morales, M. A., Leslie-Pelecky, D. L. & Labhasetwar, V. Biodistribution, clearance, and biocompatibility of iron oxide magnetic nanoparticles in rats. *Mol. Pharm.* **5**, 316–327 (2008).

36. Gloag, L., Mehdipour, M., Chen, D., Tilley, R. D. & Gooding, J. J. Advances in the Application of Magnetic Nanoparticles for Sensing. **1904385**, 1–26 (2019).

37. Cuenca, J. A. *et al.* Study of the magnetite to maghemite transition using microwave permittivity and permeability measurements. *J. Phys. Condens. Matter* **28**, (2016).

38. Panchal, V., Bhandarkar, U., Neergat, M. & Suresh, K. G. Controlling magnetic properties of iron oxide nanoparticles using post-synthesis thermal treatment. *Appl. Phys. A* **114**, 537–544 (2014).

39. Sergeev, G. B. Nanochemistry of Metals. *Usp. Khim.* **70**, 931–933 (2001).

40. Kenneth, J. *Nanoscale Materials in Chemistry*. (John Wiley & Sons, Inc., 2001). doi:10.1002/0471220620.

41. Anagnostopoulou, E. *et al.* Dense arrays of cobalt nanorods as rare-earth free permanent magnets. *Nanoscale* **8**, 4020–4029 (2016).

42. Chen, B., Michioka, C., Itoh, Y. & Yoshimura, K. Synthesis and magnetic properties of Ni3AlCx. *J. Phys. Soc. Japan* **77**, 2–5 (2008).

43. Louderback, J. G., Cox, A. J., Lising, L. J., Douglass, D. C. & Bloomfield, L. A. Magnetic properties of nickel clusters. *Zeitschrift für Phys. D Atoms, Mol. Clust.* **26**, 301–303 (1993).

44. Neeley, C., Moritz, M., Brown, J. J. & Zhou, Y. Acute side effects of three commonly used gadolinium contrast agents in the paediatric population. *Br. J. Radiol.* **89**, 0–4 (2016).

45. Abujudeh, H. H., Kosaraju, V. K. & Kaewlai, R. Acute adverse reactions to

gadopentetate dimeglumine and gadobenate dimeglumine: Experience with 32,659 injections. *Am. J. Roentgenol.* **194**, 430–434 (2010).

46. Pyykkö, P. Magically magnetic gadolinium. *Nat. Chem.* **7**, 680 (2015).

47. Elliott, J. F., Legvold, S. & Spedding, F. H. Some magnetic properties of gadolinium metal. *Phys. Rev.* **91**, 28–30 (1953).

48. Abel, F. Received May 4 ,— Read June 16 , 1892 . 228–233 (1892).

49. Guo, L., Huang, Q., Li, X. Y. & Yang, S. Iron nanoparticles: Synthesis and applications in surface enhanced Raman scattering and electrocatalysis. *Phys. Chem. Chem. Phys.* **3**, 1661–1665 (2001).

50. Arami, H., Khandhar, A., Liggitt, D. & Krishnan, K. M. In vivo delivery, pharmacokinetics, biodistribution and toxicity of iron oxide nanoparticles. *Chem. Soc. Rev.* **44**, 8576–8607 (2015).

51. Wilson, J. L. *et al.* Synthesis and magnetic properties of polymer nanocomposites with embedded iron nanoparticles. *J. Appl. Phys.* **95**, 1439–1443 (2004).

52. McGrath, A. J., Cheong, S., Henning, A. M., Gooding, J. J. & Tilley, R. D. Size and shape evolution of highly magnetic iron nanoparticles from successive growth reactions. *Chem. Commun.* **53**, 11548–11551 (2017).

53. Peng, S., Wang, C., Xie, J. & Sun, S. Synthesis and stabilization of monodisperse Fe nanoparticles. *J. Am. Chem. Soc.* **128**, 10676–10677 (2006).

54. Dumestre, F., Chaudret, B., Amiens, C., Renaud, P. & Fejes, P. Superlattices of Iron Nanocubes Synthesized from Fe[N(SiMe 3)2]2. *Science (80-.).* **303**, 821–823 (2004).

55. Wang, C. M. *et al.* Void formation during early stages of passivation: Initial oxidation of iron nanoparticles at room temperature. *J. Appl. Phys.* **98**, (2005).

56. Kim, D. *et al.* Synthesis of hollow iron nanoframes. *J. Am. Chem. Soc.* **129**, 5812–5813 (2007).

57. Cheong, S. *et al.* Simple synthesis and functionalization of iron nanoparticles for magnetic resonance imaging. *Angew. Chemie - Int. Ed.* **50**, 4206–4209 (2011).

58. Cheong, S. *et al.* Synthesis and stability of highly crystalline and stable iron/iron oxide core/shell nanoparticles for biomedical applications. *Chempluschem* **77**, 135–140 (2012).

59. Gloag, L. *et al.* Zero valent iron core-iron oxide shell nanoparticles as small magnetic particle imaging tracers. *Chem. Commun.* **56**, 3504–3507 (2020).

60. Stanicki, D., Elst, L. Vander, Muller, R. N. & Laurent, S. Synthesis and processing of magnetic nanoparticles. *Curr. Opin. Chem. Eng.* **8**, 7–14 (2015).

61. Amendola, V. *et al.* Top-down synthesis of multifunctional iron oxide nanoparticles for macrophage labelling and manipulation. *J. Mater. Chem.* **21**, 3803–3813

(2011).

62. Mignot, A. *et al.* A top-down synthesis route to ultrasmall multifunctional Gd-based silica nanoparticles for theranostic applications. *Chem. - A Eur. J.* **19**, 6122–6136 (2013).

63. Singamaneni, S., Bliznyuk, V. N., Binek, C. & Tsymbal, E. Y. Magnetic nanoparticles: Recent advances in synthesis, self-assembly and applications. *J. Mater. Chem.* **21**, 16819–16845 (2011).

64. Bedanta, S., Barman, A., Kleemann, W., Petracic, O. & Seki, T. Magnetic nanoparticles: A subject for both fundamental research and applications. *J. Nanomater.* **2013**, (2013).

65. Mendoza-Garcia, A. & Sun, S. Recent Advances in the High-Temperature Chemical Synthesis of Magnetic Nanoparticles. *Adv. Funct. Mater.* **26**, 3809–3817 (2016).

66. Mascolo, M. C., Pei, Y. & Ring, T. A. Room Temperature Co-Precipitation Synthesis of Magnetite Nanoparticles in a Large ph Window with Different Bases. *Materials (Basel).* **6**, 5549–5567 (2013).

67. Cheng, C., Xu, F. & Gu, H. Facile synthesis and morphology evolution of magnetic iron oxide nanoparticles in different polyol processes. *New J. Chem.* **35**, 1072–1079 (2011).

68. Hachani, R. *et al.* Polyol synthesis, functionalisation, and biocompatibility studies of superparamagnetic iron oxide nanoparticles as potential MRI contrast agents. *Nanoscale* **8**, 3278–3287 (2016).

69. Koutzarova, T., Kolev, S., Ghelev, C., Paneva, D. & Nedkov, I. Microstructural study and size control of iron oxide nanoparticles produced by microemulsion technique. *Phys. Status Solidi C Conf.* **3**, 1302–1307 (2006).

70. Ennas, G. *et al.* Characterization of Iron Oxide Nanoparticles in an Fe2O3-SiO2 Composite Prepared by a Sol-Gel Method. *Chem. Mater.* **10**, 495–502 (1998).

71. Hufschmid, R. *et al.* Synthesis of phase-pure and monodisperse iron oxide nanoparticles by thermal decomposition. *Nanoscale* **7**, 11142–11154 (2015).

72. Daou, T. J. *et al.* Hydrothermal synthesis of monodisperse magnetite nanoparticles. *Chem. Mater.* **18**, 4399–4404 (2006).

73. Bang, J. H. & Suslick, K. S. Sonochemical synthesis of nanosized hollow hematite. *J. Am. Chem. Soc.* **129**, 2242–2243 (2007).

74. Abou Hassan, A., Sandre, O., Cabuil, V. & Tabeling, P. Synthesis of iron oxide nanoparticles in a microfluidic device: Preliminary results in a coaxial flow millichannel. *Chem. Commun.* 1783–1785 (2008) doi:10.1039/b719550h.

75. Sugimoto, T. & Matijević, E. Formation of uniform spherical magnetite particles by crystallization from ferrous hydroxide gels. *J. Colloid Interface Sci.* **74**, 227–243

(1980).

76. Chen, Q., Rondinone, A. J., C. Chakoumakos, B. & John Zhang, Z. Synthesis of superparamagnetic MgFe2O4 nanoparticles by coprecipitation. *J. Magn. Magn. Mater.* **194**, 1–7 (1999).

77. Vaqueiro, P., López-Quintela, M. A. & Rivas, J. Synthesis of yttrium iron garnet nanoparticles via coprecipitation in microemulsion. *J. Mater. Chem.* **7**, 501–504 (1997).

78. Science, I. & Science, I. Minamiashigara-City, Kanagawa 250-01,. *Interface* **28**, 65–108 (1987).

79. Petcharoen, K. & Sirivat, A. Synthesis and characterization of magnetite nanoparticles via the chemical co-precipitation method. *Mater. Sci. Eng. B Solid-State Mater. Adv. Technol.* **177**, 421–427 (2012).

80. Wang, X., Zhuang, J., Peng, Q. & Li, Y. A general strategy for nanocrystal synthesis. *Nature* **437**, 121–124 (2005).

81. Ge, S. *et al.* Facile hydrothermal synthesis of iron oxide nanoparticles with tunable magnetic properties. *J. Phys. Chem. C* **113**, 13593–13599 (2009).

82. Unni, M. *et al.* Thermal Decomposition Synthesis of Iron Oxide Nanoparticles with Diminished Magnetic Dead Layer by Controlled Addition of Oxygen. *ACS Nano* **11**, 2284–2303 (2017).

83. Park, J. *et al.* Ultra-large-scale syntheses of monodisperse nanocrystals. *Nat. Mater.* **3**, 891–895 (2004).

84. Kim, B. H. *et al.* Large-scale synthesis of uniform and extremely small-sized iron oxide nanoparticles for high-resolution T1magnetic resonance imaging contrast agents. *J. Am. Chem. Soc.* **133**, 12624–12631 (2011).

85. Zhao, Z. *et al.* Octapod iron oxide nanoparticles as high-performance T2 contrast agents for magnetic resonance imaging. *Nat. Commun.* **4**, 1–7 (2013).

86. Kemp, S. J., Ferguson, R. M., Khandhar, A. P. & Krishnan, K. M. Monodisperse magnetite nanoparticles with nearly ideal saturation magnetization. *RSC Adv.* **6**, 77452–77464 (2016).

87. Hyeon, T. Chemical synthesis of magnetic nanoparticles. *Chem. Commun.* 927–934 (2003) doi:10.1039/b207789b.

88. Laurent, S. *et al.* Magnetic Iron Oxide Nanoparticles: Synthesis, Stabilization, Vectorization, Physicochemical Characterizations, and Biological Applications (vol 108, pg 2064, 2008). *Chem. Rev.* **108**, 2064–2110 (2008).

89. Kim, D. K., Mikhaylova, M., Zhang, Y. & Muhammed, M. Protective coating of superparamagnetic iron oxide nanoparticles. *Chem. Mater.* **15**, 1617–1627 (2003).

90. He, R. *et al.* Core/shell fluorescent magnetic silica-coated composite

nanoparticles for bioconjugation. *Nanotechnology* **18**, (2007).

91. Tartaj, P., González-Carreño, T., Bomatí-Miguel, O., Serna, C. J. & Bonville, P. Magnetic behavior of superparamagnetic Fe nanocrystals confined inside submicron-sized spherical silica particles. *Phys. Rev. B - Condens. Matter Mater. Phys.* **69**, 1–8 (2004).

92. Guerrero-Martínez, A., Pérez-Juste, J. & Liz-Marzán, L. M. Recent progress on silica coating of nanoparticles and related nanomaterials. *Adv. Mater.* **22**, 1182–1195 (2010).

93. Journal of Colloid and Interface Science 1994 - (Vigil) Interactions of Silica Surfaces.pdf.

94. Rho, W. Y. *et al.* Facile synthesis of monodispersed silica-coated magnetic nanoparticles. *J. Ind. Eng. Chem.* **20**, 2646–2649 (2014).

95. Stjerndahl, M. *et al.* Superparamagnetic Fe3O4/SiO2nanocomposites: Enabling the tuning of both the iron oxide load and the size of the nanoparticles. *Langmuir* **24**, 3532–3536 (2008).

96. Tartaj, P. & Serna, C. J. Synthesis of Monodisperse Superparamagnetic Fe/Silica Nanospherical Composites. *J. Am. Chem. Soc.* **125**, 15754–15755 (2003).

97. Lu, Y., Yin, Y., Mayers, B. T. & Xia, Y. Modifying the Surface Properties of Superparamagnetic Iron Oxide Nanoparticles through a Sol-Gel Approach. *Nano Lett.* **2**, 183–186 (2002).

98. Zhang, M., Cushing, B. L. & O'Connor, C. J. Synthesis and characterization of monodisperse ultra-thin silica-coated magnetic nanoparticles. *Nanotechnology* **19**, (2008).

99. Shim, W. *et al.* Analysis of changes in gene expression and metabolic profiles induced by silica-coated magnetic nanoparticles. *ACS Nano* **6**, 7665–7680 (2012).

100. Kang, K. *et al.* Preparation and characterization of chemically functionalized silica-coated magnetic nanoparticles as a DNA separator. *J. Phys. Chem. B* **113**, 536–543 (2009).

101. Hamouda, R. A., Hussein, M. H., Abo-elmagd, R. A. & Bawazir, S. S. Synthesis and biological characterization of silver nanoparticles derived from the cyanobacterium Oscillatoria limnetica. *Sci. Rep.* **9**, 1–17 (2019).

102. Xia, Y. N. & Sun, Y. G. Shape-controlled synthesis of gold and silver nanoparticles. *Science (80-.).* **298**, 2176–2179 (2002).

103. Daniel, M.-C. & Astruc, D. Gold Nanoparticles: Assembly, Supramolecular Chemistry, Quantum-Size-Related Properties, and Applications toward Biology, Catalysis, and Nanotechnology. *Chem. Rev.* **104**, 293–346 (2004).

104. Han, B., Choi, N., Kim, K. H., Lim, D. W. & Choo, J. Application of Silver-coated

magnetic microspheres to a SERS-based optofluidic sensor. *J. Phys. Chem. C* **115**, 6290–6296 (2011).

105. Yu, W. *et al.* Magnetic FeAg hybrid nanoparticles as surface-enhanced raman scattering substrate for trace analysis of furazolidone in fish feeds. *J. Nanomater.* **2014**, (2014).

106. Song, D., Yang, R., Wang, C., Xiao, R. & Long, F. Reusable nanosilver-coated magnetic particles for ultrasensitive SERS-based detection of malachite green in water samples. *Sci. Rep.* **6**, 1–9 (2016).

107. Mahmoudi, M. & Serpooshan, V. Silver-coated engineered magnetic nanoparticles are promising for the success in the fight against antibacterial resistance threat. *ACS Nano* **6**, 2656–64 (2012).

108. Mao, B. H., Chen, Z. Y., Wang, Y. J. & Yan, S. J. Silver nanoparticles have lethal and sublethal adverse effects on development and longevity by inducing ROS-mediated stress responses. *Sci. Rep.* **8**, 1–16 (2018).

109. Ferdous, Z. & Nemmar, A. *Health impact of silver nanoparticles: A review of the biodistribution and toxicity following various routes of exposure*. *International Journal of Molecular Sciences* vol. 21 (2020).

110. Shipelin, V. A., Gmoshinski, I. V. & Khotimchenko, S. A. Risk assessment of silver nanoparticles. *IOP Conf. Ser. Mater. Sci. Eng.* **98**, 0–5 (2015).

111. Moraes Silva, S., Tavallaie, R., Sandiford, L., Tilley, R. D. & Gooding, J. J. Gold coated magnetic nanoparticles: From preparation to surface modification for analytical and biomedical applications. *Chem. Commun.* **52**, 7528–7540 (2016).

112. Mayer, K. M. & Hafner, J. H. Localized surface plasmon resonance sensors. *Chem. Rev.* **111**, 3828–3857 (2011).

113. Willets, K. A. & Van Duyne, R. P. Localized surface plasmon resonance spectroscopy and sensing. *Annu. Rev. Phys. Chem.* (2007) doi:10.1146/annurev.physchem.58.032806.104607.

114. Unser, S., Bruzas, I., He, J. & Sagle, L. Localized surface plasmon resonance biosensing: Current challenges and approaches. *Sensors (Switzerland)* **15**, 15684–15716 (2015).

115. McFarland, A. D. & Van Duyne, R. P. Single silver nanoparticles as real-time optical sensors with zeptomole sensitivity. *Nano Lett.* **3**, 1057–1062 (2003).

116. Lee, J. U., Nguyen, A. H. & Sim, S. J. A nanoplasmonic biosensor for label-free multiplex detection of cancer biomarkers. *Biosens. Bioelectron.* **74**, 341–346 (2015).

117. Rajeeva, B. B. *et al.* Regioselective Localization and Tracking of Biomolecules on Single Gold Nanoparticles. *Adv. Sci.* **2**, 28–30 (2015).

118. Sriram, M. *et al.* A rapid readout for many single plasmonic nanoparticles using

dark-field microscopy and digital color analysis. *Biosens. Bioelectron.* **117**, 530–536 (2018).

119. Haes, A. J., Hall, W. P., Chang, L., Klein, W. L. & Van Duyne, R. P. A localized surface plasmon resonance biosensor: First steps toward an assay for Alzheimer's disease. *Nano Lett.* **4**, 1029–1034 (2004).

120. Markhali, B. P. *et al.* Single particle detection of protein molecules using dark-field microscopy to avoid signals from nonspecific adsorption. *Biosens. Bioelectron.* **169**, 112612 (2020).

121. Peiris, S., McMurtrie, J. & Zhu, H. Y. Metal nanoparticle photocatalysts: Emerging processes for green organic synthesis. *Catal. Sci. Technol.* **6**, 320–338 (2016).

122. Baryshnikova, K. V., Petrov, M. I., Babicheva, V. E. & Belov, P. A. Plasmonic and silicon spherical nanoparticle antireflective coatings. *Sci. Rep.* **6**, 1–11 (2016).

123. Armelles, G., Cebollada, A., García-Martín, A. & González, M. U. Magnetoplasmonics: Combining Magnetic and Plasmonic Functionalities. *Adv. Opt. Mater.* **1**, 10–35 (2013).

124. Levin, C. S. *et al.* Magnetic− Plasmonic Core− Shell Nanoparticles. *ACS Nano* **3**, 1379–1388 (2009).

125. Chaffin, E. A., Bhana, S., O'Connor, R. T., Huang, X. & Wang, Y. Impact of core dielectric properties on the localized surface plasmonic spectra of gold-coated magnetic core-shell nanoparticles. *J. Phys. Chem. B* **118**, 14076–14084 (2014).

126. Boyd, R. W. The Intensity-Dependent Refractive Index. *Nonlinear Opt.* 159–190 (1992) doi:10.1016/b978-0-12-121680-1.50008-4.

127. Bhatia, P., Verma, S. S. & Sinha, M. M. Tuning the optical properties of Fe-Au core-shell nanoparticles with spherical and spheroidal nanostructures. *Phys. Lett. Sect. A Gen. At. Solid State Phys.* **383**, 2542–2550 (2019).

128. Gray, S. K. Theory and modeling of plasmonic structures. *J. Phys. Chem. C* **117**, 1983–1994 (2013).

129. Chiu, M. H., Li, J. H. & Nagao, T. Optical properties of au-based and pt-based alloys for infrared device applications: A combined first principle and electromagnetic simulation study. *Micromachines* **10**, (2019).

130. Kwizera, E. A. *et al.* Size- and Shape-Controlled Synthesis and Properties of Magnetic-Plasmonic Core-Shell Nanoparticles. *J. Phys. Chem. C* **120**, 10530–10546 (2016).

131. Chauhan, N., Narang, J., Meena & Pundir, C. S. An amperometric glutathione biosensor based on chitosan-iron coated gold nanoparticles modified Pt electrode. *Int. J. Biol. Macromol.* **51**, 879–886 (2012).

132. Xin, Y. *et al.* A novel H2O2biosensor based on Fe3O 4-Au magnetic nanoparticles coated horseradish peroxidase and graphene sheets-Nafion film

modified screen-printed carbon electrode. *Electrochim. Acta* **109**, 750–755 (2013).

133. Pham, T. T. H. & Sim, S. J. Electrochemical analysis of gold-coated magnetic nanoparticles for detecting immunological interaction. *J. Nanoparticle Res.* **12**, 227–235 (2010).

134. Chuah, K. *et al.* Ultrasensitive electrochemical detection of prostate-specific antigen (PSA) using gold-coated magnetic nanoparticles as 'dispersible electrodes. *Chem. Commun.* **48**, 3503–3505 (2012).

135. Lai, L. M. H. *et al.* Gold-coated magnetic nanoparticles as 'dispersible electrodes' - Understanding their electrochemical performance. *J. Electroanal. Chem.* **656**, 130–135 (2011).

136. Goon, I. Y., Lai, L. M. H., Lim, M., Amal, R. & Gooding, J. J. 'Dispersible electrodes': a solution to slow response times of sensitive sensors. *Chem. Commun.* **46**, 8821 (2010).

137. Silva, S. M. & Justin Gooding, J. Chapter 8: Dispersible electrodes: An approach to developing sensing devices that can quickly detect ultralow concentrations of analyte. *RSC Detect. Sci.* **2016**-**Janua**, 279–295 (2016).

138. Goon, I. Y. *et al.* Fabrication and dispersion of gold-shell-protected magnetite nanoparticles: Systematic control using polyethyleneimine. *Chem. Mater.* **21**, 673–681 (2009).

139. Freitas, M., Viswanathan, S., Nouws, H. P. A., Oliveira, M. B. P. P. & Delerue-Matos, C. Iron oxide/gold core/shell nanomagnetic probes and CdS biolabels for amplified electrochemical immunosensing of Salmonella typhimurium. *Biosens. Bioelectron.* **51**, 195–200 (2014).

140. Jin, Y., Jia, C., Huang, S. W., O'Donnell, M. & Gao, X. Multifunctional nanoparticles as coupled contrast agents. *Nat. Commun.* **1**, 1–8 (2010).

141. MoraesSilva, S., Tavallaie, R., TanzirulAlam, M., Chuah, K. & Gooding, J. J. A Comparison of Differently Synthesized Gold-coated Magnetic Nanoparticles as 'Dispersible Electrodes'. *Electroanalysis* **28**, 431–438 (2016).

142. Bhalla, N., Jolly, P., Formisano, N. & Estrela, P. Introduction to biosensors. *Essays Biochem.* **60**, 1–8 (2016).

143. Mehrotra, P. Biosensors and their applications - A review. *J. Oral Biol. Craniofacial Res.* **6**, 153–159 (2016).

144. Vidotti, M., Carvalhal, R. F., Mendes, R. K., Ferreira, D. C. M. & Kubota, L. T. Biosensors based on gold nanostructures. *J. Braz. Chem. Soc.* **22**, 3–20 (2011).

145. Jazayeri, M. H., Amani, H., Pourfatollah, A. A., Pazoki-Toroudi, H. & Sedighimoghaddam, B. Various methods of gold nanoparticles (GNPs) conjugation to antibodies. *Sens. Bio-Sensing Res.* **9**, 17–22 (2016).

146. Ghosh, P., Han, G., De, M., Kim, C. K. & Rotello, V. M. Gold nanoparticles in delivery applications. *Adv. Drug Deliv. Rev.* **60**, 1307–1315 (2008).

147. Oliveira, J. P. *et al.* Impact of conjugation strategies for targeting of antibodies in gold nanoparticles for ultrasensitive detection of 17β-estradiol. *Sci. Rep.* **9**, 1–8 (2019).

148. Hill, H. D. & Mirkin, C. A. The bio-barcode assay for the detection of protein and nucleic acid targets using DTT-induced ligand exchange. *Nat. Protoc.* **1**, 324–336 (2006).

149. Tsai, T. C. *et al.* In situ study of EDC/NHS immobilization on gold surface based on attenuated total reflection surface-enhanced infrared absorption spectroscopy (ATR-SEIRAS). *Colloids Surfaces B Biointerfaces* **175**, 300–305 (2019).

150. Yu, Z., Grasso, M. F., Cui, X., Silva, R. N. & Zhang, P. Sensitive and Label-Free SERS Detection of Single-Stranded DNA Assisted by Silver Nanoparticles and Gold-Coated Magnetic Nanoparticles. *ACS Appl. Bio Mater.* **3**, 2626–2632 (2020).

151. Wang, J. *et al.* Facile Synthesis of Au-Coated Magnetic Nanoparticles and Their Application in Bacteria Detection via a SERS Method. *ACS Appl. Mater. Interfaces* **8**, 19958–19967 (2016).

152. Rawal, R., Chawla, S. & Pundir, C. S. An electrochemical sulfite biosensor based on gold coated magnetic nanoparticles modified gold electrode. *Biosens. Bioelectron.* **31**, 144–150 (2012).

153. Tavallaie, R. *et al.* Nucleic acid hybridization on an electrically reconfigurable network of gold-coated magnetic nanoparticles enables microRNA detection in blood. *Nat. Nanotechnol.* (2018) doi:10.1038/s41565-018-0232-x.

154. Chen, D., Wu, Y., Hoque, S., Tilley, R. D. & Gooding, J. J. Rapid and ultrasensitive electrochemical detection of circulating tumor DNA by hybridization on the network of gold-coated magnetic nanoparticles. *Chem. Sci.* **12**, 5196–5201 (2021).

155. Ghosh Chaudhuri, R. & Paria, S. Core/shell nanoparticles: Classes, properties, synthesis mechanisms, characterization, and applications. *Chem. Rev.* **112**, 2373–2433 (2012).

156. Bauer, E. & van der Merwe, J. H. crystalline superlattices: From. *Phys. Rev. B* **33**, 3657–3672 (1986).

157. Gilroy, K. D., Ruditskiy, A., Peng, H. C., Qin, D. & Xia, Y. Bimetallic nanocrystals: Syntheses, properties, and applications. *Chem. Rev.* **116**, 10414–10472 (2016).

158. Fan, F. R. *et al.* Epitaxial growth of heterogeneous metal nanocrystals: From gold nano-octahedra to palladium and silver nanocubes. *J. Am. Chem. Soc.* **130**, 6949–6951 (2008).

159. McMurdie, H. F. *et al.* Standard X-Ray Diffraction Powder Patterns from The JCPDS Research Associateship. *Powder Diffr.* **1**, 64–77 (1986).

160. Kwizera, E. A., Chaffin, E., Wang, Y. & Huang, X. Synthesis and properties of magnetic-optical core-shell nanoparticles. *RSC Adv.* **7**, 17137–17153 (2017).

161. Salihov, S. V. *et al.* Recent advances in the synthesis of Fe3O4@AU core/shell nanoparticles. *J. Magn. Magn. Mater.* **394**, 173–178 (2015).

162. Smith, M., McKeague, M. & DeRosa, M. C. Synthesis, transfer, and characterization of core-shell gold-coated magnetic nanoparticles. *MethodsX* **6**, 333–354 (2019).

163. Billen, A. *et al.* Novel synthesis of superparamagnetic plasmonic core-shell iron oxide-gold nanoparticles. *Phys. B Condens. Matter* **560**, 85–90 (2019).

164. Mandal, M. *et al.* Magnetite nanoparticles with tunable gold or silver shell. *J. Colloid Interface Sci.* **286**, 187–194 (2005).

165. Fouad, D. M., El-Said, W. A. & Mohamed, M. B. Spectroscopic characterization of magnetic Fe3O4@Au core shell nanoparticles. *Spectrochim. Acta - Part A Mol. Biomol. Spectrosc.* **140**, 392–397 (2015).

166. Baskakov, A. O. *et al.* Magnetic and interface properties of the core-shell Fe3O4/Au nanocomposites. *Appl. Surf. Sci.* **422**, 638–644 (2017).

167. Lin, J. *et al.* Gold-coated iron (Fe@Au) nanoparticles: Synthesis, characterization, and magnetic field-induced self-assembly. *J. Solid State Chem.* **159**, 26–31 (2001).

168. Jain, P. K., Xiao, Y., Walsworth, R. & Cohen, A. E. Surface Plasmon Resonance Enhanced Rotation Enhancement in Gold-Coated Iron Oxide Nanocrystals. *Nano Lett.* **9**, 1644 (2009).

169. Lim, J. K., Eggeman, A., Lanni, F., Tilton, R. D. & Majetich, S. A. Synthesis and single-particle optical detection of low-polydispersity plasmonic-superparamagnetic nanoparticles. *Adv. Mater.* **20**, 1721–1726 (2008).

170. Hien Pham, T. T., Cao, C. & Sim, S. J. Application of citrate-stabilized gold-coated ferric oxide composite nanoparticles for biological separations. *J. Magn. Magn. Mater.* **320**, 2049–2055 (2008).

171. Lu, Q. H. *et al.* Synthesis and characterization of composite nanoparticles comprised of gold shell and magnetic core/cores. *J. Magn. Magn. Mater.* **301**, 44–49 (2006).

172. Lo, C. K., Xiao, D. & Choi, M. M. F. Homocysteine-protected gold-coated magnetic nanoparticles: Synthesis and characterisation. *J. Mater. Chem.* **17**, 2418–2427 (2007).

173. Ahmad, T. *et al.* Gold-coated iron oxide nanoparticles as a T 2 agent in magnetic resonance imaging. *J. Nanosci. Nanotechnol.* **12**, 5132–5137 (2012).

174. Tamer, U., Gündoğdu, Y., Boyaci, I. H. & Pekmez, K. Synthesis of magnetic core-shell Fe3O4-Au nanoparticle for biomolecule immobilization and detection. *J.*

Nanoparticle Res. **12**, 1187–1196 (2010).

175. Larson, T. A., Bankson, J., Aaron, J. & Sokolov, K. Hybrid plasmonic magnetic nanoparticles as molecular specific agents for MRI/optical imaging and photothermal therapy of cancer cells. *Nanotechnology* **18**, (2007).

176. Bao, F., Yao, J. L. & Gu, R. A. Synthesis of Magnetic Fe2O3/Au core/shell nanoparticles for bioseparation and immunoassay based on surface-enhanced Raman spectroscopy. *Langmuir* **25**, 10782–10787 (2009).

177. Liang, C. H. *et al.* Iron oxide/gold core/shell nanoparticles for ultrasensitive detection of carbohydrate-protein interactions. *Anal. Chem.* **81**, 7750–7756 (2009).

178. Kumar, G. V. P. *et al.* Metal-coated magnetic nanoparticles for surface enhanced Raman scattering studies. *Bull. Mater. Sci.* **34**, 207–216 (2011).

179. Brown, K. R. & Natan, M. J. Hydroxylamine seeding of colloidal Au nanoparticles in solution and on surfaces. *Langmuir* **14**, 726–728 (1998).

180. Lyon, J. L., Fleming, D. A., Stone, M. B., Schiffer, P. & Williams, M. E. Synthesis of Fe oxide Core/Au shell nanoparticles by iterative hydroxylamine seeding. *Nano Lett.* **4**, 719–723 (2004).

181. Faraji, M., Yamini, Y. & Rezaee, M. Magnetic nanoparticles: Synthesis, stabilization, functionalization, characterization, and applications. *J. Iran. Chem. Soc.* **7**, 1–37 (2010).

182. Pal, S., Morales, M., Mukherjee, P. & Srikanth, H. Synthesis and magnetic properties of gold coated iron oxide nanoparticles. *J. Appl. Phys.* **105**, 8–11 (2009).

183. Wang, L. *et al.* Monodispersed core-shell Fe3O4@Au nanoparticles. *J. Phys. Chem. B* **109**, 21593–21601 (2005).

184. Wang, L. *et al.* Iron oxide-gold core-shell nanoparticles and thin film assembly. *J. Mater. Chem.* **15**, 1821–1832 (2005).

185. Xu, Z., Hou, Y. & Sun, S. Magnetic Core/Shell Fe 3 O 4 /Au and Fe 3 O 4 /Au/Ag Nanoparticles with Tunable Plasmonic Properties. *J. Am. Chem. Soc.* (2007) doi:10.1021/ja073057v.

186. Liu, H. L., Hou, P., Zhang, W. X. & Wu, J. H. Synthesis of monosized core-shell Fe3O4/Au multifunctional nanoparticles by PVP-assisted nanoemulsion process. *Colloids Surfaces A Physicochem. Eng. Asp.* **356**, 21–27 (2010).

187. Mikhaylova, M. *et al.* Superparamagnetism of Magnetite Nanoparticles: Dependence on Surface Modification. *Langmuir* **20**, 2472–2477 (2004).

188. Brinson, B. E. *et al.* Nanoshells Made Easy : Improving Au Layer Growth on Nanoparticle Surfaces Nanoshells Made Easy : Improving Au Layer Growth on Nanoparticle Surfaces. *Society* **120**, 14166–14171 (2008).

189. Wang, R. *et al.* Citrate-Regulated Surface Morphology of SiO2@Au Particles to Control the Surface Plasmonic Properties. *J. Phys. Chem. C* **120**, 377–385 (2016).

190. Lim, Y. T., Park, O. O. & Jung, H. T. Gold nanolayer-encapsulated silica particles synthesized by surface seeding and shell growing method: Near infrared responsive materials. *J. Colloid Interface Sci.* **263**, 449–453 (2003).

191. Hu, Y., Meng, L., Niu, L. & Lu, Q. Facile synthesis of superparamagnetic Fe3O 4@polyphosphazene@Au shells for magnetic resonance imaging and photothermal therapy. *ACS Appl. Mater. Interfaces* **5**, 4586–4591 (2013).

192. Xuan, S., Wang, Y. X. J., Yu, J. C. & Leung, K. C. F. Preparation, characterization, and catalytic activity of core/shell Fe 3O4@polyaniline@Au nanocomposites. *Langmuir* **25**, 11835–11843 (2009).

193. Xie, H. *et al.* Fe 3 O 4 Au Core Shell Nanoparticles Modified with Ni 2Nitrilotriacetic Acid Specific to.pdf. 4825–4830 (2010).

194. Zhou, J., Meng, L. & Lu, Q. Core@shell nanostructures for photothermal conversion: Tunable noble metal nanoshells on cross-linked polymer submicrospheres. *J. Mater. Chem.* **20**, 5493–5498 (2010).

195. Park, K. *et al.* Structural and magnetic properties of gold and silica doubly coated γ-Fe2O3 nanoparticles. *J. Phys. Chem. C* **111**, 18512–18519 (2007).

196. Salgueiriño-Maceira, V. *et al.* Bifunctional gold-coated magnetic silica spheres. *Chem. Mater.* **18**, 2701–2706 (2006).

197. Wang, L. *et al.* Core@shell nanomaterials: Gold-coated magnetic oxide nanoparticles. *J. Mater. Chem.* **18**, 2629–2635 (2008).

198. Monaco, I. *et al.* Synthesis of Lipophilic Core-Shell Fe3O4@SiO2@Au Nanoparticles and Polymeric Entrapment into Nanomicelles: A Novel Nanosystem for in Vivo Active Targeting and Magnetic Resonance-Photoacoustic Dual Imaging. *Bioconjug. Chem.* **28**, 1382–1390 (2017).

199. Fu, J. *et al.* Preparation of silver nanocables wrapped with highly cross-linked organic-inorganic hybrid polyphosphazenesjvia a hard-template approach. *J. Phys. Chem. C* **112**, 16840–16844 (2008).

200. Zhou, J., Meng, L., Lu, Q., Fu, J. & Huang, X. Superparamagnetic submicro-megranates: Fe3O4 nanoparticles coated with highly cross-linked organic/inorganic hybrids. *Chem. Commun.* 6370–6372 (2009) doi:10.1039/b914394g.

201. Wan, J., Cai, W., Meng, X. & Liu, E. Monodisperse water-soluble magnetite nanoparticles prepared by polyol process for high-performance magnetic resonance imaging. *Chem. Commun.* **4**, 5004–5006 (2007).

202. Allie Kwizera, E. *et al.* Size-and Shape-Controlled Synthesis and Properties of Magnetic-Plasmonic Core-Shell Nanoparticles Graphical abstract HHS Public

Access. *J Phys Chem C Nanomater Interfaces* **120**, 10530–10546 (2016).

203. Zhou, X. *et al.* Fabrication of cluster/shell Fe 3 O 4 /Au nanoparticles and application in protein detection via a SERS method. *J. Phys. Chem. C* **114**, 19607–19613 (2010).

204. Chin, S. F., Iyer, K. S. & Raston, C. L. Facile and green approach to fabricate gold and silver coated superparamagnetic nanoparticles. *Cryst. Growth Des.* **9**, 2685–2689 (2009).

205. Zhang, Q. *et al.* Tailored synthesis of superparamagnetic gold nanoshells with tunable optical properties. *Adv. Mater.* **22**, 1905–1909 (2010).

206. Hou, X. *et al.* Facile synthesis of multifunctional Fe3O4@SiO2@Au magneto-plasmonic nanoparticles for MR/CT dual imaging and photothermal therapy. *RSC Adv.* **7**, 18844–18850 (2017).

207. Adams, S. A. *et al.* Fe $_3$ O $_4$ @SiO $_2$ Nanoparticles Functionalized with Gold and Poly(vinylpyrrolidone) for Bio-Separation and Sensing Applications. *ACS Appl. Nano Mater.* acsanm.8b00225 (2018) doi:10.1021/acsanm.8b00225.

208. Dong, W. *et al.* Facile synthesis of monodisperse superparamagnetic Fe 3O 4 Core@hybrid@Au shell nanocomposite for bimodal imaging and photothermal therapy. *Adv. Mater.* **23**, 5392–5397 (2011).

209. Woodard, L. E. *et al.* Nanoparticle architecture preserves magnetic properties during coating to enable robust multi-modal functionality. *Sci. Rep.* **8**, 1–13 (2018).

210. Hu, T. T., Wang, J. X., Shen, Z. G. & Chen, J. F. Engineering of drug nanoparticles by HGCP for pharmaceutical applications. *Particuology* **6**, 239–251 (2008).

211. Kim, J. W. *et al.* Single-cell mechanogenetics using monovalent magnetoplasmonic nanoparticles. *Nat. Protoc.* **12**, 1871–1889 (2017).

212. Jang, J. T. *et al.* Critical enhancements of MRI contrast and hyperthermic effects by dopant-controlled magnetic nanoparticles. *Angew. Chemie - Int. Ed.* **48**, 1234–1238 (2009).

213. Liu, C., Zou, B., Rondinone, A. J. & Zhang, Z. J. Chemical control of superparamagnetic properties of magnesium and cobalt spinel ferrite nanoparticles through atomic level magnetic couplings. *J. Am. Chem. Soc.* **122**, 6263–6267 (2000).

214. Zhu, M., Lerum, M. Z. & Chen, W. How to prepare reproducible, homogeneous, and hydrolytically stable aminosilane-derived layers on silica. *Langmuir* **28**, 416–423 (2012).

215. Sood, A., Arora, V., Shah, J., Kotnala, R. K. & Jain, T. K. Ascorbic acid-mediated synthesis and characterisation of iron oxide/gold core–shell nanoparticles. *J. Exp. Nanosci.* **11**, 370–382 (2016).

216. Khosroshahi, M. E. & Ghazanfari, L. Physicochemical characterization of Fe3O4/SiO2/Au multilayer nanostructure. *Mater. Chem. Phys.* (2012) doi:10.1016/j.matchemphys.2011.12.047.

217. Mohapatra, J. *et al.* Size-dependent magnetic and inductive heating properties of Fe3O4nanoparticles: Scaling laws across the superparamagnetic size. *Phys. Chem. Chem. Phys.* **20**, 12879–12887 (2018).

218. Neuberger, T., Schöpf, B., Hofmann, H., Hofmann, M. & Von Rechenberg, B. Superparamagnetic nanoparticles for biomedical applications: Possibilities and limitations of a new drug delivery system. *J. Magn. Magn. Mater.* **293**, 483–496 (2005).

219. Nightingale, A. M. *et al.* A stable droplet reactor for high temperature nanocrystal synthesis. *Lab Chip* **11**, 1221–1227 (2011).

220. Arndt, D., Thöming, J. & Bäumer, M. Improving the quality of nanoparticle production by using a new biphasic synthesis in a slug flow microreactor. *Chem. Eng. J.* **228**, 1083–1091 (2013).

221. Khan, S. A., Günther, A., Schmidt, M. A. & Jensen, K. F. Microfluidic synthesis of colloidal silica. *Langmuir* **20**, 8604–8611 (2004).

222. Krishnadasan, S., Brown, R. J. C., DeMello, A. J. & DeMello, J. C. Intelligent routes to the controlled synthesis of nanoparticles. *Lab Chip* **7**, 1434–1441 (2007).

223. Jähnisch, K., Hessel, V., Löwe, H. & Baerns, M. *Chemistry in Microstructured Reactors*. *Angewandte Chemie - International Edition* vol. 43 (2004).

224. Hoang, P. H., Park, H. & Kim, D. P. Ultrafast and continuous synthesis of unaccommodating inorganic nanomaterials in droplet- and ionic liquid-assisted microfluidic system. *J. Am. Chem. Soc.* **133**, 14765–14770 (2011).

225. Krishna, K. S., Li, Y., Li, S. & Kumar, C. S. S. R. Lab-on-a-chip synthesis of inorganic nanomaterials and quantum dots for biomedical applications. *Adv. Drug Deliv. Rev.* **65**, 1470–1495 (2013).

226. Zhao, C. X., He, L., Qiao, S. Z. & Middelberg, A. P. J. Nanoparticle synthesis in microreactors. *Chem. Eng. Sci.* **66**, 1463–1479 (2011).

227. Dunne, P. W., Munn, A. S., Starkey, C. L., Huddle, T. A. & Lester, E. H. Continuous-flow hydrothermal synthesis for the production of inorganic nanomaterials. *Philos. Trans. R. Soc. A Math. Phys. Eng. Sci.* **373**, (2015).

228. Frenz, L. *et al.* Droplet-based microreactors for the synthesis of magnetic iron oxide nanoparticles. *Angew. Chemie - Int. Ed.* **47**, 6817–6820 (2008).

229. Abou-Hassan, A., Bazzi, R. & Cabuil, V. Multistep continuous-flow microsynthesis of magnetic and fluorescent γ-Fe2O3OSiO2 core/shell nanoparticles. *Angew. Chemie - Int. Ed.* **48**, 7180–7183 (2009).

230. Duraiswamy, S. & Khan, S. A. Plasmonic nanoshell synthesis in microfluidic composite foams. *Nano Lett.* **10**, 3757–3763 (2010).

231. Ahrberg, C. D., Wook Choi, J. & Geun Chung, B. Automated droplet reactor for the synthesis of iron oxide/gold core-shell nanoparticles. *Sci. Rep.* **10**, 1737 (2020).

232. Ma, J., Lee, S. M. Y., Yi, C. & Li, C. W. Controllable synthesis of functional nanoparticles by microfluidic platforms for biomedical applications-a review. *Lab Chip* **17**, 209–226 (2017).

Chapter 2

Materials and methods

This chapter layouts a detailed list of the materials and chemicals used in this project. This chapter will also provide details on how nanoparticles were cleaned after synthesis and prepared for characterisation. In addition, descriptions of all the instrumentation and characterization techniques used to achieve the results are presented in this thesis.

2.1. Materials

The list of chemicals and materials used in this project, as well abbreviations/Formula, specification/purity, and supplier of each material, are detailed in table 2.1.

Table 2.1. List of chemicals used in this thesis.

Chemical	Abbreviation/Formula	Specification/Purity	supplier
iron(III) acetylacetonate	Iron acac	99.9%	Sigma-Aldrich
oleylamine	OLA	70% & 98%	Sigma-Aldrich
oleic acid	$C_{18}H_{34}O_2$	90%	Sigma-Aldrich
trioctylamine	$C_{24}H_{51}N$	98%	Sigma-Aldrich
poly (oxyethylene)nonylphenyl ether)	Igepal CO520	-	Sigma-Aldrich
ammonium hydroxide solution	Ammonia water	28-30%	Sigma-Aldrich
tetraethyl orthosilicate	TEOS	98%	Sigma-Aldrich
(3-aminopropyl)trimethoxysilane	APTES	99%	Sigma-Aldrich
[3-(2-aminoethylamino)propyl]trimethoxysilane	AEAPTES	≥80%	Sigma-Aldrich
dimethyl sulfoxide	DMSO	Analytical grade	Chem-supply
gold (III) chloride trihydrate	$HAuCl_4.\ 3H_2O$	≥99.9	Sigma-Aldrich
sodium hydroxide	NaOH	≥97%	Sigma-Aldrich
tetrakis(hydroxymethyl)phosphonium chloride solution	THPC	80% in H_2O	Sigma-Aldrich
hydroxylamine hydrochloride	$NH_2OH.HCL$	99%	Sigma-Aldrich
trizma base	$NH_2C(CH_2OH)_3$	≥99.9%	Sigma-Aldrich
bis(p-sulfonatophenyl)phenylphosphine dihydrate dipotassium salt	BSPP	97%	Sigma-Aldrich
4-aminothiophenol	4-ATP	97%	Sigma-Aldrich
phosphate-buffered saline solution	PBS	pH ≈ 7.6	Sigma-Aldrich

sodium phosphate monobasic	NaH_2PO_4	≥98%	Sigma-Aldrich
sodium phosphate dibasic	Na_2HPO_4	99%	Sigma-Aldrich
potassium carbonate	K_2CO_3	≥99%	Sigma-Aldrich
hydrochloric acid	HCl	32%	Chem-supply
toluene	$C_6H_5CH_3$	Analytical grade	Chem-supply
cyclohexane	C_6H_{12}	Analytical grade	Chem-supply
ethanol 96%	EtOH	Analytical grade	Chem-supply
ethanol absolute	EtOH	Analytical grade	Chem-supply
hydrogen peroxide	H_2O_2	27-30% in H_2O	Sigma-Aldrich
sulfuric acid	H_2SO_4	98%	Sigma-Aldrich
nitric acid	HNO_3	70%	Sigma-Aldrich
tri-sodium citrate	$Na_3C_6H_5O_7$	≥99%	Sigma-Aldrich
sodium borohydride	$NaBH_4$	≥98%	Sigma-Aldrich
hydrofluoric acid	HF	48%	Sigma-Aldrich
4-mercaptobenzoic acid	4-MBA	99%	Sigma-Aldrich
1-octadecene	$C_{18}H_{36}$	90%	Sigma-Aldrich
iron(0) pentacarbonyl	$Fe(CO)_5$	≥99.99%	Sigma-Aldrich
gold-coated magnetic nanoparticles 100 nm	Fe_3O_4@Au	BioPure	Nanopartz
gold-coated magnetic nanoparticles 50 & 250 nm	Fe_3O_4@Au	BioPure	Creative diagnostics
gold-coated magnetic nanoparticles 150 nm	Fe_3O_4@Au	BioPure	Nanocomposix
gold-coated magnetic nanoparticles 50 & 250 nm	Fe_3O_4@Au	BioPure	Nanoimmunotech
AmiconUltra-15 centrifugal units	-	-	Sigma-Aldrich
polylactic Acid	PLA	-	Flashforge
sodium hydride	NaH	60% in mineral oil	Sigma-Aldrich
2,4-pentanedione	PD	99%	Fisher Scientific
1-iodooctadecane	1-IOD	95%	Sigma-Aldrich
diethyl ether	ether	≥99%	Sigma-Aldrich

2.1.1. Nucleic Acids

The nucleic acids that were used in this project (table 2.2) were synthesized and purchased from Biosearch Technologies (Novato).

Table 2.2. List of nucleic acid sequences used in this project.

Name	Sequence
Methylene blue label probe DNA	5′-SH-$(CH_2)_3$-p-TCAACATCAGTCTGATAAGCTA-$(CH_2)_3$- MB-3′
Complementary RNA target (miRNA-21)	5′-UAGCUUAUCAGACUGAUGUUGA-3′

2.2. Washing

All the glassware was cleaned with acetone, ethanol, and Milli-Q water before reactions. All the glassware used for gold seeding and gold coating of nanoparticles was cleaned in piranha solution (H_2SO_4:H_2O_2 in a 3:1 ratio by volume), followed by being lightly rinsed with Milli-Q water, then dried in an oven and then lastly cleaned by *aqua-regia* (HCl: HNO_3 in a 3:1 ratio by volume) that was followed by being rinsed with Milli-Q water and then dried in an oven.

2.3. 3D printing

The Y-shaped pieces used to scale up the synthesis of gold-coated magnetic nanoparticles was designed, and 3D printed by another member of the SMS group, Daniel Hagness. The program Autodesk Inventor Professional 2021 was used to design the pieces and a Flashforge Creator Pro 2016 3D printer was used to print the pieces. All the pieces were made out of Flashforge branded PLA.

2.4. Synthesis of 3-octadecyl-2,4-pentanedione (OD-PD)

To synthesize the zero-valent iron core iron oxide nanoparticles, 3-octadecyl-2,4-pentanedione (OD-PD) was used as a stabilizing surfactant. OD-PD is not commercially available and has to be synthesized in the lab. Lucy Gloag, another SMS group member, has synthesized OD-PD in our lab according to a method reported by Bleier et al[1]. In short, 0.737 g of NaH was added to a 250 mL three-neck round bottom flask and was followed by the addition of 150 mL anhydrous DMF under argon. A total of 1.54 g of PD was then added dropwise to the solution until the NaH was completely dissolved.

Next, 7 g of 1-IOD was quickly added while the argon flow was high, and then the reaction was heated to 90°C and kept at that temperature for 4 days. The reaction was cooled down to room temperature and neutralized with a 1 M HCl solution. The solution was then added to a separating funnel and the solution was extracted into diethyl ether and the diethyl ether layer was washed with 1 M HCl solution three times with the 1 M HCl solution layer being removed each time. Then the solution was heated to dissolve the rest of the solids. The solution was then put inside a freezer overnight. The solid product was filtered the following day right after removing it from the freezer and washed with diethyl ether twice and stored at $18^{\circ}C$. The product was then placed inside a vacuum oven without heating for 30 minutes. The OD-PD was then transferred into a 25 mL vial and stored at room temperature inside a desiccator.

2.5. Purification of nanoparticles post-synthesis

To remove any by-products, surfactants, solvents, and excess precursors from the nanoparticle solution after the reaction, purification was done *via* centrifugation and magnetic separation by using a neodymium magnet. Centrifugation can purify the particles from by-products because the particles have a much greater mass than solvents, surfactants, and other reaction by-products. The magnetic separation of particles separates the magnetic nanoparticles from the non-magnetic materials and purifies the magnetic nanoparticles. Centrifugation of the particles was performed by transferring the nanoparticle solution to falcon tubes and changing the speed, the time and the solvent to the antisolvent mixture to help precipitate specific nanoparticles on the bottom of the falcon tubes. The superparamagnetic iron oxide nanoparticles, silica-coated conglomerates of superparamagnetic iron oxide nanoparticles, zero-valent iron core iron oxide shell nanoparticles and silica-coated zero-valent iron core iron oxide shell nanoparticles were cleaned using a centrifuge. Gold seeded and gold-coated magnetic nanoparticles were cleaned by magnetic separation by using a neodymium magnet. Description of the required cleaning steps for each novel nanoparticle is detailed in the following chapters.

2.6. Modification of glass coverslips with APTES

In order to investigate the properties of the particles synthesized in this thesis via dark-field microscopy and scanning electron microscopy, the gold-coated magnetic nanoparticles were immobilized onto the surface of a glass coverslip (22 mm×22 mm) by following a salinization process.

The salinization process is where a layer of APTES was introduced onto the surface of a clean coverslip and the method is as following:

1. The coverslip was immersed in 1 M NaOH and left in a sonicator for 20 minutes.
2. The coverslip was washed with a copious amount of Milli-Q water.
3. The coverslip was immersed in absolute ethanol and left in a sonicator for 20 minutes.
4. The coverslip was dried by nitrogen flow.
5. The coverslip was cleaned via plasma cleaner.
6. A solution having a composition of 5% APTES, 5% Milli-Q water and 90% absolute ethanol was prepared.
7. The coverslip was immersed in the solution prepared in step 6 and left for 90 minutes.
8. The coverslip was then washed with Milli-Q water and absolute ethanol and dried.
9. To immobilize the gold-coated magnetic nanoparticles onto the surface of the coverslip, one or two drops of gold-coated magnetic suspension were introduced on the surface and left for 30 minutes.
10. After immobilization, the glass coverslip was washed with Milli-Q water and dried.

2.7. Characterization methods

Transmission electron microscopy (TEM), Scanning electron microscopy (SEM), Dynamic light scattering (DLS), UV-Vis spectroscopy, X-Ray Diffraction (XRD), Dark-field microscopy, superconducting quantum interference device (SQUID)

magnetometer, Raman spectroscopy, cyclic voltammetry (CV) and square wave voltammetry (SQWV) are measurement techniques that were used to study the properties and biosensing capabilities of the synthesized nanoparticles.

2.7.1. Electron microscopy

The fundamental principles of electron microscopy and light microscopy are similar to each other. The main difference between the two methods is related to the use of electrons instead of light as an imaging source in the case of electron microscopy. Electron microscopes were developed to overcome the limitation of light microscopy. Since the wavelength of electrons is much smaller than visible light, an image with a much higher resolution of a smaller sample can be obtained via electron microscopy. The most common electron microscopes are scanning electron microscope (SEM) and transmission electron microscope (TEM). Figure 2.1 details of the components of both microscopes are illustrated.

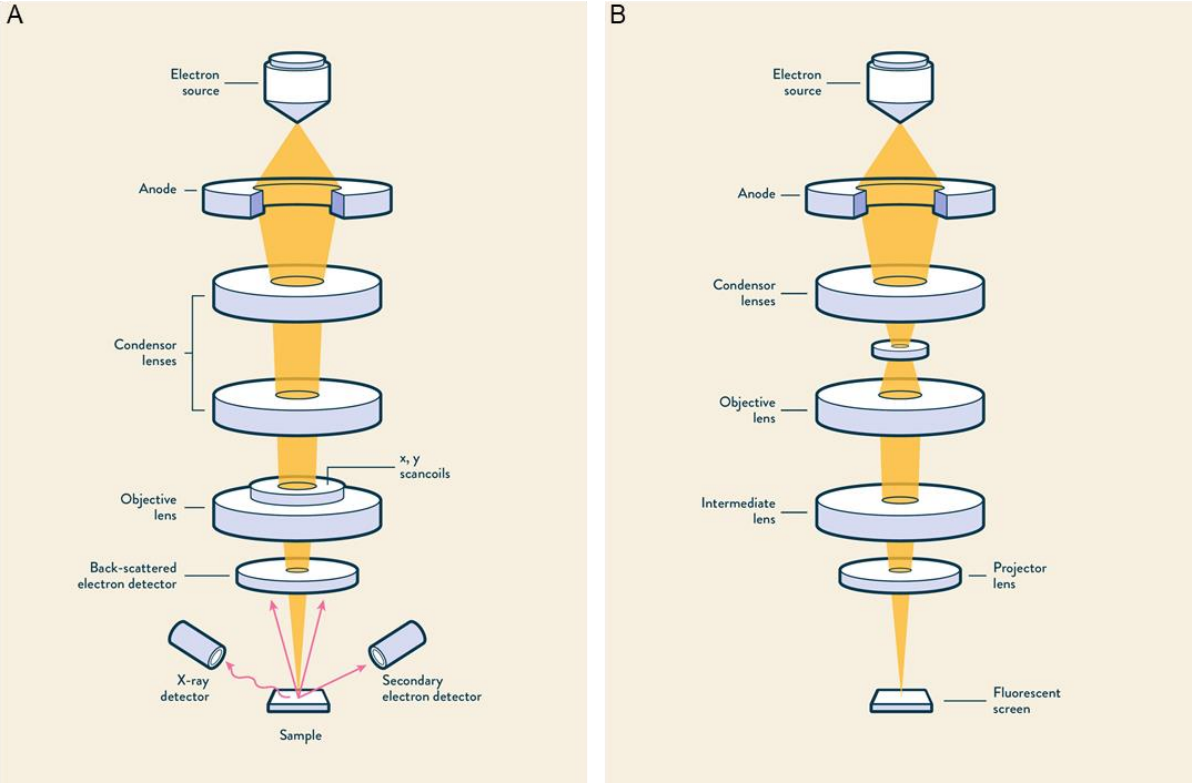

Figure 3.1. Schematic illustration of A) Scanning electron microscopy (SEM) and B) Transmission electron microscopy (TEM). The picture is taken from technology networks' website: https://www.technologynetworks.com/analysis/articles/sem-vs-tem-331262.

To create an image, a TEM uses a high voltage electron beam. The electron gun at top of the TEM microscope emits electrons that pass through the vacuum tube inside the microscope where an electromagnetic lens focuses the electrons to a fine beam of electrons. The focused beam then goes to the sample where the electrons will either scatter off or transmit through and hit the fluorescent screen to develop an image. The picture of the sample is then formed in different shades based on the density of transmitted electrons. SEM uses similar principles to create an image. In short, SEM scans a focused beam of electrons over a particular surface and produces various signals as the result of the interaction of the electron beam with the surface and creates the SEM image. The images created by both microscopes can then be captured by an imaging device, typically it is a digital camera. ImageJ software was used for the analysis of the images in this project, TEM was used to confirm the size, shape and structure of nanoparticles at each step of the synthesis. SEM was used to confirm the data obtained from the dark field microscopy measurements.

TEM images were taken using a Phillips CM200 TEM microscope and a FEI Tecnai G2 20 TEM microscope. SEM images were taken using a FEI Nova NanoSEM 450 FE-SEM. All the electron microscopy was done at the Mark Wainwright Analytical Centre at UNSW.

2.7.1.1. Sample preparation for TEM

To obtain low-resolution TEM images of nanoparticles, diluted nanoparticle suspensions were drop-casted onto 200 mesh formvar-coated Cu grids. The grids were left to dry in the air while being held by a self-closing tweezer. In the case of particles that were dispersed in milli-Q water, air drying was done overnight.

2.7.1.2. Sample preparation for SEM

Because glass coverslips are not conductive, we need to coat the surface of them with a layer of conductive elements such as platinum or palladium. To do so, the glass coverslips were first mounted on a conductive stab, then a 5 nm platinum coating was sputtered onto the surface of glass coverslips via a Leica EM ACE600 sputter coater.

2.7.2. Dynamic light scattering (DLS) and zeta potential

Measuring the hydrodynamic size of the nanoparticles floating in the solution is possible by using DLS. A Malvern Zetasizer ZS™ instrument was used to determine the nanoparticles hydrodynamic size and zeta potentials. We know that particles are constantly moving in the solution in all directions and as a result, they are colliding with liquid molecules. The nanoparticles in solution are illuminated by a laser beam and the fluctuations of the scattered light are detected at a known scattering angle θ by a fast photon detector and it measures the hydrodynamic size of the particles. In this thesis, DLS was used to investigate not only the size of the particles but also the resistance towards the magnetic aggregation of the particles and the particles' stability in Milli-Q water over time. The zeta potential was used to determine if the surface charge of the particles is positive or negative and also used for determining whether the particles are aggregated or not.

DLS and zeta potential measurements were done using a Malvern Zetasizer at the Flow Cytometry Core Facility at UNSW.

2.7.3. UV-Vis spectrophotometer

Ultraviolet-visible spectroscopy (UV-Vis) is a technique based on measuring the intensity of light before and after it passes through a sample. For nanoparticles with plasmonic properties, due to LSPR, absorbance happens in the visible region of the electromagnetic spectrum. In a normal UV-Vis spectrum, this is shown by a specific peak at a certain Wavelength. By reducing or increasing the size of the plasmonic nanoparticles the position and intensity of the peak change. This technique is also applicable to investigate whether a plasmonic shell has formed on the magnetic nanoparticles considering that magnetic nanoparticles just scatter the light and hence no peak can be observed. As soon as a plasmonic shell is formed around the magnetic nanoparticles due to LSPR, a peak at a certain wavelength with a certain intensity can be observed. This information could be used to determine if a sample is fully coated or not. Finally, based on the Beer-Lambert law (equation 2.1) and by knowing the extinction coefficient of the nanoparticles, the concentration of the nanoparticles in the solution can be calculated.

$$A = \varepsilon bC \quad (2.1)$$

Where A is the absorbance, ε is the molar absorptivity, b is the length of the light path and C is the molar concentration.

All the UV-Vis measurements were done by using a Cary 60 UV-Vis Agilent Technologies spectrophotometer.

2.7.4. Superconducting quantum interference device (SQUID) magnetometer

SQUID is an apparatus used for measuring very weak signals, such as small changes in the electromagnetic energy field. Due to its innate high sensitivity and high dynamic range, the SQUID technique can detect an extremely small disruption in a magnetic field produced by structural anomalies located on the surface or inside the material volume. Magnetic measurements of nanoparticles were done using a Quantum Design MPMS XL.

To prepare a sample for the SQUID measurement, a plastic straw was loaded with a colloidal solution of magnetic nanoparticles. The particles were left to dry at room temperature and then the straw was sealed, weighed, and sent for measurements.

M-H loops or hysteresis loops measure the generated magnetization of particles as a function of the applied magnetic field. The produced hysteresis loop can give us the magnetization saturation of the particles and can also be a good indication of the magnetic behaviour of the sample, such as superparamagnetism, ferromagnetism, ferrimagnetism.

The magnetic properties of particles in this thesis were investigated by using SQUID magnetometry with an external magnetic field ranging from 60000 Oe to -60000 Oe at 300 K.

2.7.5. Dark-field microscopy

The dark-field microscopy was performed with an Olympus BX51 dark-field microscope. A 100 W halogen lamp was used as the excitation source and was focused through a darkfield condenser (NA > 0.8). The scattered light was collected by a 40x dark-field objective. The images were directly taken by a commercially available CMOS camera

(Canon 100D, 22.3mm x 14.9mm sensor size, 4.3 µm x 4.3 µm pixel size). The images were saved and processed as Canon RAW (.CR2) 14-bit colour files.

2.7.6. X-ray diffraction (XRD)

Materials are composed of crystals and each of these crystals are composed of a regular arrangement of atoms and each atom is composed of a nucleus surrounded by a cloud of electrons. Since the wavelength of an X-ray is similar to the distance between atoms in a crystal, the diffraction of X-ray incident to a crystal plane can be used to measure the distance between the atoms. As the atomic spacing of each material is unique, this technique could be used to identify the crystal structure of each material and give insights into the composition of the nanoparticles based on the crystallographic database. Bragg's law (equation 2.2) describes the relationship between atomic spacing (d) and the angle of diffraction (θ):

$$n\lambda = 2dsin\theta \qquad 2.2$$

Where λ is the wavelength of the X-ray, d is the spacing of the crystal layers, θ is the incident angle and n is an integer. The XRD data in this thesis was acquired by an Empyrean 2 (Malvern Panalytical) X-ray diffractometer using a Co Kα (1.79°A) radiation source at Solid State & Elemental Analysis Unit at UNSW.

2.7.7. Electrochemical measurements

Electrochemical measurements were performed for two reasons. The first reason is to see if the new nanoparticles made in this thesis can satisfy the requirements needed for an electrochemical biosensing agent. Square wave voltammetry (SQWV) was chosen for this matter because this technique is highly sensitive, it can discriminate against the charging background current, and it also has a high sampling speed. The second reason was to use cyclic voltammetry (CV) to confirm the existence of a complete gold shell around the magnetic nanoparticles.

Cyclic voltammetry (CV) and square wave voltammetry (SQWV) were performed using a CHI potentiostat (CHI instruments, model no. 600-60D). To perform the electrochemical experiments a unique set-up (figure 2.2) was used.

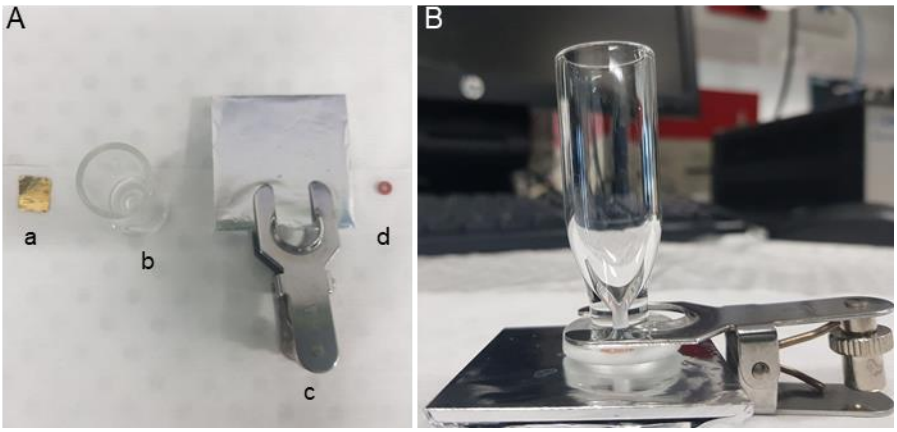

Figure 2.2. A) The components of the set up used in this project for electrochemical measurements consisted of a) gold foil, b) cup-shaped glass cell, c) clamp and base layer covered with aluminum foil, and d) plastic gasket. B) photo representative of the arrangement of all the components together for electrochemical measurements.

The set-up was comprised of a cup-shaped glass cell with a 3 mm diameter hole at the bottom, a gold foil as a working electrode and a plastic gasket (O ring with 2 mm inner diameter) which was placed on top of the gold foil and underneath the glass cup. A platinum working electrode and a saturated Ag/AgCl reference electrode were placed carefully inside the glass cup and connected to their respective terminals of the CHI potentiostat. All the electrochemical experiments were repeated three times to ensure reproducibility.

2.8. References

1. Bleier, G. C., Watt, J., Simocko, C. K., Lavin, J. M. & Huber, D. L. Reversible Magnetic Agglomeration: A Mechanism for Thermodynamic Control over Nanoparticle Size. *Angew. Chemie - Int. Ed.* **57**, 7678–7681 (2018).

Chapter 3

Commercially available gold-coated magnetic nanoparticles

3.1. Chapter overview:

This chapter aims to dive into the world of state-of-the-art commercially available gold-coated magnetic nanoparticles to give us a perspective of the challenges and properties to expect from these nanoparticles. In the two decades since the first reports on the gold coating of magnetic nanoparticles emerged, many methods and approaches for synthesizing these materials have been introduced.[1,2] The dual properties (conductivity and LSPR) of these nanomaterials make them beneficial for many applications as discussed in the introductory chapter.[3] As demand for these nanomaterials grow, companies around the world started to invest in synthesizing them. A wide range of products with different shapes, sizes, gold thicknesses and different functionalities are available commercially all around the world. This raises the question is there any reason to now synthesize these nanoparticles?

In this chapter, this question is explored. A survey of comparison of the properties of gold-coated magnetic nanoparticles acquired from the most well-known nanotechnology companies around the world. This was done to enlarge our understanding of the possible challenges and advantages these nanoparticles could provide for the scientific community. The gold-coated magnetic nanoparticles were acquired from Nanopartz™, Creative Diagnostic®, and Nanoimmunotech. These three companies were chosen as there were not many companies providing gold-coated magnetic nanoparticles at the time and also, they were the most recommended ones.

3.2. Experimental section:

Samples were ordered on two separate occasions from each company from early 2018 to the end of 2018. Each sample was characterized as it was received from the companies. All the samples were kept in the fridge at 4° C away from light by wrapping the sample with aluminium foil. TEM images of the nanoparticles were acquired by a Phillips CM200 TEM microscope at an accelerated voltage of 200 kV. EDX mapping of the gold-coated magnetic nanoparticles was acquired from an F200 TEM microscope. Images acquired from TEM was analysed using ImageJ. To prepare the TEM grid for imaging a drop of the diluted sample was drop-cast onto a carbon-coated copper grid. XRD was performed on an Empyrean 2 (Malvern Panalytical) X-ray diffractometer with

Co Kα (1.79 Å) radiation sample was analysed from 30° to 100° (2θ). To prepare the samples for XRD, nanoparticles were deposited on an XRD holder dropwise to produce a uniform layer. To measure the hydrodynamic size of the gold-coated magnetic nanoparticles a Zetasizer Nano ZS was used. To measure the absorbance spectra of the gold-coated magnetic nanoparticles a Cary 60 single-beam UV-Vis spectrophotometer was used. The magnetic property was investigated by SQUID magnetometry with an external magnetic field ranging from 20000 Oe to -20000 Oe for samples acquired from Creative Diagnostics and from 10000 to -10000 for samples acquired from Nanoimmunotech and Nanopartz. All the magnetic measurements were performed at 300 K. The SQUID data was not normalized based on ICP because the composition of nanoparticles was not fully recognized as the companies refused to reveal the exact composition of their nanoparticles. For the ICP measurements, the gold-coated magnetic nanoparticles were digested with a combination or either Hydrofluoric acid or Aqua regia (3:1 hydrochloric acid to nitric acid) mixture, and it is important to choose the acidic mixture based on the composition that needs to be digested.

3.3. Gold-coated magnetic nanoparticles acquired from Nanopartz™

Nanopartz™ is a company making a variety of nanoparticles from gold, polymers, silver, and gold-coated magnetic nanoparticles. According to the commercial brochure, gold-coated-coated magnetic nanoparticles here is comprised of magnetite nanoparticles with a layer of gold (15 nm thickness) on their surfaces. The hydrodynamic size of the nanoparticles was 100 nm with an absorbance peak at 559 nm. The concentration of the nanoparticles was reported to be 1.24×10^{12} particles/mL.

3.3.1. Nanoparticles' morphology and composition

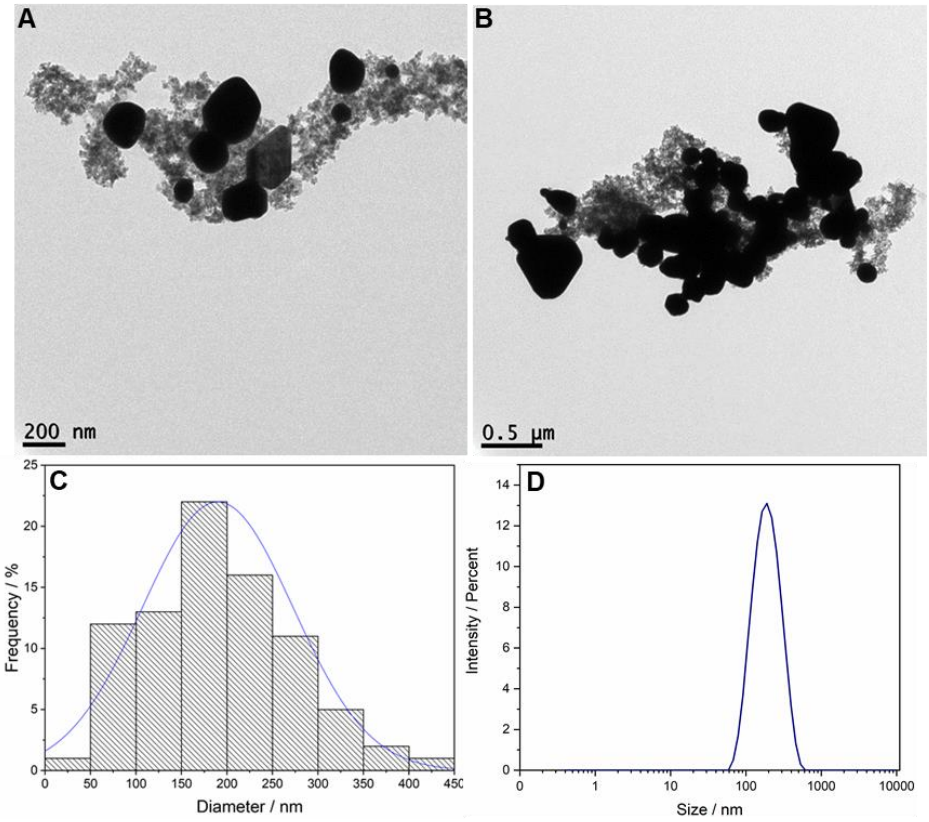

Figure 3.1. A, B) TEM images of gold-coated magnetic nanoparticles acquired from Nanopartz™, C) the corresponding histogram of the size of gold-coated magnetic nanoparticles acquired from Nanopartz™ and D) Dynamic light scattering (DLS) of the gold-coated magnetic nanoparticles.

As it can be seen from the Figure 3.1 A and B the nanoparticles are a combination of two separate nanoparticles bigger sizes with black colour and smaller sizes grey nanoparticles. The corresponding histogram in Figure 3.1 C shows that the

nanoparticles are not monodisperse with an average size of 189 ± 82 nm. It is also, worth noting that the nanoparticles have a variety of shapes from spherical to cubic and even with no specific shape. DLS revealed that the hydrodynamic size of the nanoparticles is 168 nm with a polydispersity index (PDI) of 0.192. The low PDI of the nanoparticles recorded using DLS was in contrast to the findings of the TEM which showed that the nanoparticles were quite polydisperse. This could be explained by the fact that the hydrodynamic size and DLS, in general, are hugely affected by the bigger size nanoparticles, and the effect of the smaller size nanoparticles is often not observed in DLS measurements.[4] To take a deeper look at the composition of the nanoparticles EDX mapping was performed.

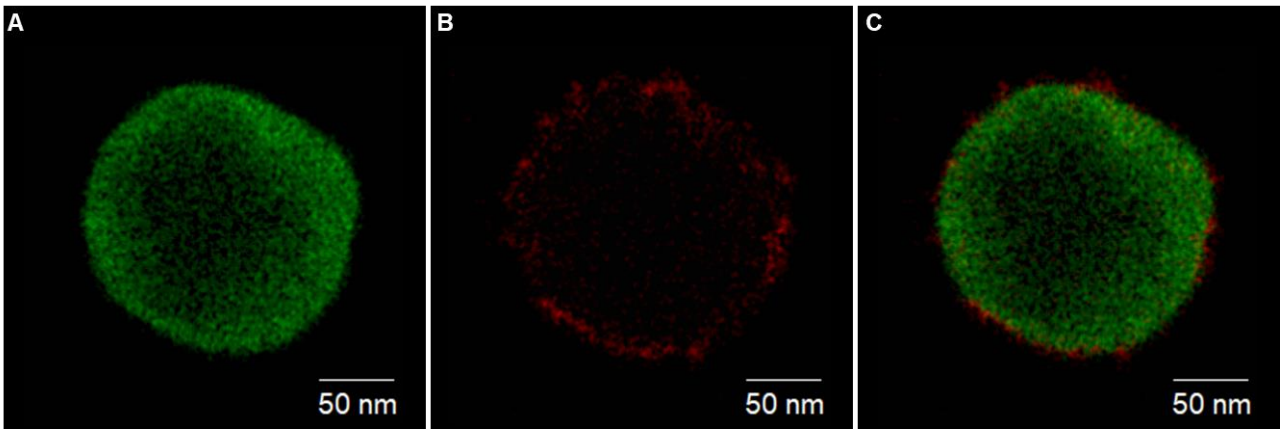

Figure 3. 2. EDX map of the elements A) gold B) iron and C) merged gold and iron of the gold-coated magnetic nanoparticles acquired from Nanopartz™.

As it can be seen from Figure 3.2 the nanoparticles seem to be a combination of gold nanoparticles and iron oxide nanoparticles. It is worth noting that a ring of iron is present around the gold, which shows that the iron could be seen if present through gold. The size of gold nanoparticles seems to be bigger than the size of the iron oxide nanoparticles. The green in Figure 3.2 which represents gold could be assigned to the black nanoparticles in Figure 3.1 A which shows that the big black nanoparticles are simply gold nanoparticles. The red dots in Figure 3.2 B are iron and could be seen in Figure 3.1 as grey which is iron oxide nanoparticles.

To further characterize the nanoparticles composition and crystal structure XRD was performed.

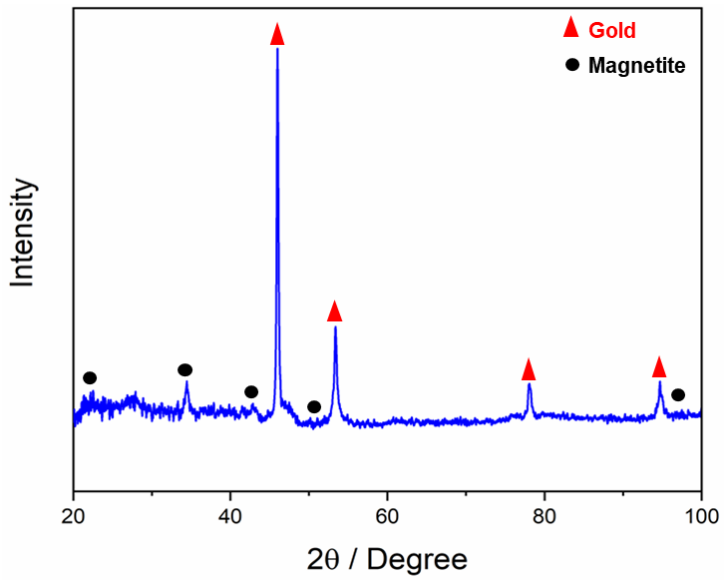

Figure 3.3. X-ray diffraction patterns of gold-coated magnetic nanoparticles acquired from Nanopartz™.

As shown in Figure 3.3, four major peaks (red triangles) could be assigned to the gold crystal structure and 5 smaller peaks (black spheres) shows the magnetite crystal structure. It is worth mentioning that the existence of other peaks in the pattern, and also slight deviation in the major peaks, could be due to the fact that the nanoparticles comprise other crystal structures such as maghemite.[5–7]

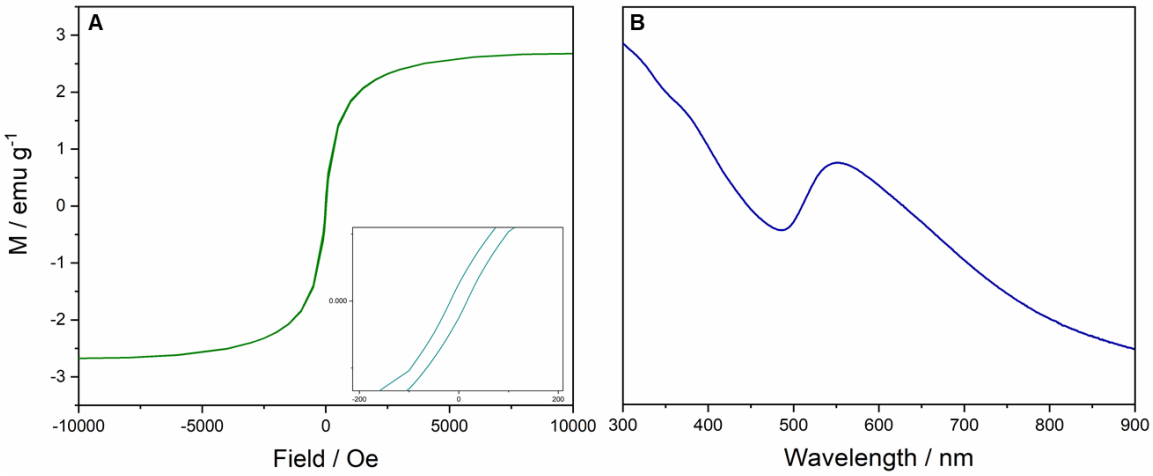

Figure 3.4. A) SQUID magnetometry measurements of gold-coated magnetic nanoparticles acquired from Nanopartz™; Inset shows the low field region. B) UV-Vis spectra of gold-coated magnetic nanoparticles acquired from Nanopartz™.

Magneto-plasmonic properties of gold-coated magnetic nanoparticles were characterized using SQUID and UV-Vis spectroscopy. SQUID magnetometry was performed to evaluate the magnetic property of the nanoparticles. As it can be seen from Figure 3.4 gold-coated magnetic nanoparticles acquired from Nanopartz™ show superparamagnetism (neglectable coercivity and remanence) with magnetization saturation of 3 emu g^{-1}.

The optical property of the nanoparticles was measured by UV-Vis spectroscopy. As it can be seen from Figure 3.4. B there are two peaks available in the UV-Vis plot one small peak at around 400 nm and a bigger peak at around 550 nm. The existence of these two peaks could lead to believe there are at least two different size gold nanoparticles available in the sample.

3.4. Gold-coated magnetic nanoparticles acquired from Creative Diagnostics®

Creative Diagnostics® is providing a wide range of products from antibodies, viral antigens, nanoparticles, and innovative diagnostic components. The gold-coated magnetic nanoparticles with two sizes of 50 nm and 250 ± 70 nm were purchased from this company on two separate occasions. The gold-coated magnetic nanoparticles have citrate as the capping agent to stabilize them. The absorbance peak of the 50 nm gold-coated magnetic nanoparticles was located at 530 nm. The absorbance peak of the gold-coated magnetic nanoparticles (250 nm) was located at 584 nm. The concentration of the gold-coated magnetic nanoparticles was 3.2×10^{10} particles/mL for 50 nm nanoparticles and 3.1×10^{10} particles/mL for 250 nm nanoparticles.

3.4.1. Nanoparticles' morphology and composition

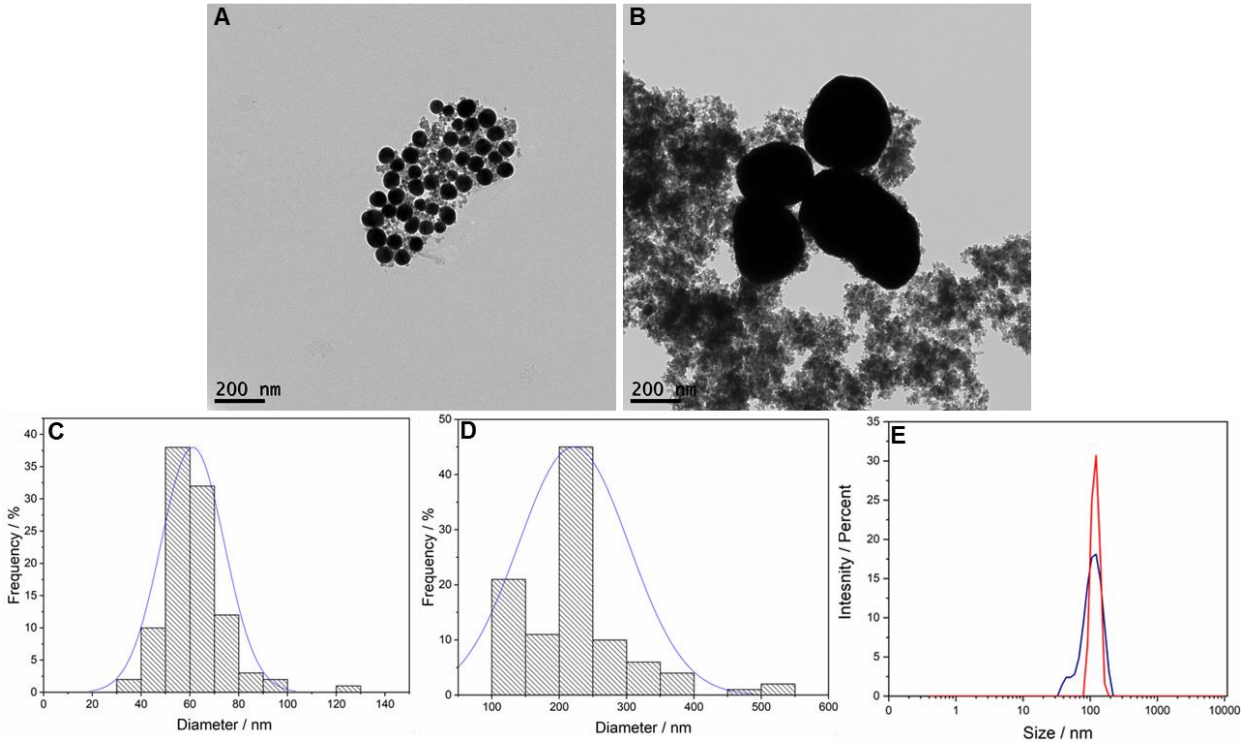

Figure 3.5. A) TEM image of the gold-coated magnetic nanoparticles acquired from Creative Diagnostics®(50 nm) B) TEM images of the gold-coated magnetic nanoparticles acquired from Creative Diagnostics® (250 nm) C) the corresponding histogram of the size of gold-coated magnetic nanoparticles acquired from Creative Diagnostics®(50 nm) D) the corresponding histogram of the size of gold-coated magnetic nanoparticles acquired from Creative Diagnostics® (250 nm) E) Dynamic light scattering (DLS) of the gold-coated magnetic nanoparticles acquired from Creative Diagnostics® 50 nm (blue) and 250 nm (red).

Figure 3.5 A and B shows the TEM images of the gold-coated magnetic nanoparticles acquired from Creative Diagnostics®. As it can be seen from Figure 3.5 A and B there are two types of nanoparticles, the ultra-small grey nanoparticles, and the bigger black nanoparticles. The corresponding histogram (Figure 3.5 C and D) of the size of the gold-coated magnetic nanoparticles showed that the nanoparticles have a size of 61.3 ± 12.8 nm and 221 ± 82 nm. The 50 nm nanoparticles are quite monodispersed with a spherical shape while the bigger gold-coated magnetic nanoparticles are not monodispersed and have no uniform shape. The hydrodynamic sizes of the gold-coated magnetic nanoparticles were measured in Milli-Q water using DLS. The hydrodynamic

size of the nanoparticles was shown to be 98 nm with a PDI of 0.351 and 204 nm and a PDI of 0.136.

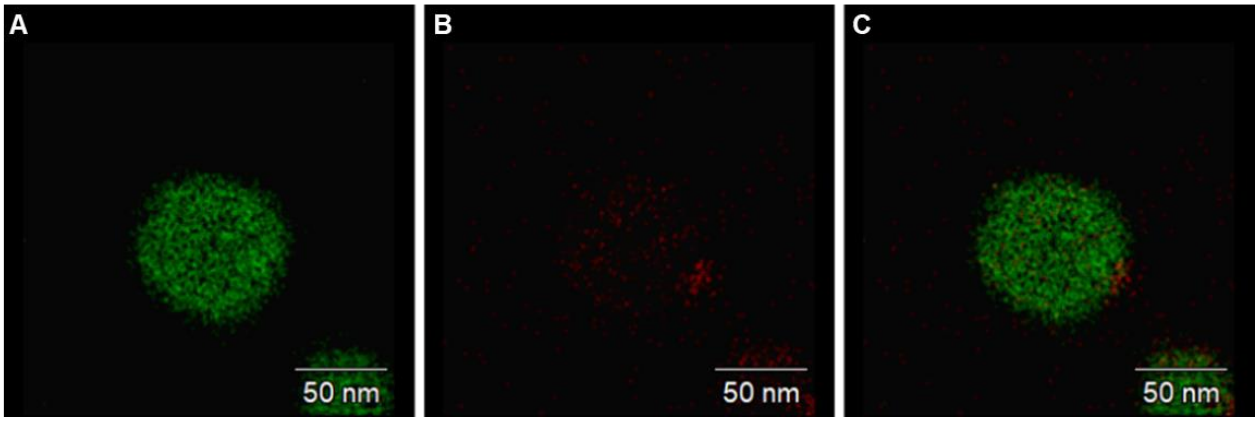

Figure 3.6. EDX map of the elements A) gold B) iron and C) merged gold and iron of the gold-coated magnetic nanoparticles acquired from Creative Diagnostics®.

In order to characterize the nanoparticles composition EDX mapping was done. As it can be seen from Figure 3.6 it seems that the nanoparticles are compromised two separate gold and iron oxide nanoparticles. The big black nanoparticles in Figure 3.5 A and B to be pure gold nanoparticles and the grey areas to be iron oxide nanoparticles.

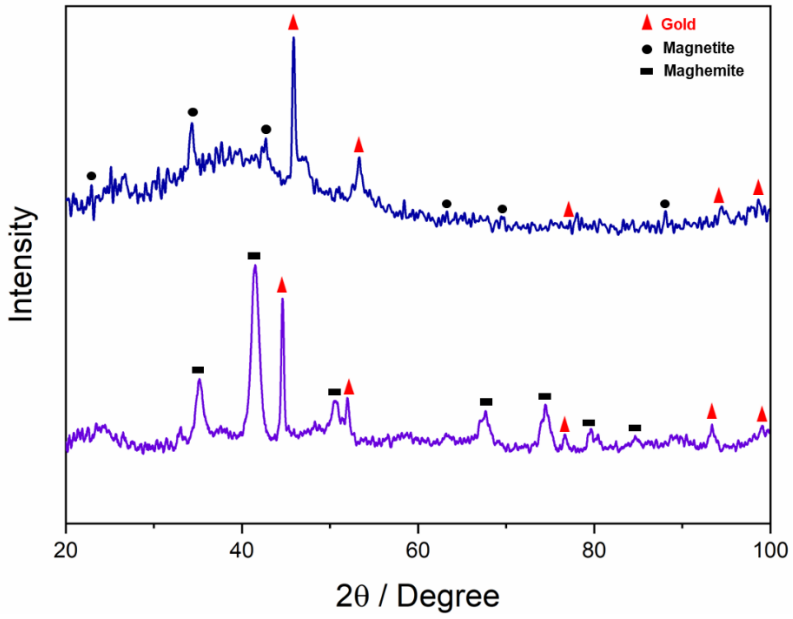

Figure 3.7. X-ray diffraction patterns of gold-coated magnetic nanoparticles acquired from Creative Diagnostics® (navy blue) 50 nm and (purple) 250 nm.

The XRD patterns of the gold-coated magnetic nanoparticles with two sizes of 50 nm and 250 nm acquired from Creative Diagnostics® are shown in Figure 3.7. as it can be seen from the patterns of the gold-coated magnetic nanoparticles peaks located at 44, 52, 76, 93 and 98 degree represents the gold crystal structure.[8–10] Analysis of the major in XRD data showed that 50 nm gold-coated magnetic nanoparticles are mostly compromised of magnetite, while in the case of 250 nm gold-coated magnetic nanoparticles matched best with maghemite. [5,11,12]

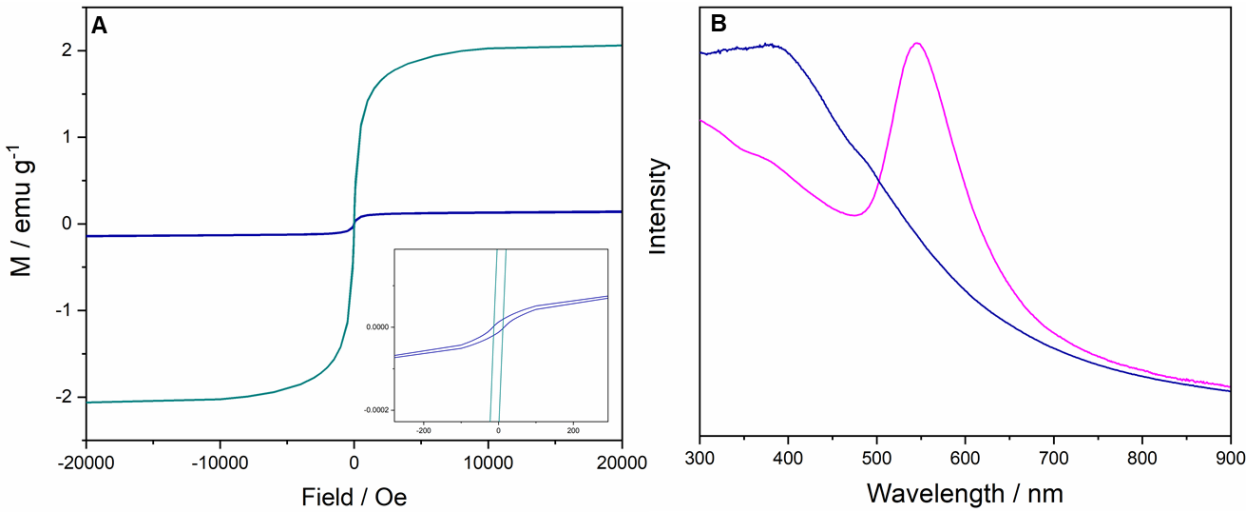

Figure 3.8. A) SQUID magnetometry measurements of gold-coated magnetic nanoparticles acquired from Creative Diagnostics® (cyan) gold-coated magnetic nanoparticles 250 nm and (navy) gold-coated magnetic nanoparticles 50 nm; Inset shows the low field region, B) UV-Vis spectra of gold-coated magnetic nanoparticles acquired from Creative Diagnostics®, (navy) gold-coated magnetic nanoparticles 50 nm, (pink) gold-coated magnetic nanoparticles 250 nm.

To evaluate the magnetic properties of the gold-coated magnetic nanoparticles SQUID magnetometry was employed. As can be seen from Figure 3.8 A the magnetization saturation of 1.9 emu g^{-1} and 0.1 emu g^{-1} were recorded for 250 nm and 50 nm gold-coated magnetic nanoparticles purchased from Creative Diagnostics® respectively. That is both nanoparticles showed superparamagnetic behaviour. The optical property of the nanoparticles was measured using UV-Vis spectroscopy (Figure 3.8 B). UV-Vis showed two major peaks for 50 nm gold-coated magnetic nanoparticles, first at 400 nm and another small peak at 470 nm. For 250 nm gold-coated magnetic nanoparticles two major peaks at 390 nm and 550 nm.

3.5. Gold-coated magnetic nanoparticles acquired from Nanoimmunotech

Nanoimmunotech is a company offering a wide range of products such as nanoparticles, bioconjugation kits, bioconjugation services and, characterization services. The gold-coated magnetic nanoparticles were purchased from Nanoimmunotech on two separate occasions early 2018 and mid-2018. Two sizes of gold-coated magnetic nanoparticles 50 nm and 250 nm were received. Both gold-coated nanoparticles were capped with citrate and were dispersed in Milli-Q water. According to the commercial datasheet, gold-coated magnetic nanoparticles were 51.8 ± 6.1 nm and 250 ± 70 nm. The concentration of 50 nm and 250 nm gold-coated magnetic nanoparticles were 3.2×10^{10} particles/millilitre and 3.1×10^{10} particles/millilitre. The optical peaks of the 50 and 250 nm gold-coated magnetic nanoparticles were located at 536 nm and 580 ± 5 nm. The company data sheet acknowledged that the product might contain some uncoated magnetic nanoparticles.

3.5.1. Nanoparticles' morphology and composition

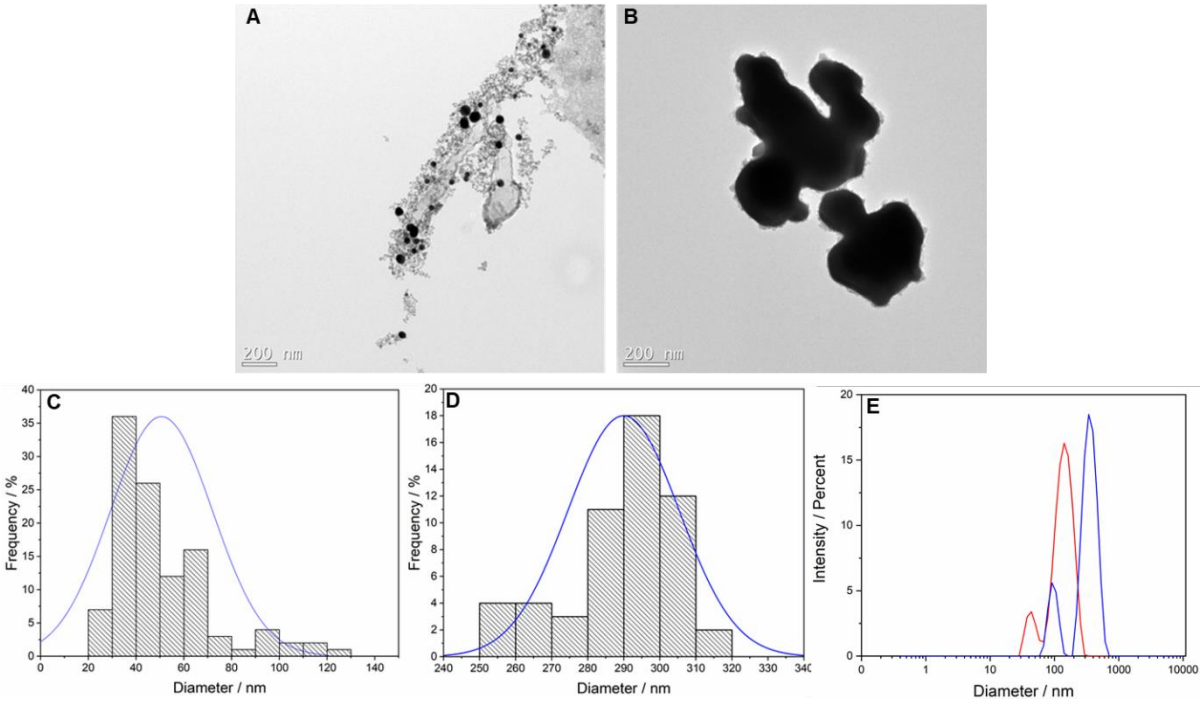

Figure 3.9. A) TEM image of the 50 nm gold-coated magnetic nanoparticles acquired from Nanoimmunotech B) TEM image of the 250 nm gold-coated magnetic nanoparticles C) the corresponding histogram of the size of 50 nm gold-coated magnetic nanoparticles acquired from Nanoimmunotech D) the corresponding histogram of the size of 250 nm gold-coated magnetic

nanoparticles acquired from Nanoimmunotech, and E) Dynamic light scattering (DLS) of the 50 nm (red) and 250 nm (blue) gold-coated magnetic nanoparticles acquired from Nanoimmunotech.

Figure 3.9 A and B shows the TEM images of the gold-coated magnetic nanoparticles purchased from the Nanoimmunutech. As it can be seen from Figure 3.9 A the nanoparticles are uniformly spherical black. There are other grey spots on the grid which could be the uncoated magnetic nanoparticles. The histogram of the size of the gold-coated magnetic nanoparticles revealed that the nanoparticles are quite monodisperse with an average size of 50.6 ± 2.1 nm. As it is depicted in Figure 3.9 B the 250 nm gold-coated magnetic nanoparticles are randomly shaped with an average size of 289 ± 60 nm. The hydrodynamic size of the gold-coated magnetic nanoparticles in Milli-Q water was measured using dynamic light scattering (DLS). The 50 nm gold-coated magnetic nanoparticles showed a hydrodynamic size of 106 nm with a PDI of 0.191. The difference between the TEM size and hydrodynamic size could be due to two main reasons. First, there might be some aggregates or bigger size nanoparticles in the gold-coated magnetic nanoparticles solution and second, the surface capping agent could be the reason for the big size difference.[13–15] The DLS revealed that the hydrodynamic size of the 250 nm gold-coated magnetic nanoparticles was 216 nm with a PDI of 0.21.

To further investigate the composition of the gold-coated magnetic nanoparticles EDX mapping was performed.

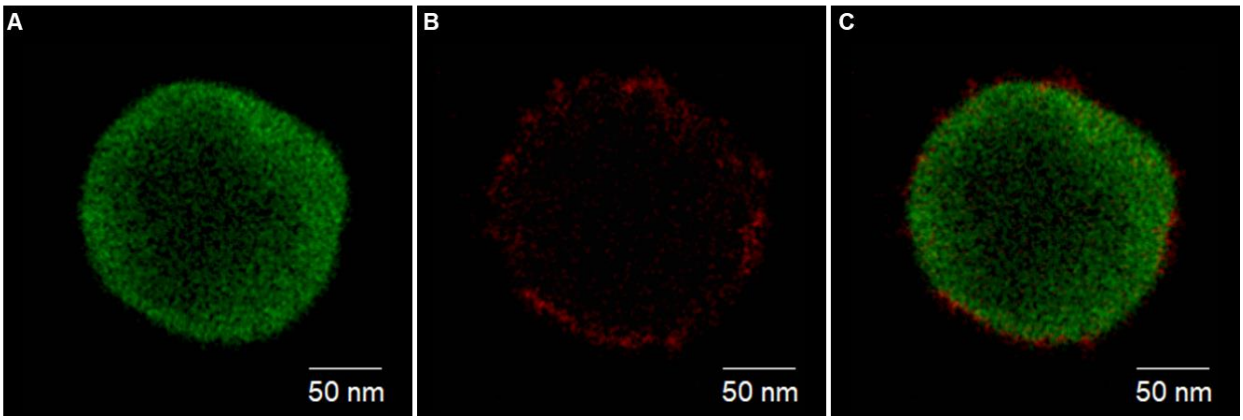

Figure 3.10. EDX map of the elements A) gold B) iron and C) merged gold and iron of the gold-coated magnetic nanoparticles acquired from Nanoimmunotech.

As it can be seen from Figure 3.10 both gold and iron are present in the nanoparticles. As it can be seen it seems that iron and gold are separated from each other, the sample contains a combination of gold nanoparticles and iron oxide nanoparticles. The ring of iron around gold could also be seen again.

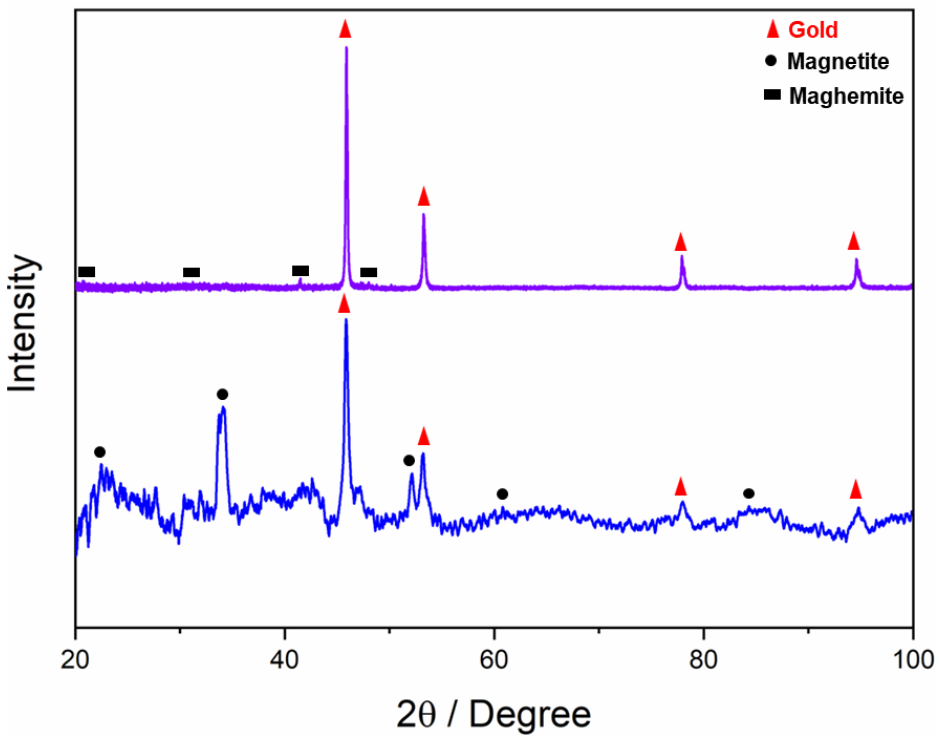

Figure 3.11. X-ray diffraction patterns of (purple) 50 nm and (blue) 250 nm gold-coated magnetic nanoparticles were acquired from Nanoimmunotech.

To further characterize the nanoparticles XRD patterns of each nanoparticle are depicted in Figure 3.11. As it is depicted in purple and blue XRD patterns, the main four gold's peaks are located at two theta degrees of 44, 52, 76 and 93 corresponding to (111), (200), (220) and (311) faces of gold crystal structure.[16–18] The peaks assigned to the iron oxide of 50 nm gold-coated magnetic nanoparticles (purple pattern) are mostly matched with maghemite, while for 250 nm gold-coated magnetic nanoparticles the peaks mostly match with magnetite.[5,16,19]

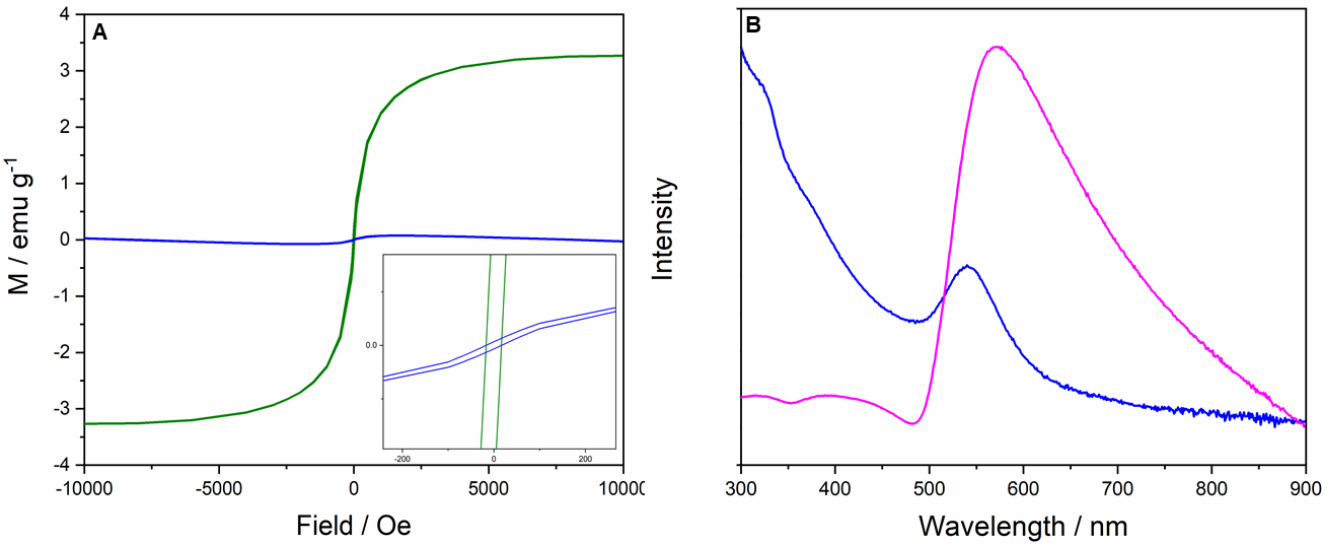

Figure 3.12. A) SQUID magnetometry measurements (blue) 50 nm gold-coated magnetic nanoparticles, (green) 250 nm gold-coated magnetic nanoparticles acquired from Nanoimmunotech, and B) UV-Vis spectroscopy measurements of (blue) 50 nm gold-coated magnetic nanoparticles, (purple) 250 nm gold-coated magnetic nanoparticles acquired from Nanoimmunotech.

The magneto-plasmonic property of the gold-coated magnetic nanoparticles was measured using SQUID magnetometry and UV-Vis spectroscopy. Figure 3.11 A shows the hysteresis curves of gold-coated magnetic nanoparticles. The 50 nm gold-coated magnetic nanoparticle show a small magnetization saturation of 0.7 emu g^{-1}, and superparamagnetic behaviour. The 250 nm gold-coated magnetic nanoparticles showed a magnetization saturation of 3.1 emu g^{-1} with superparamagnetic behaviour. It is worth noting that 250 nm gold-coated magnetic nanoparticles still show superparamagnetic behaviour.

The UV-Vis spectroscopy of the gold-coated magnetic nanoparticles is depicted in Figure 3.11 B. The 50 nm gold-coated magnetic nanoparticles show two main peaks at 330 nm and 540 nm. The 250 nm gold-coated magnetic nanoparticle showed three peaks at 310 nm, 400 nm and a big peak at 580 nm.

3.6. Conclusion

Gold-coated magnetic nanoparticles with different sizes and shapes have been bought from three different companies. The nanoparticles have been characterized *via* TEM, EDX mapping, UV-Vis spectroscopy and SQUID magnetometry. Gold-coated magnetic nanoparticles showed to be a combination of gold nanoparticles and iron oxide nanoparticles in most cases. They are all showed to have a magnetic property and behave like superparamagnetic nanoparticles. The nanoparticles showed low optical consistency with several UV-Vis peaks available in each measurement. Although the commercially available gold-coated magnetic nanoparticles might be useful for some applications it is important to note that they are not useful for applications with extreme dependence on nanoparticles composition and uniformity. Complete gold coverage around magnetic cores, fast magnetic response and high colloidal and magnetic aggregation stability are some of the main important properties south in gold-coated magnetic nanoparticles for bio-sensing. It is highly recommended to try synthesising the gold-coated magnetic nanoparticles in a lab rather than just buying from companies. Chapter 4 of this thesis is focusing on synthesizing a perfect gold-coated magnetic nanoparticle specifically for bio-sensing applications.

3.7. Disclaimer

The gold-coated magnetic nanoparticles were purchased in 2018 on two separate occasions. Data presented in this chapter is based on the nanoparticles purchased at that date. All the statement made in this chapter was based on data acquired from those samples. The quality of the nanoparticles could improve at any time.

3.8. References

1. Carpenter, E. E. & Orleans, N. Effects Of Shell Thickness. *Polyhedron* **35**, 3496–3498 (1999).
2. Carpenter, E. E., Sims, J. A., Wienmann, J. A., Zhou, W. L. & O'Connor, C. J. Magnetic

properties of iron and iron platinum alloys synthesized via microemulsion techniques. *J. Appl. Phys.* **87**, 5615–5617 (2000).

3. Moraes Silva, S., Tavallaie, R., Sandiford, L., Tilley, R. D. & Gooding, J. J. Gold coated magnetic nanoparticles: From preparation to surface modification for analytical and biomedical applications. *Chem. Commun.* **52**, 7528–7540 (2016).

4. Kim, A., Ng, W. B., Bernt, W. & Cho, N. J. Validation of Size Estimation of Nanoparticle Tracking Analysis on Polydisperse Macromolecule Assembly. *Sci. Rep.* **9**, 1–14 (2019).

5. Dar, M. I. & Shivashankar, S. A. Single crystalline magnetite, maghemite, and hematite nanoparticles with rich coercivity. *RSC Adv.* **4**, 4105–4113 (2014).

6. Chatterjee, J., Haik, Y. & Chen, C.-J. Size dependent magnetic properties of iron oxide nanoparticles. *J. Magn. Magn. Mater.* **257**, 113–118 (2003).

7. Wang, L. *et al.* Iron oxide-gold core-shell nanoparticles and thin film assembly. *J. Mater. Chem.* **15**, 1821–1832 (2005).

8. Kemp, S. J., Ferguson, R. M., Khandhar, A. P. & Krishnan, K. M. Monodisperse magnetite nanoparticles with nearly ideal saturation magnetization. *RSC Adv.* **6**, 77452–77464 (2016).

9. Shankar, S. S., Ahmad, A., Pasricha, R. & Sastry, M. Bioreduction of chloroaurate ions by geranium leaves and its endophytic fungus yields gold nanoparticles of different shapes. *J. Mater. Chem.* **13**, 1822–1826 (2003).

10. Khosroshahi, M. E. & Ghazanfari, L. Physicochemical characterization of Fe3O4/SiO2/Au multilayer nanostructure. *Mater. Chem. Phys.* (2012) doi:10.1016/j.matchemphys.2011.12.047.

11. Unni, M. *et al.* Thermal Decomposition Synthesis of Iron Oxide Nanoparticles with Diminished Magnetic Dead Layer by Controlled Addition of Oxygen. *ACS Nano* **11**, 2284–2303 (2017).

12. Akbaba, H., Karagöz, U., Selamet, Y. & Kantarcı, A. G. Synthesis and characterization of cationic lipid coated magnetic nanoparticles using multiple emulsions as microreactors. *J. Magn. Magn. Mater.* **426**, 518–524 (2017).

13. Williams, J. W., Baldwin, R. L., Van Holde, K. E. & Fujita, H. The Theory of Sedimentation Analysis. *Chem. Rev.* **58**, 715–744 (1958).

14. Stephens, J. R., Beveridge, J. S. & Williams, M. E. Analytical methods for separating and isolating magnetic nanoparticles. *Phys. Chem. Chem. Phys.* **14**, 3280–3289 (2012).

15. Hassan, P. A., Rana, S. & Verma, G. Making sense of Brownian motion: Colloid characterization by dynamic light scattering. *Langmuir* **31**, 3–12 (2015).

16. McMurdie, H. F. *et al.* Standard X-Ray Diffraction Powder Patterns from The JCPDS Research Associateship. *Powder Diffr.* **1**, 64–77 (1986).

17. Yan, W., Petkov, V., Mahurin, S. M., Overbury, S. H. & Dai, S. Powder XRD analysis and catalysis characterization of ultra-small gold nanoparticles deposited on titania-modified SBA-15. *Catal. Commun.* **6**, 404–408 (2005).

18. Gomez, S. *et al.* Gold nanoparticles from self-assembled gold(I) amine precursors. *Chem. Commun.* 1945–1946 (2000) doi:10.1039/b005327i.

19. García Reyes, L. E. 済無No Title No Title. *J. Chem. Inf. Model.* **53**, 1689–1699 (2013).

Chapter 4

Synthesis of gold-coated magnetic conglomerate nanoparticles with a fast magnetic response for bio-sensing

Publication one

Milad Mehdipour, Lucy Gloat, Danielle T. Bennett, Sharmin Hoque, Raheleh Pardehkhorram, Padmavathy Bakthavathsalam, Vinicius R. Gonçales, Richard D. Tilley, J. Justin Gooding. J. Mater. Chem. C, 2021, 9, 1034

4.1. Summery

The publication ‘’ Synthesis of gold-coated magnetic conglomerate nanoparticles with a fast magnetic response for bio-sensing’’ has been used in lieu of a chapter. The aim was to see whether it is possible to synthesis gold-coated magnetic nanoparticles with unique properties suitable specifically for bio-sensing. To do this superparamagnetic magnetite nanoparticles were made using thermal decomposition. A group of superparamagnetic magnetite nanoparticles were encapsulated inside a silica shell using the microemulsion method. Finally, the silica-coated conglomerates of superparamagnetic nanoparticles were coated with a layer of gold using the seed-mediated method. The gold-coated superparamagnetic nanoparticles were characterized and showed that the nanoparticles have a fast magnetic response, stability against magnetic aggregation and colloidal stability. Our data suggest that the existence of multiple superparamagnetic nanoparticles as magnetic cores inside the silica shell is the reason for its unique properties. The particles further showed to be powerful electrochemical and optical sensing agents.

Declaration for Chapter Four

Author	Contribution
Milad Mehdipour	Synthesized magnetite nanoparticles, silica-coated conglomerates of superparamagnetic nanoparticles, gold-coated conglomerates of superparamagnetic nanoparticles Characterised nanoparticles using TEM, SQUID magnetometry, UV-Vis spectroscopy, Carried out stability against magnetic aggregation and colloidal stability experiments Drafted and proofread the manuscript Addressed reviewer's comments
Lucy Gloag	Experimental Design Characterisation of the nanoparticles with EDX mapping and line scan Proofread the manuscript Help addressed the reviewer's comments
Danielle T. Bennett	Characterisation of gold-coated conglomerates superparamagnetic nanoparticles *via* dark-field microscopy Proofread the manuscript
Sharmin Hoque	Making the Scheme Modification of nanoparticles and all the electrochemical experiments Proofread the manuscript
Raheleh Pardehkhorram	Modification of nanoparticles Performed the Raman and SERS experiments Proofread the manuscript
Padmavathy Bakthavathsalam	Took the dark field microscopy images Proofread the manuscript
Vinicius R. Gonçales	Digestion of gold-coated and silica-coated conglomerates of nanoparticles with HF
Richard D. Tilley	Experimental design Provided fundamental understanding of the key magneto plasmonic properties and synthesis of nanoparticles Proofread manuscript
J. Justin. Gooding	Experimental design Provided fundamental understanding of the key magneto plasmonic properties and synthesis of nanoparticles Proofread manuscript

UNSW is supportive of candidates publishing their research results during their candidature as detailed in the UNSW Thesis Examination Procedure.

Publications can be used in their thesis in lieu of a Chapter if:

- The candidate contributed greater than 50% of the content in the publication and is the "primary author", ie. the candidate was responsible primarily for the planning, execution and preparation of the work for publication
- The candidate has approval to include the publication in their thesis in lieu of a Chapter from their supervisor and Postgraduate Coordinator.
- The publication is not subject to any obligations or contractual agreements with a third party that would constrain its inclusion in the thesis

Please indicate whether this thesis contains published material or not:

☐ This thesis contains no publications, either published or submitted for publication
(if this box is checked, you may delete all the material on page 2)

☐ Some of the work described in this thesis has been published and it has been documented in the relevant Chapters with acknowledgement
(if this box is checked, you may delete all the material on page 2)

☒ This thesis has publications (either published or submitted for publication) incorporated into it in lieu of a chapter and the details are presented below

CANDIDATE'S DECLARATION

I declare that:

- I have complied with the UNSW Thesis Examination Procedure
- where I have used a publication in lieu of a Chapter, the listed publication(s) below meet(s) the requirements to be included in the thesis.

Candidate's Name	**Signature**	**Date (dd/mm/yy)**
Milad Mehdipour		

POSTGRADUATE COORDINATOR'S DECLARATION *To only be filled in where publications are used in lieu of Chapters*

I declare that:

- the information below is accurate
- where listed publication(s) have been used in lieu of Chapter(s), their use complies with the UNSW Thesis Examination Procedure
- the minimum requirements for the format of the thesis have been met.

PGC's Name	PGC's Signature	Date (dd/mm/yy)
Alex William Donald		

For each publication incorporated into the thesis in lieu of a Chapter, provide all of the requested details and signatures required

Details of publication #1:

Full title: Synthesis of gold-coated magnetic conglomerate nanoparticles with fast magnetic response for bio-sensing

Authors: Milad Mehdipour, Lucy Gloag, Danielle T. Bennett, Sharmin Hoque, Raheleh Pardehkhorram, Padmavathy Bakthavathsalam, Vinicius R. Gonçales, Richard D.Tilley and J. Justin Gooding

Journal or book name: Journal of Materials Chemistry C
Volume/page numbers: **9**/ 1034-1043

Date accepted/ published: 06 Dec 2020/ 08 Dec 2020

Status	*Published*	***X***	*Accepted and In press*		*In progress (submitted)*	

The Candidate's Contribution to the Work

Synthesized magnetite nanoparticles, silica-coated conglomerates of superparamagnetic nanoparticles, gold-coated conglomerates of superparamagnetic nanoparticles

Characterised nanoparticles using TEM, SQUID magnetometry, UV-Vis spectroscopy,

Carried out stability against magnetic aggregation and colloidal stability experiments

Drafted and proofread the manuscript

Addressed reviewer's comments

Location of the work in the thesis and/or how the work is incorporated in the thesis:
In lieu of Chapter 4

PRIMARY SUPERVISOR'S DECLARATION

I declare that:

- the information above is accurate
- this has been discussed with the PGC and it is agreed that this publication can be included in this thesis in lieu of a Chapter
- All of the co-authors of the publication have reviewed the above information and have agreed

to its veracity by signing a 'Co-Author Authorisation' form.		
Primary Supervisor's name **J. Justin Gooding**	**Primary Supervisor's signature**	**Date (dd/mm/yy)**

Add additional boxes if required

Journal of Materials Chemistry C

ROYAL SOCIETY OF CHEMISTRY

PAPER

View Article Online
View Journal | View Issue

Cite this: J. Mater. Chem. C, 2021, 9, 1034

Synthesis of gold-coated magnetic conglomerate nanoparticles with a fast magnetic response for bio-sensing†

Milad Mehdipour,[a] Lucy Gloag,[a] Danielle T. Bennett,[a] Sharmin Hoque,[a] Raheleh Pardehkhorram,[a] Padmavathy Bakthavathsalam,[a] Vinicius R. Gonçales,[a] Richard D. Tilley *[abc] and J. Justin Gooding *[ac]

Received 4th October 2020,
Accepted 6th December 2020

DOI: 10.1039/d0tc04702c

rsc.li/materials-c

The versatile qualities of gold coated magnetic nanoparticles for both optical and electrochemical detection, as well as the separation of analytes, make them an excellent choice for ultrasensitive biosensing applications. The challenge with such nanoparticles however is that strongly magnetic nanoparticles that reach the magnet rapidly are prone to aggregation, whilst superparamagnetic nanoparticles that are stable against aggregation reach the magnet slowly. Here, we report a conglomerate nanostructure consisting of superparamagnetic nanoparticles coated with gold that provides a rapid magnetic response while exhibiting colloidal stability in solution. The performance of these gold coated magnetic nanoparticles for both bio-separation and biosensing was demonstrated for application in biosensors, dispersible electrodes for detecting microRNA and surface-enhanced Raman scattering.

1. Introduction

The conductivity and optical properties of gold make gold coated magnetic nanoparticles a key target for electrochemical and optical bio-sensing.[1–5] For instance, by taking advantage of the conductivity of gold and its high affinity toward the thiol (–SH) terminal group[2] and the inherent magnetic properties of iron,[6] the dispersible electrode concept was developed which provides an improvement over conventional electrochemical biosensors with regard to both response time and detection limit. This is achievable as surface functionalised gold coated magnetic nanoparticles enable bringing the analyte to the sensor rather than the conventional paradigm of the analyte finding the sensor.[7–9] In this application, it is important that gold coated magnetic nanoparticles have a fast response time when a magnetic field is applied. A fast response time is required for the implementation of magnetic nanoparticles in practical biosensing applications to detect ultralow amounts of biomarkers within minutes of testing.[7] To increase the magnetization saturation of gold coated magnetic nanoparticles, a larger magnetic core can be used. However, above 30 nm, magnetic nanoparticles tend to be irreversibly magnetized when a magnetic field is applied, resulting in aggregation due to the magnetic attraction between particles.[10] To avoid aggregation in biological systems superparamagnetic iron oxide nanoparticles (<20 nm) that can be reversibly magnetized but with lower magnetization saturation are often used.[11–13]

Direct coating of small iron oxide nanoparticles with gold is synthetically challenging. To overcome this, an intermediate layer like silica has been used to improve the adhesion of gold to the magnetic core.[14–17] We hypothesize that if many of these superparamagnetic nanoparticles are combined in a silica matrix, their magnetic domains can interact to produce a particle with a fast magnetic response that can be readily coated with gold.[18,19]

Herein, we developed a synthetic method to prepare gold coated magnetic nanoparticles that combine magnetic, optical and conductivity properties. The nanoparticles are designed to have multiple 16 nm superparamagnetic magnetite nanoparticles embedded in a silica matrix to create a conglomerate nanoparticle. These conglomerates can be readily coated with a complete gold shell. The combined magnetic response of the superparamagnetic nanoparticles within the conglomerates creates a stronger magnetic signal from the particle, thus producing a faster response to the external magnetic field while avoiding magnetic aggregation. A complete characterization of the structural, magnetic, optical and conductivity properties

[a] School of Chemistry, The University of New South Wales, Sydney, New South Wales, 2052, Australia. E-mail: r.tilley@unsw.edu.au, justin.gooding@unsw.edu.au
[b] Electron Microscope Unit, Mark Wainwright Analytical Centre, The University of New South Wales, Sydney, New South Wales, 2052, Australia
[c] Australian Centre for Nanomedicine, The University of New South Wales, Sydney, New South Wales, 2052, Australia

† Electronic supplementary information (ESI) available. See DOI: 10.1039/d0tc04702c

has been performed to demonstrate their applicability in bio-separation and optical and electrochemical bio-sensing.

2. Experimental methods

2.1. Materials

Iron(III) acetylacetonate, oleylamine (98%), oleic acid, trioctylamine, Igepal CO-520, ammonium hydroxide solution 30%, tetraethyl orthosilicate (TEOS), (3-aminopropyl)trimethoxy silane (APTES), dimethyl sulfoxide (DMSO), gold(III) chloride trihydrate ($HAuCl_4 \cdot 3H_2O$), sodium hydroxide, tetrakis(hydroxymethyl)phosphonium chloride solution (THPC), hydroxylamine hydrochloride ($NH_2OH \cdot HCl$), 4-aminothiophenol (4-ATP, 97%), Trizma base, bis(*p*-sulfonatophenyl)phenylphosphine dihydrate dipotassium salt (BSPP), phosphate buffered saline (PBS) solution, NaH_2PO_4 and Na_2HPO_4 solution were purchased from Sigma-Aldrich. Potassium carbonate (K_2CO_3), toluene, ethanol (96%), cyclohexane, methanol, hydrogen peroxide (27–30%), sulfuric acid (98%), hydrochloric acid (32%), and nitric acid (69%) were purchased from Chem-Supply Pvt. Ltd. Methylene blue labelled probe DNA: 5′-SH-$(CH_2)_3$-*p*-TCAACATCAGTCTGATAAGCTA-$(CH_2)_3$-MB-3′ and complementary RNA target (miRNA-21): 5′-UAGCUUAUCAGACUGAUGUUGA-3′ were purchased from Biosearch Technologies (Novato). Gold coated magnetic nanoparticles were also purchased from Creative Diagnostics for comparison and henceforth are referred to as commercial gold coated magnetic nanoparticles. Amicon Ultra-15 centrifugal units were purchased from Sigma-Aldrich. All the chemicals except for oleylamine were used as received. Oleylamine was distilled prior to reaction. All glassware was washed with freshly prepared piranha solution (H_2SO_4 : H_2O_2 in a 3 : 1 ratio by volume), followed by rinsing with ultrapure water (18.2 Milli-Q) and then washing with freshly prepared aqua regia (HCl : HNO_3 in a 3 : 1 ratio by volume), followed by rinsing with ultrapure water (18.2 Milli-Q).

2.2. General procedure for the synthesis and modification of gold coated conglomerates of superparamagnetic nanoparticles

2.2.1. Synthesis of superparamagnetic iron oxide nanoparticles. Magnetite nanoparticles were prepared via a slightly modified thermal decomposition method previously reported in the literature.[20] To a 25 mL round-bottom flask, 260 mg of iron(III) acetylacetonate was added. Then, 0.6 mL of oleic acid, 2.4 mL of oleylamine and 2.4 mL of trioctylamine were added. The flask was connected to a Schlenk line and the solution was magnetically stirred throughout the reaction. The reaction was performed in 7 steps: (1) heating to 120 °C under vacuum, (2) constant heating at 120 °C under vacuum for 90 minutes, (3) switching to Ar and gradual heating to 200 °C (10 °C per 5 minutes), (4) constant heating at 200 °C under Ar flow for 60 minutes, (5) gradual heating to 330 °C under Ar (10 °C per 5 minutes), (6) constant heating at 330 °C under Ar for 50 minutes, and (7) cooling to room temperature. A total of 15 mL of ethanol was then added to the solution and the precipitated particles were collected by centrifugation at 8000 rpm, followed by washing three times with ethanol. The as-prepared nanoparticles were dispersed in 1.5 mL of toluene.

2.2.2. Synthesis of amine-terminated silica coated conglomerates of superparamagnetic nanoparticles. Silica coating was achieved through the well-known water-in-oil reverse microemulsion method with minor modifications reported in the literature.[21,22] An aliquot of 10 mL of cyclohexane was added to a 50 mL vial, followed by the addition of 600 μL of Igepal CO-520. The solution was vortexed for 5 minutes to dissolve the Igepal completely. Then 100 μL of magnetite nanoparticles were added while shaking the solution. Subsequently, 80 μL of ammonium hydroxide solution and 30 μL of TEOS were added. The vial was shaken for 1 min and then left inside a fume hood for 36 h. To functionalize the nanoparticles so that they possess distal amines to aid the dispersion of the nanoparticles 4 mL of methanol was added to break the microemulsion. The brown layer was carefully transferred to a new vial and the nanoparticles were magnetically separated *via* a neodymium square block magnet ($50 \times 50 \times 25.4$ mm^3) and washed with 3 mL ethanol 3 times to remove any trace of by-products. The nanoparticles were dispersed in 3 mL of ethanol. An aliquot of 4 μL of APTES was added and the mixture was rotated on a rotating wheel for 2 h. Amine-terminated particles were magnetically separated, washed 3 times with ethanol and dispersed in 500 μL of DMSO.

2.2.3. Synthesis of gold seed nanoparticles (<5 nm) and attachment of seeds to the amine-terminated silica coated conglomerates of superparamagnetic nanoparticles. A colloidal dispersion of gold nanoparticles (<5 nm) was prepared according to a method reported in the literature with modifications.[23] An aliquot of 50 mL of Milli-Q water was added to a 100 mL glass beaker, followed by the addition of 600 μL of 1 M sodium hydroxide solution and 15 μL of THPC. The solution was vigorously stirred and after 30 seconds 2.2 mL of 1 wt% Au(III) chloride trihydrate was added rapidly, resulting in the solution undergoing an immediate colour change to brown. Gold seeds were concentrated in 2 mL using an Amicon Ultra-15 centrifugal unit at 6000 rpm for 30 minutes and washed with water twice. Then 0.1 mL of amine-terminated silica coated iron oxide nanoparticles were added to the seed solution and then the solution was covered with aluminium foil and rotated for 12 h on a rotating wheel. Gold seeded silica coated nanoparticles were separated magnetically and dispersed in 3 mL of Trizma–HCl (pH = 8) buffer.

2.2.4. Growth of the gold shell on the surface of gold seeded silica coated conglomerates of superparamagnetic nanoparticles. To form the gold shell around the already gold seeded particles,[24] a mass of 45 mg of Au(III) chloride trihydrate and 75 mg of K_2CO_3 were added to 600 mL of Milli-Q water and stirred with a mechanical stirrer at 500 rpm overnight. The gold seeded silica coated conglomerates of iron oxide nanoparticles in 3 mL Trizma–HCl buffer were added to the above solution, followed by the addition of 20 mL of 1 mg mL^{-1} BSPP aqueous solution. Then 20 mL of 120 μg mL^{-1} $NH_2OH \cdot HCl$ was added and the solution was stirred for 24 h. The nanoparticles were separated magnetically and dispersed in 3 mL of Milli-Q. The solution after gold shell growth and purification turns pale green. The particles were stable when stored at 4 °C away from light for several months. The synthesis is highly reproducible

(<90% success rate) when fresh reagents were used, especially gold chloride.

2.2.5. **Modification of the gold coated conglomerates of superparamagnetic nanoparticles and commercial gold coated magnetic nanoparticles with 4-ATP molecules.** To immobilize the 4-ATP molecules on the surface of the gold coated conglomerates of superparamagnetic nanoparticles and commercial gold coated magnetic nanoparticles,[25] 1.5 μL (2 mM) of 4-ATP was added to 100 μL of the particle solution and the solution was stirred for 2 h at room temperature, followed by magnetic separation 3 times, and the supernatant was discarded to remove the unbonded 4-ATP from solution.

2.2.6. **Modification of gold coated conglomerates of superparamagnetic nanoparticles with methylene blue labelled probe DNA.** In the first step,[26] 100 μL of gold coated conglomerates of superparamagnetic nanoparticles (1.6×10^9 particles per mL) were dispersed into 0.5 mL of 10 mM NaH_2PO_4 and Na_2HPO_4 solution, followed by 30 second sonication. The dispersed particles were added to 0.5 mL of freshly prepared 20 nM probe DNA solution in 10 mM NaH_2PO_4 and Na_2HPO_4 containing 0.15 M NaCl. This mixture was rotated on a rotating wheel for 8 h. The DNA functionalized gold coated conglomerates of superparamagnetic nanoparticles were separated by centrifugation at 12 000 rpm for half an hour and washed with 1 mL phosphate buffer containing 0.075 M NaCl 3 times. The modified nanoparticles were re-dispersed in 1 mL of 10 mM NaH_2PO_4 and Na_2HPO_4 containing 0.075 M NaCl.

2.2.7. **Hybridization with target miRNA.** A solution of miR21 with a concentration of 1 N m was prepared by dilution of a stock solution of 0.1 μM miR-21 in hybridization buffer (150 Mm NaCl in 10 Mm PBS). To hybridize the modified nanoparticles with target miRNA,[26] modified gold coated conglomerates of superparamagnetic nanoparticles were separated from the supernatant (30 min centrifugation at 12000 rpm) and incubated overnight with 2 mL of target miRNA solution with gentle mixing in a rotating wheel. Hybridized particles were then separated from the supernatant solution (30 min centrifugation at 12 000 rpm), rinsed two times using PBS solution and re-dispersed in 1 mL of PBS solution.

2.3. Instruments and characterization

A Philips CM 200 transmission electron microscope (TEM) was used to acquire images at an acceleration voltage of 200 kV. HRTEM images, EDX maps and line scan images were acquired using an F200 transmission electron microscope (TEM). The TEM samples were prepared by drop-casting the nanoparticle solution on carbon coated copper grids, followed by air-drying overnight. An FEI Nova NanoSEM 450 was used to take the SEM images of the nanoparticles at an acceleration voltage in the range of 4–25 kV. The average size of the particles was analysed using ImageJ software. A Cary 60 single-beam UV-vis spectrophotometer was used to measure the absorption spectra of gold coated conglomerates of magnetic nanoparticles and commercial gold coated magnetic nanoparticles at room temperature. The hydrodynamic diameters of the magnetite nanoparticles, silica coated conglomerates of magnetic nanoparticles, gold coated conglomerates of magnetic nanoparticles and commercial gold coated magnetic nanoparticles were measured on a Zetasizer Nano ZS (Malvern Panalytical) in toluene, DMSO and Milli-Q water, respectively. The colloidal stability of the gold coated conglomerates of superparamagnetic nanoparticles and the commercial gold coated magnetic nanoparticles in water was investigated over time. To evaluate the stability of the gold coated conglomerates of superparamagnetic nanoparticles and commercial gold coated magnetic nanoparticles against magnetic aggregation, cycles of collection and redispersion of particles *via* a magnet and sonication (5 minutes) were repeated 25 times. After each cycle, the hydrodynamic diameter was measured. The magnetic properties were investigated by SQUID magnetometry with an external magnetic field ranging from 60 000 Oe (6 T) to −60 000 Oe (−6 T) at 300 K. To compare the separation duration of the gold coated conglomerates of superparamagnetic nanoparticles and the commercial gold coated magnetic nanoparticles, a sequence of images were taken at 5 seconds intervals of their response to the neodymium square block magnet ($50 \times 50 \times 25.4$) up to the point that their respective solutions were emptied. A MATLAB™ script (see the ESI†) was written to analyse the intensity of a user selected area on a sequence of images. First, the user is prompted to select an image and then to select an area of pixels in the image (Fig. S1, ESI†). The image is converted to black and white to get a more consistent pixel value. Each pixel is assigned an integer value depending on its intensity, and those pixel values within the selected rectangle are recorded. The median of the recorded values is found. Successive images are then analysed to give an intensity value; as the particles move towards the magnet the intensity value will change accordingly. Each intensity is normalized by the initial intensity when no magnet is applied, to get a more comparative measurement. To obtain the localized surface plasmon resonance (LSPR) histogram of the particles a dark-field microscope was calibrated to attain the corresponding Hue values for wavelengths of the visible spectrum.[27] Images were then taken in the dark field of each sample to observe the LSPR. Using an in-house MATLAB™ script, the location of each particle was found and then each pixel around the centre was recorded for colour information up to 8 pixels. These pixel colours were then compiled using a probability density estimate to create a computational spectrum of the LSPR profile of the nanoparticle. The peak of each of these LSPR spectra was taken as the 'colour' of the nanoparticle and compiled in a histogram to observe the optical consistency of the plasmonic response. This corresponds to consistency in the size and shape of the particles. XRD was performed on an Empyrean 2 (Malvern Panalytical) X-ray diffractometer with Co Kα (1.79 Å) radiation with all samples analysed from 20° to 110° (2θ). The particle concentration was measured with Nanoparticle Tracking Analysis (NanoSight NS300, Malvern Panalytical). A dark-field microscope (Olympus BX51) was used to acquire dark field images. To obtain the dark field images, gold coated conglomerates of superparamagnetic nanoparticles and commercial gold coated magnetic nanoparticles were immobilized onto APTES modified coverslips and left for 5 minutes. Coverslips were then rinsed with ultrapure water and then dried under a stream of nitrogen. The coverslip

was mounted on the aluminium holder and imaged using an Olympus BX51 microscope. A 100 W halogen lamp was used as the excitation source and was focused through a dark-field condenser with NA > 0.8. The scattered light was collected by an objective of 100× magnification and imaged using a Canon 100D CMOS camera (22.3 mm × 14.9 mm sensor size, 4.3 μm × 4.3 μm pixel size). The single particle spectra were obtained using an Ocean Optics USB2000+ spectrometer. Firstly, absorbance reference spectra were taken of a bare spot on the glass coverslip and of background light. Then a spot containing a single particle was found and scanned over a period of 30 seconds to allow suitable light intensity. The final spectra were obtained from an average of three scans. Raw data were fitted with the 'multiple peak fit' option in Origin to obtain a Gaussian fit (Fig. S2, ESI†). To verify the accuracy of the plasmonic properties, single nanoparticle spectra were obtained from more than one individual particle and compared with the ensemble spectra taken from all the particles in the view. Raman spectra were measured using a Renishaw inVia confocal Raman microscope with an excitation laser wavelength of 785 nm and a diffraction grating of 1200 g mm^{-1}. Raman measurements were conducted by applying a laser power of ~2.01 mW, an accumulation time of 3 seconds and an exposure time of 10 seconds. To generate the SERS data, three measurements were averaged. All the spectra were calibrated with respect to the silicon peak located at 520–521 cm^{-1}. To evaluate the electrochemical properties of the gold coated particles a unique electrochemical cup shaped glass cell with a 3 mm diameter hole at the bottom was used. Gold foil was used as the working electrode and a plastic gasket having a 2 mm diameter hole on top of it was placed underneath the glass cell, and a platinum counter electrode and a saturated Ag/AgCl reference electrode were placed securely inside the glass cell, all of which were connected to the terminals of a CHI potentiostat (CHI instruments, model no. 600-60D). 1 mL of degassed PBS electrolyte was added to the electrochemical cell. Next, a magnetic field was applied at the base of the cell for 5 min using a neodymium disc magnet (6 mm radius, 6 mm thickness) to allow the magnetically assisted collection of nanoparticles on the gold foil working electrode surface. All electrochemical measurements were repeated 3 times.

3. Results and discussion

3.1. Nanoparticle architecture and composition

The scheme in Fig. 1A outlines the synthesis procedure required to prepare the nanostructure. In step I, small (<20 nm) magnetite iron oxide nanoparticles were synthesized because magnetite has the highest magnetization saturation of the iron oxide phase.[28,29] The thermal decomposition of iron precursor in a hot boiling surfactant solution at 330 °C resulted in monodisperse 16 nm spherical nanoparticles, as shown in Fig. 1B (hydrodynamic size: 19 nm and polydispersity index (PDI): 0.141, Fig. S3, ESI†).[11] The crystal structure was confirmed to be magnetite by X-ray diffraction (XRD) as shown in Fig. S4 (ESI†).[28,30]

The encapsulation of multiple superparamagnetic nanoparticles, in step II of scheme 1A, produced conglomerates of nanoparticles with an average size of 97 nm (hydrodynamic size: 137 nm and PDI: 0.118, Fig. S3, ESI†). Surfactant is the key component in the microemulsion system to provide a framework to connect the hydrophobic magnetite nanoparticles and the aqueous domain of the microemulsion.[31] The conglomerates were formed by coating a thin layer of silica on each of the superparamagnetic nanoparticles which then aggregate together into a larger particle.[32,33] The characterisation of 100 silica coated conglomerates of superparamagnetic nanoparticles (Fig. S5, ESI†)

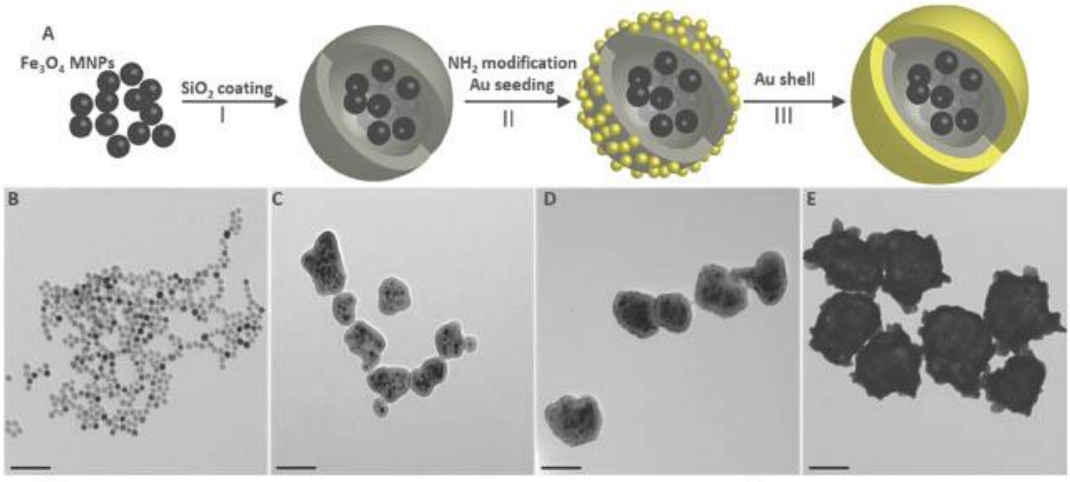

Fig. 1 (A) Schematic illustration of the synthesis procedure and the corresponding TEM images of (B) iron oxide superparamagnetic nanoparticles (16 nm), (C) silica coated conglomerates of superparamagnetic nanoparticles (100 nm), (D) gold seeded silica coated conglomerates of superparamagnetic nanoparticles (100 nm) and (E) gold coated conglomerates of superparamagnetic nanoparticles (165 nm). Scale bars: 100.

shows that 84% of the conglomerates contain at least 20 or more magnetite nanoparticles and less than 10% of the particles have only one magnetic core. The silica shell does not affect the crystalline structure of the magnetite nanoparticles, as shown by the XRD patterns depicted in Fig. S4B (ESI†).

To grow Au onto the SiO_2 shells, it is important to modify the silica surface with distal amine moieties on the silica surface, followed by the decoration of at least 25% of the surface with gold seeds (<4 nm).[34,35] Electrostatic attraction between the positively charged amine-functionalized silica surface and the negatively charged gold seeds drives the surface association. The ultra-small gold nanoparticles then act as gold shell nucleation sites.[36] The small gold seeds in Fig. 1D and Fig. S6 (ESI†) can be observed as black dots that uniformly cover the surface of the conglomerates.

Finally, to grow a complete gold shell, step III of scheme 1A involves the slow deposition of gold onto the silica surface. In this step, Au(III) was reduced to Au(0) under mild conditions using hydroxylamine hydrochloride, which deposits onto the surface of the already gold seeded particles to fully coat the surface of silica with gold (Fig. 1E and Fig. S7, ESI†). The complete coating of gold over the silica surface was confirmed by HR-STEM. As can be seen by the bright field and dark field STEM images in Fig. S8 (ESI†), there are darker and lighter patches over the nanoparticles, consistent with an uneven gold shell. The EDX map and line scan shown in Fig. S8 and S9 (ESI†), respectively, show that gold is detected across the entire particle, with lighter contrast regions of the shell corresponding to lower levels of gold rather than gaps in the shell. Moreover, the gold-to-iron ratio was 87 at% to 13 at%. After the growth of the gold shell around the particles, the size of the particles reaches 165 nm (hydrodynamic size: 188 nm and PDI: 0.197, Fig. S3, ESI†). Although the particles are not uniformly shaped, the formation of the complete shell and their good dispersity in solution make them ideal for application in dispersible electrodes and SERS.[8,37] Fig. S4C (ESI†) shows the XRD patterns of gold coated conglomerates of superparamagnetic nanoparticles with peaks that match both magnetite and gold.[38,39]

The nanostructure of gold coated conglomerates with multiple superparamagnetic cores encapsulated inside a synthesised gold shell differs from gold coated magnetic nanoparticles reported to date, as shown by comparison with commercially available state-of-the-art gold coated magnetic nanoparticles in Fig. S10 (ESI†). The commercial particles appear to be a combination of separate gold nanoparticles and iron oxide nanoparticles as can be seen from the EDX map of gold and iron (Fig. S11, ESI†) with an average size of 201 nm (hydrodynamic size: 192 nm and PDI: 0.245, Fig. S3, ESI†).

3.2. Magnetic properties and nanoparticle stability in dispersion

For any sensor system based on magnetic nanoparticles, three features are sought: (1) high magnetic saturation (fast response to a magnet), (2) colloidal stability, and (3) low magnetic aggregation.[1] Moreover, gold coated magnetic nanoparticles >100 nm are suitable to be applied in *in vitro* sensors of biomarkers on a comparable size scale.[40] Having superparamagnetic nanoparticle components in the larger conglomerate ensures that when the magnetic field is removed, the individual domains of the magnetite nanoparticles easily relax and no permanent magnetism is retained in the conglomerate nanoparticle.[41] This is shown by the hysteresis loops (Fig. S12, ESI†) that show all the nanoparticles display superparamagnetic behaviour, with a remnant magnetization of ~7 emu g^{-1} and a coercivity of <9 Oe. Negligible remanence and coercivity demonstrate that the coating process encapsulated the superparamagnetic nanoparticles separately and did not cause the aggregation of magnetite nanoparticles.

Having multiple superparamagnetic nanoparticles in each conglomerate is crucial to compensate for the addition of a non-magnetic silica layer[15] and maintain a high magnetic susceptibility while retaining the superparamagnetic behaviour. Each magnetite nanoparticle contributes to individual magnetizations that sum to the total magnetization of the conglomerate. From the field-dependent magnetization measurements at 300 K in Fig. 2A, the magnetization saturation (M_s) values of 60, 34, 22 and 13 emu g^{-1} were observed for magnetite, silica coated conglomerates of superparamagnetic nanoparticles, gold coated conglomerates of superparamagnetic nanoparticles and the commercial gold coated magnetic nanoparticles, respectively. These values are typical for magnetite nanoparticles (58 emu g^{-1})[20] and for gold coated superparamagnetic nanoparticles (3.54 emu g^{-1} (ref. 16) and 7 emu g^{-1} (ref. 42)). The decrease in M_s after the addition of silica and the gold layer is simply because these materials are nonmagnetic and provide no magnetic contribution to the nanostructure.

Furthermore, to investigate the response time of the gold coated magnetic nanoparticles toward the magnet, a sequence of images and the corresponding intensity (the solution being depleted from particles as gold coated magnetic nanoparticles being attracted to the external magnetic field placed next to the cuvette) *vs.* time graph over 60 seconds for the different nanoparticles are shown in Fig. S13A–C (ESI†). The figures show that, after applying an external magnetic field, both synthesized and commercial gold coated nanoparticles are instantly attracted to the side of the cuvette where the magnet is placed. Furthermore, the transparency of the liquid in the cuvette increases which shows that nanoparticles are being drawn to the magnet. The increasing trend of transparency continues for up to 35–40 seconds and then stabilizes, indicating that all the nanoparticles have been drawn to the side of the cuvette. The speed at which the conglomerate particles responded to an external magnetic field is faster than that at which the reported gold coated magnetic nanoparticles with bigger or similar size magnetic cores (30 seconds and less than 3 minutes) responded to the external magnetic field.[43,44]

To investigate the colloidal stability, the change in hydrodynamic diameter and polydispersity index (PDI) in deionized water over time was measured for both the gold coated conglomerates of superparamagnetic nanoparticles and the commercially available gold coated magnetic nanoparticles (see Fig. 2B and

Fig. S14, ESI†). For the gold coated conglomerates of superparamagnetic nanoparticles, there were no significant changes observed in hydrodynamic diameter (~190 nm) and PDI (~0.195) for a period of 120 minutes. After this period, there was a decrease in hydrodynamic diameter from 189 nm to 183 nm and in the PDI from 0.197 to 0.166 which suggests some particle sedimentation. This sedimentation continues over a further 120 minutes as the measured hydrodynamic diameter approaches 144 nm and then stabilizes. In contrast, the commercial gold coated magnetic nanoparticles underwent a rapid decrease in both hydrodynamic diameter (192 nm to 174 nm) and PDI (0.245 to 0.208) after just 20 minutes, which is ascribed to particle sedimentation. The average size of the commercial nanoparticles continued to decrease to 116 nm and PDI as low as 0.118, and then started to stabilize.

The magnetic aggregation stability of both the gold coated conglomerates of superparamagnetic nanoparticles and the commercial gold coated magnetic nanoparticles were explored by observing the change in hydrodynamic diameter as a function of repeated cycles of collection and dispersion of particles via a magnet and sonication. As evident from Fig. 2C, Fig. S15A and B (ESI†), little to no aggregation was observed after repeated application and removal of a magnet, which shows that the conglomerates are stable against magnetic aggregation for at least 25 uses. This is because the nanoparticles were superparamagnetic and no remnant magnetization was observed (as shown by Fig. 2A). In comparison, the commercial nanoparticles begin to permanently aggregate after just 15 dispersion–collection cycles. The gold coated conglomerates of superparamagnetic nanoparticles have sufficient re-usability for use in commercial sensor applications, which require magnetic nanoparticles to respond to a magnet and be re-dispersed multiple times.

3.3. Optical properties

A qualitative demonstration of the optical properties of the gold coated nanoparticles was performed using dark field microscopy and Raman spectroscopy.

From Fig. 3, it is evident that gold artefacts appear in both the synthesized and commercial particle samples. The optical peak at around 460 nm in Fig. 3A and B is expected from the green appearance of pure gold aggregates under a dark field microscope. However, comparing Fig. 3A and B shows less aggregates as a proportion of the sample for the synthetic particles as opposed to the commercial particles, where they are the majority. The localised surface plasmonic resonance (LSPR) wavelength is influenced by particle size, shape, and composition, and therefore for identical particles one would expect close groupings in the histogram as all the peak wavelengths should be identical.

Slight variations in the nanoparticle diameter can cause a large change in LSPR, so a broader histogram is expected. Fig. 3A shows no real grouping of peak LSPR wavelengths and is dominated by the aggregates in the sample, and this lack of optical consistency suggests a lack of consistency within the sample, supported by the dark field and SEM images in the inset. Fig. 3B, aside from the aggregate peak at 460 nm, shows three major peaks at 495 nm, 570 nm and 625 nm demonstrating more optical consistency in the synthetic nanoparticles, as the width of the magnetic nanoparticle peak at 580 nm in Fig. 3A is far narrower than the wide distribution of 3B. This suggests three different sizes of particles, which could also be due to slight variations in the shape or surface smoothness of the particles. LSPR peak positions were estimated for dark field microscopy sensing purposes. As the LSPR of these particles is highly sensitive to the surrounding medium and thus the LSPR peak positions may be used for sensing. As the plasmonic biosensors are so highly sensitive, the narrower LSPR peaks of particles could be an important sign of the applicability of the particles for optical biosensing. Multiple peaks at 495 nm, 570 nm, and 625 nm result from the LSPR of the entire conglomerate nanoparticles, distortions from the perfect sphere shape and the surface roughness of the gold coated magnetic nanoparticles.[45,46] Illuminatingly, single particle spectra (Fig. S16A and B, ESI†) show a broad spectrum with a

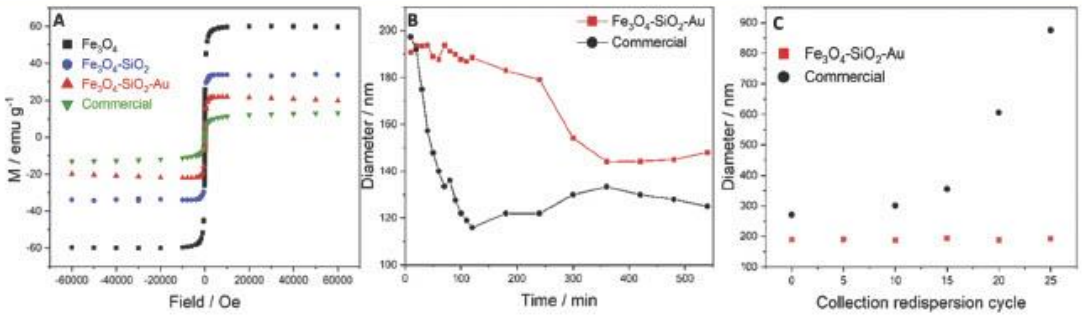

Fig. 2 (A) SQUID magnetometry measurements of the magnetization behavior of iron oxide superparamagnetic nanoparticles (black), silica coated conglomerates of superparamagnetic nanoparticles (blue), gold coated conglomerates of superparamagnetic nanoparticles (red), and commercial gold coated magnetic nanoparticles (green). Dynamic light scattering measurement of (B) the colloidal stability of the gold coated conglomerates of superparamagnetic nanoparticles (red) and commercial gold coated magnetic nanoparticles (black) over time, (C) stability behavior of gold coated conglomerates of superparamagnetic nanoparticles (red) and commercial gold coated magnetic nanoparticles (black) after collecting by a magnet and redispersion by sonication (repeated for 25 cycles).

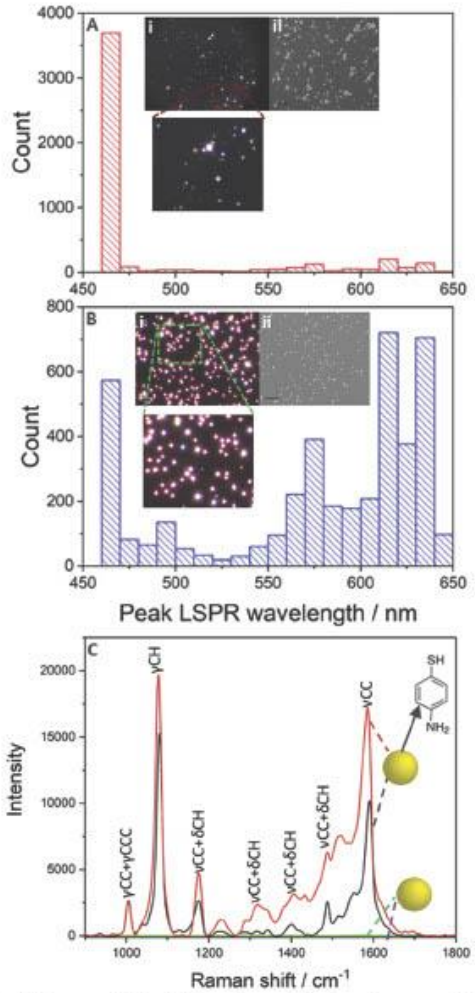

Fig. 3 Histogram of the LSPR peak wavelength of commercial gold coated magnetic nanoparticles in a dark-field image; the inset shows (i) the dark field microscopy image of the commercial gold coated magnetic nanoparticles and (ii) the corresponding SEM image of the commercial gold coated magnetic nanoparticles; scale bar: 5 μm. (B) Histogram of the LSPR peak wavelength of gold coated conglomerates of superparamagnetic nanoparticles in a dark-field image; the inset shows (i) the dark field microscopy image of the gold coated conglomerates of superparamagnetic nanoparticles and (ii) the corresponding SEM image of the gold coated conglomerates of superparamagnetic nanoparticles; scale bar: 5 μm. (C) Raman spectra of bare gold coated conglomerates of superparamagnetic nanoparticles (green), bare commercial gold coated magnetic nanoparticles (purple), SERS spectra of 4-aminothiolphenol (4-ATP) modified gold coated conglomerates of superparamagnetic nanoparticles (red) and 4-aminothiolphenol (4-ATP) modified commercial gold coated magnetic nanoparticles (black). The Raman peak assignments are shown for the corresponding vibration modes.

peak at 490 nm and 700 nm, which corresponds to the brown colour of the nanoparticles. From the dark field inset in Fig. 3B two different sizes of nanoparticles may be observed, but the broadness of the histogram may be attributed to the broad overall spectrum of the individual nanoparticles, with the peak at 490 nm remaining consistent. This is supported by the overall uniformity of the shape and size of gold coated magnetic nanoparticles, which can be seen from the SEM image of the nanoparticles (Fig. 3B(ii)).

As the particles are quite large, a broad single particle spectrum is expected but it may also point to a slight variation from a perfectly spherical particle.[45,47] The peak at 700 nm in Fig. S16A–C (ESI†) remains even when there are numerous particles on the surface indicating the overall optical consistency of the gold coated conglomerates of superparamagnetic nanoparticles. This consistency is particularly important for optical sensing functions. Narrowing of the LSPR peaks by improving the uniformity in the shape and size of the nanoparticles would enable smaller optical shifts to be detected and enhance the sensor sensitivity. The particle spectra and LSPR histogram of commercially available gold coated magnetic nanoparticles (Fig. S16D, ESI†) show two major peaks at 580 nm and 820 nm corresponding to the orange colour of the particles observed under dark field microscopy. Moreover, the broad range of the particle size in the LSPR histogram implies far less consistency in optical properties. The UV-vis spectrum of gold coated conglomerates of superparamagnetic particles shows a broad peak at 800 nm. The absorbance peak moves to around 570 nm in the case of commercial gold coated magnetic nanoparticles (Fig. S17, ESI†).

As gold coated magnetic nanoparticles in the presence of gold can enhance both the incident laser field and the scattered field, and thus amplify the Raman signal, to give surface enhanced Raman scattering (SERS),[48] we next demonstrate that the gold coated conglomerates of superparamagnetic nanoparticles are suitable for SERS tags.[49] To achieve this, gold coated conglomerates and commercial particles were modified with 4-aminothiolphenol (4-ATP) as a Raman reporter molecule. Fig. 3B depicts the SERS spectra obtained from gold coated conglomerates of superparamagnetic nanoparticles and commercial gold coated magnetic nanoparticles labelled with 4-ATP.

Distinctive vibrational modes at 1078, 1140, 1388, 1430 and 1582 cm^{-1} originated from 4-ATP can be observed when the molecules are attached on the surface of the gold coated conglomerates of the superparamagnetic nanoparticles. Furthermore, the main peaks assigned to 4-ATP molecules are in good agreement with the literature[25,50] suggesting the complete replacement of the capping surfactant on the surface of gold coated conglomerates of superparamagnetic nanoparticles by the 4-ATP molecules. Note that no detectable signal was observed when the unmodified gold coated nanoparticles were used for the Raman measurement (green and purple spectra).

3.4. Electrochemical properties

The electrochemical properties of gold coated conglomerates of superparamagnetic nanoparticles and commercial gold coated magnetic nanoparticles were studied in 0.5 M H_2SO_4 aqueous solution using cyclic voltammetry (CV), aiming to confirm the

presence of the gold shell around the magnetic cores. The calculated electroactive area is 0.195 cm^2 and around 400 μL of 2.8×10^9 particles per mL is required to form a monolayer of particles on the gold foil. Fig. 4 shows the CV of the bare gold electrode (black) in comparison to the gold coated conglomerates of superparamagnetic nanoparticles in 0.5 M H_2SO_4 aqueous solution at a scan rate of 0.1 V s^{-1}. An aliquot of 500 μL of (2.8×10^9 particles per mL) gold coated conglomerates of superparamagnetic nanoparticles and 600 μL (3.1×10^{10} particles per mL) of commercial gold coated magnetic nanoparticles were used for this measurement to obtain a typical gold CV curve in 0.5 M H_2SO_4 aqueous solution. The addition of gold coated conglomerates of superparamagnetic nanoparticles on the surface of the gold foil was evident by the small enhancement of the faradaic peaks at 0.9 and 1.5 V, where the reduction and oxidation of the gold surface occur.

This only slight increase in the apparent electroactive surface area despite the approximately 10 layers of nanoparticles was consistent with previous studies employing gold-coated magnetic nanoparticles.[51] It should be noted that if not for the complete formation of a conducting gold coat on the surface, the addition of the nanoparticles could have resulted in a diminution of the current.[43] The electrochemical behaviour of commercial gold coated magnetic nanoparticles in 0.5 M H_2SO_4 is depicted in Fig. S18 (ESI†).

Although the enhancement of faradaic current at 1.5 V could be a sign of the existence of gold, the decrease in faradaic current at 0.9 V shows that the apparent electroactive area of the gold foil has decreased (despite the addition of more particles) probably because of the existence of the iron oxide or other non-electroactive component.

To demonstrate the ability of our nanocomposites to serve as electrochemical biosensors, square-wave voltammograms of gold coated conglomerates of superparamagnetic nanoparticles before and after immobilization of the methylene-blue-labelled probe DNA were recorded (Fig. 5).

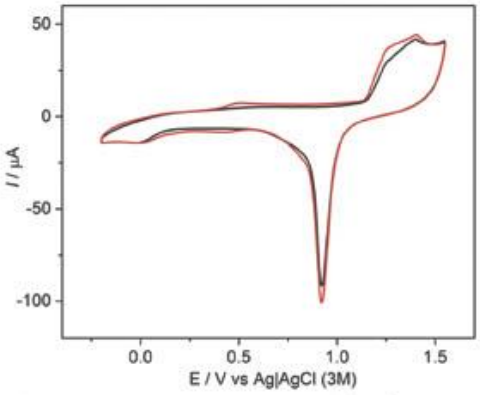

Fig. 4 Cyclic voltammograms of a bare gold foil (black) and gold coated conglomerates of superparamagnetic nanoparticles (red) in an aqueous solution of 50 mM H_2SO_4 at 0.1 V s^{-1}.

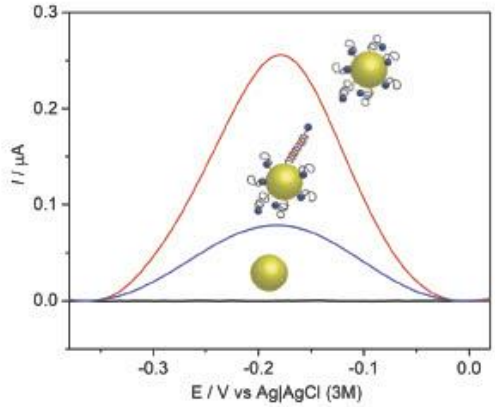

Fig. 5 Square-wave voltammograms of gold coated conglomerates of superparamagnetic nanoparticles before (black) and after (red) modification with methylene-blue-labelled probe DNA and after hybridization (blue) with the target miRNA miR-21.

The surface of gold coated conglomerates of superparamagnetic nanoparticles was modified with probe DNA *via* Au–S linkage at one end and methylene blue redox label at the other end. As can be seen from Fig. 5, the square-wave voltammograms of gold coated conglomerates of superparamagnetic nanoparticles act similarly to a gold disk electrode when modified with methylene-blue-labelled probe DNA molecules and show an increased current due to faster electron transfer between the redox molecules and the surface, while there is no current observed for unmodified particles.

To further investigate the electrochemical performance of the gold coated conglomerates of superparamagnetic nanoparticles as dispersible electrodes, complementary miRNA miR-21 were used to hybridize with the MB labelled probe DNA that has already been modified on the gold coated nanoparticles. Compared to the probe DNA the current response has decreased upon hybridization with DNA/miRNA 21, which is ascribed to two phenomena: first, the increase in the distance between the MB redox label and the electrode surface; second, the increased rigidity of the DNA/miRNA double helix compared to the probe DNA.[26]

4. Conclusions

In conclusion, this work shows a new methodology to prepare gold coated magnetic nanoparticles with a high load of superparamagnetic cores. The resulting particles showed a fast response to the external magnetic field and high resistibility against magnetic aggregation. The optical consistency of particles was demonstrated by dark field single particle spectra, and the presence of the gold shell on the surface was shown by CV in sulfuric acid solution. The conglomerate nanoparticle was able to bind to the 4-ATP molecule and methylene-blue-labelled probe DNA. The ability of gold coated conglomerates of superparamagnetic nanoparticles to target, bind and separate a target molecule and further be used as optical or electrochemical

biosensors was demonstrated by employing SERS and square wave voltammograms.

Conflicts of interest

There are no conflicts to declare.

Acknowledgements

JJG and RDT acknowledge funding under the Australian Research Council Linkage grant (LP150101014), the Australian Laureate Fellowship (FT150100060), ARC Centre of Excellence in Convergent Bio-Nano Science and Technology (CE140100036) and the Discovery Project (DP190102659 and DP200100143). LG and RDT acknowledge the Dementia Australia Research Foundation Yulgilbar innovation grant.

Notes and references

1 L. Gloag, M. Mehdipour, D. Chen, R. D. Tilley and J. J. Gooding, *Adv. Mater.*, 2019, 31, 1904385.
2 S. Moraes Silva, R. Tavallaie, L. Sandiford, R. D. Tilley and J. J. Gooding, *Chem. Commun.*, 2016, 52, 7528–7540.
3 E. Lueshen, I. Venugopal, J. Kanikunnel, T. Soni, A. Alaraj and A. Linninger, *Nanomedicine*, 2014, 9, 1155–1169.
4 A. Ángeles-Pascual, J. R. Piñón-Hernández, M. Estevez-González, U. Pal, S. Velumani, R. Pérez and R. Esparza, *Mater. Charact.*, 2018, 142, 237–244.
5 L. León Félix, B. Sanz, V. Sebastián, T. E. Torres, M. H. Sousa, J. A. H. Coaquira, M. R. Ibarra and G. F. Goya, *Sci. Rep.*, 2019, 9, 1–11.
6 L. Gloag, M. Mehdipour, M. Ulanova, K. Mariandry, M. A. Nichol, D. J. Hernández-Castillo, J. Gaudet, R. Qiao, J. Zhang, M. Nelson, B. Thierry, M. A. Alvarez-Lemus, T. T. Tan, J. J. Gooding, N. Braidy, P. S. Sachdev and R. D. Tilley, *Chem. Commun.*, 2020, 56, 3504–3507.
7 I. Y. Goon, L. M. H. Lai, M. Lim, R. Amal and J. J. Gooding, *Chem. Commun.*, 2010, 46, 8821.
8 S. M. Silva and J. Justin Gooding, *RSC Detect. Sci.*, 2016, 2016, 279–295.
9 K. Chuah, L. M. H. Lai, I. Y. Goon, S. G. Parker, R. Amal and J. Justin Gooding, *Chem. Commun.*, 2012, 48, 3503–3505.
10 H. Rui, R. Xing, Z. Xu, Y. Hou, S. Goo and S. Sun, *Adv. Mater.*, 2010, 22, 2729–2742.
11 A. H. Lu, E. L. Salabas and F. Schüth, *Angew. Chem., Int. Ed.*, 2007, 46, 1222–1244.
12 M. Mahmoudi, H. Hofmann, B. Rothen-Rutishauser and A. Petri-Fink, *Chem. Rev.*, 2012, 112, 2323–2338.
13 Z. Zhao, Z. Zhou, J. Bao, Z. Wang, J. Hu, X. Chi, K. Ni, R. Wang, X. Chen, Z. Chen and J. Gao, *Nat. Commun.*, 2013, 4, 1–7.
14 J. W. Kim, D. Seo, J. U. Lee, K. M. Southard, Y. Lim, D. Kim, Z. J. Gartner, Y. W. Jun and J. Cheon, *Nat. Protoc.*, 2017, 12, 1871–1889.
15 M. E. Khosroshahi and L. Ghazanfari, *Mater. Chem. Phys.*, 2012, 133, 55–62.
16 A. Sood, V. Arora, J. Shah, R. K. Kotnala and T. K. Jain, *J. Exp. Nanosci.*, 2016, 11, 370–382.
17 S. I. Uribe Madrid, U. Pal, Y. S. Kang, J. Kim, H. Kwon and J. Kim, *Nanoscale Res. Lett.*, 2015, 10, 217.
18 L. E. Woodard, C. L. Dennis, J. A. Borchers, A. Attaluri, E. Velarde, C. Dawidczyk, P. C. Searson, M. G. Pomper and R. Ivkov, *Sci. Rep.*, 2018, 8, 1–13.
19 L. Gutiérrez, R. Costo, C. Grüttner, F. Westphal, N. Gehrke, D. Heinke, A. Fornara, Q. A. Pankhurst, C. Johansson, S. Veintemillas-Verdaguer and M. P. Morales, *Dalton Trans.*, 2015, 44, 2943–2952.
20 D. Maity, S. G. Choo, J. Yi, J. Ding and J. M. Xue, *J. Magn. Magn. Mater.*, 2009, 321, 1256–1259.
21 S. T. Selvan, T. T. Tan and J. Y. Ying, *Adv. Mater.*, 2005, 17, 1620–1625.
22 Y. Han, J. Jiang, S. S. Lee and J. Y. Ying, *Langmuir*, 2008, 24, 5842–5848.
23 J. L. Hueso, V. Sebastián, Á. Mayoral, L. Usón, M. Arruebo and J. Santamaría, *RSC Adv.*, 2013, 3, 10427–10433.
24 B. E. Brinson, J. B. Lassiter, C. S. Levin, R. Bardhan, N. Mirin and N. J. Halas, *Society*, 2008, 120, 14166–14171.
25 R. Pardehkhorram, S. Bonaccorsi, H. Zhu, V. R. Gonçales, Y. Wu, J. Liu, N. A. Lee, R. D. Tilley and J. J. Gooding, *Chem. Commun.*, 2019, 55, 7707–7710.
26 R. Tavallaie, J. McCarroll, M. Le Grand, N. Ariotti, W. Schuhmann, E. Bakker, R. D. Tilley, D. B. Hibbert, M. Kavallaris and J. J. Gooding, *Nat. Nanotechnol.*, 2018, 13, 1066–1071.
27 M. Sriram, B. P. Markhali, P. R. Nicovich, D. T. Bennett, P. J. Reece, D. Brynn Hibbert, R. D. Tilley, K. Gaus, S. R. C. Vivekchand and J. J. Gooding, *Biosens. Bioelectron.*, 2018, 117, 530–536.
28 M. I. Dar and S. A. Shivashankar, *RSC Adv.*, 2014, 4, 4105–4113.
29 J. H. L. Beal, S. Prabakar, N. Gaston, G. B. The, P. G. Etchegoin, G. Williams and R. D. Tilley, *Chem. Mater.*, 2011, 23, 2514–2517.
30 T. Hyeon, S. Seong Lee, J. Park, Y. Chung and H. Bin Na, *J. Am. Chem. Soc.*, 2001, 123, 12798–12801.
31 M. Zhang, B. L. Cushing and C. J. O'Connor, *Nanotechnology*, 2008, 19, 085601.
32 M. Stjerndahl, M. Andersson, H. E. Hall, D. M. Pajerowski, M. W. Meisel and R. S. Duran, *Langmuir*, 2008, 24, 3532–3536.
33 E. Tombácz, R. Turcu, V. Socoliuc and L. Vékás, *Biochem. Biophys. Res. Commun.*, 2015, 468, 442–453.
34 S. L. Westcott, S. J. Oldenburg, T. R. Lee and N. J. Halas, *Langmuir*, 1998, 14, 5396–5401.
35 I. Monaco, F. Arena, S. Biffi, E. Locatelli, B. Bortot, F. La Cava, G. M. Marini, G. M. Severini, E. Terreno and M. Comes Franchini, *Bioconjugate Chem.*, 2017, 28, 1382–1390.
36 D. V. Leff, L. Brandt and J. R. Heath, *Langmuir*, 1996, 12, 4723–4730.
37 J. Reguera, J. Langer, D. Jiménez De Aberasturi and L. M. Liz-Marzán, *Chem. Soc. Rev.*, 2017, 46, 3866–3885.
38 S. S. Shankar, A. Ahmad, R. Pasricha and M. Sastry, *J. Mater. Chem.*, 2003, 13, 1822–1826.

39 M. Aslam, L. Fu, M. Su, K. Vijayamohanan and V. P. Dravid, *J. Mater. Chem.*, 2004, 14, 1795–1797.
40 S. A. Adams, J. L. Hauser, A. C. Allen, K. P. Lindquist, A. P. Ramirez, S. Oliver and J. Z. Zhang, *ACS Appl. Nano Mater.*, 2018, 1(3), 1406–1412.
41 Y. Gossuin, P. Gillis, A. Hocq, Q. L. Vuong and A. Roch, *Wiley Interdiscip. Rev.: Nanomed. Nanobiotechnol.*, 2009, 1, 299–310.
42 E. Iglesias-Silva, J. L. Vilas-Vilela, M. A. López-Quintela, J. Rivas, M. Rodríguez and L. M. León, *J. Non-Cryst. Solids*, 2010, 356, 1233–1235.
43 S. MoraesSilva, R. Tavallaie, M. TanzirulAlam, K. Chuah and J. J. Gooding, *Electroanalysis*, 2016, 28, 431–438.
44 J. Wang, X. Wu, C. Wang, Z. Rong, H. Ding, H. Li, S. Li, N. Shao, P. Dong, R. Xiao and S. Wang, *ACS Appl. Mater. Interfaces*, 2016, 8, 19958–19967.
45 S. K. Gray, *J. Phys. Chem. C*, 2013, 117, 1983–1994.
46 B. B. Rajeeva, D. S. Hernandez, M. Wang, E. Perillo, L. Lin, L. Scarabelli, B. Pingali, L. M. Liz-Marzán, A. K. Dunn, J. B. Shear and Y. Zheng, *Adv. Sci.*, 2015, 2, 28–30.
47 B. P. Markhali, M. Sriram, D. T. Bennett, P. S. Khiabani, S. Hoque, R. D. Tilley, P. Bakthavathsalam and J. J. Gooding, *Biosens. Bioelectron.*, 2020, 169, 112612.
48 N. Li, P. Zhao and D. Astruc, *Angew. Chem., Int. Ed.*, 2014, 53, 1756–1789.
49 X. Zhou, W. Xu, Y. Wang, Q. Kuang, Y. Shi, L. Zhong and Q. Zhang, *J. Phys. Chem. C*, 2010, 114, 19607–19613.
50 M. Osawa, N. Matsuda, K. Yoshii and I. Uchida, *J. Phys. Chem.*, 1994, 98, 12702–12707.
51 L. M. H. Lai, I. Y. Goon, M. Lim, D. B. Hibbert, R. Amal and J. J. Gooding, *J. Electroanal. Chem.*, 2011, 656, 130–135.

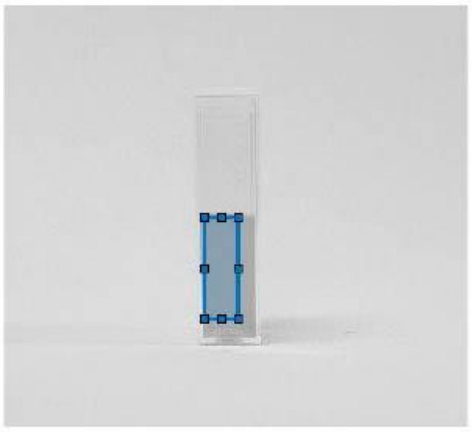

Figure S1. A black and white image showing the commercial particles before a magnet was applied. The blue overlay is a user selected area of pixels, the same area is then used for successive images

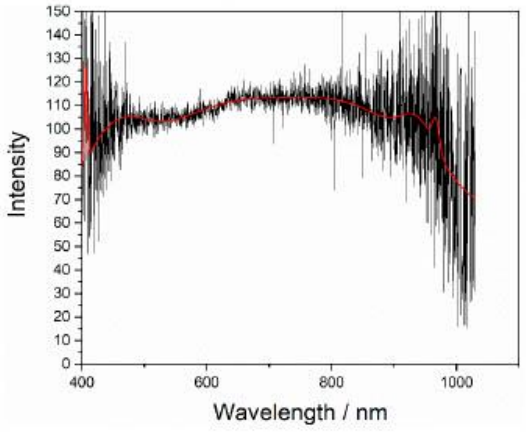

Figure S2. Graph of the raw data acquired from dark field single particle spectra (black) and the interpolated fit (red) from the origin multiple peak fit

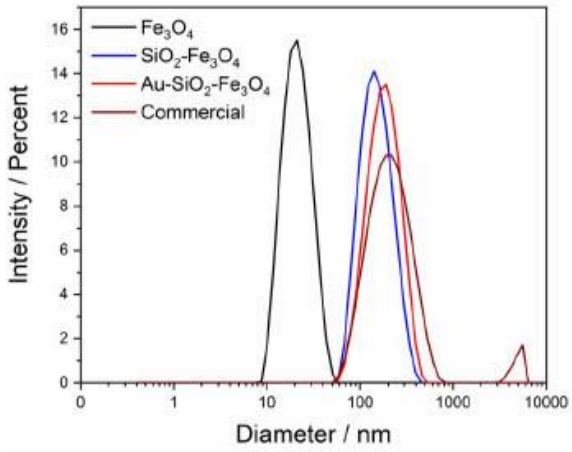

Figure S3. Dynamic light scattering (DLS) of Magnetite nanoparticles (black), Silica coated conglomerates of superparamagnetic nanoparticles (blue), gold coated conglomerates of superparamagnetic nanoparticles (red) and commercial gold coated magnetic nanoparticles (wine)

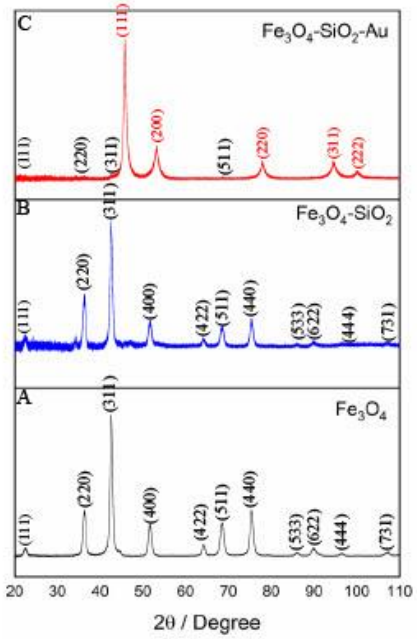

Figure S4. X-ray diffraction patterns of A) magnetite nanoparticles B) Silica coated conglomerates of superparamagnetic nanoparticles and C) gold coated conglomerates of superparamagnetic nanoparticles, with representative index on typical peaks

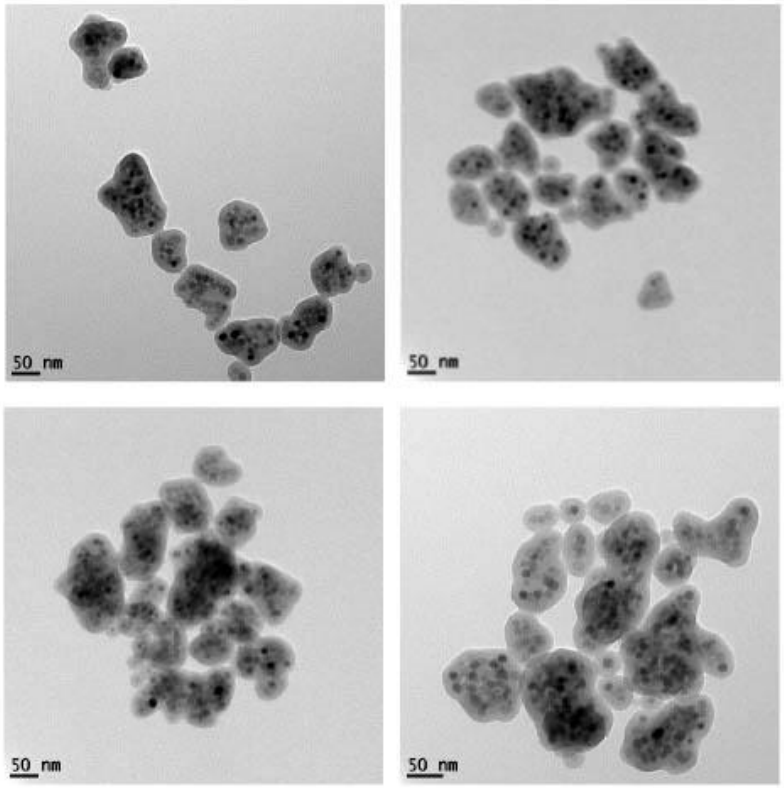

Figure S5.TEM images of silica coated conglomerates of superparamagnetic nanoparticles showing the high loads of magnetic nanoparticles inside silica shell

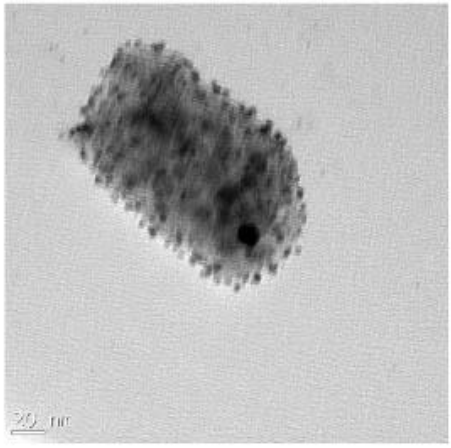

Figure S6. TEM image of gold nanoparticle decorated (<4 nm) silica coated conglomerates of superparamagnetic nanoparticles (black dots show the small gold nanoparticles)

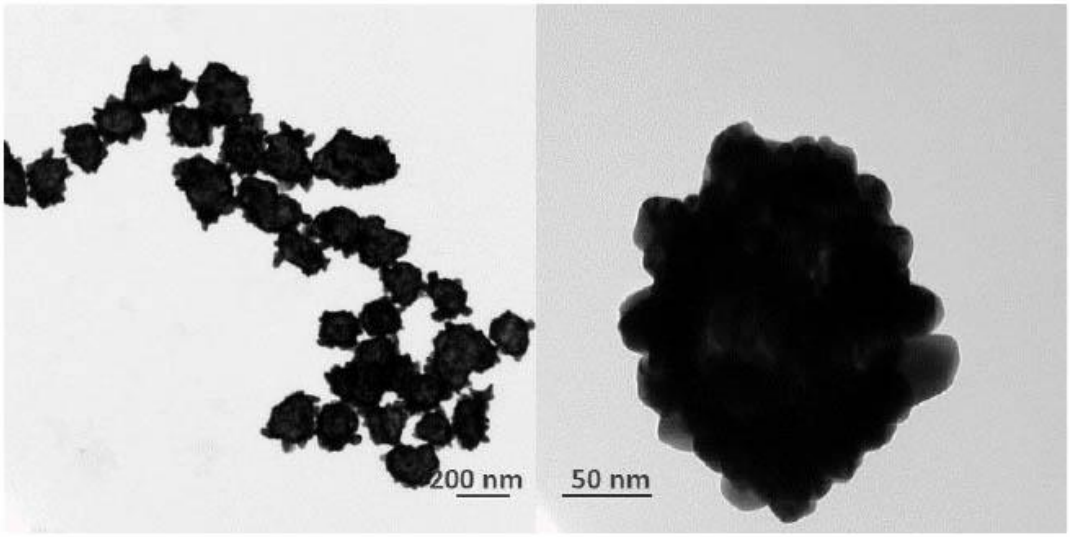

Figure S7. TEM images of the gold coated conglomerates of superparamagnetic nanoparticles

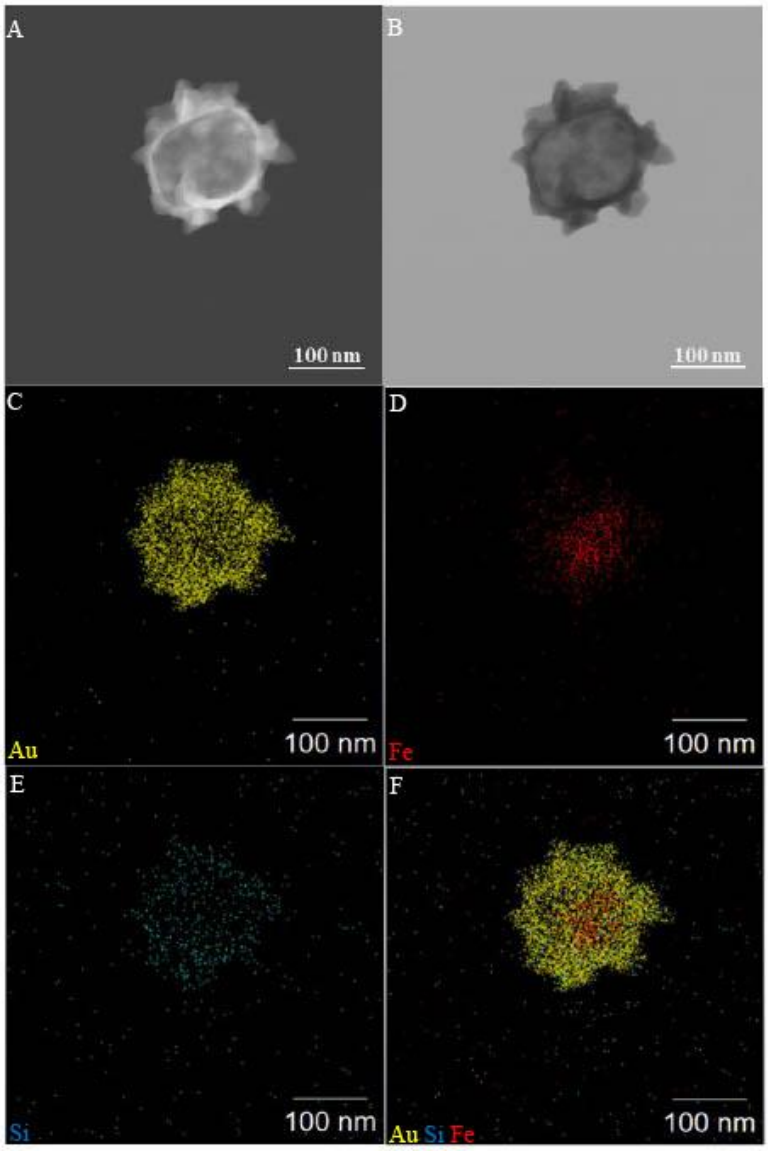

Figure S8. A) Bright field, B) dark field STEM images and STEM-EDX map of the elements C) gold D) iron E) silicon and F) merged gold silicon and iron of the gold coated conglomerates of superparamagnetic nanoparticles

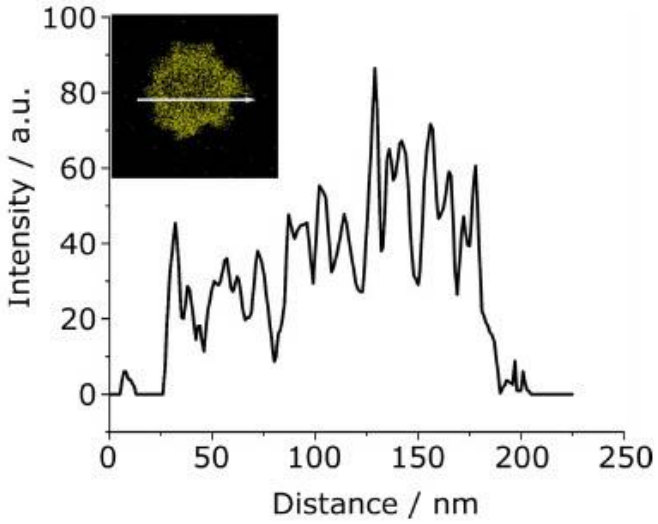

Figure S9. Line scan analysis of element gold of the gold coated conglomerates of superparamagnetic nanoparticles inset shows the EDX map of the element gold

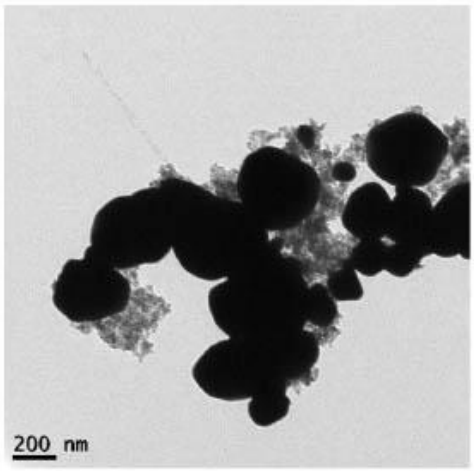

Figure S10. TEM image of commercially available gold coated magnetic nanoparticles acquired from Creative Diagnostics

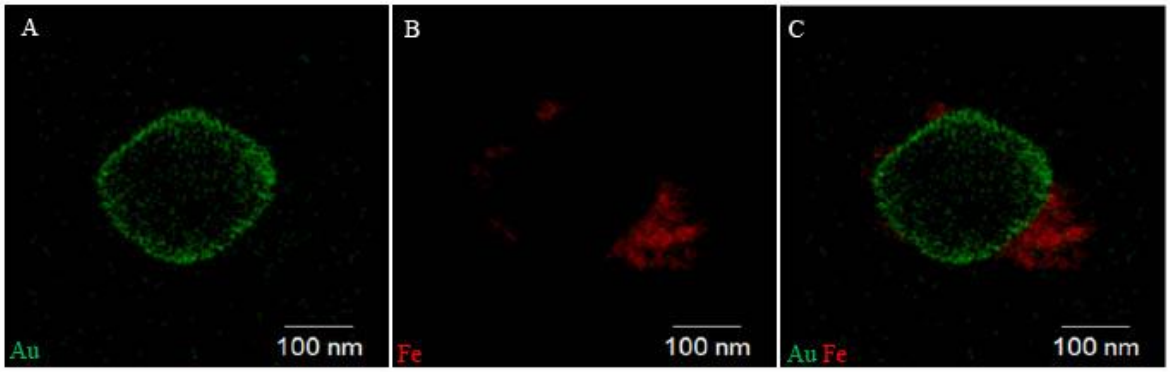

Figure S11. EDX map of the elements A) gold B) iron and C) merged gold and iron of the commercial gold coated magnetic nanoparticles

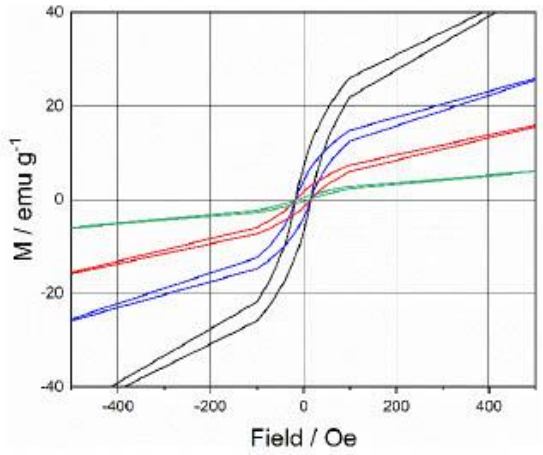

Figure S12. SQUID magnetometry measurements of magnetization behavior of (black) iron oxide superparamagnetic nanoparticles, (blue) silica coated conglomerates of superparamagnetic nanoparticles, (red) gold coated conglomerates of superparamagnetic nanoparticles, (green) commercial gold coated magnetic nanoparticles

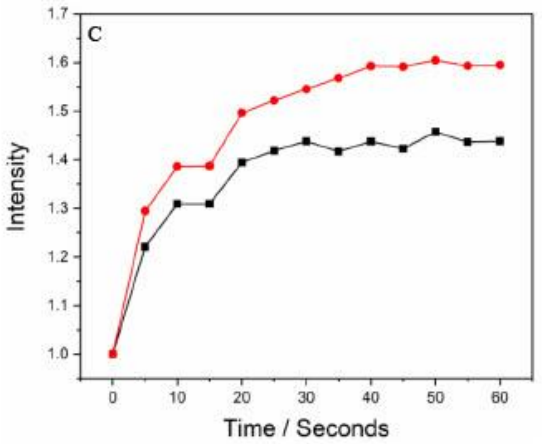

Figure S13. Sequence of images taken by interval of 5 seconds of A) gold coated conglomerates of superparamagnetic nanoparticles, B) commercial gold coated magnetic nanoparticles and C) Graph of intensity vs time as (red) gold coated conglomerates of superparamagnetic nanoparticles and (black) commercial gold coated magnetic nanoparticles respond to a magnet

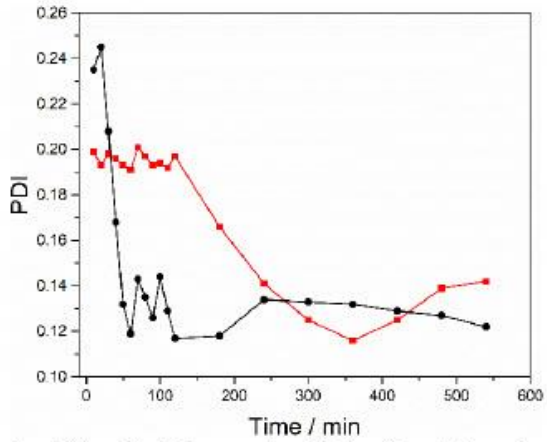

Figure S14. Variation of polydispersity index over time (red) gold coated conglomerates of superparamagnetic nanoparticles and (black) commercial gold coated magnetic nanoparticles

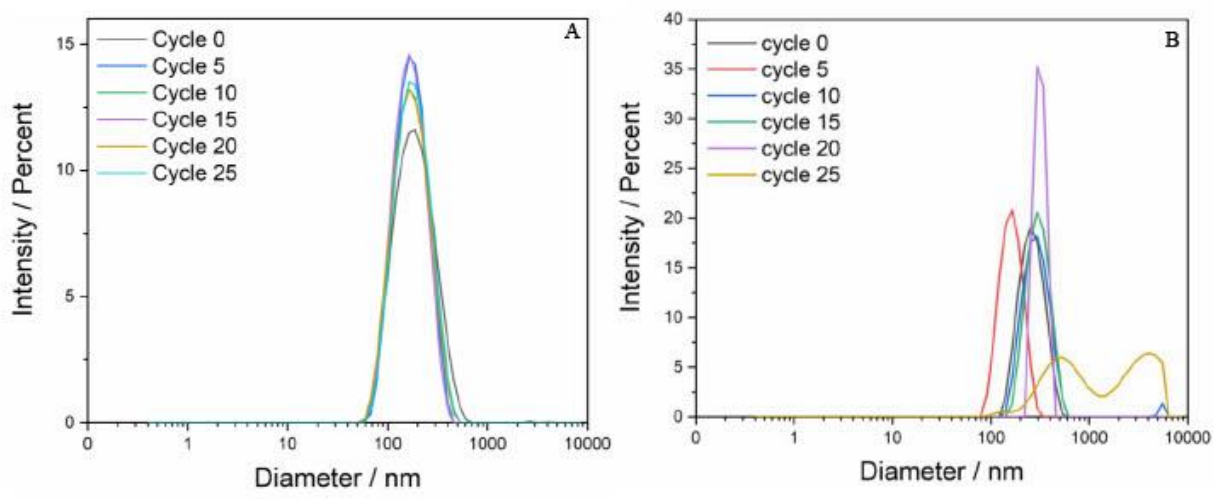

Figure S15. Dynamic light scattering (DLS) measurements of stability behavior of (A) gold coated conglomerates of magnetic nanoparticles and (b) commercial gold coated magnetic nanoparticles after collecting by a magnet and redispersion by sonication

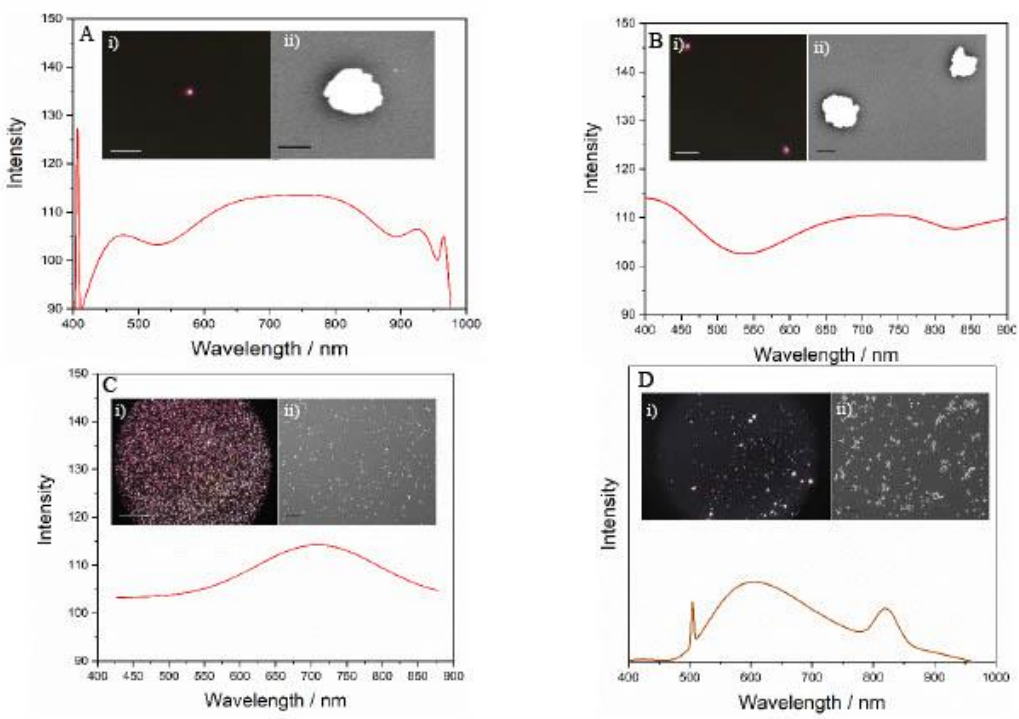

Figure S16. A) Single-particle dark-field spectroscopy of a gold coated conglomerates of superparamagnetic nanoparticle, Inset shows i) dark field microscopy image of a gold coated conglomerates of superparamagnetic nanoparticles, scale bar 500 nm and ii) corresponding SEM image of the gold coated conglomerates of superparamagnetic nanoparticles, scale bar 100 nm. and B) particle dark-field spectroscopy of two gold coated conglomerates of superparamagnetic nanoparticles, Inset shows i) dark field microscopy image of numerous gold coated conglomerates of superparamagnetic nanoparticles, scale bar 500 nm and ii) corresponding SEM image of the gold coated conglomerates of superparamagnetic nanoparticles, scale bar 100 nm. C) particle dark-field spectroscopy of numerous gold coated conglomerates of superparamagnetic nanoparticle, Inset shows i) dark field microscopy image of numerous gold coated conglomerates of superparamagnetic nanoparticles, scale bar 500 nm and ii) corresponding SEM image of the gold coated conglomerates of superparamagnetic nanoparticles, scale bar 5 μm and D) particle dark-field spectroscopy of commercial gold coated magnetic nanoparticles, inset shows i) dark field microscopy image of commercial gold coated magnetic nanoparticles ii) Corresponding SEM image of the commercial gold coated magnetic nanoparticles and

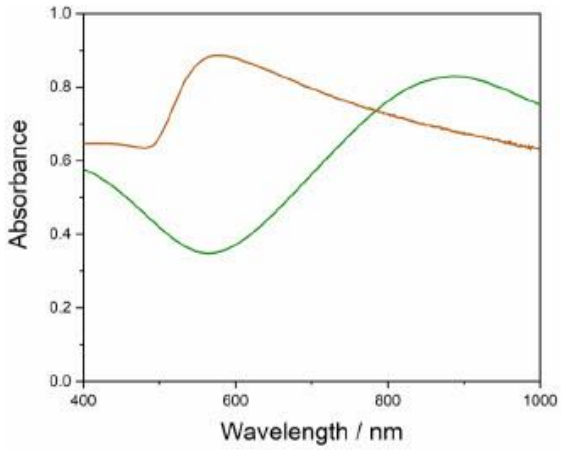

Figure S17. UV-Vis spectra of (green) gold coated conglomerates of superparamagnetic nanoparticles and (brown) commercial gold coated magnetic nanoparticles

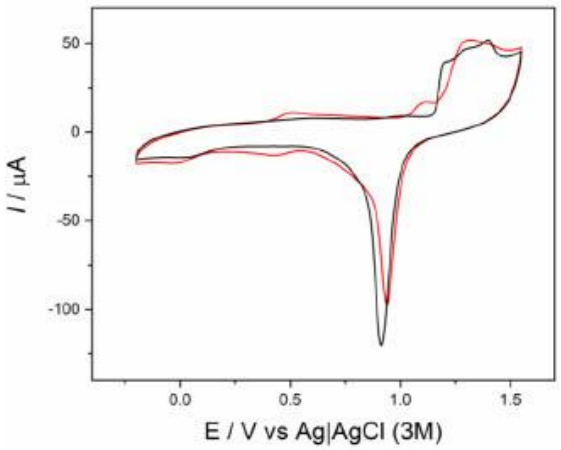

Figure S18. Cyclic voltammograms of bare gold foil (black) and commercial gold coated magnetic nanoparticles (red) in aqueous solution of 50 mM H_2SO_4 at 0.1 Vs^{-1}

Matlab script

```
[file,path] = uigetfile(' *.jpg',...
   'Select One or More Files', ...
   'MultiSelect', 'on');
selectedfile = fullfile(path,file);
im=imread(selectedfile);
BW = im(:,:,3);

figure()
imshow(BW)
hold on
u=gca;
roi=drawrectangle(u);
positionroi=roi.Position;
waitfor(gcf)
hold off
cropim=imcrop(BW,positionroi);
meanintensity=median(cropim(:));
answer = questdlg('Are there further images?', ...
    'Options', ...
    'Yes,No');
i=2;
while(strcmp(answer,'Yes')==1)
  [file,path] = uigetfile(' *.jpg',...
   'Select One or More Files', ...
   'MultiSelect', 'on');
        selectedfile = fullfile(path,file);
        im=imread(selectedfile);
        BW = rgb2gray(im);
        figure()
        u=gca;
        imshow(BW)
        roi=drawrectangle(u,'Position',positionroi);
        waitfor(gcf)
        hold off
        cropim=imcrop(BW,positionroi);
        meanintensity(:,i)=mean(cropim(:));
        answer = questdlg('Are there further images?', ...
            'Options', ...
            'Yes,No');
        i=i+1;
end
```

Chapter 5

Synthesis of strongly magnetic gold-coated zero-valent iron core-iron oxide shell nanoparticles with superparamagnetic behaviour

Publication two

Milad Mehdipour, Lucy Gloag, Jiaxin Lian, Richard D Tilley and J. Justin Gooding, submitted to ChemComm September 2021

5.1. Summery

The publication ‘’Synthesis of strongly magnetic gold-coated zero-valent iron core-iron oxide shell nanoparticles with superparamagnetic behaviour’’ has been used in lieu of a chapter. The aim of this paper was to synthesis gold-coated magnetic nanoparticles with high magnetization saturation while keeping the superparamagnetic behaviour intact. To achieve this, a highly magnetic zero-valent iron core-iron oxide shell was first synthesized *via* thermal decomposition of iron pentacarbonyl. The capping agent on the surface of zero-valent iron nanoparticles was changed from OD-PD to oleic acid. The nanoparticles were then exposed to air and become zero-valent iron core-iron oxide shell and were coated with a silica layer *via* the microemulsion method. A gold layer was introduced on the surface of nanoparticles *via* a seed-mediated method. The result of SQUID magnetometry showed a magnetization saturation of 63 emu g^{-1} for the gold-coated zero-valent iron core-iron oxide shell while the nanoparticles kept their superparamagnetic behaviour. The nanoparticles further demonstrated high stability against magnetic aggregation.

Declaration for Chapter Five

Author	**Contribution**
Milad Mehdipour	Synthesized zero-valent iron nanoparticles, silica-coated zero-valent iron core-iron oxide shell nanoparticles, gold-coated zero-valent iron core-iron oxide shell nanoparticles Characterised nanoparticles using TEM, SQUID magnetometry, UV-Vis spectroscopy, Darkfield image Carried out stability against magnetic aggregation and colloidal stability experiments Drafted and proofread the manuscript
Lucy Gloag	Experimental design Proofread manuscript
Jiaxin Lian	Digestion of silica-coated zero-valent iron core-iron oxide shell nanoparticles, gold-coated zero-valent iron core-iron oxide shell nanoparticles with HF
Richard. D Tilley	Experimental design Provided fundamental understanding of the key magneto plasmonic properties and synthesis of nanoparticles Proofread manuscript
J. Justin Gooding	Experimental design Provided fundamental understanding of the key magneto plasmonic properties and synthesis of nanoparticles Proofread manuscript

UNSW is supportive of candidates publishing their research results during their candidature as detailed in the UNSW Thesis Examination Procedure.

Publications can be used in their thesis in lieu of a Chapter if:

- The candidate contributed greater than 50% of the content in the publication and is the "primary author", ie. the candidate was responsible primarily for the planning, execution and preparation of the work for publication
- The candidate has approval to include the publication in their thesis in lieu of a Chapter from their supervisor and Postgraduate Coordinator.
- The publication is not subject to any obligations or contractual agreements with a third party that would constrain its inclusion in the thesis

Please indicate whether this thesis contains published material or not:

☐ This thesis contains no publications, either published or submitted for publication
(if this box is checked, you may delete all the material on page 2)

☐ Some of the work described in this thesis has been published and it has been documented in the relevant Chapters with acknowledgement
(if this box is checked, you may delete all the material on page 2)

☒ This thesis has publications (either published or submitted for publication) incorporated into it in lieu of a chapter and the details are presented below

CANDIDATE'S DECLARATION

I declare that:

- I have complied with the UNSW Thesis Examination Procedure
- where I have used a publication in lieu of a Chapter, the listed publication(s) below meet(s) the requirements to be included in the thesis.

Candidate's Name	**Signature**	**Date (dd/mm/yy)**
Milad Mehdipour		

POSTGRADUATE COORDINATOR'S DECLARATION *To only be filled in where publications are used in lieu of Chapters*

I declare that:

- the information below is accurate
- where listed publication(s) have been used in lieu of Chapter(s), their use complies with the UNSW Thesis Examination Procedure
- the minimum requirements for the format of the thesis have been met.

PGC's Name	PGC's Signature	Date (dd/mm/yy)
Alex William Donald		

For each publication incorporated into the thesis in lieu of a Chapter, provide all of the requested details and signatures required

Details of publication #2:

Full title: Synthesis of strongly magnetic gold-coated zero-valent iron core-iron oxide shell nanoparticles with superparamagnetic behaviour

Authors: Milad Mehdipour, Lucy Gloag, Jiaxin Lian, Richard D Tilley and J. Justin Gooding

Journal or book name: *ChemComm*

Volume/page numbers:

Date accepted/ published:

Status	*Published*		*Accepted and In press*		*In progress (submitted)*	***X***

The Candidate's Contribution to the Work

Synthesized zero-valent iron nanoparticles, silica-coated zero-valent iron core-iron oxide shell nanoparticles, gold-coated zero-valent iron core-iron oxide shell nanoparticles

Characterised nanoparticles using TEM, SQUID magnetometry, UV-Vis spectroscopy, Darkfield image

Carried out stability against magnetic aggregation and colloidal stability experiments

Drafted and proofread the manuscript

Location of the work in the thesis and/or how the work is incorporated in the thesis:

In lieu of Chapter 5

PRIMARY SUPERVISOR'S DECLARATION

I declare that:

- the information above is accurate
- this has been discussed with the PGC and it is agreed that this publication can be included in this thesis in lieu of a Chapter
- All of the co-authors of the publication have reviewed the above information and have agreed to its veracity by signing a 'Co-Author Authorisation' form.

Primary Supervisor's name	Primary Supervisor's signature	Date (dd/mm/yy)
J. Justin Gooding		

Add additional boxes if required

COMMUNICATION

Synthesis of strongly magnetic gold-coated zero-valent iron core-iron oxide shell nanoparticles with superparamagnetic behaviour

Milad Mehdipour, [a] Lucy Gloag, [a] Jiaxin Lian, [a] Richard D Tilley [abc*] and J. Justin Gooding [ac*]

Received 00th January 20xx,
Accepted 00th January 20xx

DOI: 10.1039/x0xx00000x

A new type of gold-coated magnetic nanoparticles with a strongly magnetic zero-valent iron core-iron oxide shell as magnetic cores were synthesized. The small size of the magnetic cores and the zero-valent iron ensured superparamagnetic behaviour and high magnetization saturation of the overall nanoparticles. The nanoparticles showed stability against magnetic aggregation and also good colloidal stability, which is important for many biomedical applications.

Gold-coated magnetic nanoparticles are increasingly important for a variety of biomedical applications.[1,2] The combination of two properties, localized surface plasmon resonance and magnetism in a composite nanostructure requires careful and precise synthesis.[3] Nanoparticles with these dual properties are usually composed of iron oxide cores (magnetite) encapsulated inside an intermediate layer (normally silica) and coated with a gold nanoshell. The addition of a layer of non-magnetic materials on the surface of the iron oxide nanoparticles decreases the magnetization saturation of the overall nanoparticle and the susceptibility in an external magnetic field.[4,5]

Strategies to preserve the saturation magnetization of the gold-coated magnetic nanoparticles include using bigger iron oxide nanoparticles (≥20 nm for example).[6–8] However, iron oxide nanoparticles above 20 nm tend to aggregate easily as they can become irreversibly magnetized when exposed to an external magnetic field.[9] To overcome this issue, we recently used multiple superparamagnetic magnetite nanoparticles (16 nm) as magnetic cores encased in silica and coated in gold to give gold-coated nanoparticle with a fast magnetic response and superparamagnetic behaviour.[10]

Zero-valent iron (Fe^0) nanoparticles produce the highest magnetization saturation of any superparamagnetic nanoparticles.[12] Although iron rapidly oxidizes when exposed to air or water, for iron nanoparticles above 10 nm a 2-3 nm oxide shell forms on the surface and the nanoparticle becomes a zero-valent iron core-iron oxide shell.[13] The zero-valent iron core-iron oxide shell nanoparticles showed some of the highest magnetization saturation for magnetic nanoparticles, reaching values as high as 176 emu g^{-1}.[14,15] So one alternative, as yet unexplored strategy to reach high magnetization saturation, and maintain the superparamagnetic behaviour, is to use small Fe^0 nanoparticles whilst decreasing the amount of non-magnetic layers (gold and silica).[11]

To make the zero-valent iron core-iron oxide shell nanoparticles thermal decomposition of iron pentacarbonyl ($Fe(CO)_5$) in 1-octadecene as solvent and 3-octadecyl-2,4-pentanedione (OD-PD) as a stabilizing surfactant at 220°C.[16] The zero-valent iron core-iron oxide shell nanoparticles were then coated with silica using a microemulsion approach and finally seed mediated method to produce the gold shell was used. Figure 1 shows the TEM images of the multistep synthesis method to make the gold-coated conglomerates of zero-valent iron core-iron oxide shell nanoparticles. As depicted in Figure 1A, spherical zero-valent iron core-iron oxide nanoparticles show two different contrasts. The darker contrast (black) in the middle corresponds to the zero-valent iron core and the lighter contrast (grey) shell shows the iron oxide shell around the nanoparticle (Figure S1, ESI).[17] The histogram of the size of nanoparticles showed the particles are monodisperse with an average size of 14.1±0.7 nm, Figure 1B. 14 nm zero-valent iron core-iron oxide shell nanoparticles were chosen as bigger size (≥14 nm) nanoparticles show soft ferromagnetic behaviour.[13]

[a]*School of Chemistry, The University of New South Wales, Sydney, New South Wales, 2052, Australia. E-mail: r.tilley@unsw.edu.au, justin.gooding@unsw.edu.au*
[b]*Electron Microscope Unit, Mark Wainwright Analytical Centre, The University of New South Wales, Sydney, New South Wales, 2052, Australia.*
[c]*Australian Centre for NanoMedicine, The University of New South Wales, Sydney, New South Wales, 2052, Australia.*
Electronic Supplementary Information (ESI) available: See DOI: 10.1039/x0xx00000x

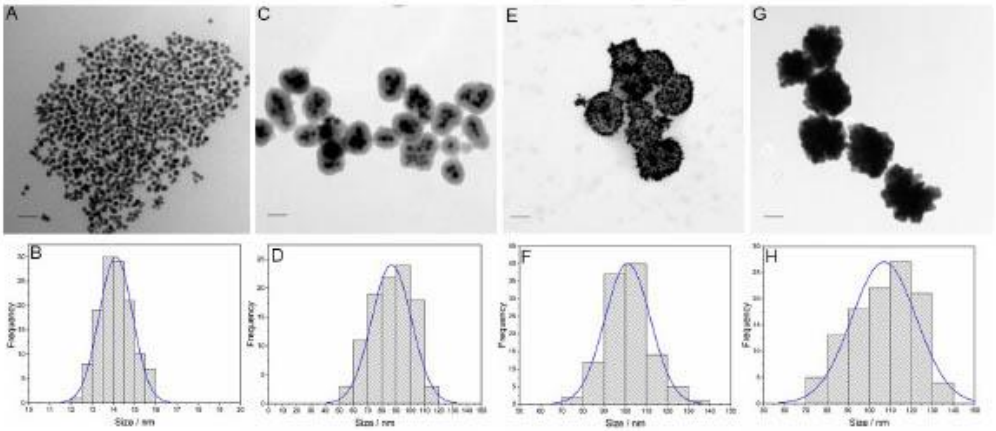

Figure 1. A) TEM image of zero-valent iron core – iron oxide shell magnetic nanoparticles B) Histogram of the size of zero-valent iron core – iron oxide shell magnetic nanoparticles C) TEM image of silica-coated zero-valent iron core – iron oxide shell magnetic nanoparticles D) Histogram of the size of silica-coated zero-valent iron core – iron oxide shell magnetic nanoparticles E) TEM image of gold-seeded silica-coated zero-valent iron core – iron oxide shell magnetic nanoparticle F) Histogram of the size of gold-seeded silica-coated zero-valent iron core – iron oxide shell magnetic nanoparticle G) TEM image of Gold-coated zero-valent iron core – iron oxide shell magnetic nanoparticles and histogram of the size of gold-coated- zero-valent iron core – iron oxide shell magnetic nanoparticles. Scale bars 50 nm.

The crystal structure by X-ray diffraction (XRD) in Figure S2 (ESI) shows two main peaks located at 52° and 77° corresponding to (110) and (200) faces of bcc iron and several peaks that could be indexed to either magnetite or maghemite iron oxide phases.[18–20]

To encapsulated the zero-valent iron core-iron oxide shell nanoparticles inside a silica shell, a well-known microemulsion method was used.[21] Hydrolysis and condensation of TEOS at the interface of the nanoreactors (micelles) result in formation of silica shell around magnetic nanoparticles.[22] This involves a two-step ligand exchange process was followed. First, the surface of the zero-valent iron core-iron oxide shell nanoparticles was modified with an amine rich layer with oleylamine and then the weakly-binding oleylamine surfactant was exchanged with oleic acid. The weak binding of oleylamine means the surface is not protected and the particles can easily oxidize during purification. An oleic acid coating is stronger-binding and forms denser monolayers, which allows us to recover the nanoparticles by precipitation and centrifugation without oxidation and then further coated with a silica layer.[15,16] Silica not only provides a favourable surface for the gold coating of particles but also preserve the zero-valent iron core–iron oxide shell nanoparticles from further oxidation during the gold coating process.[23] A TEM image of the silica-coated zero-valent iron core – iron oxide shell nanoparticles is depicted in Figure 1C. The particles have an irregular shape with an average size of 86.8 ± 13.9 nm, as could be seen from the histogram in Figure 1D. It is worth noting that after coating the particles with silica (Figure S3, ESI) the darker and lighter contrast of the zero-valent iron core – iron oxide shell nanoparticles remained (≈3 nm iron oxide shell and ≈ 8 nm zero-valent iron core). Dynamic light scattering (DLS) measurement of the nanoparticles showed the hydrodynamic size of 100 nm with PDI 0.217 (Figure S4, ESI). XRD showed that the silica coating process has not caused the zero-valent iron core to oxidize, and two 2 theta peaks positioned at 52° and 77° of the (110) and (200) face of zero-valent iron. (Figure S2, ESI).[18]

To fully coat the surface of the nanoparticles with a gold nanoshell a seed-mediated method was used.[24] To form a complete gold shell first we have to attach the ultra-small gold seeds (≤4 nm) to the surface of the silica to produce catalytic sites. These ultra-small gold nanoparticles on the surface of the silica are very active due to their big surface to volume ratio and want to reduce their surface energy and grow and become a gold shell.[25] To achieve that surface of silica has to be positively charged. [3-(2-Aminoethylamino)propyl]trimethoxysilane (AEAPTMS) was used to modify the silica surface with an amine terminal group.[26] Electrostatic interaction between negatively charged gold seeds and positively charged silica surface produces the gold seeded silica-coated zero-valent iron core – iron oxide shell nanoparticles. As it can be seen from Figure 1E and Figure S5 (ESI), The surface of the silica is fully covered with gold seeds (black dots).

A full gold shell was grown on the surface of the silica by slow reduction (24 hours) of the Au^3 to Au^0 *via* hydroxylamine hydrochloride on the catalytic sites. As it can be seen from Figure 1G and Figure S6 (ESI) a complete gold shell was grown and gold-coated- zero-valent iron core – iron oxide shell magnetic nanoparticles were formed. The particles size reached 107 ±17 nm as can be seen from the histogram in Figure 1H. The hydrodynamic size of the nanoparticles reached 120 nm with PDI 0.213. XRD pattern in Figure S2 (ESI) matches well with gold-coated magnetic nanoparticles reported in the literature.[18,27,28] The demonstration of the magneto-plasmonic properties of the gold-coated nanoparticles was performed using UV-Vis spectroscopy, darkfield microscopy and SQUID magnetometer.

Overall the magnetic properties of nanoparticles, and especially saturation magnetization and superparamagnetic behaviour of the nanoparticles, can significantly affect their application. Having multiple superparamagnetic nanoparticles with strong magnetization saturation as magnetic engines ensures that the nanoparticles have good magnetization saturation while retaining their superparamagnetic behaviour.[10] Magnetization

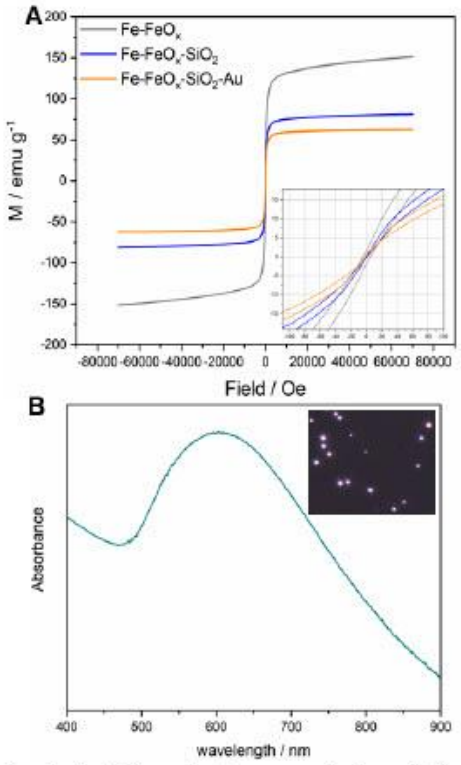

Figure 2. A) SQUID magnetometry measurements of magnetization behavior of (grey) zero-valent iron core – iron oxide shell magnetic nanoparticles, (blue) silica-coated zero-valent iron core – iron oxide shell magnetic nanoparticles, (orange) gold-coated zero-valent iron core – iron oxide shell magnetic nanoparticles and B) UV-Vis spectrum of gold-coated zero-valent iron core – iron oxide shell magnetic nanoparticles. Inset shows the dark-field microscopy image of the gold-coated zero-valent iron core-iron oxide shell.

saturation of 151, 81 and 63 emu g^{-1} were recorded for zero-valent iron core-iron oxide shell, silica-coated zero-valent iron core-iron oxide shell and gold-coated zero-valent iron core-iron oxide shell (Figure 2A). The high magnetization saturation of the nanoparticles here could be assigned to the existence of the zero-valent iron cores in all three nanoparticles.[14]

Furthermore, all the nanoparticles show superparamagnetic behaviour, with a neglectable coercivity of ≈4 Oe and remanence magnetization of ≈2 emu g^{-1}. The magnetic properties of the particles demonstrate that the coating process has not caused the zero-valent iron core-iron oxide shell to further oxidize and become iron oxide nanoparticles (typical magnetization saturation between 50-70 emu g^{-1}).[29,30] It is also worth noting that previous reports on gold-coated magnetic nanoparticles with even bigger magnetic cores (≥ 100 nm) have not reached the magnetization saturation managed to be achieved here from the 14 nm Fe(0) magnetic nanoparticles.[6,31]

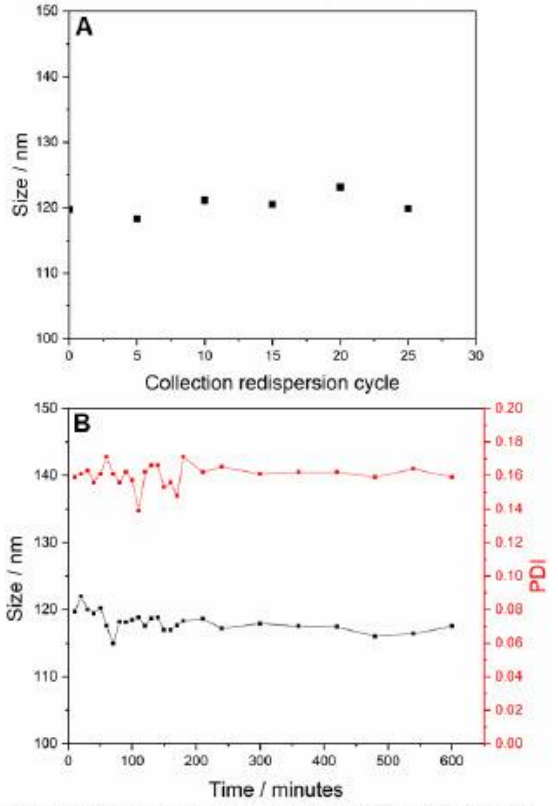

Figure 3. A) DLS measurements of magnetic aggregation stability of the gold-coated zero-valent iron core-iron oxide shell magnetic nanoparticles and B) colloidal stability of the gold-coated zero-valent iron core-iron oxide shell magnetic nanoparticles in Milli-Q water over time.

The UV-Vis spectrum shows a broad peak at 610 nm (Figure 2B). The darkfield microscopy image in the inset of Figure 2B shows that the nanoparticles have a pink scattering colour with no sign of intense scattering indicative of aggregation which shows that the nanoparticles are well dispersed on the surface of the glass coverslip (Figure S7).[32]

In order to design a perfect gold-coated magnetic nanoparticle for biomedical applications, having high magnetization saturation is just one of the required properties. Having good colloidal stability in solution in order to perform all kinds of biomolecules modifications and stability toward magnetic aggregation are two more important features south.[1]

To investigate the stability of the gold-coated magnetic nanoparticles against magnetic aggregation, the hydrodynamic size was measured before and after 25 cycles of collection *via* a

magnet and redispersion *via* sonication. As it can be seen from Figure 3A no significant size difference could be detected as nanoparticles were collected and redispersed in the solution for 25 cycles. This is because the gold-coated magnetic nanoparticles have superparamagnetic cores that are only magnetic when an external magnetic field is applied and by removing the external magnetic field they are not magnetic anymore. Hence, less magnetic attraction toward each other.

Finally, to test the colloidal stability of the gold-coated zero-valent iron core-iron oxide shell in Milli-Q water over time was investigated. As it can be seen from Figure 3B, the hydrodynamic size of the particles show no significant reduction and stays stable for 10 h. This illustrates the excellent colloidal stability of the nanoparticles. The gold-coated zero-valent iron core-iron oxide shell has a zeta potential of -36±3 mV which are typical values for gold surface capped by citrate and as a result good electrostatic stabilization. This colloidal stability could be crucial for applications requiring the nanoparticles to be modified with a variety of biomolecules and reagents.

In conclusion, we have demonstrated that using zero-valent iron core-iron oxide magnetic nanoparticles it is possible to achieve high magnetization saturation (M_s=63 emu g^{-1}) after coating the nanoparticles with silica and gold. The small size of the magnetic cores ensures that the overall particles show superparamagnetic behaviour and as the result, they are stable against magnetic aggregation. The particles also showed good colloidal stability with at least 10 h of no significant change in their hydrodynamic size and zeta potential of -36±3 mV. All and all these results demonstrate that these particles could be used in many biomedical applications.

We acknowledge funding under the Australian Research Council Linkage grant (LP150101014, JJG and RDT), the Australian Laureate Fellowship (FT150100060, JJG), ARC Centre of Excellence in Convergent Bio-Nano Science and Technology (CE140100036, JJG) and the Discovery Project (DP190102659 and DP200100143, RDT). JJG also acknowledges a National Health and Medical Research Investigator grant (APP1196648). LG, JJG and RDT acknowledge the Dementia Australia Research Foundation Yulgilbar innovation grant.

Conflicts of interest

There are no conflicts to declare

Notes and references

1 L. Gloag, M. Mehdipour, D. Chen, R. D. Tilley and J. J. Gooding, *Adv. Mater.*, 2019, **31**, 1–26.

2 R. Tavallaie, J. McCarroll, M. Le Grand, N. Ariotti, W. Schuhmann, E. Bakker, R. D. Tilley, D. B. Hibbert, M. Kavallaris and J. J. Gooding, *Nat. Nanotechnol.*, , DOI:10.1038/s41565-018-0232-x.

3 S. Moraes Silva, R. Tavallaie, L. Sandiford, R. D. Tilley and J. J. Gooding, *Chem. Commun.*, 2016, **52**, 7528–7540.

4 A. Sood, V. Arora, J. Shah, R. K. Kotnala and T. K. Jain, *J. Exp. Nanosci.*, 2016, **11**, 370–382.

5 M. E. Khosroshahi and L. Ghazanfari, *Mater. Chem. Phys.*, , DOI:10.1016/j.matchemphys.2011.12.047.

6 S. A. Adams, J. L. Hauser, A. C. Allen, K. P. Lindquist, A. P. Ramirez, S. Oliver and J. Z. Zhang, *ACS Appl. Nano Mater.*, 2018, acsanm.8b00225.

7 I. Y. Goon, L. M. H. Lai, M. Lim, P. Munroe, J. J. Gooding and R. Amal, *Chem. Mater.*, 2009, **21**, 673–681.

8 L. E. Woodard, C. L. Dennis, J. A. Borchers, A. Attaluri, E. Velarde, C. Dawidczyk, P. C. Searson, M. G. Pomper and R. Ivkov, *Sci. Rep.*, 2018, **8**, 1–13.

9 M. Mahmoudi, H. Hofmann, B. Rothen-Rutishauser and A. Petri-Fink, *Chem. Rev.*, 2012, **112**, 2323–2338.

10 M. Mehdipour, L. Gloag, D. T. Bennett, S. Hoque, R. Pardehkhorram, P. Bakthavathsalam, V. R. Gonçales, R. D. Tilley and J. J. Gooding, *J. Mater. Chem. C*, 2021, **9**, 1034–1043.

11 J. W. Kim, D. Seo, J. U. Lee, K. M. Southard, Y. Lim, D. Kim, Z. J. Gartner, Y. W. Jun and J. Cheon, *Nat. Protoc.*, 2017, **12**, 1871–1889.

12 D. L. Huber, *Small*, 2005, **1**, 482–501.

13 S. Cheong, P. Ferguson, K. W. Feindel, I. F. Hermans, P. T. Callaghan, C. Meyer, A. Slocombe, C. H. Su, F. Y. Cheng, C. S. Yeh, B. Ingham, M. F. Toney and R. D. Tilley, *Angew. Chemie - Int. Ed.*, 2011, **50**, 4206–4209.

14 L. Gloag, M. Mehdipour, M. Ulanova, K. Mariandry, M. A. Nichol, D. J. Hernández-Castillo, J. Gaudet, R. Qiao, J. Zhang, M. Nelson, B. Thierry, M. A. Alvarez-Lemus, T. T. Tan, J. J. Gooding, N. Braidy, P. S. Sachdev and R. D. Tilley, *Chem. Commun.*, 2020, **56**, 3504–3507.

15 A. J. McGrath, S. Cheong, A. M. Henning, J. J. Gooding and R. D. Tilley, *Chem. Commun.*, 2017, **53**, 11548–11551.

16 G. C. Bleier, J. Watt, C. K. Simocko, J. M. Lavin and D. L. Huber, *Angew. Chemie - Int. Ed.*, 2018, **57**, 7678–7681.

17 D. A. J. Herman, S. Cheong-Tilley, A. J. McGrath, B. F. P. McVey, M. Lein and R. D. Tilley, *Nanoscale*, 2015, **7**, 5951–5954.

18 H. F. McMurdie, E. H. Evans, M. C. Morris, B. Paretzkin, W. Wong-Ng, L. Ettlineer and C. R. Hubbard, *Powder Diffr.*, 1986, **1**, 64–77.

19 J. H. L. Beal, S. Prabakar, N. Gaston, G. B. The, P. G. Etchegoin, G. Williams and R. D. Tilley, *Chem. Mater.*, 2011, **23**, 2514–2517.

20 X. Wang, R. D. Tilley and J. J. Watkins, *Langmuir*, 2014, **30**, 1514–1521.

21 S. T. Selvan, T. T. Tan and J. Y. Ying, *Adv. Mater.*, 2005, **17**, 1620–1625.

22 M. Zhang, B. L. Cushing and C. J. O'Connor, *Nanotechnology*, , DOI:10.1088/0957-4484/19/8/085601.

23 Y. Lu, Y. Yin, B. T. Mayers and Y. Xia, *Nano Lett.*, 2002, **2**, 183–186.

24 N. Phonthammachai, J. C. Y. Kah, G. Jun, C. J. R. Sheppard, M. C. Olivo, S. G. Mhaisalkar and T. J. White, *Langmuir*, 2008, **24**, 5109–5112.

25 B. E. Brinson, J. B. Lassiter, C. S. Levin, R. Bardhan, N. Mirin and N. J. Halas, *Society*, 2008, **120**, 14166–14171.

26 M. Zhu, M. Z. Lerum and W. Chen, *Langmuir*, 2012, **28**,

416–423.
27 X. Zhou, W. Xu, Y. Wang, Q. Kuang, Y. Shi, L. Zhong and Q. Zhang, *J. Phys. Chem. C*, 2010, **114**, 19607–19613.
28 Z. Ban, Y. A. Barnakov, F. Li, V. O. Golub and C. J. O'Connor, *J. Mater. Chem.*, 2005, **15**, 4660–4662.
29 D. Maity, S. G. Choo, J. Yi, J. Ding and J. M. Xue, *J. Magn. Magn. Mater.*, 2009, **321**, 1256–1259.
30 P. Guardia, A. Labarta and X. Batlle, *J. Phys. Chem. C*, 2011, **115**, 390–396.
31 J. Wang, X. Wu, C. Wang, Z. Rong, H. Ding, H. Li, S. Li, N. Shao, P. Dong, R. Xiao and S. Wang, *ACS Appl. Mater. Interfaces*, 2016, **8**, 19958–19967.
32 B. P. Markhali, M. Sriram, D. T. Bennett, P. S. Khiabani, S. Hoque, R. D. Tilley, P. Bakthavathsalam and J. J. Gooding, *Biosens. Bioelectron.*, 2020, **169**, 112612.

Synthesis of highly magnetic gold-coated zero-valent iron core-iron oxide shell nanoparticles with superparamagnetic behaviour

Milad Mehdipour,[a] Lucy Gloag,[a] Jiaxin Lian,[a] Richard D Tilley [abc*] and J. J. Gooding [ac*]

a. School of Chemistry, The University of New South Wales, Sydney, New South Wales, 2052, Australia.

b. Electron Microscope Unit, Mark Wainwright Analytical Centre, The University of New South Wales, Sydney, New South Wales, 2052, Australia.

c. Australian Centre for NanoMedicine, The University of New South Wales, Sydney, New South Wales, 2052, Australia.

Experimental:

Chemicals: iron pentacarbonyl (99.99%), 1-octadecene (1-ODE, 90%), oleylamine (98%), oleic acid (90%) sodium hydride (60 % dispersion in mineral oil), anhydrous *N,N*-dimethylformamide (DMF, 99.8%), 1-iodooctadecane (1-IOD, 95%), 2,4-pentanedione (PD, 99%), Igepal CO-520, ammonium hydroxide (30%), tetraethyl orthosilicate (TEOS, 98%), 3-(2-aminoethylamino)propyltrimethoxysilane (AEAPTMS, 80%), gold(III) chloride trihydrate (99.9%), tetramethylammonium hydroxide in methanol solution (25% (wt/vol) TMAOH in methanol solution), hydroxylamine hydrochloride (NH2OH.HCl), sodium citrate dihydrate, sodium borohydride were purchased from Sigma-Aldrich. Acetone, toluene, cyclohexane, methanol, nitric acid (69%), hydrochloric acid (32%) were purchased from Chem-Supply Australia. With the exception of oleylamine, all chemicals were used as received. Oleylamine was distilled under reduced pressure before reaction. Glassware was cleaned with freshly prepared *aqua regia* (HCl: HNO_3 in a 3:1 ratio by volume) followed by rinsing with Milli-Q water.

Synthesis of zero-valent iron core-iron oxide nanoparticles: magnetic nanoparticles were synthesized with a slightly modified thermal decomposition method reported in the literature.[1]

To ensure all reagents were air-free, all liquids were degassed under vacuum and argon before use. The chemicals and glassware were first transferred to a glovebox. A sum of 20 mg of 3-Octadecyl-2,4-Pentanedione (OD-PD)[1] and 5 mL of 1-ODE was added to a 25 mL two neck round bottom flask and vortexed to dissolve. The flask was sealed with a stopper and a closed condenser to ensure no air or moisture could go inside. To a 25 mL vial were added 48 mg of OD-PD, 1.47 mL of iron pentacarbonyl and 9 mL of the 1-ODE and vortexed to dissolve. The solution was transferred to a 20 mL syringe tube and sealed. The two necks round bottom flask and 20 mL syringe were carefully transferred to a laboratory fume hood. The flask was connected to a Schlenk line and opened to Ar gas flow. The syringe was loaded onto a syringe pump. The flask was heated *via* a hot plate to 220° C while under a continuous flow of Ar. After reaching 220° C the solution inside the syringe was added dropwise into the flask with a rate of 0.03 mL/min. Once the syringe was emptied the reaction was heated at 220° C for another hour and then cooled down to room temperature. The two neck flask was carefully transferred to the glovebox. To change the ligand on the surface of the nanoparticles 500 µL of the sample was mixed with 2 mL of 1-ODE and 60 µL

of oleylamine and transferred to a 25 mL round bottom flask while making sure the flask was totally sealed and then transferring the solution to a fume hood and heating to 70◦ C and kept at 70◦ C for one hour while stirring (under Ar atmosphere). The particles were cooled down to room temperature and transferred back to the glovebox. The particles were magnetically separated and transferred to a new round bottom flask. A total of 2 mL of 1-ODE and 1 mL of oleic acid were added to a new flask. The flask was sealed and then transferred to a fume hood heated to 70◦ C while stirring and left for one hour (under Ar atmosphere). The nanoparticles were transferred to 5 mL centrifuge tubes and 2 mL of a solution 10:1 toluene to oleylamine and 1 mL of ethanol was added to the solution. The particles were centrifuged at 13500 rcf for 12 min and the supernatant was removed (repeated two more times). The particles were dispersed in 500µL of toluene (the concentration of nanoparticles was adjusted to 2.75 nM according to ICP).

Addition of a silica shell on the surface of the nanoparticles: a well-known microemulsion method was used to form the silica layer on the surface of the oleic acid capped zero-valent iron core-iron oxide shell nanoparticles.[2] An aliquot of 12 mL of cyclohexane was added to a 40 mL vial followed by addition of 770 µL of Igepal CO-520. The solution was vortex for 5 min to dissolve Igepal completely. Then 100 µL of the zero-valent iron core-iron oxide shell nanoparticles in toluene was added to the solution and shake with hand. Then an aliquot of 60 µL of the ammonium hydroxide was added. The solution was shaken by hand for few seconds and subsequently, 30 µL of TEOS was added and the vial was shaken for few more seconds. The vial then was left inside a fume hood for two days. A 7 µL of the AEAPTMS was added to the vial and the vial was shaken for 2 h at 200 rpm. 4 mL of the 50 mM TMAOH in methanol solution was added to the microemulsion system and the dark brown layer was carefully transferred to a new vial. To clean the particles 8 mL of acetone was added to the solution and the solution was transferred to centrifuge tubes. Particles were centrifuged at 1600 rcf for 15 min and the supernatant was carefully removed. To each centrifuge tube was added 4 mL of acetone and nanoparticles were centrifuged at 1600 rcf for 15 min again. The supernatant was removed and particles were dispersed in DMSO. To make sure that the free silica nanoparticles are removed, magnetic separation was done twice and final silica-coated zero-valent iron core-iron oxide shell nanoparticles were dispersed in 500 µL of DMSO (concentration of the particles was adjusted to 400 nM).

Gold seeding and gold shell growth: To form the gold nanoshell a seed-mediated method with modification was used.[3,4] A 40 mL beaker was set in the middle of a container full of ice. A sum of 1.7 mg of gold(III) chloride trihydrate was added to 20 mL of Milli-Q water and transferred to the beaker. The solution was stirred at 500 rpm with a mechanical stirrer. This was followed by the addition of 110 µL of the nanoparticles in DMSO to the beaker. An aqueous solution of sodium citrate (0.17 M) was made and 150 µL of the solution was injected into the beaker. Finally, 1 mL of sodium borohydride aqueous solution (378.3 µg to 1 mL of MQ) was injected rapidly into the beaker. The solution was stirred for 6 min and then transferred into a vial. Gold seeded nanoparticles were separated magnetically and cleaned by adding Milli-Q water (repeated twice). The particles were dispersed in 2 mL of Milli-Q water. A sum of 0.367 mg of the gold(III) chloride trihydrate was added to 3.6 mL of Milli-Q and was stirred *via* a mechanical stirrer at 400 rpm for 6 h. Subsequently, the gold solution was added to the vial containing the nanoparticles. An aqueous solution of sodium citrate (4.8 mM) was prepared and 3.6 mL of the solution was added to the vial containing nanoparticles and gold solution. Finally, 40 µL of aqueous solution (40 mM) of hydroxylamine hydrochloride was added to the vial. The vial was wrapped with aluminium foil and left

inside a fridge at 4◦ C for 24 h. The gold-coated zero-valent iron core-iron oxide shell was magnetically separated and washed with Milli-Q water (twice) and dispersed in Milli-Q water.

Characterization:

A CM200 transmission electron microscope was used to acquire the TEM images at an accelerating voltage of 200 kV. Nanoparticles were drop-casted onto a carbon-coated grid followed by air drying. An FEI Nova NanoSEM 450 was used to acquire the SEM images at an accelerating voltage of 4-25 kV. TEM and SEM images were characterized by ImageJ software. Cary 60 single-beam UV-Vis spectrophotometer was used to acquire the UV-Vis spectra of the gold-coated zero-valent iron core-iron oxide shell nanoparticles at room temperature. Zetasizer Nano ZS (Malvern Panalytical) was used to measure the hydrodynamic size and zeta potential of the nanoparticles. Colloidal stability of gold-coated iron core-iron oxide shell nanoparticles was investigated for the changes in the hydrodynamic size of the particles and PDI over time. To investigate the magnetic stability of the nanoparticles. cycles of collection and redispersion of particles via magnet and sonication (5 min) were repeated 25 times after each cycle, the hydrodynamic diameter was measured. The magnetic property was investigated by SQUID magnetometry with an external magnetic field ranging from 60,000 Oe (6 T) to -60,000 Oe (-6 T) at 300 K. X-ray diffraction (XRD) was performed on an Empyrean 2 (Malvern Panalytical) X-ray diffractometer with Co Kα (1.79 Å) radiation with all samples analyzed from 30° to 90° (2θ). nanoparticles concentration was measured with Nanoparticle tracking analysis (NanoSight NS300, Malvern Panalytical). A dark-field microscope (Olympus BX51) was used to acquire dark field images. Gold-coated zero-valent iron core-iron oxide shell was immobilized onto APTES modified glass coverslips and left for 10 min. Glass coverslips were then rinsed with Milli-Q water and then dried under a stream of nitrogen. The coverslip was mounted on the aluminium holder and imaged in an Olympus BX51 dark-field microscope. A 100 W halogen lamp was used as the excitation source and was focused through a dark-filed condenser with NA>0.8. the scattered light was collected by an objective of 100 x magnification and imaged using a Canon 100D CMOS camera (22.3 mm x 14.9 mm sensor size, 4.3 µm x 4.3 µm pixel size).

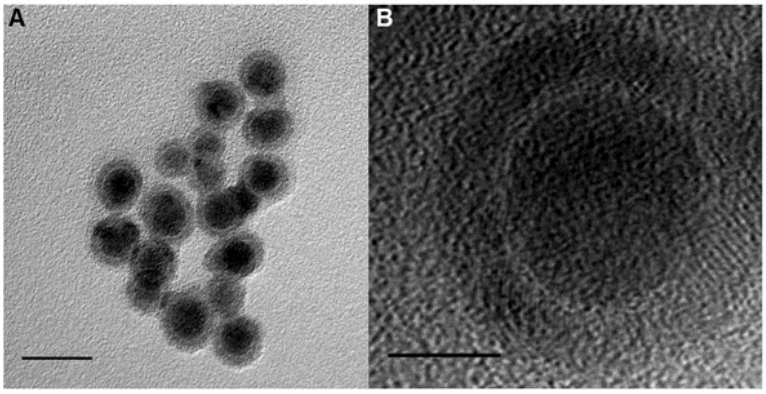

Figure S1. A and B) TEM images of the zero-valent iron core-iron oxide shell magnetic nanoparticles. Scale bars A) 20 nm and B) 5 nm.

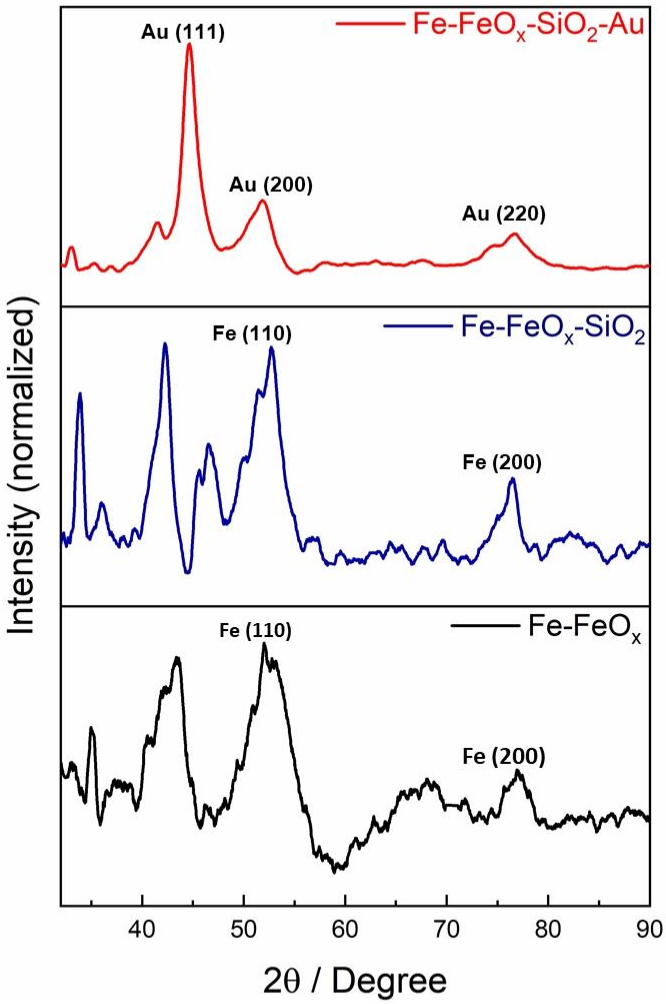

Figure S2. X-ray diffraction (XRD) spectra of zero-valent iron core – iron oxide shell magnetic nanoparticles (black), silica-coated zero-valent iron core – iron oxide shell magnetic nanoparticles (blue) and gold-coated zero-valent iron core – iron oxide shell magnetic nanoparticles (red).

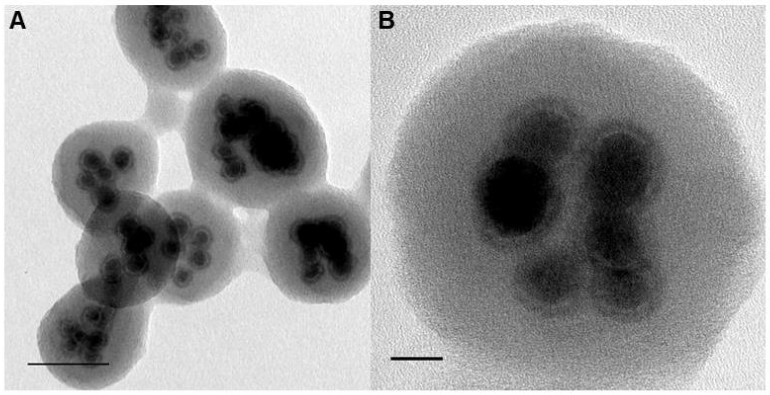

Figure S3. A and B) TEM images of the silica-coated zero-valent iron core-iron oxide shell magnetic nanoparticles. Scale bars A) 50 nm and B) 10 nm.

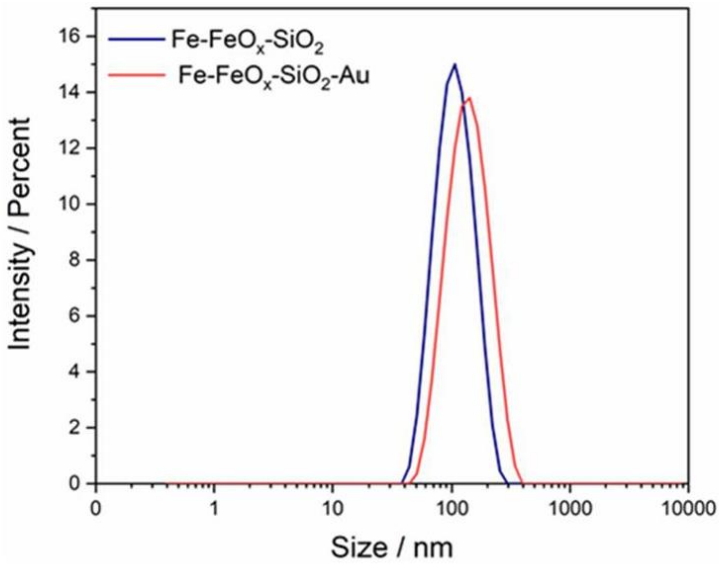

Figure S4. Dynamic light scattering (DLS) measurements of silica-coated zero-valent iron core – iron oxide shell magnetic nanoparticles (hydrodynamic size=100 nm; PDI=0.217) (blue) and Gold-coated zero-valent iron core – iron oxide shell magnetic nanoparticles (hydrodynamic size=120nm; PDI=0.213) (red).

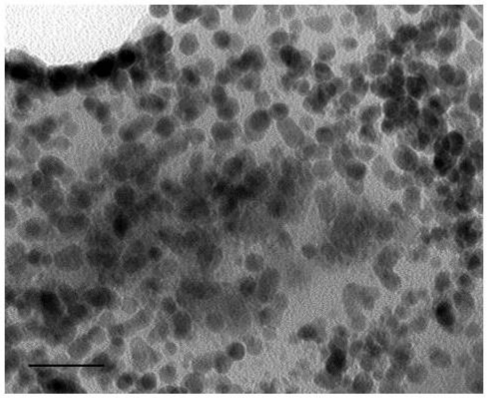

Figure S5. TEM image of the surface of the silica-coated zero-valent iron core-iron oxide shell magnetic nanoparticles seeded with ultra-small gold nanoparticles (≤4 nm). Scale bar 20 nm.

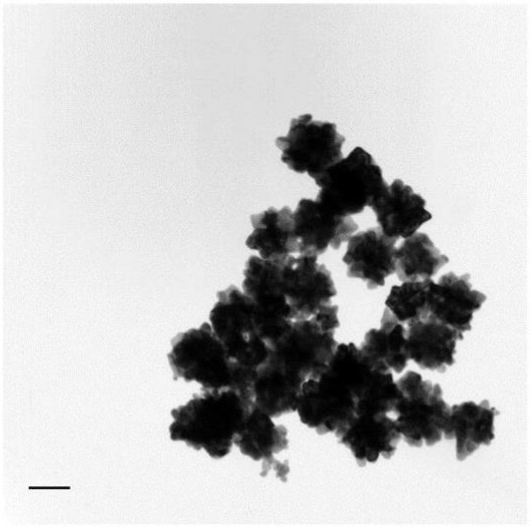

Figure S6. TEM image of the gold-coated zero-valent iron core-iron oxide shell magnetic nanoparticles. Scale bar 100 nm.

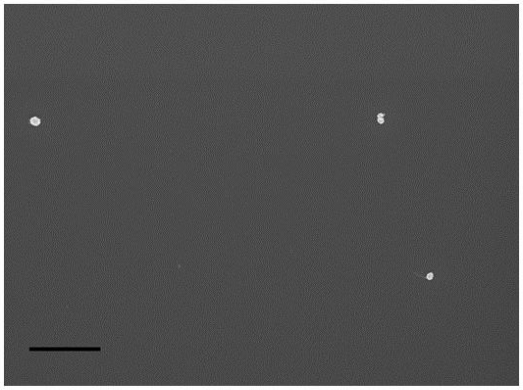

Figure S7. SEM image of the gold-coated zero-valent iron core-iron oxide shell magnetic nanoparticles. scale bar 1 μm.

References:

1 G. C. Bleier, J. Watt, C. K. Simocko, J. M. Lavin and D. L. Huber, *Angew. Chemie - Int. Ed.*, 2018, **57**, 7678–7681.

2 M. Mehdipour, L. Gloag, D. T. Bennett, S. Hoque, R. Pardehkhorram, P. Bakthavathsalam, V. R. Gonçales, R. D. Tilley and J. J. Gooding, *J. Mater. Chem. C*, 2021, **9**, 1034–1043.

3 A. Espinosa, M. Bugnet, G. Radtke, S. Neveu, G. A. Botton, C. Wilhelm and A. Abou-Hassan, *Nanoscale*, 2015, **7**, 18872–18877.

4 R. Wang, X. Ji, Z. Huang, Y. Xue, D. Wang and W. Yang, *J. Phys. Chem. C*, 2016, **120**, 377–385.

Chapter 6

Facile, flow reactor synthesis of gold-coated magnetic nanoparticles for biosensing applications

Publication three

Milad Mehdipour, Lucy Gloag, Daniel Hagness, Jiaxin Lian, Md Saiful Alam, Xueqian Chen, Richard. D Tilley, and J. Justin Gooding, submitted to aggregate October 2021

6.1. Summery

The publication ‘’ Facile, flow reactor synthesis of gold-coated magnetic nanoparticles for biosensing applications’’ has been used in lieu of a chapter. The goal was to develop a fast and scalable method for the synthesis of gold-coated magnetic nanoparticles. To achieve this aim, two Y-shaped pieces were designed, and 3D printed. The pieces were used for pre-seeding the silica-coated magnetic nanoparticles with ultra-small gold seeds and to grow gold shell on the pre-seeded silica-coated magnetic nanoparticles. The strategy was to use a fluidic system to produce the gold-coated magnetic nanoparticles. It was shown that the concentration of pre-gold seeded silica-coated magnetic nanoparticles could affect the quality of the final gold-coated magnetic nanoparticles. Low and high concentrations of pre-gold seeded silica-coated magnetic nanoparticles resulted in heavy and partial aggregation of the gold-coated magnetic nanoparticles respectively. When the concentration of the pre-gold seeded silica-coated magnetic nanoparticles was balanced the particles were fully coated with gold and no sign of aggregation was observed. Further investigation showed that the gold-coated magnetic nanoparticles produced were able to be used as biosensing agents.

Declaration for Chapter Six

Author	**Contribution**
Milad Mehdipour	Experimental design Synthesized magnetite nanoparticles, silica-coated conglomerates of superparamagnetic nanoparticles, gold-coated conglomerates of superparamagnetic nanoparticles Characterised nanoparticles using TEM, SQUID magnetometry, UV-Vis spectroscopy Design of the Y-shaped pieces Drafted and proofread the manuscript
Lucy Gloag	Experimental design Proofread the manuscript
Daniel Hagness	Design of the Y-shaped pieces 3D printing of the pieces Proofread the manuscript
Jiaxin Lian	Digestion of silica-coated zero-valent iron core-iron oxide shell nanoparticles, gold-coated zero-valent iron core-iron oxide shell nanoparticles with HF
Md Saiful Alam	Nanoparticles modification Raman and SERS
Xueqian Chen	Darkfield microscopy images Proofread the manuscript
Richard. D Tilley	Experimental design Provided fundamental understanding of the key magneto plasmonic properties and synthesis of nanoparticles Proofread manuscript
J. Justin Gooding	Experimental design Provided fundamental understanding of the key magneto plasmonic properties and synthesis of nanoparticles Proofread manuscript

UNSW is supportive of candidates publishing their research results during their candidature as detailed in the UNSW Thesis Examination Procedure.

Publications can be used in their thesis in lieu of a Chapter if:

- The candidate contributed greater than 50% of the content in the publication and is the "primary author", ie. the candidate was responsible primarily for the planning, execution and preparation of the work for publication
- The candidate has approval to include the publication in their thesis in lieu of a Chapter from their supervisor and Postgraduate Coordinator.
- The publication is not subject to any obligations or contractual agreements with a third party that would constrain its inclusion in the thesis

Please indicate whether this thesis contains published material or not:

☐ This thesis contains no publications, either published or submitted for publication
(if this box is checked, you may delete all the material on page 2)

☐ Some of the work described in this thesis has been published and it has been documented in the relevant Chapters with acknowledgement
(if this box is checked, you may delete all the material on page 2)

☒ This thesis has publications (either published or submitted for publication) incorporated into it in lieu of a chapter and the details are presented below

CANDIDATE'S DECLARATION

I declare that:

- I have complied with the UNSW Thesis Examination Procedure
- where I have used a publication in lieu of a Chapter, the listed publication(s) below meet(s) the requirements to be included in the thesis.

Candidate's Name	**Signature**	**Date (dd/mm/yy)**
Milad Mehdipour		

POSTGRADUATE COORDINATOR'S DECLARATION *To only be filled in where publications are used in lieu of Chapters*

I declare that:

- the information below is accurate
- where listed publication(s) have been used in lieu of Chapter(s), their use complies with the UNSW Thesis Examination Procedure
- the minimum requirements for the format of the thesis have been met.

PGC's Name	PGC's Signature	Date (dd/mm/yy)
Alex William Donald		

For each publication incorporated into the thesis in lieu of a Chapter, provide all of the requested details and signatures required

Details of publication #3:

Full title: Facile, flow reactor synthesis of gold-coated magnetic nanoparticles for biosensing applications

Authors: Milad Mehdipour, Lucy Gloag, Daniel Hagness, Jiaxin Lian, Md Saiful Alam, Xueqian Chen, Richard. D Tilley, and J. Justin Gooding

Journal or book name: Aggregate

Volume/page numbers:

Date accepted/ published:

Status	*Published*		*Accepted and in press*		*In progress (submitted)*	***X***

The Candidate's Contribution to the Work

Experimental design

Synthesized magnetite nanoparticles, silica-coated conglomerates of superparamagnetic nanoparticles, gold-coated conglomerates of superparamagnetic nanoparticles

Characterised nanoparticles using TEM, SQUID magnetometry, UV-Vis spectroscopy

Design of the Y-shaped pieces

Drafted and proofread the manuscript

Location of the work in the thesis and/or how the work is incorporated in the thesis:

In lieu of Chapter 6

PRIMARY SUPERVISOR'S DECLARATION

I declare that:

- the information above is accurate
- this has been discussed with the PGC and it is agreed that this publication can be included in this thesis in lieu of a Chapter
- All of the co-authors of the publication have reviewed the above information and have agreed to its veracity by signing a 'Co-Author Authorisation' form.

Primary Supervisor's name	Primary Supervisor's signature	Date (dd/mm/yy)
J. Justin Gooding		

Add additional boxes if required

AGGREGATE WILEY

Facile, flow reactor synthesis of gold-coated magnetic nanoparticles for biosensing applications

Milad Mehdipour, Lucy Gloag, Daniel Hagness, Jiaxin Lian, Md Saiful Alam, Xueqian Chen, Richard. D Tilley, and J. Justin Gooding

M. Mehdipour, L. Gloag, Daniel Hagness, Jiaxin Lian, Md Saiful Alam, Xueqian Chen, Richard. D Tilley, and J. Justin Gooding
School of Chemistry, The University of New South Wales, Sydney, New South Wales,2052, Australia.
Prof. R. D. Tilley
Electron Microscope Unit, Mark Wainwright Analytical Centre, The University of New South Wales, Sydney, New South Wales,2052, Australia.
Prof. R. D. Tilley and Prof. J. J. Gooding
Australian Centre for Nanomedicine, The University of New South Wales, Sydney, New South Wales,2052, Australia.

Keywords: plasmonics, magnetic nanoparticles, gold, biosensing, nanoshell, flow reactor

Gold-coated magnetic nanoparticles are a promising candidate for a variety of applications due to their optical, electrical and magnetic properties. However, the availability of a robust, and scalable synthesis method to form a complete gold nanoshell around magnetic nanoparticles remains unfulfilled. Herein, we present a new methodology for the synthesis of gold-coated magnetic nanoparticles *via* a fluid manufacturing system that can easily be scaled up. The developed method could produce gold-seeded silica coated magnetic nanoparticles and further gold-coated magnetic nanoparticles with a complete gold shell within 2 minutes with relatively uniform size and shape. The particles show both excellent magnetic and plasmonic properties. The potential of the gold-coated magnetic nanoparticles for biosensing was investigated using dark-field microscopy and surface-enhanced Raman scattering (SERS).

1. Introduction

Magneto-plasmonic nanoparticles and especially gold-coated magnetic nanoparticles are attracting enormous interest for biosensing.[1] This is because the combination of properties such as conductivity, simplicity of bioconjugation, chemical stability, localized surface plasmon resonance (LSPR) and magnetism in a nanoparticle opens numerous possibilities for

facilitating diagnostics and treatment of diseases.[2–4] Colloidal synthesis methods have been the primary approach for researchers to make gold-coated magnetic nanoparticles.[5–13] However, the absence of viable synthesis method for mass production hinders the transition of gold-coated magnetic nanoparticles for commercial applications[18–20] Thus, exploring synthetic routes for facile large-scale production is very important for the widespread promotion of the new nanotechnology.

Flow-based synthesis is promising method to achieve scalable and precise nanomaterial production.[17–20] Flow reactors are preferable to conventional batch synthesis due to superior reagents mixing and homogeneity, controllable heat and mass transfer and reproducibility of final products. [21–25] Recently Ahrberg et al,[26] reported an automated system based on a capillary droplet reactor to synthesis gold-coated magnetic nanoparticles. They have synthesized iron oxide nanoparticles *via* co-precipitation of ferric and ferrous ions in basic pH inside the tube channel. Continuous reduction of gold precursor on the surface of iron oxide nanoparticles formed the gold nucleation sites and then these sites grow into a full gold shell. Duraiswamy et al,[27] managed to coat the already gold seeded silica nanoparticles with good control over the size with gold *via* a microfluidic composite foam system in 2 minutes. They found that rapid electroless gold plating occurring on the catalytic sites (gold seeds) could be as high as 200 nm/s and shell growth could finish in few seconds. Thus, reaction kinetics and full shell growth are highly dependent on the diffusion of ionic species to the catalytic sites. These finding of rapid gold shell growth on silica nanoparticles is in line with other reports from the colloidal synthesis of gold shell on silica and silica-coated magnetic nanoparticles.[28,29] Yet further advances are needed to overcome existing hurdles such as channel clogging, expensive substrates, and the need for cleanroom facilities to mould the subtracts hinders the widespread application of these methods for the synthesis of nanomaterials.[30,31]

Herein we report a unique system for both seedings with gold nanoparticles and the growth of gold shell on the surface of silica-coated magnetic nanoparticles. The simple design of the system developed here not only solves the problem of clogging but offers a disposable system capable of coating the magnetic nanoparticles with a gold shell in a scalable fashion. The strategy here was to use syringe pumps and a Y-shaped piece with channels just long enough for both attachments of small gold seed nanoparticles to, and the growth of a gold shell around, silica-coated magnetic nanoparticles. Moreover, since this system has been designed with main channel of 2.8 cm length, and the pieces are disposable, continuous flow system can be used instead of a segmented droplet system. The reaction conditions were optimized to achieve the fully gold-coated magnetic nanoparticles. Finally, the ability of the synthesized particles to bind to biomolecules and act as bio-sensing agents was demonstrated by SERS.

2. Results and discussion:

The simplified schematic of our method Figure 1, and Y-shaped pieces Figure S1 show the approach used to synthesis the gold-coated magnetic nanoparticles. As it can be seen, unlike normal fluidic set-ups in the literature, the system presented herein was rationalized into just two small Y-shaped tube connectors; one with two streams merging onto one and the second three streams are combined.

The system starts with the synthesis of magnetic nanoparticle which are conglomerates of superparamagnetic nanoparticles encapsulated in silica using an approach we reported previously.[32] The importance of these conglomerate magnetic nanoparticles are they move rapidly to a magnet, as needed for many applications but, as they are not magnetic when not exposed to a magnetic field, they are far more stable against deleterious aggregation than larger magnetic nanoparticles.

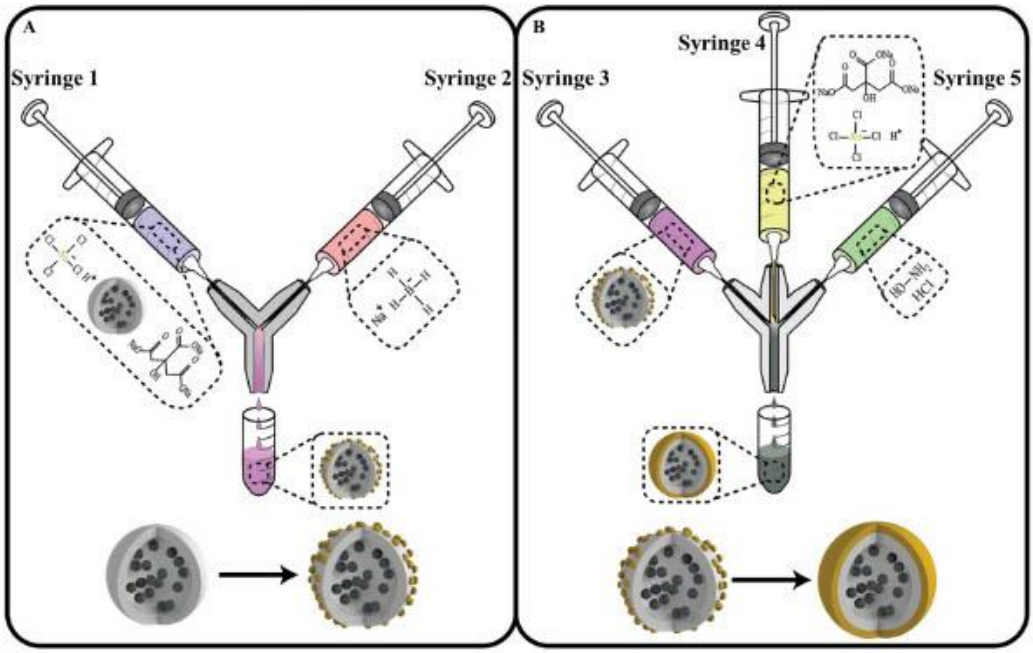

Figure 1. Schematic of A) seeding manufacturing method using a two-channel syringe set-up and B) gold nanoshell manufacturing method using a three-channel syringe set-up.

Figure S2 shows the TEM images of iron oxide magnetic nanoparticles and silica-coated magnetic nanoparticles clearly show the aggregates of superparamagnetic nanoparticles encapsulate within the silica. The corresponding histogram of the size of the particles reveals that the individual iron oxide superparamagnetic nanoparticles are 16 nm in size and silica-coated magnetic nanoparticles are 100 nm in size. Each silica shell contained around 20 superparamagnetic nanoparticles. After synthesis of magnetic iron oxide nanoparticles *via* thermal decomposition of iron precursor, base-catalyzed hydrolysis, and condensations of TEOS result in the formation of a silica shell around magnetic nanoparticles with a hydroxyl group on the surface. The modification of silica surface with amine terminal group results in positively charged particles that can electrostatically bind to the negatively charged gold seeds. Routinely, (3-aminopropyl)triethoxysilane (APTES) is being used to perform silane ligand exchange. Since we needed the gold seeds to quickly bind to the surface of the silica, instead

of APTES we used [3-(2-aminoethylamino)propyl]trimethoxysilane (AEAPTMS). The higher amine content of the AEAPTMS facilitates the attachment of gold seeds to the surface of the silica and results in seeding with higher density within a shorter time-frame.[33]

To attach the small gold nanoparticles to the surface of silica, particles along with gold chloride and sodium citrate aqueous solution were loaded into Syringe 1 and Syringe 2 contained an aqueous solution of sodium borohydride (0.01 M). The flow rate of Syringe 1 was 230 µL/ min, and Syringe 2 was 70 µL/min. A deposition-precipitation method was used for the synthesis and simultaneous attachment of gold seeds to the silica surface.[34] Reducing the gold chloride with a strong reducing agent like sodium borohydride in the presence of sodium citrate produces small gold nanoparticles with a negative charge on the surface. Figure S3 shows the TEM images of the gold seeded nanoparticles and a corresponding histogram of the size of gold nanoparticles. From these Figures, it can be seen that the surface area of the silica-coated magnetic nanoparticles is fully covered with ~3 nm gold nanoparticles (visible as black dots). A dense seeding of the surface with ultra-small gold nanoparticles is the key to the formation of a complete gold shell as these small gold nanoparticles act as catalytic sites for gold nanoshell formation.[35]

The growth of the gold shell around pre-gold seeded silica-coated magnetic nanoparticles was achieved by using a three-syringe setup. Gold seeded silica-coated magnetic nanoparticles with three different concentrations (2 nM, 24 nM and 58 nM) were loaded inside Syringe 3, Syringe 4 was loaded with an aqueous solution of gold chloride and sodium citrate and finally, Syringe 5 contained the aqueous solution of hydroxylamine hydrochloride as the reducing agent. By adjusting the flow rate for Syringe 3 to 30 µL/min, Syringe 4 to 120 µL/min and Syringe 5 to 50 µL/min and keeping the concentration of gold chloride, sodium citrate, and hydroxylamine hydrochloride constant gold shell growth was performed. It is worth noting that sodium citrate only starts acting as a reducing agent for gold if the temperature is above 70°C.[36]

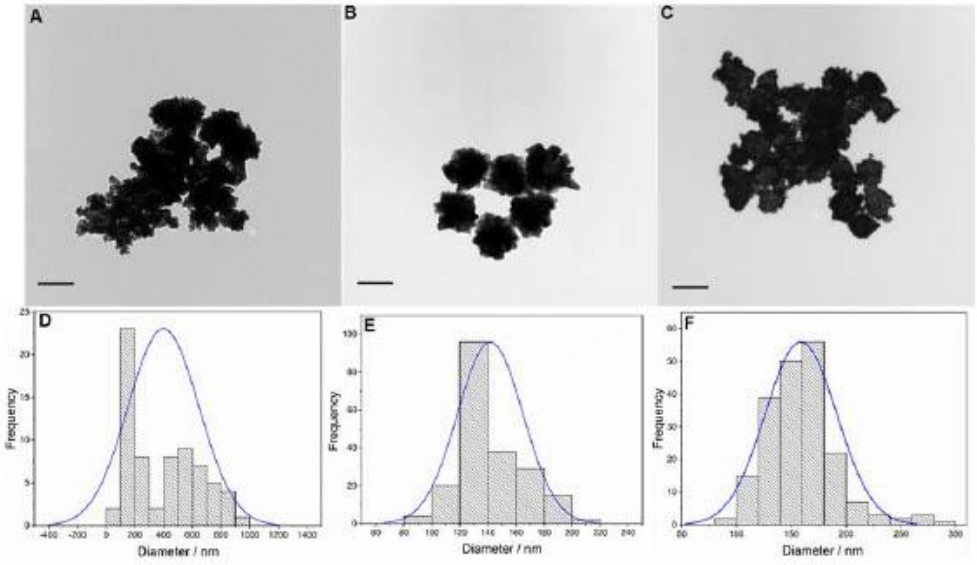

Figure 2. TEM images of gold-coated magnetic nanoparticles prepared with different initial pre-gold seeded silica-coated magnetic nanoparticles concentration A) 2 nM B) 24 nM and C) 58 nM and corresponding histograms of the size of gold-coated magnetic nanoparticles prepared with different initial pre-gold seeded silica-coated magnetic nanoparticles concentration D) 2 nM E) 24 nM and F) 58 nM. The scale bars are 200 nm in length.

To make sure that the pre-gold seeded silica-coated magnetic nanoparticles are fully gold-coated before leaving the channel, a TEM grid was loaded with a drop of the reaction solution at the end of the channel before the reagents drop into the vial. The particles were investigated by TEM (see Figure S4). The TEM grid shows fully coated particles and no sign of partial coating although other deposits are visible. Figure 2 shows the TEM images of gold-coated magnetic nanoparticles after the reaction. The initial concentration of pre-gold seeded silica-coated magnetic nanoparticles is important in controlling whether the final particles after gold nanoshell growth are aggregates or fully gold-coated and monodisperse nanoparticles.

Low concentration of pre-gold seeded silica-coated magnetic nanoparticles, as can be seen from Figure 2A, lead to aggregation. Continuous supply of fresh gold precursor and simultaneous reduction by hydroxylamine hydrochloride on the surface of pre-gold seeded silica will lead to aggregated particles. The corresponding histogram of the size of particles in Figure 2D shows

the polydispersity of the particles with an average size of 400 ± 245 nm. Dynamic light scattering (DLS) shown in Figure S5 also confirmed the results acquired by TEM as the hydrodynamic size of the gold-coated particles was 856 nm with PDI: 0.579.

The shape and monodispersity of nanoparticles are significantly improved by increasing the concentration of the pre-gold seeded silica-coated magnetic nanoparticles to 24 nM (Figure 2B and Figure S6). The corresponding histogram of the size of the particles shows better monodispersity with an average size of 141±23 nm from TEM. DLS (Figure S5) results showed that the hydrodynamic size of the particles was 158 nm with PDI: 0.181. The optimal ratio of gold precursor and a reducing agent to the surface area of the pre-gold seeded silica-coated magnetic nanoparticles results in fully gold-coated magnetic nanoparticles with no sign of aggregation.

Figure 2C shows the gold-coated magnetic nanoparticles synthesized after increasing the concentration of pre-gold seeded silica-coated magnetic nanoparticles to 58 nM. Although the particles are coated with gold, the gold shell is thinner as evident by the less intense black colour of the particles in Figure S7. The histogram from the TEM images of the size of the particles revealed that the particles are more polydispersed as the average size of the particles reaches 159±32 nm. The hydrodynamic size and PDI (Figure S5) of the particles increased to 330 nm and 0.311 respectively. The fact that the gold shell seems to be thinner, while the hydrodynamic radius of the particles is large, reflects a minor amount of aggregation of the nanoparticles during coating. This phenomenon could be explained by the basic origin of the DLS measurement. Scattered light from the Brownian motion of nanoparticles determines the hydrodynamic size of the nanoparticles. As the intensity of the scattered light is proportional to the volume of the particles, existence of bigger particles could have a dominant effect on the DLS data.[37,38]

To test the colloidal stability of the gold-coated magnetic nanoparticles acquired by the initial concentration of 24 nM in Milli-Q water, the changes in hydrodynamic size and PDI vs time were recorded. As it can be seen from Figure S5 B (supporting information) no sign of the flocculation of the particles is observed up to 270 minutes with the PDI remaining stable. After 270 minutes, a sudden decrease in hydrodynamic size from 153 nm to 134 nm along with a reduction of the PDI from 0.134 to 0.117 suggest the few bigger particles may have deposited as sediment at the bottom of the vessel. Further measurements up to 750 minutes showed no significant changes in size or PDI hence, showing a stable dispersion of particles in solution.

The XRD patterns for gold-coated magnetic nanoparticles is shown in Figure S8. The peaks corresponding to the (111), (200), (220), (311) and (222) of the gold. The 2 theta peaks at 33.92° and 41.65°corresponding to the (104) and (006) faces of the iron oxide crystal structure respectively.[39–42]

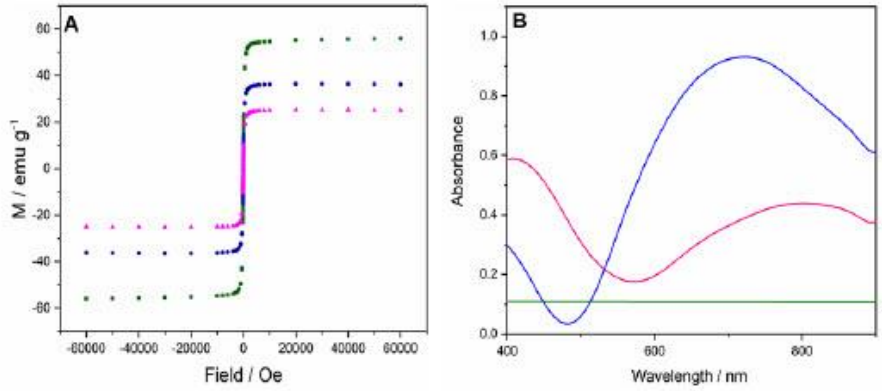

Figure 3. A) SQUID magnetometry measurements of iron oxide nanoparticles (green) silica-coated magnetic nanoparticles (blue) and gold-coated magnetic nanoparticles (magenta), B) UV-Vis spectra of gold-coated magnetic nanoparticles prepared with different initial pre-gold seeded silica-coated magnetic nanoparticles concentration 2 nM (green), 24 nM (blue), and 58 nM (magenta).

The magneto-plasmonic properties of the synthesized particles were investigated using a SQUID magnetometer and UV-Vis spectroscopy. The magnetization (M) - applied field (H)

relationship of the particles is shown in Figures 3A and S9. It is evident from Figure 3 that the decrease in the saturation magnetization is a result of the addition of non-magnetic layers to the magnetic nanoparticles. The saturation magnetization of 56 emu/g, 36 emu/g and 25 emu/g were recorded for iron oxide magnetic nanoparticles, silica-coated magnetic nanoparticles and gold-coated magnetic nanoparticles respectively. It is also evident from the hysteresis curves in Figure S9 that the particles show superparamagnetic behaviour regardless of the coating, with the remnant magnetization of ≈5 emu /g and a coercivity of ≈ 11 Oe. These saturation magnetization values are in agreement with previous work.[32]

The UV-Vis spectra of the particles can be seen in Figure 3B. While no visible peak was observed in the case of the particles made with the initial pre-gold seeded silica-coated magnetic nanoparticles concentration of 2 nM of the pre-gold seeded silica-coated magnetic nanoparticles. Two peaks at 710 nm and 780 nm were observed for the particles which were prepared with the initial pre-gold seeded silica-coated magnetic nanoparticles concentration of 24 nM and 58 nM respectively. This is in agreement with the classical electromagnetic scattering theory, as by varying the thickness ratio of the dielectric core to the metallic shell optical resonance could be transferred to any region of the optical spectrum.[35,43] As shown in Figure 3B, the UV-Vis spectrum of the particles made with the initial concentration of 2 nM pre-gold seeded silica-coated magnetic nanoparticles does not show any strong absorption in the visible region because of the sedimentation as a result of the aggregation of that group of particles.

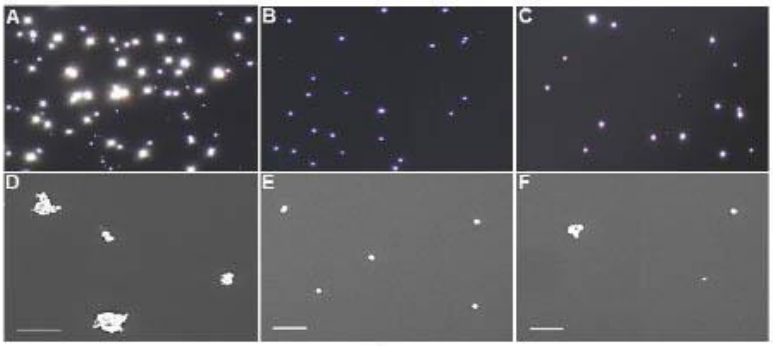

Figure 4. Dark-field microscopy images of gold-coated magnetic nanoparticles prepared with different initial pre-seeded silica-coated magnetic nanoparticles concentration A) 2 nM B) 24 nM and C) 58 nM and corresponding SEM images of gold-coated magnetic nanoparticles prepared with different initial pre-gold seeded silica-coated magnetic nanoparticles concentration D) 2 nM E) 24 nM and F) 58 nM. Scale bars 1 μm.

The optical properties of the gold-coated magnetic nanoparticles made with different concentration of pre-gold seeded silica-coated magnetic nanoparticles were further investigated using dark-field microscopy and SEM. The large bright spots in Figure 4A from the gold-coated magnetic nanoparticles made from 2 nM pre-seed nanoparticles is due to light scattered by these nanoparticles. The whiteish color nanoparticles in the image suggests that this image is showing many scattering spots where the nanoparticles are aggregated. The corresponding SEM images confirm that the particles are mostly aggregated. As it can be seen from Figure 4B, with the gold-coated magnetic nanoparticles made from 24 nM of the pre-seeded particles, the purple hue from the scattering images indicates that these nanoparticles are well dispersed. The SEM image confirms the well-dispersity and monodispersity of the nanoparticles. Finally, the dark-field microscopy image of the gold-coated magnetic nanoparticles made from 58 nM of the pre-gold seeded silica-coated magnetic nanoparticles (Figure 4C) has a less intense purple and pinkish color which could be because these particles have a thinner gold shell.[44] It is also important to note that sign of particles aggregation on small scale could be seen from the picture in form of bright and bigger spots in the dark-field image. The SEM image in Figure 4F and Figure S10 confirms the co-existence of both well-dispersed particles along with a small number of aggregated nanoparticles.

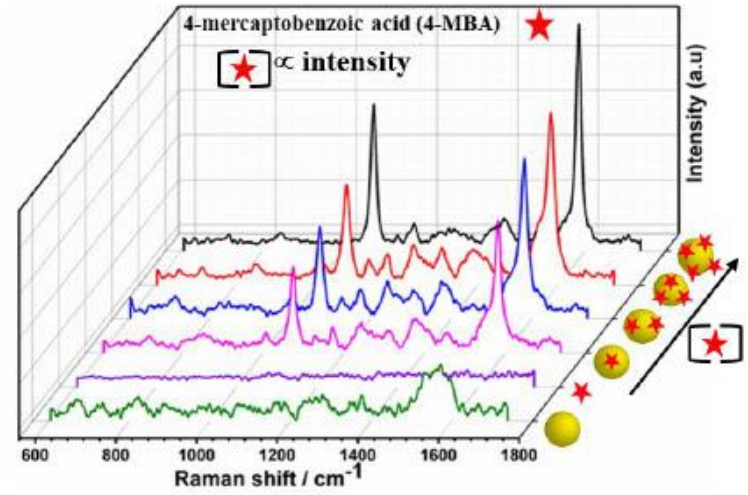

Figure 5. Raman spectra of bare gold-coated magnetic nanoparticles (Green), 4-mercaptobenzoic acid (4-MBA) Raman active molecule (Purple), and SERS spectra of gold-coated magnetic nanoparticles modified with 3μM of 4-mercaptobenzoic acid (4-MBA) (Magenta), gold-coated magnetic nanoparticles modified with 5μM of 4-mercaptobenzoic acid (4-MBA) (Blue), gold-coated magnetic nanoparticles modified with 20 μM of 4-mercaptobenzoic acid (4-MBA) (Red) and gold-coated magnetic nanoparticles modified with 1 mM of 4-mercaptobenzoic acid (4-MBA) (Black)

To verify the SERS performance, gold-coated magnetic nanoparticles were modified with Raman probe molecules. Thiol based (-SH) 4-mercaptobenzoic acid was considered as the Raman active molecule to prepare the SERS particles.[45] The obtained SERS spectra from these SERS particles prepared from gold-coated magnetic nanoparticles is illustrated in Figure 5. Two distinct SERS bands are observed at 1076 cm^{-1} and 1586 cm^{-1} corresponding to the aromatic ring vibrations such as ν_{12} – ring breathing and ν_{8a} – ring breathing of 4-mercaptobenzoic acid. This was observed in the resultant SERS spectra which have a good agreement with the literature indicates the chemisorption of 4-mercaptobenzoic acid on gold-coated magnetic nanoparticles surface.[46,47] The SERS performance of these particles was validated by investigating the effect of concentration of 4-mercaptobenzoic molecules (indicated by an arrow in Figure 5) where the enhancement of SERS intensity was found with

the increase in coverage of the Raman active molecules to the point where a full monolayer coverage is achieved.[48]

3. Conclusion

In conclusion, here we have developed a new rapid synthetic method for the preparation of the gold-coated magnetic nanoparticles that solves the long-standing challenge of reliable gold-coating of magnetic nanoparticles. The synthesis strategy reported here starts by attaching ultra-small gold nanoparticles to the surface of the silica and then a gold shell form around the pre-seeded silica-coated magnetic nanoparticles. The fluidic-based synthesis method reported here is simple, scalable, cost-effective and fast. We showed that the quality of the final gold-coated magnetic nanoparticles is highly related to the initial concentration of pre-gold seeded silica-coated magnetic nanoparticles. Magneto-plasmonic properties of the particles were investigated using SQUID magnetometry and UV-Vis spectrometer. The optical consistency of the final products was investigated using dark-field microscopy. Finally, the ability of the particles to be used as biosensing agent was investigated.

4. Experimental Section

Materials: iron (III) acetylacetonate, oleylamine (70%), oliec acid, trioctylamine, igepal CO-520, ammonium hydroxide 30%, tetraethylorthosilicate (TEOS), [3-(2-aminoethylamino) propyl]trimethoxysilane 80 % (AEAPTMS), (3-aminopropyl)triethoxysilane (APTES), dimethyl sulfoxide (DMSO), gold (III)trihydrate ($HAuCl_4$. $3H_2O$), tetramethylammonium hydroxide in methanol solution (25% (wt/vol) TMAOH in methanol solution), hydroxylamine hydrochloride (NH_2OH. HCl), sodium citrate dihydrate, sodium borohydride, 4-mercaptobenzoic acid were purchased from Sigma-Aldrich. acetone, toluene, cyclohexane, methanol, nitric acid (69%), and hydrochloric acid (32%) were purchased from Chem-Supply Australia. Polylactic acid (PLA) was purchased from Flashforge. Except for oleylamine chemicals were used as received. oleylamine was distilled before reaction. Syringes were

purchased from Terumo syringe, needles (0.7×38 mm) were purchased from BD. Glassware was cleaned with freshly prepared *aqua regia* (HCl: HNO_3 in a 3:1 Ratio by volume) followed by rinsing with a copious amount of Milli-Q water.

Magnetic and silica-coated magnetic nanoparticles were synthesized following our previously reported with small modification method using thermal decomposition and microemulsion.[32] In short, iron (III) acetylacetonate was thermally decomposed in a boiling solution of oleylamine, oleic acid and triactolamine at 330˚C. A silica shell was formed around the iron oxide nanoparticles using a standard microemulsion sol-gel method. Base-catalyzed hydrolysis and polycondensation of TEOS on the surface of magnetic nanoparticles produced a dielectric shell around the magnetic nanoparticles. To achieve that 12 mL of cyclohexane was added to a 40 mL vial and then 700 µL of igepal CO-520 was added to the cyclohexane. The solution was vortexed to dissolve the igepal CO-520 in cyclohexane completely. A 100 µL of the 3µM of iron oxide nanoparticles in toluene was added to the solution. Next 85 µL of ammonium hydroxide was added to the solution and the vial was shaken by hand for few seconds. Finally, a sum of 30 µL of TEOS was added to the solution and the vial was left inside a fume hood for 42 hours. To terminate the surface of the silica-coated magnetic nanoparticles with amine group, AEAPTMS was used. An amount of 7 µL of 80% analytical grade AEAPTMS was added to the microemulsion solution of the silica-coated magnetic nanoparticles and shaken for 120 minutes. The microemulsion was broken by adding 4 mL of the 50 mM TMAOH in methanol and then carefully collecting the brown layer from the solution. Then 8 mL of acetone was added to the solution and the particles solution were transferred to the centrifuge tubes. Particles were centrifuged at 1600 rcf for 15 minutes then the supernatant was removed (this step was repeated twice). The acquired nanoparticles were redispersed in 1 mL of DMSO sonicated and transferred to the centrifuge tube again. The particles were centrifuged at 3800 rcf for 5 minutes and the supernatant was collected. Particles that precipitated out of the solution from the

centrifuge tubes are not well-dispersed and should be discarded. Next, the silica-coated magnetic nanoparticles were transferred to a syringe containing gold chloride aqueous solution (0.25 mM) and sodium citrate aqueous solution (0.17 M). The second syringe was loaded with an aqueous solution of sodium borohydride (0.01 M). Nanoparticles and streams of reagents were dropped into a 40 mL vial. The seeded particles were separated from the solution and washed using a neodymium square block magnet. Different concentrations of the pre-gold seeded silica-coated magnetic nanoparticles were dispersed in Milli-Q water and then loaded into a syringe. A second syringe was loaded with gold chloride aqueous solution (0.3 mM) and sodium citrate aqueous solution (10.8 mM) and a third and final syringe were loaded with the hydroxylamine hydrochloride aqueous solution (40 mM). Nanoparticles at the end of a piece were collected inside a vial and then further washed with Milli-Q water *via* magnetic separation. The reaction could theoretically be continuous as long as the supply of the chemicals and nanoparticles are available. After adding any sets of syringes containing the chemicals and particles a new Y-shaped piece was used to avoid clogging.

SERS particles were prepared by the immobilization of 4-mercaptobenzoic acid on the surface of gold-coated magnetic nanoparticles. Briefly 50 μL gold-coated magnetic nanoparticles (6×10^{12} particles/mL) was mixed with 50 μL of diffrent concentration of 4-mercaptobenzoic and the resulting mixture was incubated for 2 h under shaking conditions at room temperature to form SAM over the surface of the gold-coated magnetic nanoparticles.

Instruments and characterization: TEM images were acquired using a Phillips CM 200 microscope at an acceleration voltage of 200 kV. The TEM samples were prepared by drop-casting a diluted solution of the nanoparticles on a carbon-coated copper grid, this was followed by air drying at room temperature. An FEI Nova Nano SEM 450 was used for acquiring SEM images of the gold-coated magnetic nanoparticles in the range of 4-25 kV. Both TEM and SEM

images were analyzed by ImageJ software. A Cary 60 single-beam UV-Vis spectrophotometer was used to acquire the absorbance spectra of the gold-coated nanoparticles in solution. The hydrodynamic size of the gold-coated magnetic nanoparticles in Milli-Q water was measured on a Zetasizer Nano ZS. The colloidal stability of the gold-coated magnetic nanoparticles was measured over time using Zetasizer Nano ZS. Particle concentration was measured using Nanoparticle tracking analyzes (Nano-sight NS300, Malvern Panalytical). Olympus BX51 dark-field microscopy was used to acquire dark-field images of the gold-coated magnetic nanoparticles. To achieve this, the gold-coated magnetic nanoparticles were immobilized onto APTES modified coverslips and then coverslips were rinsed with Milli-Q water and dried under a stream of argon. The coverslip was mounted on the aluminium holder and imaged using an Olympus BX51 microscope. Raman spectra were measured using a Renishaw in Via confocal Raman microscope with excitation laser wavelengths of 785 nm and the diffraction grating of 1200g/mm. Raman measurements were recorded by applying the laser power of ~ 2.01 mW, accumulation time of three and exposure time of 10 seconds. The average of 3 measurements was used to present in SERS data and all the spectra were calibrated to silicon peak located at 520-521 cm^{-1}. XRD was performed on an Empyrean 2 (Malvern Panalytical) X-ray diffractometer with Co Kα (1.79 Å) radiation sample was analyzed from 30° to 100° (2θ).

Supporting Information

Supporting Information is available from the Wiley Online Library or the author.

Acknowledgements

We acknowledge funding under the Australian Research Council Linkage grant (LP150101014, JJG and RDT), the Australian Laureate Fellowship (FT150100060, JJG) and the Discovery Project (DP190102659 and DP200100143, RDT). JJG also acknowledges a National Health and Medical Research Investigator grant (APP1196648). LG, JJG and RDT acknowledge the Dementia Australia Research Foundation Yulgilbar innovation grant.

Received: ((will be filled in by the editorial staff))
Revised: ((will be filled in by the editorial staff))
Published online: ((will be filled in by the editorial staff))

References

[1] L. Gloag, M. Mehdipour, D. Chen, R. D. Tilley, J. J. Gooding, *Adv. Mater.* **2019**, *31*, 1.

[2] R. Tavallaie, J. McCarroll, M. Le Grand, N. Ariotti, W. Schuhmann, E. Bakker, R. D. Tilley, D. B. Hibbert, M. Kavallaris, J. J. Gooding, *Nat. Nanotechnol.* **2018**, 13, 1066

[3] F. Mohammad, G. Balaji, A. Weber, R. M. Uppu, C. S. S. R. Kumar, *J. Phys. Chem. C. Nanomater. Interfaces* **2010**, *114*, 19194.

[4] L. Gloag, M. Mehdipour, M. Ulanova, K. Mariandry, M. A. Nichol, D. J. Hernández-Castillo, J. Gaudet, R. Qiao, J. Zhang, M. Nelson, B. Thierry, M. A. Alvarez-Lemus, T. T. Tan, J. J. Gooding, N. Braidy, P. S. Sachdev, R. D. Tilley, *Chem. Commun.* **2020**, *56*, 3504.

[5] E. E. Carpenter, J. A. Sims, J. A. Wienmann, W. L. Zhou, C. J. O'Connor, *J. Appl. Phys.* **2000**, *87*, 5615.

[6] E. E. Carpenter, N. Orleans, *Polyhedron* **1999**, *35*, 3496.

[7] W. L. Zhou, E. E. Carpenter, J. Lin, A. Kumbhar, J. Sims, C. J. O'Connor, *Eur. Phys. J. D* **2001**, *16*, 289.

[8] M. Mandal, S. Kundu, S. K. Ghosh, S. Panigrahi, T. K. Sau, S. M. Yusuf, T. Pal, *J. Colloid Interface Sci.* **2005**, *286*, 187.

[9] X. Zhou, W. Xu, Y. Wang, Q. Kuang, Y. Shi, L. Zhong, Q. Zhang, *J. Phys. Chem. C* **2010**, *114*, 19607.

[10] S. Moraes Silva, R. Tavallaie, L. Sandiford, R. D. Tilley, J. J. Gooding, *Chem. Commun.* **2016**, *52*, 7528.

[11] Z. Xu, Y. Hou, S. Sun, *J. Am. Chem. Soc.* **2007**, DOI 10.1021/ja073057v.

[12] X. Hou, X. Wang, R. Liu, H. Zhang, X. Liu, Y. Zhang, *RSC Adv.* **2017**, *7*, 18844.

[13] J. Lin, W. Zhou, A. Kumbhar, J. Wiemann, J. Fang, E. E. Carpenter, C. J. O'Connor, *J. Solid State Chem.* **2001**, *159*, 26.

[14] C. X. Zhao, L. He, S. Z. Qiao, A. P. J. Middelberg, *Chem. Eng. Sci.* **2011**, *66*, 1463.

[15] S. V. Salihov, Y. A. Ivanenkov, S. P. Krechetov, M. S. Veselov, N. V. Sviridenkova, A. G. Savchenko, N. L. Klyachko, Y. I. Golovin, N. V. Chufarova, E. K. Beloglazkina, A. G. Majouga, *J. Magn. Magn. Mater.* **2015**, *394*, 173.

[16] S. MoraesSilva, R. Tavallaie, M. TanzirulAlam, K. Chuah, J. J. Gooding, *Electroanalysis* **2016**, *28*, 431.

[17] A. M. Nightingale, J. C. Demello, *Adv. Mater.* **2013**, *25*, 1813.

[18] G. Niu, A. Ruditskiy, M. Vara, Y. Xia, *Chem. Soc. Rev.* **2015**, *44*, 5806.

[19] H. J. Kwon, K. Shin, M. Soh, H. Chang, J. Kim, J. Lee, G. Ko, B. H. Kim, D. Kim, T. Hyeon, *Adv. Mater.* **2018**, *1704290*, 1.

[20] D. Arndt, J. Thöming, M. Bäumer, *Chem. Eng. J.* **2013**, *228*, 1083.

[21] S. He, T. Kohira, M. Uehara, T. Kitamura, H. Nakamura, M. Miyazaki, H. Maeda, *Chem. Lett.* **2005**, *34*, 748.

[22] J. M. Köhler, M. Held, U. Hübner, J. Wagner, *Chem. Eng. Technol.* **2007**, *30*, 347.

[23] S. A. Khan, A. Günther, M. A. Schmidt, K. F. Jensen, *Langmuir* **2004**, *20*, 8604.

[24] A. Knauer, A. Thete, S. Li, H. Romanus, A. Csáki, W. Fritzsche, J. M. Köhler, *Chem. Eng. J.* **2011**, *166*, 1164.

[25] H. Nakamura, Y. Yamaguchi, M. Miyazaki, H. Maeda, M. Uehara, P. Mulvaney, *Chem. Commun.* **2002**, *23*, 2844.

[26] C. D. Ahrberg, J. Wook Choi, B. Geun Chung, *Sci. Rep.* **2020**, *10*, 1737.

[27] S. Duraiswamy, S. A. Khan, *Nano Lett.* **2010**, *10*, 3757.

[28] R. Wang, X. Ji, Z. Huang, Y. Xue, D. Wang, W. Yang, *J. Phys. Chem. C* **2016**, *120*,

377.

[29] L. E. Woodard, C. L. Dennis, J. A. Borchers, A. Attaluri, E. Velarde, C. Dawidczyk, P. C. Searson, M. G. Pomper, R. Ivkov, *Sci. Rep.* **2018**, *8*, 1.

[30] J. Ma, S. M. Y. Lee, C. Yi, C. W. Li, *Lab Chip* **2017**, *17*, 209.

[31] L. Shang, Y. Cheng, Y. Zhao, *Chem. Rev.* **2017**, *117*, 7964.

[32] M. Mehdipour, L. Gloag, D. T. Bennett, S. Hoque, R. Pardehkhorram, P. Bakthavathsalam, V. R. Gonçales, R. D. Tilley, J. J. Gooding, *J. Mater. Chem. C* **2021**, DOI 10.1039/d0tc04702c.

[33] J. W. Kim, D. Seo, J. U. Lee, K. M. Southard, Y. Lim, D. Kim, Z. J. Gartner, Y. W. Jun, J. Cheon, *Nat. Protoc.* **2017**, *12*, 1871.

[34] M. Dmsmcd, N. Com, **n.d.**

[35] S. J. Oldenburg, R. D. Averitt, S. L. Westcott, N. J. Halas, *Chem. Phys. Lett.* **1998**, *288*, 243.

[36] X. Ji, X. Song, J. Li, Y. Bai, W. Yang, X. Peng, *J. Am. Chem. Soc.* **2007**, *129*, 13939.

[37] A. Kim, W. B. Ng, W. Bernt, N. J. Cho, *Sci. Rep.* **2019**, *9*, 1.

[38] P. A. Hassan, S. Rana, G. Verma, *Langmuir* **2015**, *31*, 3.

[39] A. Sood, V. Arora, J. Shah, R. K. Kotnala, T. K. Jain, *J. Exp. Nanosci.* **2016**, *11*, 370.

[40] H. Yu, M. Chen, P. M. Rice, S. X. Wang, R. L. White, S. Sun, *Nano Lett.* **2005**, *5*, 379.

[41] J. H. L. Beal, S. Prabakar, N. Gaston, G. B. The, P. G. Etchegoin, G. Williams, R. D. Tilley, *Chem. Mater.* **2011**, *23*, 2514.

[42] X. Wang, R. D. Tilley, J. J. Watkins, *Langmuir* **2014**, *30*, 1514.

[43] Y. T. Lim, O. O. Park, H. T. Jung, *J. Colloid Interface Sci.* **2003**, *263*, 449.

[44] J. K. Lim, R. D. Tilton, A. Eggeman, S. A. Majetich, *J. Magn. Magn. Mater.* **2007**, *311*, 78.

[45] R. Pardehkhorram, S. Bonaccorsi, H. Zhu, V. R. Gonçales, Y. Wu, J. Liu, N. A. Lee, R.

D. Tilley, J. J. Gooding, *Chem. Commun.* **2019**, *55*, 7707.

[46] A. Michota, J. Bukowska, *J. Raman Spectrosc.* **2003**, *34*, 21.

[47] A. Williams, K. J. Flynn, Z. Xia, P. R. Dunstan, *J. Raman Spectrosc.* **2016**, *47*, 819.

[48] Y. Wang, S. Schlücker, *Analyst* **2013**, *138*, 2224.

AGGREGATE WILEY

Supporting Information

Facile, flow reactor synthesis of gold-coated magnetic nanoparticles for bio-sensing applications

Milad Mehdipour, Lucy Gloag, Daniel Hagness, Jiaxin Lian, Md Saiful Alam, Xueqian Chen, Richard. D Tilley, and J. Justin Gooding

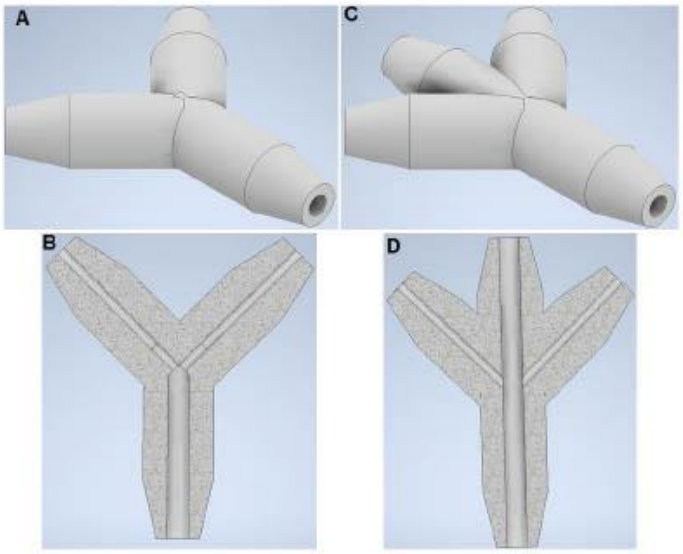

Figure S1. Schematic illustration of A) the Y-shaped piece used for seeding of the silica-coated magnetic nanoparticles with small gold nanoparticles, B) cross-section of the two-channel Y-shaped piece used for seeding, C) the three-channel Y-piece used for the growth of the gold shell around the already gold-seeded silica-coated magnetic nanoparticles and D) cross-section of the three-channel Y-shaped piece used for the growth of gold shell.

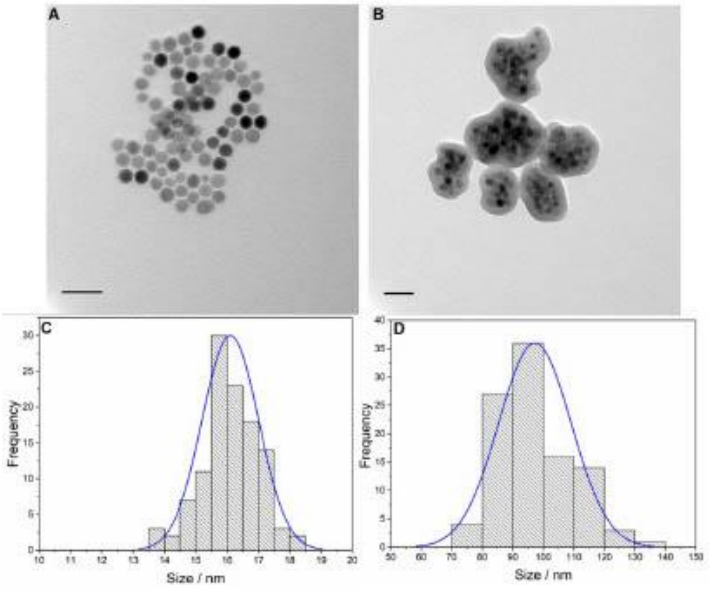

Figure S2. TEM images of A) iron oxide magnetic nanoparticles B) silica-coated conglomerate magnetic nanoparticles. The scale bars are 50 nm long.

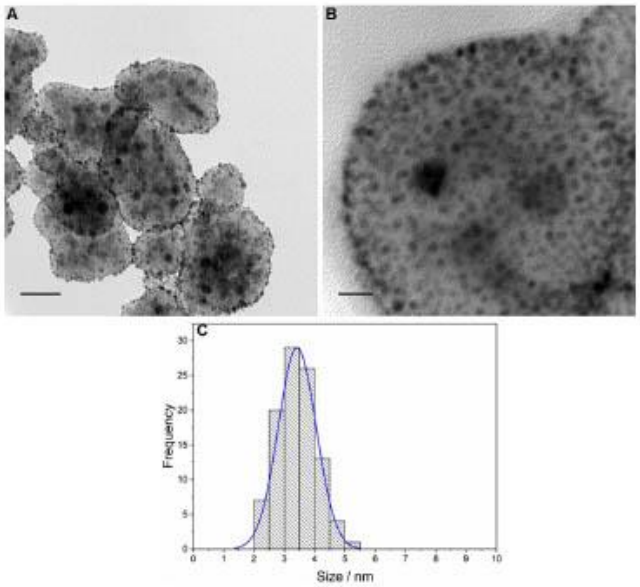

Figure S3. TEM images of A) silica-coated magnetic nanoparticles after seeding with small gold nanoparticles. The scale bar is 50 nm, B) higher resolution image of the silica-coated magnetic nanoparticles seeded with small gold nanoparticles. Scale bar 10 nm, and C) Histogram of the size of gold seeds on the surface of silica-coated magnetic nanoparticles.

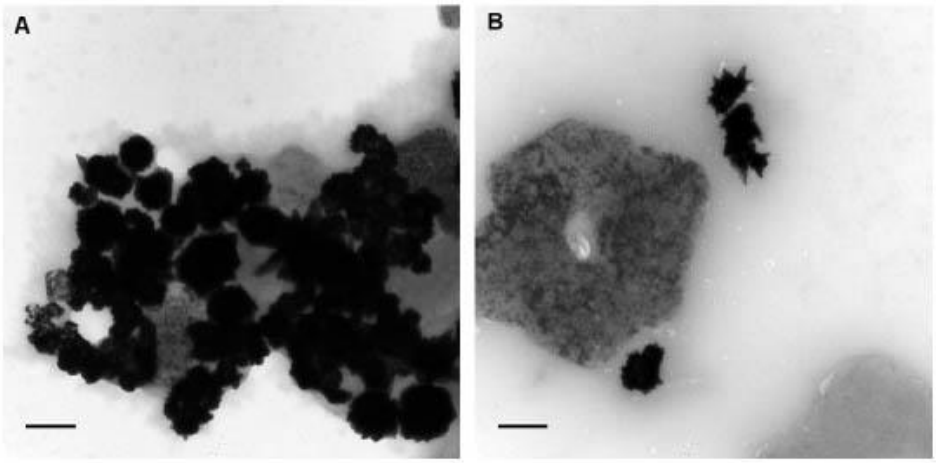

Figure S4. A and B TEM images of two separate spots of the TEM grid of the gold-coated magnetic nanoparticles right after the end of the long channel of the Y-shaped piece (no washing step was performed). The scale bars are 200 nm.

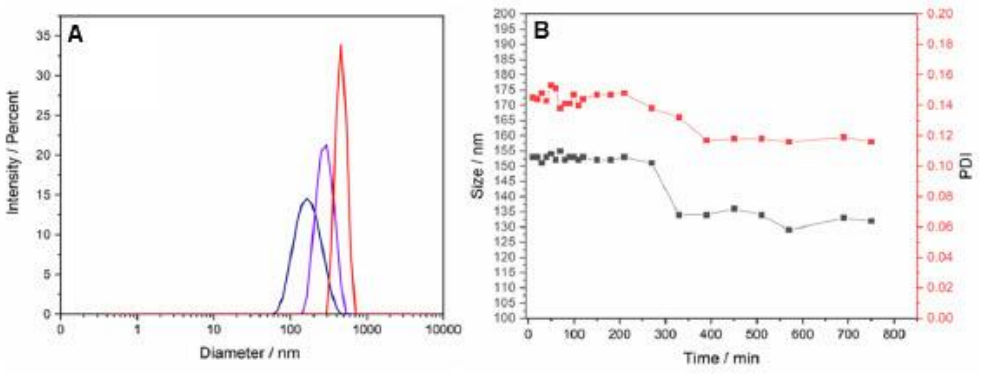

Figure S5. Dynamic light scattering measurement of A) gold-coated magnetic nanoparticles of initial pre-gold seeded silica-coated magnetic nanoparticles concentration of 2 nM (red), 24 nM (blue), and 58 nM (purple) and B) colloidal stability of gold-coated magnetic nanoparticles (24 nM) over time. The black points represent the hydrodynamic size of the particles as on the black y-axis and the red points refer to the PDI as on the red y-axis.

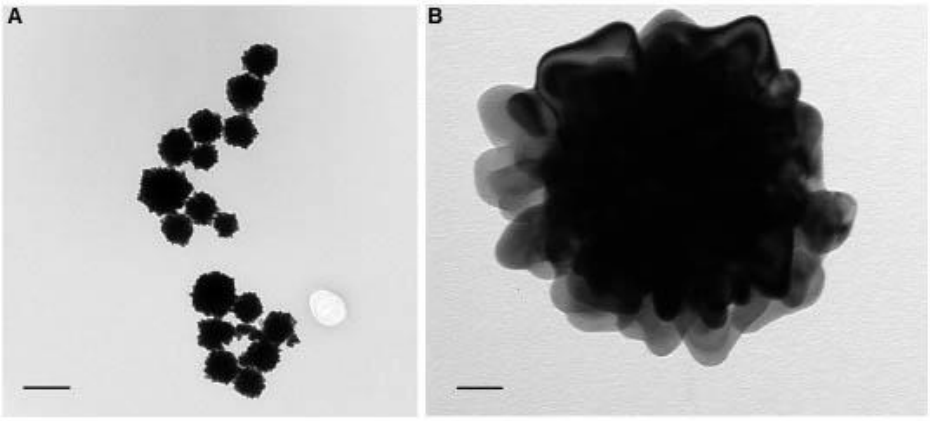

Figure S6. TEM images of A) the gold-coated magnetic nanoparticles (24 nM). The scale bar is 200 nm B) higher resolution TEM image of a gold-coated magnetic nanoparticle. The scale bar is 20 nm.

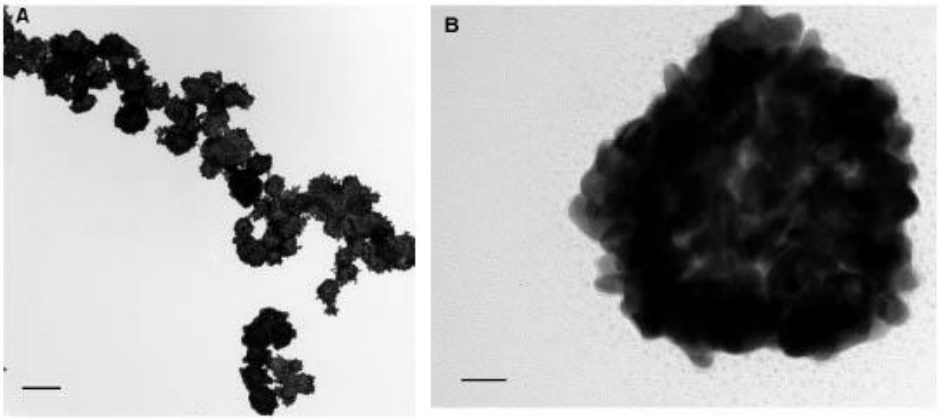

Figure S7. TEM images of A) the gold-coated magnetic nanoparticles (58 nM). The scale bar is 200 nm B) higher resolution TEM image of a gold-coated magnetic nanoparticle. The scale bar is 20 nm.

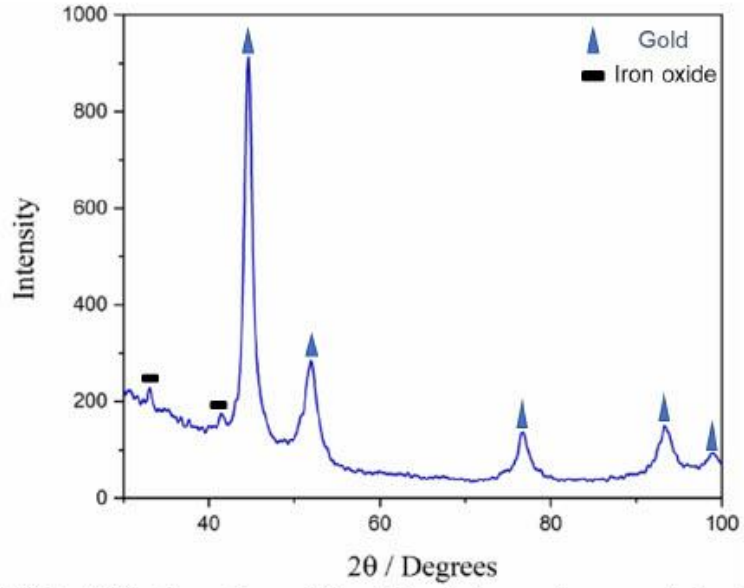

Figure S8. X-Ray Diffraction patterns of the gold-coated magnetic nanoparticles with representative index typical peaks.

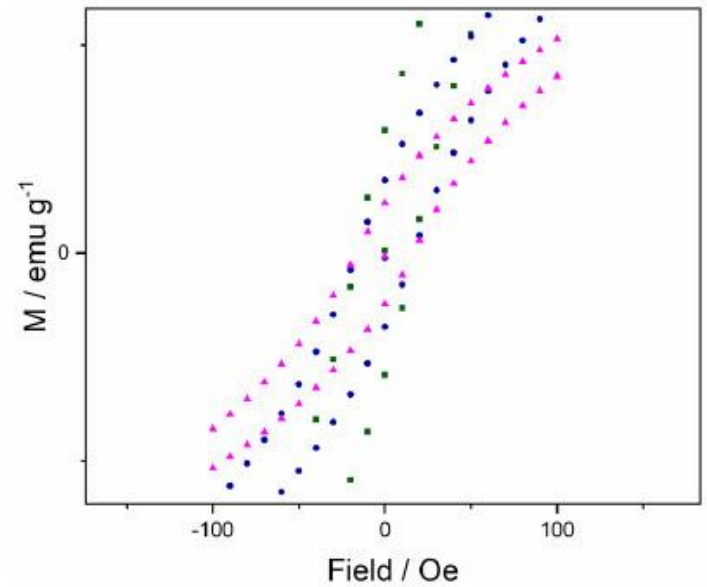

Figure S9. SQUID magnetometry measurements of magnetization behavior of iron oxide magnetic nanoparticles (green), silica-coated magnetic nanoparticles (blue), gold-coated magnetic nanoparticles (magenta).

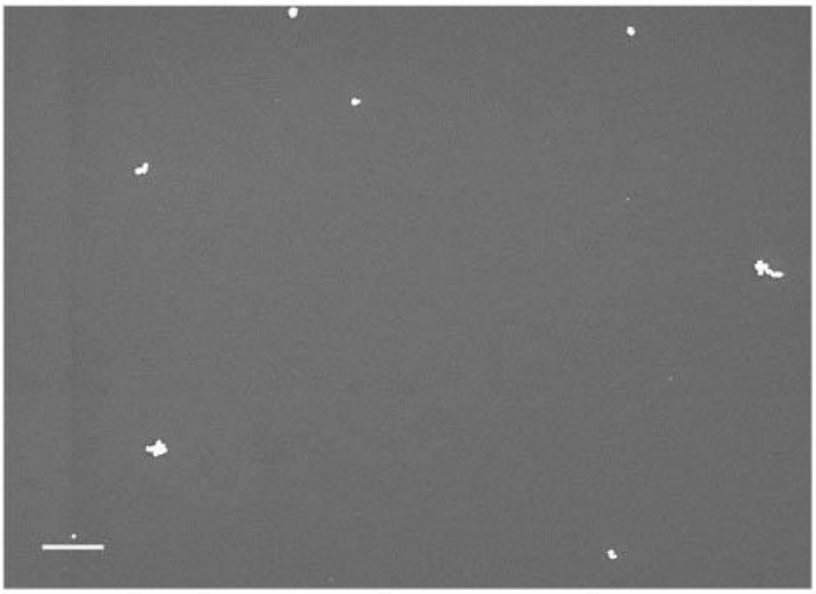

Figure S10. SEM image of the gold-coated magnetic nanoparticles acquired from the initial pre-gold seeded silica-coated magnetic nanoparticles concentration of 58 nM. The scale bar is 1 μm.

Chapter 7

Conclusion and future work

7.1. Conclusion and summary

The current thesis focuses on gold-coated magnetic nanoparticles for bio-sensing applications. As it was discussed in length in chapter one gold-coated magnetic nanoparticles can provide versatile properties for bio-sensing applications. Conductivity, localized surface plasmon resonance (LSPR), ease of modification with biological entities, and magnetism are among the most important properties provided by these types of nanoparticles. Challenges such as partial coating, low magnetization saturation, weak magnetic response toward an external magnetic field, and lack of robust and scalable synthesis procedures hinder the widespread use of gold-coated magnetic nanoparticles. This thesis aims to address some of these issues with novel nanoparticles and innovative synthesis methods.

First, to understand the biggest challenges and merits of the gold-coated magnetic nanoparticles, a survey of properties of the state-of-the-art commercially available gold-coated magnetic nanoparticles were conducted in chapter 3. Five different samples from three companies Nanopartz™, Creative Diagnostic®, and Nanoimmunotech were purchased on two separate occasions. The samples have undergone a series of characterization techniques *via* TEM, EDX mapping, UV-Vis spectroscopy, SQUID magnetometry, Dynamic light scattering (DLS), and X-ray diffraction (XRD) to evaluate their properties. This was mainly performed to give scientists a perspective of expected challenges and whether the commercially available nanoparticles could address requirements needed for intended applications. The data acquired from TEM and EDX mapping showed that the commercial gold-coated magnetic nanoparticles seem to be mostly a combination of the iron oxide nanoparticles and gold nanoparticles with different sizes and shapes. The XRD patterns mostly showed that particles compromise gold and iron oxide (maghemite and magnetite). In the case of magneto-plasmonic properties, UV-Vis results showed that the optical property of commercial gold-coated magnetic nanoparticles seemed to be mostly in line with pure gold nanoparticles of different sizes. The SQUID magnetometry data showed that although most of the gold-coated magnetic nanoparticles showed magnetism yet some do not show either any sign or neglectable magnetism. Overall, this study showed that commercially available

gold-coated magnetic nanoparticles could not fulfil the requirements of applications such as bio-sensing. These nanoparticles showed no uniformity in case of shape and more importantly, they were a combination of gold nanoparticles and magnetic nanoparticles.

To address the challenges discussed in chapter one and the fact that commercially available gold-coated nanoparticles investigated in chapter 3 showed no sign of solving these challenges, a new type of gold-coated magnetic nanoparticle was designed in chapter 4. As discussed in chapter one, partial gold-coating of magnetic nanoparticles, aggregation and slow magnetic response are some of the main concerns related to gold-coated magnetic nanoparticles and bio-sensing. To address these challenges a novel nanoparticle called ‘’gold-coated conglomerates of superparamagnetic nanoparticles’’ was designed. When magnetic nanoparticles are coated with non-magnetic layers such as silica and gold their magnetization saturation decreases. This means that gold-coated magnetic nanoparticles respond to the external magnetic field weakly. One solution to this challenge could be using bigger size magnetic nanoparticles in which can produce stronger magnetic force. The problem with magnetic nanoparticles (≥20 nm) is that they also attract each other even in absence of an external magnetic field which makes them highly prone to aggregation. To address this issue superparamagnetic nanoparticles which are only magnetic in presence of an external magnetic field could be used, but superparamagnetic nanoparticles are not as magnetic. Gold-coated conglomerates of superparamagnetic nanoparticles were designed to solve the issue of aggregation while at the same time being rapidly responsive toward the external magnetic field. Magnetite nanoparticles with an average size of 16 nm were synthesized through thermal decomposition, and then *via* a reverse microemulsion method, a group of magnetite nanoparticles were encapsulated inside a silica shell. Finally, through a seed mediation growth method a complete gold shell was introduced around the silica-coated conglomerates of superparamagnetic nanoparticles. The obtained gold-coated conglomerates of superparamagnetic nanoparticles were rapidly attracted to the external magnetic field (within 35-40 seconds) while extremely stable against magnetic aggregation. Each of the superparamagnetic nanoparticles inside the silica shell act as a magnetic engine for the overall nanoparticle and as the

result a rapid response toward the external magnetic field. The rapid response toward the external magnetic field and high stability against magnetic aggregation is crucial for the modification of nanoparticles with different molecules and detecting biomolecules promptly.

The utility of the nanoparticles as bio-sensing agents was demonstrated by using them as SERS agents (Optical sensing) and dispersible electrodes (electrochemical sensing). First, the optical consistency of the nanoparticles was established using dark-field microscopy. The colour analyses and single-particle spectra showed that the nanoparticles have good optical consistency which is very important for optical sensing. Furthermore, gold-coated conglomerates of superparamagnetic nanoparticles were modified with 4-aminothiolphenol molecules and the performance of modified nanoparticles as SERS agents was demonstrated by comparing the data with unmodified nanoparticles. Finally, the gold-coated conglomerates of superparamagnetic nanoparticles were used as dispersible electrodes. The nanoparticles were modified with methylene-blue-labelled probe DNA and then a square-wave voltammogram was measured for nanoparticles with and without the probe DNA. While no current was detected in the case of unmodified nanoparticles, an increase in current was observed in nanoparticles modified with the methylene-blue-labelled probe DNA due to the faster electron transfer between the redox molecules and the surface. Furthermore, hybridizing the modified nanoparticles with the miRNA miR-21 decreased the current due to two facts: first increase in the distance between the redox label and the surface and second increased rigidity of the DNA/miRNA double helix. Although, the gold-coated conglomerates of superparamagnetic nanoparticles showed a fast magnetic response toward an external magnetic field, stability against magnetic aggregation, colloidal stability and bio-sensing applicability, their magnetization saturation was 22 emu g^{-1} which could be a sign of concern and a point that need to be a focus on more. It should be noted that increasing magnetization saturation of nanoparticles not only could affect the magnetic response time of the nanoparticles but also nanoparticles with high magnetization saturation could be useful for other types of application such as bio-imaging and hyperthermia.

To address the main challenge (magnetization saturation of gold-coated conglomerates of superparamagnetic nanoparticles) that arose from the work in chapter 4 a new type of nanoparticle was designed in chapter 5. As was discussed in chapter 1 and 4 addition of non-magnetic layers to magnetic nanoparticles decrease their magnetization saturation and response time to the external magnetic field. To address this challenge by encapsulating multiple superparamagnetic nanoparticles inside a silica shell, a nanoparticle with a fast magnetic response was developed in chapter 4 but the magnetization saturation of the gold-coated conglomerates of nanoparticles was still low. To address this challenge a novel nanoparticle called ‘’gold-coated zero-valent iron core-iron oxide shell’’ was synthesized in chapter 5. Zero-valent iron has the highest magnetization saturation among other magnetic elements. The issue with a zero-valent iron nanoparticle is that it oxidizes almost immediately to other types of iron oxide nanoparticles once in contact with air or water. According to the literature which was discussed in chapter one if zero-valent iron nanoparticles grow to a size bigger than 8 nm even after exposure to air and water a part of the nanoparticle remains intact and as the result, a core-shell nanoparticle of zero-valent iron core-iron oxide shell nanoparticles will form. To make the zero-valent iron core-iron oxide shell nanoparticles iron pentacarbonyl was thermally decomposed at 220°C. The synthesized 14 nm nanoparticles then underwent a series of surface modification steps to ensure that the zero-valent iron core-iron oxide shell was protected against further oxidation and the iron core did not become iron oxide. First, the surface of nanoparticles was capped with oleylamine and second the amine rich ligand was exchanged with oleic acid which is more resistant toward oxidation. The oleic acid capped zero-valent iron core-iron oxide shell was then encapsulated inside a silica shell using a reverse microemulsion method. Seed mediated method was then used to attach 3-4 nm gold nanoparticles on the surface and then form a complete gold shell around the nanoparticles. After coating the nanoparticles with gold size of the nanoparticles reached 107 nm. The gold-coated zero-valent iron core-iron oxide shell was shown to have superparamagnetic behaviour with magnetization saturation of 63 emu g^{-1}. The high magnetization saturation of the gold-coated zero-valent iron core-iron oxide shell is because the zero-valent iron core of the nanoparticles generates high magnetization saturation and as the result, the overall

nanoparticles showed high magnetization saturation. The particles further showed high stability against magnetic aggregation and very long colloidal stability time.

So far two different gold-coated magnetic nanoparticles with unique properties were synthesized. To form the gold shell around the magnetic nanoparticles and synthesize the gold-coated magnetic nanoparticles. In both cases, a seed-mediated method was used. Although the seed-mediated method can produce gold-coated magnetic nanoparticles with a complete gold shell, there are still some important challenges regarding this method that needs to be deal with. The most important challenges are related to the long and complicated procedure and the inability to scale up the procedure.

To address these challenges in chapter 6 a new methodology was developed based on a microfluidic system. As it was discussed in chapter 1 section 1.5.3, although the microfluidic method has made great progress in the synthesis of nanoparticles and gold-coated magnetic nanoparticles, there are challenges such as channel clogging and the need for expensive facilities and subtracts facing scientists. In chapter 6 a new methodology was developed for the attachment of gold seeds and further formation of a complete gold shell around silica-coated magnetic nanoparticles. A two and three channel Y-shape pieces were made to be used for attachment of small gold seeds and growth of gold shell respectively. The simple and cheap design and manufacturing of the pieces was the key difference between the method proposed in chapter 6 and other reports in the literature. Furthermore, the effect of the concentration of pre-gold seeded silica-coated magnetic nanoparticles on the quality of the gold shell growth was investigated. Three different concentrations of 2 nM, 24 nM and 58 nM pre-gold seeded silica-coated magnetic nanoparticles were used. The TEM and DLS data showed that nanoparticles made with a 2 nM concentration of pre-gold seeded silica-coated magnetic nanoparticles are heavily aggregated. When the concentration of pre-gold seeded silica-coated magnetic nanoparticles increased to 24 nM a complete gold shell was formed around the silica-coated magnetic nanoparticles and the nanoparticles showed no sign of aggregation. Increasing the concentration of pre-gold seeded silica-coated magnetic nanoparticles to 58 nM showed to produce gold-coated magnetic

nanoparticles with thinner gold shell and also produce small aggregation but overall, the quality of gold-coated nanoparticles produced was decent. Magneto-plasmonic properties of gold-coated magnetic nanoparticles produced with different concentrations of pre-gold seeded silica-coated magnetic nanoparticles were investigated using SQUID magnetometry, UV-Vis spectroscopy and dark-field microscopy. The SQUID measurement showed that the gold-coated magnetic nanoparticles showed superparamagnetic behaviour with 25 emu g^{-1}. The UV-Vis and darkfield microscopy showed that nanoparticles made with 2 nM pre-gold seeded silica-coated magnetic nanoparticles showed heavy aggregation, while in the case of nanoparticles made with 58 nM small aggregation was observed. The nanoparticles made with a 24 nM concentration of pre-gold seeded silica-coated magnetic nanoparticles showed the best result and no sign of aggregation. The darkfield microscopy showed well-separated gold-coated magnetic nanoparticles with uniform purple colour. The key to getting the best gold-coated magnetic nanoparticles with a complete gold shell and no sign of aggregation was the balance between the concentration of pre-gold seeded silica-coated magnetic nanoparticles, gold precursor and reducing agent. Finally, to show that the gold-coated magnetic nanoparticles' effectiveness for biosensing the nanoparticles were modified with 4-mercaptobenzoic acid (4-MBA). The gold-coated magnetic nanoparticles showed to be able to bind to biomolecules, be separated with a help of a magnet and also showed good SERS performance. Overall, this chapter showed a new system for the synthesis of gold-coated magnetic nanoparticles with the ability to scale up the procedure.

7.2. Future work

In this section, some possible future works for the synthesis of gold-coated magnetic nanoparticles and possible expansion of a microfluidic system will be suggested.

7.2.1. Improving the synthesis of gold-coated iron nanoparticles

In chapter 5 a new type of gold-coated magnetic nanoparticle was synthesized. The gold-coated iron core-iron oxide shell synthesized in this chapter showed high magnetization saturation with superparamagnetic behaviour. One way to increase the

magnetization saturation, even more, is to keep the iron core intact and keep the iron nanoparticles from becoming iron core-iron oxide shell. To do that the iron nanoparticles could be first coated with an intermediate layer such as Sn using glovebox and Fisher-Porter bottle. The coated iron nanoparticles further could be coated with gold by the slow reduction in the Fisher-Porter bottle and finally, by simple ligand exchange, the gold-coated iron core nanoparticles could be transferred to the water phase.

7.2.2. Improving the fluidic system to produce gold-coated magnetic nanoparticles

Although the fluidic system introduced in chapter 6 solved the issue of scaling up and made the synthesis of gold-coated magnetic nanoparticles easier, the purification of the nanoparticles after seeding and before gold shell growth could be a pivotal point to work on in order to improve the system. To address the issue of purification of nanoparticles before gold shell growth it is possible to use a capillary tubing system that connects the two Y-shaped pieces together. The tubing should be designed in a way that an outlet for unwanted bio-products is available while the gold seeded magnetic nanoparticle could be separated from the bio-products *via* an external magnetic field. The gold-seeded magnetic nanoparticles could be separated from by-products in multiple steps *via* several magnets and then followed by introduction into the three channel Y-shape piece. In this way, the system can be more automated and most of the time consumed on purification cleaning of nanoparticles could be saved.